ParisTech
INSTITUT DES SCIENCES ET TECHNOLOGIES
PARIS INSTITUTE OF TECHNOLOGY

AgroParisTech
INSTITUT DES SCIENCES ET INDUSTRIES DU VIVANT ET DE L'ENVIRONNEMENT
PARIS INSTITUTE OF TECHNOLOGY FOR LIFE, FOOD AND ENVIRONMENTAL SCIENCES

ECOLE DOCTORALE RP2E

Doctorat ParisTech

THÈSE

pour obtenir le grade de docteur délivré par

L'Institut des Sciences et Industries du Vivant et de l'Environnement (AgroParisTech)

Spécialité : Science du sol

présentée et soutenue publiquement par

Pierre-Joseph HATTON

Le 07/09/2012

Séquestration du carbone et de l'azote des feuilles de hêtre dans les associations organo-minérales du sol: Approches macroscopiques, nanométriques & moléculaires

Directeur de thèse : **Etienne DAMBRINE**
Co-encadrement de la thèse : **Delphine DERRIEN**

Jury

Mme Claire CHENU, Professeur, UMR Bioemco, AgroParisTech	Rapporteur
M. Wulf AMELUNG, Professeur, Division Soil Science, University of Bonn	Rapporteur
Mme Isabelle BASILE-DOELSCH, Maître de Conférences, CEREGE	Examinateur
M. Manuel NICOLAS, Ingénieur Responsable RENECOFOR, ONF R&D	Examinateur
M. Etienne DAMBRINE, Professeur, UMR Carrtel, Université de Savoie	Directeur de thèse
Mme Delphine DERRIEN, Chargé de Recherche, UR BEF, INRA-Nancy	Co-directeur de thèse
M. Laurent REMUSAT, Chargé de Recherche, UMR LMCM, MNHN	Invité

INRA

AgroParisTech
UR 1138 Biogéochimie des Ecosystèmes Forestiers
INRA Nancy – 54280 Champenoux

UNIVERSITÉ DE LORRAINE

Résumé

Les associations organo-minérales jouent un rôle prépondérant dans la séquestration à long terme des matières organiques des sols forestiers, mais les contributions des différents types d'association organo-minérale à la stabilisation, ainsi que les processus microbiens qui en sont responsables, restent mal connus. Pour y remédier, des techniques de traçage isotopique ont été combinées à la séparation densitométrique séquentielle des associations organo-minérales. Ces dernières ont été investiguées *in* et *ex situ*, à différentes échelles spatiales (macroscopique, submicrométrique et moléculaire) et temporelles (de 8 heures à 12 ans).

Quatre types d'association organo-minérale ont été distingués : les débris végétaux associés à quelques rares minéraux, les agrégats végétaux, les agrégats microbiens et les grains minéraux. Le traçage isotopique du carbone et de l'azote dérivés des litières de feuilles a mis en évidence, à l'échelle de la décennie, des transferts entre les différentes associations organo-minérales. Tous deux entrent dans le sol sous forme de fragments végétaux, puis migrent progressivement vers les agrégats végétaux et microbiens. Les agrégats apparaissent pertinents pour la stabilisation du carbone et de l'azote à l'échelle décennale. Une petite fraction du carbone et de l'azote apparaît rapidement stabilisée dans les grains minéraux denses. Nos observations du devenir du ^{15}N indiquent que l'activité des microorganismes du sol est responsable de ces transferts. Les fragments de feuilles colonisés par les microorganismes sont progressivement incorporés dans les agrégats végétaux. A mesure que la décomposition se poursuit, les agrégats végétaux se disloquent pour former des agrégats plus stables, plus pauvres en matières organiques, plus enrichis en produits microbiens et plus compacts : les agrégats microbiens.

La stabilisation microbienne a été étudiée aux échelles macroscopique, submicrométrique et moléculaire, principalement par NanoSIMS et LC-IRMS. Elle opère (i) directement par immobilisation dans les cellules microbiennes et (ii) indirectement via une abondante production de métabolites extracellulaires. La calibration des C/N obtenus par NanoSIMS a permis de déterminer qu'ils sont stabilisés dans les associations organo-minérales sans contrôle apparent de la chimie des matières organiques. L'incorporation du ^{13}C dans les sucres aminés, biomarqueurs des biomasses bactériennes et fongiques, indique que les microorganismes vivants croissent où la ressource se trouve. Ils s'accumulent dans les agrégats microbiens via les processus de transfert précédemment évoqués.

Ce travail souligne l'importance des agrégats pour la séquestration du carbone et de l'azote dérivés des litières à l'échelle de la décennie. Il met également en évidence le rôle des microorganismes dans les transferts et la stabilisation du carbone et de l'azote dérivés des feuilles au sein d'associations organo-minérales.

Mots clés: Sol forestier, Litière; Stabilisation, Traçage isotopique, Azote, Carbone, Association organo-minérale; Microorganismes; NanoSIMS; STXM-NEXAFS; LC-IRMS; Sucres amines

Abstract

Organo-mineral associations play a key role in the long-term sequestration of organic matter in forest soils. However, knowledge about the contribution of the different types of organo-mineral associations and the microbial processes involved in soil organic matter stabilisation is scant. To solve it, stable isotope techniques have been combined with the sequential density fractionation of organo-mineral associations. Isolated fractions were investigated in field and in lab, at different temporal (from 8 hours to 12 years) and spatial scales (macro-, submicron- and molecular scales).

Four types of organo-mineral associations were distinguished: plant debris with little mineral attached, plant aggregates, microbial aggregates and mineral grains. Isotopically labeled beech leaf litters were tracked at a decadal time-scale to reveal transfers in between organo-mineral associations. Both litter-derived carbon and nitrogen entered the soil as plant fragments to progressively pass through plant and microbial aggregates. Aggregates appeared particularly meaningful for the stabilisation of litter-derived carbon and nitrogen at a decadal time-scale. Little of the litter-derived carbon and nitrogen was found quickly stabilized to mineral grains. Microbial activities appeared as a major controlling factor for the evolvement of organo-mineral associations, responsive for the transfers of litter-derived carbon and nitrogen. Indeed, plant debris colonized by microorganisms are progressively trapped into plant aggregates. As decomposition proceeds, plant aggregates disrupt into denser microbial aggregates. These aggregates are loaded with lesser organic matter, but enriched in stable microbial materials.

Stabilisation by soil microorganisms has been studied at the macro-, submicron- and molecular- scales, using mostly NanoSIMS and LC-IRMS. Microbial stabilization operated (i) directly through immobilization in microbial cells and, (ii) indirectly through large production of extracellular microbial products. By calibrating the NanoSIMS for accurate C/N ratios, extracellular microbial products have been shown to be stabilized onto organo-mineral associations without apparent control of the mineral-attached organic matter chemistry. The incorporation of ^{13}C tracers into amino sugars, biomarkers of bacterial and fungal biomasses, revealed that living microorganisms grow where the resource is, but accumulate in microbial aggregates. Microbial biomasses moved from plant debris to microbial aggregates, likely along with the transfers of decaying litter residues as described above.

This work points aggregates as meaningful organo-mineral associations for the sequestration of litter-derived carbon and nitrogen at the decadal time-scale. It also revealed the role of microorganisms in the transfers and stabilization of litter-derived carbon and nitrogen within organo-mineral associations.

Keywords: Forest soil, Litter ; Isotopique labeling ; Stabilization ; Nitrogen, Carbon, Organo-mineral asociation; Microorganisms ; NanoSIMS ; STXM-NEXAFS ; LC-IRMS ; Amino sugars

Sommaire

Résumé ... 3

Abstract ... 4

Publications ... 7

Abréviations ... 8

1. Introduction ... 9
1.1. Contexte ... 9
1.2. Les formes de MOS ... 10
1.3. Stabilisation et accumulation des MOS ... 11
1.4. L'étude des MOS ... 12
1.4.1. Le traçage ... 12
1.4.1.1. L'isotopie ... 12
1.4.1.2. Les biomarqueurs ... 13
1.4.2. La séparation des MOS ... 13
1.5. Couplage et découplage du C et du N dérivés des litières de feuilles ... 14
1.6. Objectifs & démarche ... 15

2. Matériels & méthodes ... 17
2.1. Sites d'étude & sols ... 17
2.2. Marquage isotopique ... 17
2.3. Incubations au laboratoire ... 18
2.4. Séparation des associations organo-minérales ... 18
2.5. Caractérisation des échantillons ... 18
2.5.1. Echelle macroscopique ... 18
2.5.2. Echelle submicrométrique ... 19
2.5.3. Echelle moléculaire ... 20
2.6. Calculs et statistiques ... 21

3. Synthèse ... 24
3.1. Associations organo-minérales isolées par densité (Article II) ... 24
3.2. Transferts du carbone et de l'azote dérivés des litières de feuilles dans les associations organo-minérales ... 25
3.2.1. Devenirs de l'N dérivé des litières de feuilles à l'échelle décennale (Article II) ... 26
3.2.2. Modèle conceptuel de transfert dynamique de l'N organique des feuilles dans les associations organo-minérales du sol (Article II) ... 28
3.2.3. Couplage des C et N dérivés des litières de feuilles & validation du modèle pour C (Article III) ... 31
3.3. Microorganismes et associations organo-minérales ... 32
3.3.1. Mise en lumière des processus microbiens (Articles V et III) ... 32
3.3.2. Caractérisation des processus microbiens de stabilisation de C et N 34

3.3.2.1. Pertinence de l'utilisation de la glycine (Article VI) 35
3.3.2.2. Nature des produits microbiens stabilisés 38
3.3.2.2.1. Produits extracellulaires (Article VI) 38
3.3.2.2.2. Biomasse microbienne (Article VII) 41

4. Conclusions 46

5. Perspectives 50

Références 52

Remerciements 65

I. Density Fractions versus Size Separates: Does Physical Fractionation Isolate Functional Soil Compartments? 67

II. Transfer of litter-derived N to soil mineral-organic associations: Evidence from decadal N-15 tracer experiments 101

III. Flows of leaf litter-derived C and N through density-isolated soil organo-mineral associations 115

IV. A multi-scale approach to determine accurate and isotopic ratios by nano-scale secondary ion mass spectrometry imaging 125

V. NanoSIMS study of organic matter associated with soil aggregates: advantages, limitations and combination with STXM 135

VI. Shedding light on the formation of stable soil organic matter through microbial processes 147

VII. Contribution of dead and fresh bacterial and fungal biomasses to soil organo-mineral associations 171

Publications

Ce manuscrit fait la synthèse de travaux publiés ou en préparation listés en annexe. Ces articles sont numérotés de I à VII par ordre d'apparition :

I Moni C, Derrien D, Hatton P-J, Zeller B, Kleber M (Submitted to Biogeosciences). Density Fractions versus Size Separates: Does Physical Fractionation Isolate Functional Soil Compartments?

II Hatton P-J, Kleber M, Zeller B, Moni C, Plante AF, Townsend K, Gelhaye L, Lajtha K, Derrien D (2012). Transfer of litter-derived N to soil mineral-organic associations: Evidence from decadal N-15 tracer experiments. *Organic Geochemistry* **42:** 1489-1501.

III Hatton P-J, Zeller B, Remusat L, Boiry S, Derrien D (In prep.). Flows of leaf litter-derived C and N through density-isolated soil organo-mineral associations.

IV Hatton P-J, Remusat L, Zeller B, Derrien D (2012). A multi-scale approach to determine accurate and isotopic ratios by nano-scale secondary ion mass spectrometry imaging. *Rapid Communications in Mass Spectrometry* **26:** 1363-1371.

V Remusat L, Hatton P-J, Nico PS, Zeller B, Kleber M, Derrien D (2012). NanoSIMS study of organic matter associated with soil aggregates: advantages, limitations and combination with STXM. *Environmental Science & Technology* **46**: 3943-3949.

VI Hatton P-J, Remusat L, Zeller B, Brewer E A, Derrien D (In prep.). Formation of stable soil organic matter through microbial processes.

VII Hatton P-J, Bodé S, Angeli N, Boeckx P, Zeller B, Derrien D (In prep.). Contribution of dead and fresh bacterial and fungal biomasses to soil organo-mineral associations.

Abréviations

MO(S) : matière organique (du sol)

C : carbone

N : azote

EA-IRMS : elemental analyzer coupled with isotope ratio mass spectrometry.

NanoSIMS : nano-scale secondary ions mass spectrometry.

STXM-NEXAFS : scanning transmission X-ray microscopy (STXM) coupled with near edge X-ray absorption fine structure spectroscopy (NEXAFS).

LC-IRMS : liquid chromatography coupled with isotope ratio mass spectrometry.

MEB : microscope électronique à balayage.

1. Introduction

1.1. Contexte

Les écosystèmes forestiers sont sous les pressions conjointes des récents changements de pratiques sylvicoles et des changements globaux. L'intensification des pratiques sylvicoles, via notamment la réduction des cycles sylvicoles et l'exportation des rémanents (Puech, 2009), conduisent à un appauvrissement progressif en nutriments menaçant la fertilité à long terme des sols forestiers (Heijden *et al.*, 2011; Nicolas and Ranger, 2009). Parallèlement, les activités humaines ont contribué, entre autres, à l'élévation moyenne des températures (+0.7°C) et des dépôts atmosphériques (x3-5) au cours du siècle passé (Courtillot *et al.*, 2007; Galloway *et al.*, 2004). Ces dernières se poursuivront très probablement au cours des décennies à venir (IPCC, 2007). Ces changements affectent directement et indirectement le fonctionnement des écosystèmes (Bertrand *et al.*, 2011; Campbell *et al.*, 2009; Janssens *et al.*, 2010; Jonard *et al.*, 2012).

Comprendre les conséquences de ces changements sur les sols forestiers s'avère nécessaire pour l'élaboration de pratiques de gestion durables répondant à des conditions environnementales changeantes. Il s'agit, entre autre, de maintenir ou d'accroitre de la disponibilité en N pour les peuplements et de lutter contre les effets des changements globaux (IPCC, 2007), via, par exemple, la séquestration de C dans les sols. L'élaboration de telles pratiques de gestion requiert une meilleure compréhension des fonctionnements biogéochimiques des sols et, plus particulièrement, des matières organiques des sols (MOS) (Sollins *et al.*, 2007). Deux raisons principales à cela : (1) les sols constituent une réserve colossale de carbone (C) (Post *et al.*, 1982) et d'azote (N) (Post *et al.*, 1984) en équilibre dynamique entre eux et avec l'atmosphère, la biosphère et l'hydrosphère (Gardenas *et al.*, 2011; Gruber and Galloway, 2008). Bien qu'abondant dans les sols, (2) L'N est un facteur limitant la croissance arborée (Chapman *et al.*, 2006; Rennenberg *et al.*, 2009). Alors que les arbres absorbent préférentiellement les formes inorganiques de l'N (Schimel and Bennett, 2004), la majorité de l'N présent dans les sols se retrouve sous forme organique associé au C et relativement peu accessible pour les peuplements (Andrianarisoa *et al.*, 2009; Holub and Lajtha, 2004; Lajtha *et al.*, 2005). Les expérimentations menées par Bernd Zeller ont permis le suivi à long terme de l'N dérivé des litières par traçage isotopique. La figure 1 montre que 4 ans après la chute des litières de feuilles de hêtre, moins de 4% de l'N dérivé desdites litières est retrouvé dans les arbres environnants. Même si cette part augmente avec le temps, 40% à 50% de l'N dérivé des litières reste dans les premiers centimètres du sol sous forme organique au cours de la première décennie suivant la chute des feuilles. L'N dérivé des litières passe progressivement des litières de feuilles à l'horizon O, puis s'accumule dans les premiers centimètres de l'horizon A sous forme de MOS.

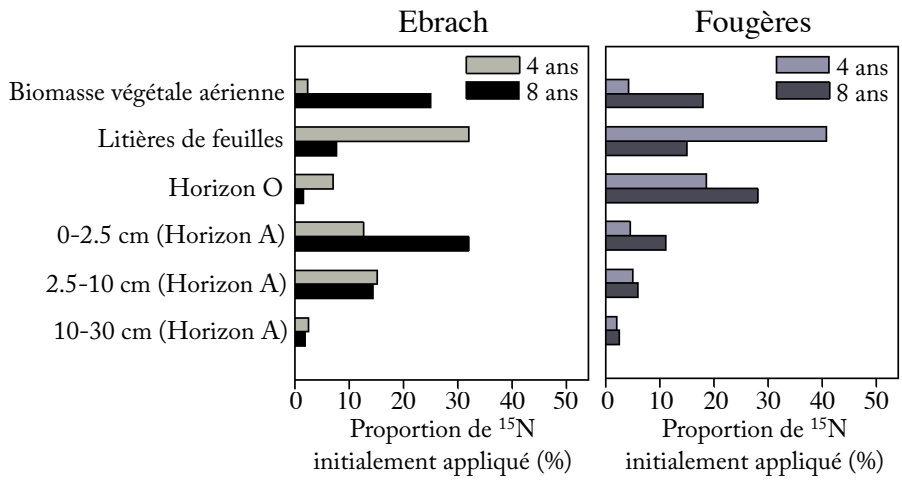

Figure 1: Distribution de l'N dérivé des litières de feuilles de hêtre dans différents compartiments des forêts tempérées d'Ebrach et de Fougères, en fonction du temps. L'azote dérivé des litières est suivi *in situ* par traçage isotopique - Cf. section 1.4.1.1.- au ^{15}N provenant de feuilles enrichies en ^{15}N déposées 4 et 8 ans auparavant (Zeller *et al.*, 1998; Zeller *et al.*, 2001; Zeller *et al.*, 2000). La biomasse végétale aérienne correspond au ^{15}N contenu dans les feuilles produites par les arbres environnants après marquage au ^{15}N.

Les MOS ont donc fait l'objet de nombreuses recherches au cours des dernières décennies. Ces recherches ont, entre autres, permis de caractériser les formes sous lesquelles elles se présentent et les mécanismes de stabilisation responsables de leur accumulation au cours du temps. Une brève synthèse de ces différents points, des méthodes de suivi des devenirs des MOS et leur application aux devenirs du C et du N dérivés des litières est proposée ci-après.

1.2. Les formes de MOS

Les sols forestiers sont principalement alimentés en C et N par les cohortes successives de litières végétales (Christensen, 2001). Ces litières subissent une succession de changements physiques, chimiques et surtout biologiques (macro-, méso-, micro- faunes et microorganismes) produisant une myriade de composés organiques et inorganiques associés ou non aux minéraux du sol pour constituer un mélange complexe et hétérogène de différents composés (Grandy and Neff, 2008; Koegel-Knabner, 2002). Bien que difficiles à déterminer avec précision (Derrien and Amelung, 2011), ces composés présentent des temps moyens de résidence très contrastés (Amelung *et al.*, 2008; Bol *et al.*, 2009) variant avec les conditions environnementales (Schmidt *et al.*, 2011).

On distingue les MOS libres et associées aux assemblages de sol. Leurs proportions varient selon les pratiques culturales, la végétation, les différents facteurs contrôlant la décomposition des litières (climats, types de sol, activités biologiques) et l'horizon de sol étudié (Christensen, 2001; Eusterhues *et al.*, 2005). Les MOS des horizons de surface se caractérisent de la manière suivante :

(1) Les formes libres représentent 10 à 40% des MOS totales et sont soumises à de fortes variations saisonnières liées à l'irrégularité des apports de litières (Christensen, 2001). Elles sont caractérisées par des temps moyens de résidence de quelques mois à quelques années et sont perçues comme un pool transitoire entre les litières et les associations organo-minérales (von Lützow *et al.*, 2008). Ces formes libres sont principalement particulaires et, dans une moindre mesure, dissoutes. Les MOS particulaires sont principalement constitués de fragments végétaux en cours de décomposition (Wagai *et al.*, 2009), mais également de résidus de la micro, méso et macro faune du sol (Christensen, 2001; Gregorich and Janzen, 1996). 10 à 25% des litières se trouvent dissoutes (Guggenberger and Kaiser, 2003) en un mélange complexe de composés rapidement lessivés ou stabilisés (Bolan *et al.*, 2011).

(2) L'essentiel des MOS se trouve sous forme de complexes organo-minéraux : 60% à 90% sont sous formes d'associations organo-minérales (Basile-Doelsch *et al.*, 2007; Mikutta *et al.*, 2009; Sollins *et al.*, 2009). Plus ou moins agrégées, ces associations organo-minérales impliquent des minéraux de tous types en association avec des MOS dans un état de décomposition généralement plus avancé que les MOS libres (Koegel-Knabner *et al.*, 2008; Kogel-Knabner and Kleber, 2011; Mikutta *et al.*, 2010; Sollins *et al.*, 2006). Leurs temps moyens de résidence sont de l'ordre de la décennie, du siècle et au delà. Ces formes de MOS sont perçues comme des pools intermédiaires et passifs (Kogel-Knabner *et al.*, 2008b; Kogel-Knabner and Kleber, 2011; von Lützow *et al.*, 2008). Les transformations microbiennes et l'association aux minéraux sont donc suspectées stabiliser les MOS à long terme.

1.3. Stabilisation et accumulation des MOS

L'accumulation des MOS résulte de leur stabilisation via les mécanismes suivants (Ekschmitt *et al.*, 2008; Rillig *et al.*, 2007; Sollins *et al.*, 1996; von Lützow *et al.*, 2006) :

- *Récalcitrance à la décomposition par les microorganismes*. Il s'agit des caractéristiques intrinsèques des MOS qui les rendent difficilement dégradables par les microorganismes et les enzymes;
- *Non-utilisation par les microorganismes*. Il s'agit de MOS non altérées par l'activité des décomposeurs qui leur préfèrent d'autres types de substrats. Ces mécanismes concernent essentiellement des MO transformées par l'activité des microorganismes du sol ;
- *Inaccessibilité physique aux décomposeurs*. L'organisation spatiale des particules de sol restreint ou interdit l'entrée des décomposeurs, enzymes ou oxygène à la MO occluse, principalement dans les agrégats ;
- *Interactions avec les phases organiques, minérales et métalliques*. Attachement des MOS opérant à des échelles fines et impliquant des interactions faibles (forces de Van der Walls, hydrophobicité, liaisons H), électrovalente (interactions électrostatiques impliquant ou non des cations polyvalents) et/ou covalente (échange anionique).

Alors que la récalcitrance à court terme des MOS non carbonisées est de plus en plus discutée (Kleber, 2010; Marschner *et al.*, 2008), les autres mécanismes semblent jouer un rôle prépondérant dans la stabilisation à long terme des MOS (Kogel-Knabner *et al.*, 2008a; Trumbore, 2009; von Lützow *et al.*, 2008). Si ces mécanismes opèrent simultanément, leur contribution à la stabilisation des MOS varie au cours du temps comme illustré en Figure 2.

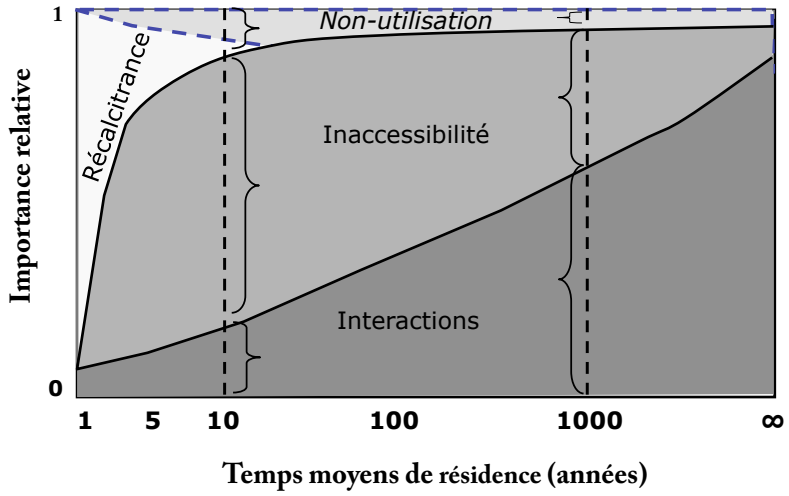

Figure 2: Contribution des différents mécanismes de stabilisation des MOS opérant au cours du temps – figure modifiée de Kögel-Knabner et Kleber (2011).

Les larges proportions de MOS contenues dans les associations organo-minérales (Cf. section 1.2.), ainsi que leur capacité à les séquestrer sur le long terme via des processus de stabilisation minéraux et microbiens (Kogel-Knabner *et al.*, 2008a; Kogel-Knabner and Kleber, 2011; Sollins *et al.*, 2009), en font des compartiments particulièrement pertinents pour l'étude dynamique des MOS (Grandy and Neff, 2008; von Lützow *et al.*, 2007).

1.4. L'étude des MOS

L'étude des devenirs des litières et/ou des MOS dans un milieu aussi complexe que le sol a donc nécessité le développement de méthodes de traçage des matériels d'intérêts ainsi que de séparation des MOS en compartiments partageant des caractéristiques structurelles et fonctionnelles suffisamment proches pour être considérées comme homogènes.

1.4.1.Le traçage

1.4.1.1. L'isotopie

Les atomes constitutifs des litières végétales et MOS présentent un nombre constant de protons et, éventuellement, un nombre variable de neutrons définissant des isotopes. Ces derniers présentent des propriétés physico-chimiques très légèrement

différentes à l'origine de variations dans les différents compartiments de l'écosystème. Ainsi, la composition isotopique des végétaux varie naturellement entre plantes ayant des métabolismes différents (végétaux de type C3 et C4), entre les compartiments d'une même plante (feuilles, tronc, racines), et selon l'état de décomposition d'un même matériel (Dijkstra *et al.*, 2006). Ces variations naturelles sont exploitées pour étudier les dynamiques des MO (Balesdent *et al.*, 1993; Balesdent and Mariotti, 1996). Une autre méthode consiste à enrichir artificiellement une MO en un isotope, par exemple l'enrichissement en ^{13}C et/ou ^{15}N des litières de feuilles (Aita *et al.*, 1997; Zeller *et al.*, 1998). L'excès isotopique, correspondant à la différence avec l'abondance naturelle, permet le suivi d'une cohorte de matériels marqués isotopiquement dans les différents compartiments de l'écosystème comme illustré en Figure 1.

1.4.1.2. Les biomarqueurs

Les litières végétales et les microorganismes sont constitués de molécules organiques dont certaines leurs sont spécifiques. Ces biomarqueurs sont utilisés, éventuellement combinés à des techniques isotopiques, pour tracer la composition et le devenir des résidus végétaux et microbiens (Amelung *et al.*, 2008; Glaser, 2005). C'est ainsi que le devenir des produits microbiens, suspectés jouer un rôle prépondérant dans la stabilisation des MOS (Cf. section 1.3.), peut être investigué. Par exemple, les sucres aminés des parois cellulaires des microorganismes sont utilisés comme biomarqueurs des biomasses microbiennes totales. Ils sont spécifiques car quasiment exclusivement produits par les microorganismes pour la formation des parois cellulaires (Amelung *et al.*, 2001). Particulièrement persistants dans les sols, ils restent inaltérés longtemps après la mort des cellules microbiennes qui les ont produits si bien que la majorité des sucres aminés sont retrouvés dans les biomasses microbiennes mortes (Glaser *et al.*, 2004; Guggenberger *et al.*, 1999). Ils représentent 1-5% des MOS. Bien que 26 sucres aminés aient été identifiés, seulement quatre sont quantifiables dans les sols : la glucosamine, la galactosamine, l'acide muramique et, plus rarement, la mannosamine. La glucosamine provient presque exclusivement des parois cellulaires fongiques alors que l'acide muramique provient uniquement des parois cellulaires bactériennes (Glaser *et al.*, 2004; Liang *et al.*, 2009). Appuhn et Joergensen (2006) ont proposés des facteurs de conversion moyens de 9 [8-10 ; 95% confiance] pour convertir la glucosamine en C fongique et de 45 [30-90 ; 95% confiance] pour la conversion de l'acide muramique en C bactériens (Table 1 ; Article VI). La galactosamine a des origines moins spécifiques. Elle est principalement produite par les bactéries, mais également par quelques champignons (He *et al.*, 2011). Les origines de la mannosamine restent quant à elles mal connues (Liang *et al.*, 2007).

1.4.2.La séparation des MOS

Les MOS sont séparées par des procédures chimiques et/ou physiques. Il s'agit pour les premières d'extraire les MOS grâce à divers solutions aqueuses (d'électrolytes, solvants organiques, acides, etc.) alors que les secondes séparent les structures de sol contenant les MOS selon leur taille et/ ou leur densité. Leurs avantages, limites et

pertinences ont été évalués par von Lützow et al. (2007). Ces différentes méthodes de séparation ont permis l'identification de pools qui se singularisent par leurs propriétés physico-chimiques, leurs degrés d'agrégation et leurs temps moyens de résidence (Grandy and Neff, 2008; Schmidt *et al.*, 2011; Trumbore, 2009). Les procédures de séparation physique ont reçu une attention particulière dans la mesure où les associations organo-minérales apparaissent jouer un rôle majeur dans la dynamique des MOS (Christensen, 2001; Mikutta *et al.*, 2006). Parmi elles, les séparations granulométriques et densitométriques ont été évaluées pour l'étude dynamique du devenir des litières végétales (Article I) : la séparation granulométrique s'avère plus pertinente dans l'étude du devenir des MO particulaires ; la séparation densitométrique s'avère supérieure pour l'étude du devenir des MO associées à différentes structures organo-minérales de sol.

La densitométrie permet la séparation d'associations organo-minérales selon la densité des minéraux et le rapport MO/ minéraux. Les fractions isolées diffèrent par (i) leurs niveaux de transformation par les microorganismes ($\delta^{13}C$ et $\delta^{15}N$ et C/N); (ii) leurs teneurs en C, N et en composés phénoliques ; (iii) leur composition minéralogique et (iv) leur capacité à incorporer le ^{14}C provenant des essais nucléaires de la moitié du siècle passé (Golchin *et al.*, 1994; Mikutta *et al.*, 2009; Prior *et al.*, 2007; Sollins *et al.*, 2009; Sollins *et al.*, 2006; Swanston *et al.*, 2004; Torn *et al.*, 2009). Les taux d'incorporation du ^{14}C "bombe" suggèrent que les temps moyens de résidence des MOS augmentent avec la densité des associations organo-minérales. Sollins *et al.* (2006) ont proposé d'interpréter ces variations par une structuration des MOS en couches successives, où l'efficience de stabilisation décroit depuis la surface minérale vers l'extérieur de l'association organo-minérale, des densités faibles aux densités élevées.

1.5. Couplage et découplage du C et du N dérivés des litières de feuilles

Les différentes méthodes de séparation des sols combinées à des techniques isotopiques et/ ou spectrométriques ont permis d'étudier simultanément les devenirs des C et N dérivés des litières. Ils sont rapidement découplés au cours de la décomposition des litières via la minéralisation préférentielle du C et l'immobilisation l'N dans les biomasses microbiennes (Bird *et al.*, 2003; Trinsoutrot *et al.*, 2000). En dépit de ces différences, les C et N résiduels se répartissent de manière comparable au sein des associations organo-minérales de sol isolées selon deux méthodes granulométriques différentes (Aita *et al.*, 1997; Angers *et al.*, 1997) et des pools de MOS extraits par voie chimique (Bird *et al.*, 2008; Bird and Torn, 2006). Même s'ils ne se retrouvent pas systématiquement dans les mêmes composés organiques (Mambelli *et al.*, 2011), les C et N résiduels semblent rester intimement liés au cours des processus de transfert (Fahey *et al.*, 2011). Bien que plus pertinente pour l'étude des associations organo-minérales (Article I), la densitométrie n'a jamais été utilisée pour l'étude simultanée des C et N dérivés des litières et du rôle qu'y jouent les microorganismes du sol.

1.6. Objectifs & démarche

Les associations organo-minérales occupent un rôle central dans la dynamique des MOS, mais les devenirs du C et du N au sein de ces dernières restent mal compris. Si la contribution des microorganismes au processus de stabilisation est largement reconnue, les processus par lesquels ils opèrent restent méconnus. Les objectifs de cette thèse sont donc d'approfondir la compréhension des devenirs du C et du N dérivés des feuilles de hêtre, espèces abondantes des forêts européennes (FAO, 2011), dans différentes associations organo-minérales des horizons de surface de sols forestiers tempérés et des processus microbiens qui s'y jouent. Plus spécifiquement, les objectifs suivis sont :

1. Le suivi temporel du C et du N dérivés des litières de feuilles dans les associations organo-minérales ;
2. La caractérisation du rôle des microorganismes dans la stabilisation du C et du N au sein des associations organo-minérales.

Pour répondre à ces objectifs, les 2,5 premiers centimètres de sol, où l'essentiel de l'N dérivé des litières de feuilles est retrouvé au cours de la première décennie après la chute des feuilles (Cf. Figure 1), ont été investigués pour :

1. Caractériser des associations organo-minérales séquentiellement séparées par densité : description visuelle des structures et caractérisation des phases organique (composition, qualité) et minérale (identification). La séparation densitométrique a été choisie pour sa pertinence dans l'étude des associations organo-minérales (Article I);
2. Suivre dans le temps des transferts de C et/ ou N des litières de feuilles au sein des associations organo-minérales:
    - L'azote : Les expériences de décomposition de litières mises en place par Bernd Zeller ont permis le suivi *in situ* d'une cohorte de feuilles enrichies en ^{15}N à l'échelle décennale (Zeller *et al.*, 2001), échelle pertinente pout l'étude des mécanismes de stabilisation (Figure 2).
    - Le couplage du C et du N: Des incubations de feuilles enrichies en ^{13}C et ^{15}N, produites par le GRAP au CEA Cadarache, ont permis de suivre simultanément les traceurs pendant un an de décomposition *ex situ*, en conditions contrôlées, de sorte à accélérer les processus de décomposition.
3. Caractériser, dans chaque association organo-minérale, le rôle des microorganismes dans la stabilisation du C et du N issus des litières de feuilles et de glycine. La glycine a été utilisée en complément des litières de feuilles afin d'accélérer les processus microbiens (Jones and Murphy, 2007; van Hees *et al.*, 2005). Les processus microbiens ont été décrits après incubation *ex situ*, en conditions contrôlées, sur des périodes de temps plus courtes (≤12 semaines).

Les différentes associations organo-minérales ont été caractérisées et les traceurs isotopiques ont été suivis à des échelles macroscopique (description visuelle, composition élémentaires et isotopiques, analyses des phases minérales), submicrométrique (description visuelle, cartographie de la spéciation des MOS et de leurs rapports élémentaires et isotopiques) et moléculaire (suivi de biomarqueurs de la biomasse microbienne).

Cette synthèse des travaux menés au cours de cette thèse traite successivement de :

1. La caractérisation des associations organo-minérales (section 3.1. ; p. 23 à 24 ; Articles I, II) ;
2. L'étude des transferts de C et N dérivés des litières entre associations organo-minérales (section 3.2. ; p. 25 à 31 ; Articles II, III)) ;
3. La caractérisation du rôle des microorganismes dans la stabilisation du C et du N (section 3.3. ; p. 31 à 43 ; Articles III, IV, V, VI, VII).

2. Matériels & méthodes

2.1. Sites d'étude & sols

Les travaux menés au cours de cette thèse ont été effectués sur les horizons de surface des sols prélevés à Ebrach, Allemagne (49°52'N, 10°27'E), et Fougères, France (48°23'N, 1°8'W). Ces deux sites sont décrits dans l'article II. Tous deux sont sous statuts forestiers depuis plusieurs siècles et aujourd'hui conduits en futaie régulière de hêtre (*Fagus sylvalica* L.). Ebrach se trouve 430m au dessus du niveau de la mer, sous un climat continental caractérisé par une température annuelle moyenne de 7,5°C et des précipitations annuelles moyennes de 750mm. Le sol est un dystic Cambisol (WRB, 2006) acide (pH_{H20}=3,9) à texture limono-sableuse, développé sur un substrat granitique et couvert d'un humus de type moder (Kaiser *et al.*, 2002; Matzner, 2004; Zeller *et al.*, 2001). Fougères se trouve à 150m au dessus du niveau de la mer, sous un climat océanique caractérisé par une température annuelle moyenne de 12,9°C et des précipitations annuelles moyennes de 870mm. Le sol de Fougères est un glossalbic Cambisol (WRB, 2006) acide (pH_{H20}=3,8) à texture argilo-limoneuse, développé sur un substrat granitique couvert d'une épaisse couche de limons aériens non carbonatés (Legout *et al.*, 2008; Nys, 1998). L'humus est de type moder.

Les 2,5 premiers centimètres de l'horizon A ont été collectés sur des surfaces de 2 m^2, mélangés et tamisés à 2mm. Les racines ont été enlevées. Les sols ainsi collectés ont été conservés en chambre froide à +4°C. Leur humidité pondérale a été mesurée à +105°C.

2.2. Marquage isotopique

Différents matériels marqués ont été ajoutés aux sols étudies: $^{13}C^{15}N$ glycine (Sigma-Aldrich, France ; Articles IV, VI, VII) et feuilles de hêtre enrichies en ^{15}N et/ou en ^{13}C :

- Les feuilles ^{15}N ont été produites *in situ* à Puvenelle par application foliaire de ^{15}N-urée et collectées après sénescence (Zeller *et al.*, 1998). En Février 1996 et 2000, les litières des sites de Ebrach et Fougères ont été remplacées par les feuilles ^{15}N séchées (Zeller *et al.*, 2001). Les sols ont été collectés 4, 8 et 12 ans plus tard à Ebrach et après 4 et 8 ans à Fougères (Articles I, II, V).
- Les feuilles $^{13}C^{15}N$ ont été produites dans une chambre de culture du CEA Cadarache (France), par enrichissement de l'atmosphère en $^{13}CO_2$ et vaporisation de ^{15}N-urée durant la période de végétation (avril-septembre). Les feuilles sénescentes ont été collectées à l'automne, séchées et broyées avant incubation au laboratoire avec les sols d'Ebrach (Articles III, VII). Les sols ont été collectés après 92, 184 et 365 jours.

2.3. Incubations au laboratoire

Les études menées sur des sols incubés au laboratoire sont reportées en Articles III, IV, VI et VII. Ces sols ont été systématiquement pré-incubés pendant 15 jours dans les conditions suivantes : (i) 50% de la capacité de rétention en eau, (ii) volume sol/air de 1/3, (iii) noir, (iv) 20°C et (v) aération régulière.

Ces derniers ont été traités en conditions stériles (Article VII) et non stériles (Articles III, IV, VI et VII). La stérilisation a été obtenue sur sols humides par rayonnement gamma (2kGy.h^{-1} pendant 20 heures ; CEA Cadarache, France). Le choix de la méthode et l'intensité d'irradiation ont été sélectionnés de sorte à (i) préserver les propriétés physico-chimiques des sols (McNamara *et al.*, 2003) ; (ii) quantifier les processus de stabilisation microbiens et abiotiques par comparaison des traitements stériles et non stériles (Berns *et al.*, 2008).

Les deux traitements ont été amendés avec 15$\mu g_N.g_{sol}^{-1}$, soit 25$\mu g_C.g_{sol}^{-1}$ pour les sols amendés avec la glycine (Articles IV, VI et VII) et 1.1$mg_C.g_{sol}^{-1}$ pour ceux amendés avec des litières de feuilles (Articles III et VII). Les sols homogénéisés ont été incubés au laboratoire dans les mêmes conditions que pour la pré-incubation. Le traitement stérile a été amendé et incubé dans des environnements stériles.

2.4. Séparation des associations organo-minérales

Les sols ont tous été séquentiellement fractionnés par densité selon la méthode décrite par Sollins et al. (2006). Brièvement, les sols ont été suspendus dans des solutions de sodium polytungsate (SPT0 ; TC-Tungsten, Allemagne) sélectionnées pour leur faible teneur en C et N (Kramer *et al.*, 2009). La densité du mélange a été ajustée à 1.65 $g.cm^{-3}$ avant séparation des fractions de densités inférieure et supérieure par centrifugation. La fraction la plus légère (surnageant) a été aspirée, rincée et séchées. La même procédure a été répétée sur la fraction la plus dense (culot) avec des solutions de densité croissante. Les coupures densitométriques effectuées sont : 1.65, 1.85, 2.0, 2.2, 2.4 et 2.65 $g.cm^{-3}$.

2.5. Caractérisation des échantillons

Des aliquotes des fractions de sol ont été caractérisées à différentes échelles :

2.5.1. Echelle macroscopique

La composition en débris végétaux, structures organo-minérales agrégées (agrégats) et non agrégées (grains minéraux) a été décrite par microscopie optique (Articles I, II, IV).

Les teneurs en C et N, ainsi que les rapports isotopiques $^{13}C/^{12}C$ et $^{15}N/^{14}N$ ont été déterminés en triplicats par analyse élémentaire couplée à un spectromètre de masse à rapport isotopique (EA-IRMS ; PDZ Europa Ltd., Corvallis, USA / CE Inst., NA 1500 type II – Finnigan, Delta S, PTEF-INRA, Nancy, France).

La minéralogie a été estimée par diffraction des rayons X (DR-X ; PANanalyticalX'Pert Pro Inst., Corvallis, USA). Les formes amorphes et cristallines

du fer (Fe), de l'aluminium (Al) et de la silice (Si) on été extraites à l'oxalate selon la méthode de Balkemore et al (1987). Les formes cristallines ont été estimées par différence avec l'extraction à la dithionite selon la méthode de Holmgren (1967). Les mesures ont été effectuées par spectrométrie d'émission atomique à plasma à couplage inductif (ICP-AES ; Corvallis, USA). Le détail des matériels et méthodes est précisé dans l'article II.

2.5.2. Echelle submicrométrique

La composition des fractions densitométriques en structures organo-minérales agrégées (agrégats) et non agrégées (grains minéraux) a été estimée par microscopie électronique à balayage (MEB ; LMCM, MNHN, Paris, France) (Article IV).

La cartographie des ions $^{12}C^-$, $^{13}C^-$, $^{16}O^-/^{18}O^-$, $^{12}C^{14}N^-$ et $^{12}C^{15}N^-$ à la surface des particules de sol a été obtenue à l'aide d'une micro-sonde ionique NanoSIMS 50 (Cameca, Gennevilliers, France ; LMCM, MNHN, Paris, France). Les particules imagées ont été déposées sur une feuille d'or et métallisées avec 20 nm d'or. Les images NanoSIMS (128x128 à 256x256 pixels) ont été obtenues après pre-ionisation (120pA, 10-25min) puis ionisation (1.5pA ; 2ms.pixel^{-1}) au Cs^+. Le rapport $^{16}O^-/^{18}O^-$ a été utilisé comme proxy pour les particules de sol ; le rapport $^{12}C^-$ pour les MOS. Les images ont été traitées à l'aide du logiciel L'IMAGE® (L. Nittler, Carnegie Institution, Washington DC, USA). Les articles IV, V et VI donnent le détail de la préparation des échantillons, des réglages effectués. Conformément aux travaux réalisées dans l'article IV, les rapports $^{13}C/^{12}C$ déterminés par NanoSIMS ont été corrigés à l'aide un standard externe (kérogène de type III) et les rapports C/N et $^{15}N/^{14}N$ par calibration interne. Brièvement, la calibration des rapports C/N et $^{15}N/^{14}N$ mesurés par NanoSIMS a été obtenue sur des fractions densitométriques marquées en ^{13}C et ^{15}N. La comparaison d'organisation spatiale des particules de sol (agrégée *vs* non-agrégée) et des variations des rapports C/N et $^{15}N/^{14}N$ observés aux échelles macroscopique (microscopie, EA-IRMS) et submicrométrique (MEB, NanoSIMS) ont révélé des analogies fortes ($R>0.8$) pour les surfaces >500µm^2. Aucune analogie n'a été observée pour les rapports $^{13}C/^{12}C$. Les rapports C/N et $^{15}N/^{14}N$ mesurés sur les fractions densitométriques par EA-IRMS et NanoSIMS ont été confrontés pour obtenir des équations de corrections. Les rapports corrigés selon cette méthode se sont révélés plus précis que ceux obtenus à l'aide de la méthode de correction traditionnelle utilisant le kérogène de type III (Figure 3). Le détail de la calibration se trouve dans l'article IV.

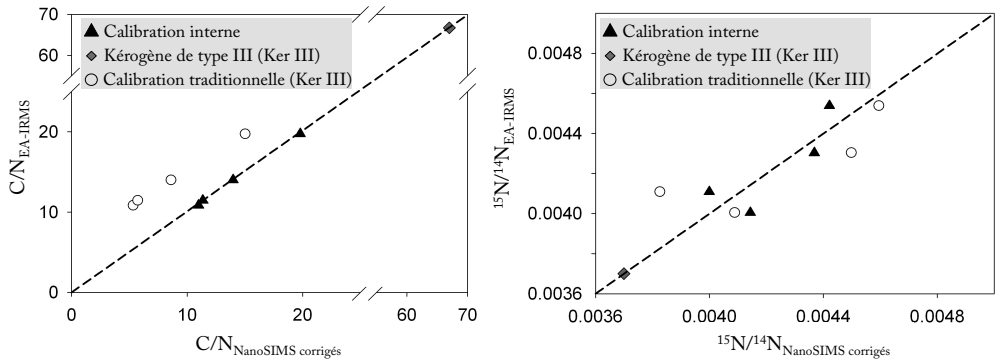

Figure 3: Rapports C/N et $^{15}N/^{14}N$ obtenus par NanoSIMS après calibration 'traditionnelle' au kérogène de type III (ronds blancs) et calibration interne (triangles noirs) en comparaison des valeurs EA-IRMS de référence (n=3). Les valeurs mesurées pour le standard kérogène de type III sont représentées à l'aide d'un losange grisé. La ligne en pointillés est la ligne 1 :1. Le détail des calculs se trouve dans l'article IV.

La spéciation du C et N à la surface des particules de sol a été obtenue par spectrométrie d'absorption des rayons X (STXM) couplée à de la spectroscopie de structure près du front d'absorption de rayons X (NEXAFS) (beamline 5.3.2.2, ALS, LBNL, Berkeley, USA). Les images ont été obtenues entre 278eV et 330eV pour le C et entre 390eV et 440eV pour le N. Les images ont été traitées avec aXis2000 (A.P. Hitchcock, McMaster University, Hamilton, Ontario, Canada) et Athena (Ravel and Newville, 2005). Le détail de la préparation et des réglages est dans l'article V.

2.5.3. Echelle moléculaire

La composition en ^{12}C et ^{13}C des sucres aminés a été obtenue en duplicats par chromatographie liquide couplée à un spectromètre de masse à rapport isotopique (LC-IRMS) (LAPC-ISOFYS, Gand, Belgique – PTEF-INRA, Nancy, France), selon la méthode décrite par Bodé *et al.* (2009). Pour chaque échantillon, l'équivalent de 0.3mg d'N a été successivement hydrolysé (HCl 6M, 105°C, 8h) et filtré (0.45µm). Les composés chargés négativement ont été séparés du filtrat à l'aide de résines protonées (AG50W-X8, ∅100-200, Biorad). Glucosamine, galactosamine et acide muramique ont été séparés et quantifiés par chromatographie en phase liquide (PA20, Thermo Electron), convertis en CO_2 à l'aide de persulfate de sodium ($Na_2S_2O_8$ 0.4M à 99.9°C ; Isolink Interface, Thermo Electron) et analysés pour leur composition isotopique par IRMS (Deltaplus XP, Thermo Electron). La préparation des échantillons et les réglages machine sont décrits dans l'article VII.

2.6. Calculs et statistiques

Les quantités de traceur isotopique ($Q_{traceur}$) ont été calculées comme suit:

$$Q_{traceur} = \frac{A(\%)_{marqué} - A(\%)_{témoin}}{100} \times \left[élément\right]_{marqué} \quad \text{(Eq.1)}$$

$A(\%)_{marqué}$ et $A(\%)_{témoin}$ sont les abondances naturelles en ^{13}C or ^{15}N, exprimées en pourcent, déterminées sur les traitements marqués et témoins, respectivement. $[élément]_{marqué}$ est la concentration en C ou N déterminée sur le traitement marqué. Les enrichissement isotopiques en ^{13}C et ^{15}N sont également exprimés en δ (‰) par rapport aux standards Vienna Pee Dee Belemnite (Craig, 1957) et N_2 atmosphérique (Mariotti, 1983), respectivement.

Les distributions isotopiques et élémentaires sont comparées via le coefficient de corrélation de Pearson et le test *t* de Student ($p<.05$), après vérification de la normalité et de l'homogénéité des variances.

Les anomalies isotopiques détectées par NanoSIMS ont été définies dans l'article V comme devant répondre à deux critères : (i) >0.3 μm^2 et (ii) l'enrichissement mesuré ($R_{anomalie}$) est strictement supérieur à trois fois à l'enrichissement mesuré sur la particule hébergeant l'anomalie (R_{image}):

$$R_{anomalie} > R_{image} + 3 \times \sigma_{anomalie} \quad \text{(Eq. 2)}$$

$\sigma_{anomalie}$ est l'erreur associée à $R_{anomalie}$.

Tableau 1: Caractérisation des fractions densitométriques. Les masses sont exprimées en % de la masse sèche recouvrée après séparation densitométrique (somme des fractions). La composition des fractions en débris végétaux, agrégats et grains minéraux non agrégés a été déterminée par microscopie optique (Article I) ; *n.d.* signifie non déterminé, - non observé. Les taux de couverture des surfaces minérales ont été déterminés par NanoSIMS (Article IV) ; * signifie que les surfaces investiguées ont été jugées représentatives. Les composantes minérales et organiques ont été reprises de l'article II. La contribution des biomasses microbiennes a été estimée à partir des concentrations en sucres aminés dans un intervalle de confiance (95%) représenté entre crochets (Article VII). Les accolades indiquent l'ensemble des fractions auxquelles la valeur est attribuée. Les valeurs sont arrondies à l'unité ou au dixième.

Fraction		Composition			Surface couverte par MOS	Carbone		Azote		Indicateurs de qualité			Contribution des biomasses microbiennes		Phases minérales dominates
Densité (g cm^{-3})	Masse (%)	Débris organiques	Agrégats	Grains minéraux	% surface totale investiguée*	mg .g$_{fraction}^{-1}$	Distribution (%)	mg .g$_{fraction}^{-1}$	Distribution (%)	C/N	δ^{13}C (‰)	δ^{15}N (‰)	Biomasse bactérienne (% fraction C)	Biomasse fongique (% fraction C)	(DR-X; Oxalate-Dithionite)
EBRACH															
Bulk soil	100	*n.d.*	*n.d.*	*n.d.*	*n.d.*	48.1 ± 2.6	100	2.6 ± 0.1	100	0.23	-27.2 ± 0.1	- 3.3 ± 0.2	48 [32;96]	22 [20;24]	*n.d.*
Fractions densitométriques															
<1.65	4	>99%	-	<1%	*n.d.*	386 ± 3.7	41 ± 0.4	18 ± 0.2	34 ± 0.4	24 ± 3	-27.6± 0.0	-4.7 ± 0.0	16 [11; 33]	13 [11; 14]	Phyllosilicates, oxides amorphes (traces)
1.65-1.85	4	<1%	>89%	10%	46%	263 ± 2.8	22 ± 0.2	15 ± 0.1	22 ± 0.1	19 ± 2	-26.9 ± 0.0	-3.8 ± 0.1	22 [15; 45]	16 [14; 18]	Phyllosilicates
1.85-2.0	3	<1%	>83%	16%	57%	210.± 1.8	16 ± 0.1	13 ± 0.0	17 ± 0.1	16 ± 1	-26.1 ± 0.1	-3.6 ± 0.0			Phyllosilicates
2.0-2.2	4	-	>73%	26%	*n.d.*	137 ± 5.3	13 ± 0.5	8.5 ± 0.3	14 ± 0.5	14 ± 2	-27.0 ± 0.1	-3.1 ± 0.0	37 [24; 73]	23 [20; 25]	Phyllosilicates
2.2-2.4	4	-	>59%	40%	31%	38 ± 0.4	3.2 ± 0.0	3.3 ± 0.0	5.0 ± 0.1	11 ± 1	-25.6 ± 0.0	-0.3 ± 0.1			Phyllosilicates
2.4-2.65	81	-	-	>99%	16%	0.8 ± 0.1	1.6 ± 0.1	0.1 ± 0.0	3.5 ± 0.3	10 ± 2	-25.7± 0.1	+1.7 ± 0.1	85 [57; 170]	32 [29; 36]	Quartz, Feldspaths
>2.65	1	-	-	>99%	2%	125 ± 0.3	3.1 ± 0.0	8.0 ± 0.0	3.5 ± 0.0	13 ± 2	-23.5 ± 0.0	-2.4 ± 0.1	*n.d.*	*n.d.*	Quartz, Feldspaths, oxides critallins
Somme des fractions	101					88.4		91.2					31 [21; 63]	19 [17; 21]	
FOUGERES															
Bulk soil	100	*n.d.*	*n.d.*	*n.d.*	*n.d.*	84 ± 4.8	100	4.7 ± 0.3	100	17	-28.0 ± 0.1	-5.0 ± 0.1	*n.d.*		*n.d.*
Fractions densitométriques															
<1.65	9	>99%	-	<1%	*n.d.*	341 ± 9.1	41 ± 1.1	16.7 ± 0.3	35 ± 0.7	21 ± 2	-28.4 ± 0.1	-5.6 ± 0.0	*n.d.*		Phyllosilicates, oxides amorphes (traces)
1.65-1.85	10	<1%	>89%	10%	*n.d.*	226 ± 5.2	31 ± 0.7	13.4 ± 0.3	31 ± 0.8	18 ± 1	-27.9 ± 0.1	-4.8 ± 0.1	*n.d.*		Phyllosilicates
1.85-2.0	5	<1%	>83%	16%	*n.d.*	181 ± 1.2	13 ±0.1	11.7 ± 0.2	14 ± 0.2	16 ± 1	-26.7 ± 0.1	-3.5± 0.0	*n.d.*		Phyllosilicates
2.0-2.2	7	-	>78%	21%	*n.d.*	108 ± 0.3	9 ± 0.0	7.5 ± 0.1	11 ± 0.1	15 ± 1	-27.5 ± 0.0	-2.9 ± 0.0	*n.d.*		Phyllosilicates
2.2-2.4	3	-	>64%	35%	*n.d.*	72 ± 1.4	3.1 ± 0.0	5.6 ± 0.2	4.1 ± 0.2	14 ± 1	-27.1 ± 0.1	-2.0 ± 0.1	*n.d.*		Phyllosilicates
2.4-2.65	60	-	-	>99%	*n.d.*	2.3 ± 0.4	1.8 ± 0.3	0.3 ± 0.0	3.1 ± 0.5	10 ± 0	-27.0 ± 0.0	+1.0 ± 0.1	*n.d.*		Quartz, Feldspaths
>2.65	4	-	-	>99%	*n.d.*	3.1 ± 0.0	0.1 ± 0.0	0.4 ± 0.1	0.3 ± 0.0	11 ± 0	-27.3 ± 0.1	+2.1 ± 0.0	*n.d.*		Quartz, Feldspaths, oxides critallins
Somme des fractions	98					92.8		95.2							

3. Synthèse

3.1. Associations organo-minérales isolées par densité (Article II)

Le fractionnement densitométrique séquentiel isole des associations organo-minérales contrastées (Kogel-Knabner and Kleber, 2011). L'élévation de densité est suspectée isoler des associations contenant des couches de MO de plus en plus minces à mesure que la densité augmente (Sollins *et al.*, 2006). Cette théorie a été évaluée par la caractérisation des associations organo-minérales séquentiellement séparées par densité (sans sonication) depuis les sols d'Ebrach et Fougères (Tableau 1). Quatre types d'associations organo-minérales ont été distingués :

Les *débris végétaux* sont isolés <1.65 g.cm^{-3}. Les observations visuelles et les teneurs en C et N indiquent que les matériels isolés sont majoritairement des débris végétaux. L'ensemble des indicateurs de qualité de la MO - $\delta^{13}C$, $\delta^{15}N$, C/N (Baisden *et al.*, 2002) - ainsi que la présence de sucres aminés (Article VI) indiquent que ces débris végétaux sont partiellement colonisés par les microorganismes (Derrien *et al.*, 2006; Rovira and Vallejo, 2003; Watteau *et al.*, 2006; Zeller and Dambrine, 2011). Les analyses DR-X révèlent la présence de traces de quartz, feldspaths et phyllosilicates. Les extractions oxalate-dithionite indiquent la présence d'oxydes amorphes.

Les *agrégats « végétaux »* sont isolés entre 1.65 et 1.85 g.cm^{-3}. Les observations au microscope optique indiquent que près de 90% des structures isolées sont agrégées. Les fortes teneurs en C et N révèlent une forte proportion de MO, traduisant la matrice végétale des agrégats. Comme le montre la revue de Wagaï *et al.* (2009), les indicateurs de qualité de la MO révèlent un état de décomposition plus avancé que pour les débris végétaux libres. Ceci est confirmé par l'analyse des sucres aminés. L'application des facteurs de conversion proposés par Appuhn et Joergensen (2006), fournit une estimation des biomasses microbiennes de l'ordre de ±30% du C total présent dans ces agrégats. La fraction minérale est plus importante que précédemment et nettement dominée par les phyllosilicates.

Les *agrégats « microbiens »* sont isolés entre 1.85 et 2.4 g.cm^{-3}. Les structures agrégées représentent l'essentiel des matériels isolés et leur minéralogie est dominée par les phyllosilicates. Les taux de couverture des MO décroissent avec la densité. En parallèle, les teneurs en MO diminuent et deviennent de plus en plus microbiennes (Golchin *et al.*, 1994; Prior *et al.*, 2007; Sollins *et al.*, 2009; Sollins *et al.*, 2006). Les teneurs en sucres aminés augmentant fortement par rapport au C, indiquant une forte contribution des biomasses bactériennes et fongiques estimée à ±60% du C de ces agrégats. Bien que les structures non agrégées représentent une part croissante des matériels isolés dans ces fractions, leur faible teneur en MO ne semble pas affecter la signature globale de la faction (Article II).

Les *grains minéraux*, principalement constitués de minéraux primaires, présentant de faibles teneurs en MO sont isolés >2.4 g.cm^{-3}. La composition minéralogique et les

indicateurs de qualité de matière organique permettent la distinction de deux types d'associations organo-minérales. Les grains minéraux isolés entre 2.4 et 2.65 $g.cm^{-3}$ sont très nettement dominés par des minéraux primaires bien cristallisés, principalement quartz et feldspaths. Bien que constituant l'essentiel des sols étudiés, ces derniers ne contiennent que très peu de MO (Basile-Doelsch *et al.*, 2007; Basile-Doelsch *et al.*, 2005). Les indicateurs de qualité de la MO pointent cette fraction comme étant très fortement transformée par l'activité des microorganismes. Les fortes teneurs en sucres aminés, relativement aux teneurs en C, sont plus élevées que dans n'importe quelle autre type d'association organo-minérale et suggèrent que l'ensemble des MO a été transformé par les microorganismes. Les matériels isolés >2.65 $g.cm^{-3}$ sont principalement des grains quartz et feldspaths, mais d'autres minéraux plus réactifs tels que des oxydes de fer et d'aluminium (Kaiser and Guggenberger, 2007; Wagai and Mayer, 2007) y sont également trouvés en quantité. Oxydes et concrétions ferromagnésiennes représentent 20% des structures observées au microscope optique (Article I). Ce changement notable de minéralogie s'accompagne d'un changement quantitatif et qualitatif de MO. Les teneurs en MO sont nettement supérieures à celles mesurées dans la fraction 2.4-2.65 $g.cm^{-3}$, mais, paradoxalement, couvrent moins de surface. Les indicateurs de qualité de la MO révèlent une nature plus contrastée, suggérant une association des MO indépendamment de leur origine. Pour des raisons techniques (Article VII), les fortes teneurs en oxydes n'ont pas permis la quantification des sucres aminés et l'estimation de la contribution des biomasses microbiennes aux MO présentes dans cette fraction.

Contrairement à ce qui a été postulé par Sollins *et al.,* (2006), le fractionnement densitométrique séquentiel sans sonication ne sépare pas des associations organo-minérales contenant des couches de MOS de plus en plus minces à mesure que la densité augmente. Ce fractionnement ségrége différents types d'associations organo-minérales aux propriétés physico-chimiques contrastées: débris végétaux, agrégats végétaux, agrégats microbiens et grains minéraux de différentes réactivités. Les changements de densité s'expliquent par les variations des rapports MO/ minéraux, de densité des minéraux et de porosité au sein des agrégats.
Tester la théorie de l'empilement en couches des MOS nécessite l'emploi de traitements dispersifs puissants pour détruire les agrégats, bien que la dispersion de ces derniers soit difficile à obtenir (Chenu and Plante, 2006).

3.2. Transferts du carbone et de l'azote dérivés des litières de feuilles dans les associations organo-minérales

Les associations organo-minérales jouent un rôle important dans la stabilisation à long terme des MOS (Kogel-Knabner *et al.*, 2008b; Kogel-Knabner and Kleber, 2011; von Lützow *et al.*, 2006). En dépit de la pertinence de la séparation

densitométrique pour l'étude des MOS des associations organo-minérales (Article I), les dynamiques de transferts entre associations séparées par densité restent mal connues (Wagai *et al.*, 2009). Les transferts du $^{15}N_{traceur}$ dérivé des litières de ^{15}N-feuilles ont donc été étudiés *in situ* à l'échelle de la décennie à Ebrach (après 4 et 12 ans) et Fougères (après 8 ans). Ces derniers ont ensuite été confrontés aux processus biologiques et physico-chimiques opérant dans les associations organo-minérales artificiellement isolées par densité pour l'élaboration d'un modèle conceptuel de transfert de l'N résiduel issu des litières de feuilles. Finalement, ce modèle est testé *ex situ* pour le C grâce au suivi simultané des $^{13}C_{traceur}$ et $^{15}N_{traceur}$ dérivés des $^{13}C^{15}N$-feuilles.

3.2.1. Devenirs de l'N dérivé des litières de feuilles à l'échelle décennale (Article II)

L'incorporation des feuilles marquées enrichies ^{15}N dans le sol minéral est initialement retardée par transformations microbiennes de fragmentation prenant place dans l'horizon O (Zeller *et al.*, 2000). La figure 1 montre que 4 et 12 ans après l'apport des ^{15}N-feuilles à Ebrach, 12% et 15% du $^{15}N_{traceur}$ initialement appliqué ont été retrouvés dans l'horizon étudié, contre 5% et 11% après 4 et 8 ans à Fougères (Article II).

Les quantités de $^{15}N_{traceur}$ résiduel sont inégalement réparties entre les associations organo-minérales isolées (Figure 4). Dans les deux sites d'étude, la plupart du $^{15}N_{traceur}$ résiduel se trouve sous forme de débris végétaux tout au long de la première décennie. A Ebrach, cette quantité décroit significativement au cours du temps au profit des agrégats : 57% et 40% du $^{15}N_{traceur}$ sont retrouvés dans les débris végétaux et les agrégats après 4 ans, contre 41% et 56% après 12 ans. Ceci suggère un transfert des débris végétaux aux agrégats. Les ~3% restant sont retrouvés associés aux grains minéraux où, en dépit des différences statistiquement nettes mais quantitativement faibles, le $^{15}N_{traceur}$ résiduel reste relativement stable au cours du temps. Ceci suggère que le $^{15}N_{traceur}$ résiduel est rapidement incorporé et efficacement stabilisé ou activement échangé dans ces grains minéraux. La distribution du $^{15}N_{traceur}$ résiduel mesurée à Fougères après 8 ans est globalement comparable à celle mesurée à Ebrach après 12 ans, suggérant que les mécanismes de transfert opèrent à des échelles de temps similaires. Les agrégats microbiens apparaissent cependant sensiblement moins riches en $^{15}N_{traceur}$ résiduel. Ceci est attribué au fait que l'expérimentation soit moins longue à Fougères qu'à Ebrach et que les temps moyens de résidence déterminés dans l'horizon O y soient plus longs : 3.45 ans contre 2.78 à Ebrach (d'Annuzio et al., 2008; Zeller et al., 2000). Ces différences suggèrent que le degré de décomposition de la MO exerce un important contrôle sur l'interaction organo-minérale et la dynamique de transfert entre associations organo-minérales.

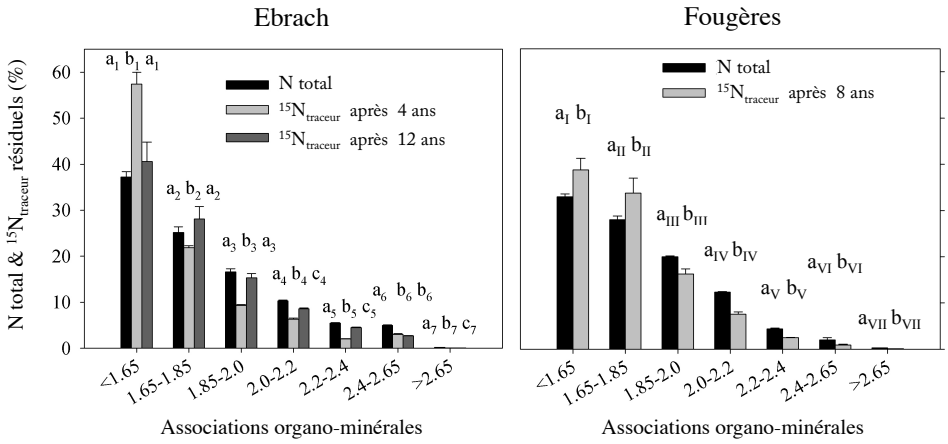

Figure 4: Distributions de l'N total et du $^{15}N_{traceur}$ résiduel dans différentes associations organo-minérales séquentiellement isolées par densité (% total recouvré après fractionnement densitométrique) des horizons de surface de Ebrach et Fougères (n=3). N total correspond à la moyenne sur des différents traitements. A Ebrach, 12 et 15% du $^{15}N_{traceur}$ initialement appliqué ont été retrouvés dans l'horizon étudié, contre 11% après 8 ans à Fougères. Les débris végétaux sont isolés <1.65 g.cm^{-3} ; les agrégats végétaux entre 1.65-1.85 g.cm^{-3} ; les agrégats microbiens entre 1.85-2.4 g.cm^{-3} ; les grains minéraux de faible et forte réactivité entre 2.4-2.65 g.cm^{-3} et >2.65 g.cm^{-3}, respectivement. Les comparaisons statistiques entre les différentes distributions ont été réalisées à l'aide d'un test-*t* de Student au seuil de 95% : deux lettres identiques indiquent une égalité statistique, alors qu'une différence significative est notée par deux lettres différentes.

Parallèlement à ces transferts, les potentiels de minéralisation nette (Cf. Article II) mesurés pour le $^{15}N_{traceur}$ résiduel à Ebrach 4 et 12 ans diminuent de 2.5±0.1% à 0.5±0.1% du $^{15}N_{traceur}$ résiduel, contre 0.8±0.1% de l'N total aux deux dates. Cette diminution indique que le $^{15}N_{traceur}$ résiduel devient moins accessible aux décomposeurs au cours du temps, probablement via l'association progressive du $^{15}N_{traceur}$ aux agrégats et grains minéraux.

Les transferts verticaux, de l'horizon O vers l'horizon étudié, et horizontaux, i.e. entre fractions, mettent en évidence des délais variables pour l'incorporation du $^{15}N_{tracer}$ résiduel dans les différentes fractions de sol. Ces transferts se superposent aux différentes probabilités de contact entre le $^{15}N_{traceur}$ résiduel et les surfaces accessibles et inaccessibles (occluses) pour contraindre l'accessibilité du $^{15}N_{traceur}$ aux différentes associations organo-minérales du sol. Ces derniers rendent le calcul de temps moyens de résidence délicat (Derrien and Amelung, 2011). Cependant, les différences de distribution entre N total et $^{15}N_{traceur}$ renseignent sur la dynamique du transfert de la cohorte de litière marquée dans chacune des fractions de sol étudiée. Contrairement à l'N total qui renseigne sur l'état intégré de l'N issus des cohortes successives de litières au cours du temps, le $^{15}N_{traceur}$ résiduel indique la distribution de l'N issu d'une cohorte de feuilles à un instant *t*. Les débris végétaux incorporent préférentiellement le $^{15}N_{traceur}$ après 4 ans à Ebrach et 8 ans à Fougères. Ce trait

s'estompe après 12 ans à Ebrach, suggérant que cette fraction se renouvelle en une décennie. Les différences entre les proportions de $^{15}N_{traceur}$ résiduel et d'N total vont croissantes avec la densité des agrégats et des grains minéraux traduisant l'augmentation des délais de transferts. Ces dernières ne permettent pas la caractérisation des vitesses de renouvellement des agrégats et des grains minéraux.

Au cours de la première décennie après la chute des litières, l'N n'est que peu prélevé par la végétation et s'accumule sous forme organique dans l'horizon de surface étudié (Figure 1). Dans les deux sites d'étude, la plupart de l'N résiduel reste sous forme de débris végétaux tout au long de la première décennie. A Ebrach, cette quantité décroit significativement au cours du temps au profit des agrégats : 57% et 40% du $^{15}N_{traceur}$ sont retrouvés dans les débris végétaux et les agrégats après 4 ans, contre 41% et 56% après 12 ans. l'N issu des litières migre donc progressivement des débris végétaux aux agrégats végétaux et microbiens. Les ~3% restant sont retrouvés associés aux grains minéraux où l'N résiduel semble stabilisé au cours du temps. La distribution de l'N résiduel observée 8 ans après la chute des feuilles à Fougères est semblable à celle observée après 12 ans à Ebrach.
Parallèlement à ces transferts, l'N dérivé des litières apparaît de moins en moins disponible pour les microorganismes jusqu'à devenir moins disponible que l'N total. La diminution de la disponibilité semble indiquer que l'N qui a migré dans les agrégats et les grains minéraux y est stabilisé.
Pour réconcilier les résultats obtenus en 3.1. et 3.2.1., un modèle conceptuel pour le transfert de l'N organique dérivé des litières dans les différents compartiments de sols séparés par densité a été élaboré.

3.2.2. Modèle conceptuel de transfert dynamique de l'N organique des feuilles dans les associations organo-minérales du sol (Article II)

Les transferts dynamiques de l'N dérivé des feuilles dans les associations organo-minérales des horizons de surface peuvent s'expliquer par des processus biologiques et les propriétés physico-chimiques desdites associations (Figure 5) :

Les résidus de litières de feuilles entrent dans le sol principalement par bioturbation et fragmentation par les macro- et méso- faunes (Zeller *et al.*, 2000). Ces résidus sont pour partie minéralisés par les microorganismes et pour partie altérés ou transformés en une myriade de sous produits (Christensen, 2001; Mambelli *et al.*, 2011). Ces derniers s'associent aux minéraux selon trois mécanismes principaux : (i) association médiée par la dynamique des agrégats et les activités microbiennes ; (ii) capture dans la porosité des agrégats et (iii) sorption des composés labiles (MO dissoute et nutriments tels que le NH_4^+).

Les fragments végétaux, représentant la majorité des résidus de litières de feuilles, sont incorporés dans des agrégats au gré de leur dynamique de formation. La

probabilité de désagrégation dépend pour partie de la nature de la MO occluse : les complexes organo-minéraux impliquant des produits microbiens sont plus stables que ceux impliquant des débris végétaux hydrophobes (Christensen, 2001; De Gryze *et al.*, 2006; Oades, 1993; Plante and McGill, 2002). Les agrégats végétaux, plus sensibles à désagrégation que les agrégats microbiens, offrent donc une plus grande probabilité de recombinaison aux débris végétaux.

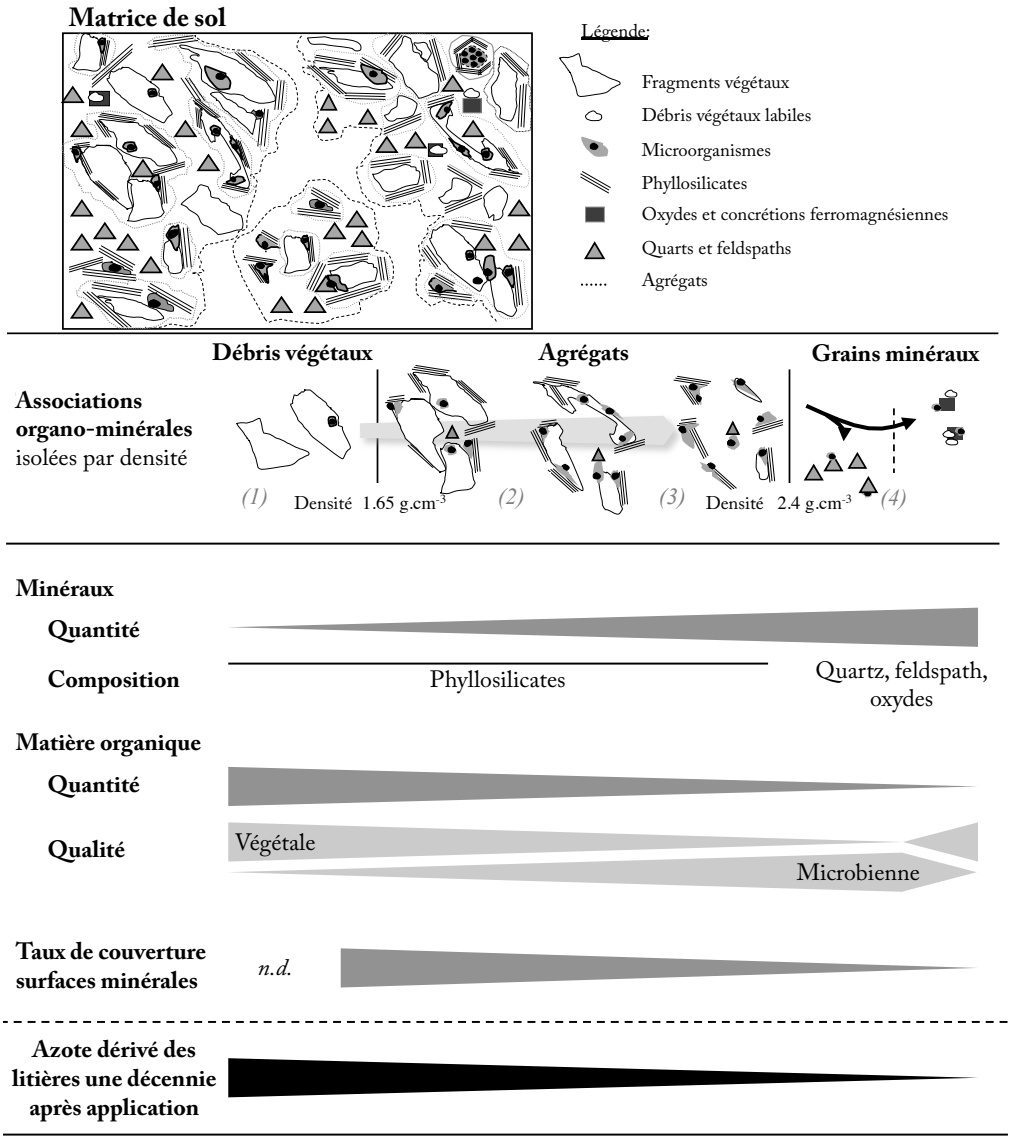

Figure 5: Modèle conceptuel de transfert de l'N dérivé des litières de feuilles dans les associations organo-minérales isolées par densité. (1) Les fragments végétaux entrent dans le sol minéral progressivement incorporés dans des agrégats. Les fragments végétaux occlus dans les agrégats sont progressivement dégradés par l'activité des microorganismes jusqu'à (2) affaiblissement de leur structure aboutissant à leur destruction. (3) Les petits agrégats

ainsi libérés sont plus denses, moins poreux et plus riches en produits microbiens. (4) Les grains minéraux composent les fractions les plus denses, où les produits microbiens dominent. Cependant, la présence d'oxydes dans les fractions les plus denses adsorbe les MO indépendamment de leurs origines végétales ou microbiennes via leurs surfaces hydroxylées.

A mesure que les fragments de litières occlus dans les agrégats végétaux sont décomposés par les microorganismes qui les colonisent, la proportion de MO diminue relativement aux matière minérales entrainant une élévation de la densité desdits agrégats (Golchin *et al.*, 1994; Oades and Waters, 1991; Six *et al.*, 2002). La décomposition des résidus de litières altère progressivement la structure des agrégats jusqu'à causer leur désagrégation. Plus riches en produits microbiens fortement associés aux surfaces minérales, les entités ainsi produites sont donc de petites tailles et n'offrent qu'une porosité réduite. La diminution de porosité se superpose à la diminution du rapport MO/ matière minérale dans l'élévation de densité des agrégats. Ce phénomène perdure jusqu'à désagrégation totale des agrégats ou jusqu'à la réintégration de ladite structure lors de la formation d'un nouvel agrégat.

Les composés produits lors de la décomposition des résidus de litières, qu'ils soient organiques (≥97% à Ebrach) ou minéraux (≤3% à Ebrach), sont susceptibles d'interagir avec toutes surfaces minérales réactives et accessibles, telles que celles des phyllosilicates (Kinyangi *et al.*, 2006; Kleber *et al.*, 2005) et des oxydes (Kaiser and Guggenberger, 2007; Wagai and Mayer, 2007). Ces interactions opèrent également à l'intérieur des agrégats après incorporation par diffusion via le système de pores (Smucker *et al.*, 2007).

Ce modèle conceptuel pour le transfert de l'N organique dans les associations organo-minérales de sol rend compte des changements de densité, de dynamiques et de propriétés physico-chimiques des associations (section 3.1.). Les transformations microbiennes des MO occluses dans les agrégats sont responsables des changements de densité et du transfert progressif de l'N dérivé des litières au sein des agrégats de densité croissante. Il en résulte des délais de transfert de plus en plus importants à mesure que la densité augmente. La minéralogie des grains minéraux non agrégés explique la densité des associations organo-minérales qu'ils hébergent, la nature contrastée des MO qui s'y trouvent ainsi que leur faible quantité.

3.2.3. Couplage des C et N dérivés des litières de feuilles & validation du modèle pour C (Article III)

Bien que le modèle précédemment exposé puisse théoriquement s'appliquer au C organique résiduel issu des feuilles, il n'a pas été testé. Pour y remédier, le suivi simultané et dynamique des $^{13}C_{traceur}$ et $^{15}N_{traceur}$ résiduels issus de $^{13}C^{15}N$-feuilles a été étudié *ex situ* sur les 2,5 premiers centimètres de sol d'Ebrach précédemment étudiés.

92, 184 et 364 jours après l'apport des $^{13}C^{15}N$-feuilles, 79±3%, 70±4% et 68±4% du $^{13}C_{traceur}$ initialement appliqué ont été retrouvés dans l'horizon étudié. Aucune perte significative de $^{15}N_{traceur}$ n'a été observée au cours de la période d'incubation. Conformément à ce qui a été montré auparavant (Bird *et al.*, 2008; Bird and Torn, 2006; Fahey *et al.*, 2011; Trinsoutrot *et al.*, 2000), $^{13}C_{traceur}$ et $^{15}N_{traceur}$ résiduels issus des feuilles sont rapidement découplés suite à la minéralisation préférentielle du C.

La Figure 6 montre cependant que tous deux partagent des distributions et des cinétiques similaires à travers les différents types d'associations organo-minérales de sol (Aita *et al.*, 1997; Angers *et al.*, 1997). $^{13}C_{traceur}$ et $^{15}N_{traceur}$ résiduels diminuent à mesure que la densité des associations organo-minérales augmente. Les débris végétaux restent le plus grand pool de traceurs résiduels tout au long de la première année d'incubation, mais ce dernier diminue progressivement au cours du temps. Inversement, les traceurs résiduels augmentent significativement au cours du temps dans les agrégats et les grains minéraux. Sur un an, $^{13}C_{traceur}$ et $^{15}N_{traceur}$ résiduels augmentent respectivement de 38% à 48% et de 48% à 55% dans les agrégats. Dans le même temps, $^{13}C_{traceur}$ et $^{15}N_{traceur}$ résiduels augmentent respectivement de 5% à 9% et de 4,5% à 5,3% dans les grains minéraux. Comme observé précédemment (section 3.2.1.), les délais relatifs à ces transferts tendent à s'accroître à mesure que la densité des associations organo-minérale augmente, des agrégats aux grains minéraux.

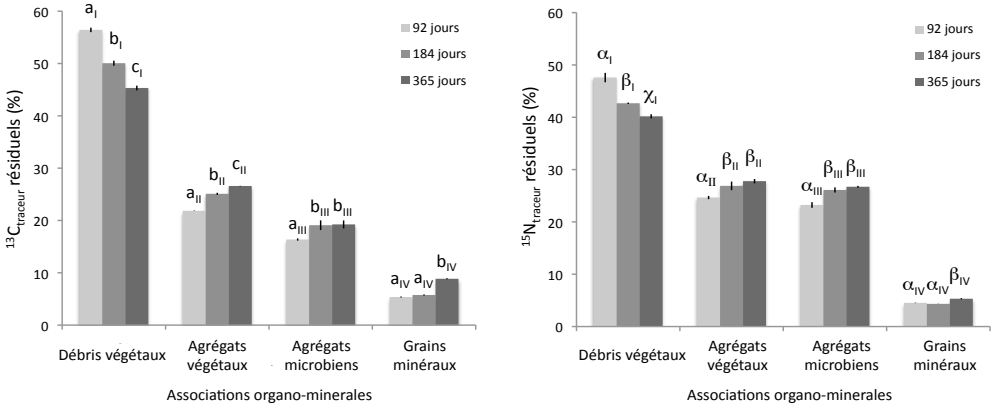

Figure 6: Distributions des $^{13}C_{traceur}$ (gauche) et $^{15}N_{traceur}$ (droite) résiduels issus de litières de feuilles dans différentes associations organo-minérales séquentiellement séparées par densité (% total recouvré après séparation). Les débris végétaux sont isolés <1.65 g.cm^{-3} ; les agrégats végétaux entre 1.65-1.85 g.cm^{-3} ; les agrégats microbiens entre 1.85-2.4 g.cm^{-3} ; les grains minéraux >2.4 g.cm^{-3}. Les distributions ont été comparées à l'aide d'un test-*t* de Student au

seuil de 95% : deux lettres identiques indiquent une égalité statistique, alors qu'une différence significative est notée par deux lettres différentes (n=3).

Bien qu'il y ait substantiellement moins de $^{13}C_{traceur}$ résiduels que de $^{15}N_{traceur}$ résiduels suite à minéralisation préférentielle du $^{13}C_{traceur}$, les $^{13}C_{traceur}$ et $^{15}N_{traceur}$ résiduels dérivés des litières suivent tous deux les mêmes chemins et sont similairement transférés depuis les débris végétaux vers les agrégats et, en de moindres proportions, vers les grains minéraux. Le modèle conceptuel pour le transfert de l'N résiduel dérivé des litières s'applique également pour le C à l'échelle des associations organo-minérales isolées par densité.

3.3. Microorganismes et associations organo-minérales

Les microorganismes sont suspectés jouer un rôle important dans la mise en place des associations organo-minérales (Grandy and Neff, 2008; Sollins *et al.*, 2009). La section 3.2. de ce manuscrit met en évidence le contrôle exercé par les microorganismes dans l'évolution des associations organo-minérales responsable des transferts de C et de N dérivés des litières. Cependant, les processus par lesquels les microorganismes opèrent la stabilisation des MOS, ainsi que leur distribution dans les sols, restent mal connus (Chenu and Stotzky, 2002). Les transformations microbiennes des litières ont d'abord été mises en évidence dans la section 3.3.1., à l'aide de deux méthodes distinctes de traçage isotopique aux échelles submicrométrique (couplage NanoSIMS-STXM/NEXAFS) et macroscopique (EA-IRMS). Les processus microbiens impliqués dans la mise en place des associations organo-minérales ont ensuite été caractérisés par traçage isotopique aux échelles submicrométriques par NanoSIMS (section 3.3.2.2.) et moléculaires par LC-IRMS (section 3.3.2.3.).

3.3.1. Mise en lumière des processus microbiens (Articles V et III)

Les transformations microbiennes des litières ont été investiguées par les suivis (1) de $^{15}N_{traceur}$ résiduels à la surface d'agrégats séparés 12 ans après la chute des ^{15}N-feuilles (section 3.2.1.) par le couplage NanoSIMS et STXM/NEXAFS (Article V) et (2) des rapports $^{13}C_{traceur}$ résiduels/ $^{15}N_{traceur}$ résiduels mesurés après 92, 184 et 365 jours d'incubation de $^{13}C^{15}N$-feuilles au laboratoire (Article III).

Dans un premier temps, les transformations microbiennes ont été investiguées sur une vingtaine de micro agrégats isolés depuis les sols collectés après 12 ans de marquage *in situ* par apport de feuilles enrichies en ^{15}N (Article V). Ces derniers ont été sélectionnés en raison de leurs forts enrichissements en $^{15}N_{traceur}$. Ils ont été alternativement analysés à l'échelle submicrométrique de sorte à déterminer la spéciation des MO, par STXM-NEXAFS, contenant le $^{15}N_{traceur}$ localisé par NanoSIMS (Eq. 2). Malgré des contraintes techniques fortes liées à la combinaison de ces deux techniques de pointe, un micro agrégat contenant le $^{15}N_{traceur}$ a été identifié et caractérisé (Figure 7). Le $^{15}N_{traceur}$ est localisé en région 1. Il se trouve en

présence d'une MO riche en C, vraisemblablement dominée par des groupements carboxyliques et/ou amides comme le serait un mélange de protéines, sucres aminés et de composés polysaccharidiques. Après comparaison avec des MO microbiennes (Chan *et al.*, 2009) et litières de feuilles (Lehman *et al.*, 2008), la MO contenant le $^{15}N_{traceur}$ s'avère chimiquement plus proche des MO microbiennes, suggérant que le $^{15}N_{traceur}$ est contenu dans des produits microbiens issus de la décomposition des litières de feuilles.

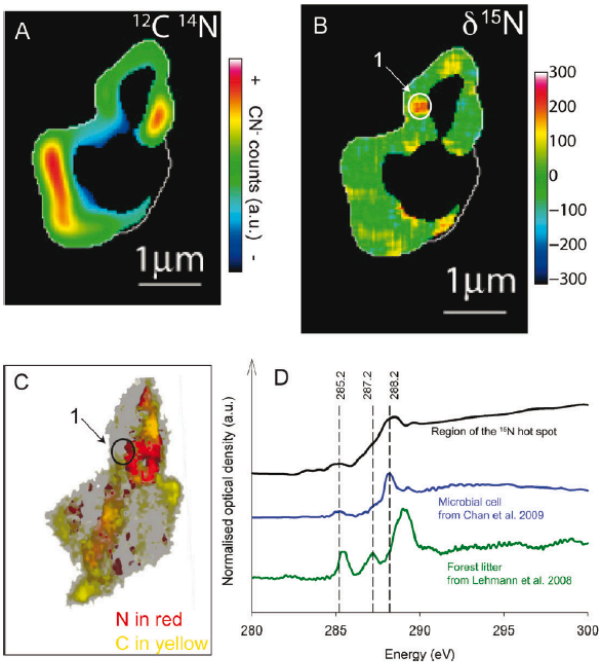

Figure 7: Analyse submicrométrique d'un micro agrégat microbien par NanoSIMS (A & B) et STXM-NEXAFS (C & D). A: image $^{26}CN^-$; B: image $\delta^{15}N$; C: image C (278->330 eV) et N (390->440eV); D: spectres NEXAFS de la région 1 contenant le $^{15}N_{traceur}$ (noir) ($\delta^{15}N$=213±132‰), de MO microbiennes (bleu) (Chan *et al.*, 2009) et de litières de feuilles (vert) (Lehman *et al.*, 2008). Les raies d'absorption à 285.2eV, 287.2eV et 288.2eV sont respectivement spécifiques des C aromatiques (Keiluweit *et al.*, 2010; Lehman *et al.*, 2007), C aliphatiques (Brandes *et al.*, 2004) et C carboxyliques et groupements amides (Kinyangi *et al.*, 2006).

Dans un second temps, les rapports $^{13}C_{traceur}$ résiduels/$^{15}N_{traceur}$ résiduels mesurés après 92, 184 et 365 jours d'incubation de $^{13}C^{15}N$-feuilles au laboratoire (Cf. section 3.2.3. ; Article III) révèlent des découplages au sein même des fractions (Figure 8). Ces derniers traduisent des transformations microbiennes importantes des feuilles incubées. Plus spécifiquement, les agrégats deviennent progressivement plus riches en $^{15}N_{traceur}$ résiduels relativement au $^{13}C_{traceur}$ résiduels au cours du temps, suggérant que la minéralisation préférentielle du $^{13}C_{traceur}$ s'y combine à l'immobilisation du $^{15}N_{traceur}$ (Trinsoutrot *et al.*, 2000). A contrario, les grains minéraux montrent un enrichissement relatif en $^{13}C_{traceur}$ par rapport au $^{15}N_{traceur}$ qui s'accentue au cours du

temps. Ces différences suggèrent une compartimentation des processus de stabilisation, vraisemblablement, microbiens entre agrégats et grains minéraux et/ ou un cloisonnement des activités microbiennes.

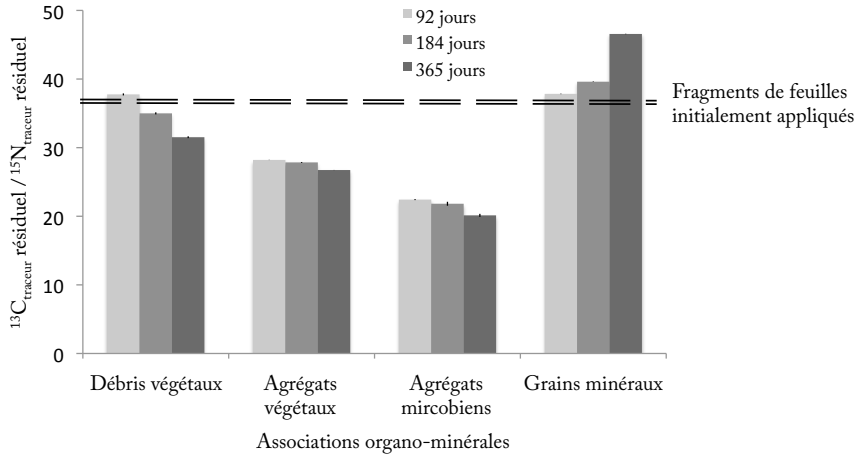

Figure 8: $^{13}C^{traceurs}$ résiduels/ $^{15}N_{traceurs}$ résiduels dans différentes associations organo-minérales séquentiellement isolées par densité après 92, 184 et 365 jours après apport des feuilles $^{13}C^{15}N$ (n=3). Les débris végétaux sont isolés <1.65 g.cm^{-3} ; les agrégats végétaux entre 1.65-1.85 g.cm^{-3} ; les agrégats microbiens entre 1.85-2.4 g.cm^{-3} ; les grains minéraux de faible et forte réactivité >2.4 g.cm^{-3}. La ligne discontinue indique le rapport mesuré sur les fragments de feuilles initialement appliquées.

Le couplage NanoSIMS-STXM/NEXAFS a montré que l'N résiduel issu d'une cohorte de feuilles vieille de 12 ans pouvait se trouver sous forme de produit microbien. Plus représentatif, le suivi des rapports $^{13}C_{traceur}$ résiduels /$^{15}N_{traceur}$ résiduels a confirmé les transformations microbiennes des résidus de feuilles. Ces transformations apparaissent importantes et inféodées à des types d'association organo-minérales distincts, avec un enrichissement progressif en N dans les agrégats et en C dans les grains minéraux. Ces résultats mettent en évidence la transformation par les microorganismes du sol des résidus de feuilles associées aux différents types d'associations organo-minérales.

3.3.2.Caractérisation des processus microbiens de stabilisation de C et N

La caractérisation des processus microbiens responsables de la stabilisation des MOS a été effectuée à l'aide de $^{13}C^{15}N$-feuilles et de $^{13}C^{15}N$-glycine. La glycine a été

utilisée en complément des feuilles pour accélérer les processus de transformation microbiens et évaluer les modes de stabilisation de leurs produits (Jones and Murphy, 2007). La pertinence de l'utilisation de la glycine pour l'étude de la stabilisation microbienne a d'abord été évaluée dans la section 3.3.2.1. Les produits microbiens ainsi stabilisés dans les différents types d'association organo-minérales ont ensuite été caractérisés par traçage isotopique à l'échelle submicrométrique par NanoSIMS et à l'échelle moléculaire par LC-IRMS. Le suivi des $^{15}N_{traceur}$ résiduels et $^{13}C_{traceur}$ résiduels dérivés de $^{13}C^{15}N$-glycine a d'abord été effectué à la surface des particules de sol isolées depuis différents types d'associations organo-minérale (section 3.3.2.2.). L'incorporation de $^{13}C_{traceur}$ issus de $^{13}C^{15}N$-glycine et $^{13}C^{15}N$-feuilles dans les sucres aminés des différentes associations organo-minérales a ensuite été étudiée par LC-IRMS (section 3.3.2.3.).

3.3.2.1. Pertinence de l'utilisation de la glycine (Article VI)

La pertinence de l'utilisation de la glycine pour étudier les processus microbiens impliqués dans la stabilisation des C et N qui en sont issus a été testée à l'aide de $^{13}C^{15}N$-glycine. Pour chaque association organo-minérale, la différentiation des processus de stabilisation microbiens et abiotiques a été obtenue par comparaison des quantités de traceurs résiduels isolés depuis les traitements stérile et non stérile (Berns *et al.*, 2008).

Après seulement 8 heures d'incubation, $^{15}N_{traceur}$ résiduels et $^{13}C_{traceur}$ résiduels retrouvés dans les associations organo-minérales représentent 7% des apports initiaux. Ces derniers sont considérés comme étant stabilisés (Sollins *et al.*, 2009; Sollins *et al.*, 2006). Les $^{15}N_{traceur}$ résiduels et $^{13}C_{traceur}$ résiduels sont stabilisés à 90% et 85% par des processus microbiens dont la contribution varie selon les types d'association organo-minérale avec lesquels ils sont stabilisés. La Figure 9 montre que la contribution des processus microbiens à la stabilisation des traceurs augmente avec la densité des agrégats. La stabilisation microbienne représente 87% à 95% des $^{15}N_{traceur}$ résiduels stabilisés dans les agrégats contre 93% à 99% pour les $^{13}C_{traceur}$ résiduels. La part de la stabilisation microbienne diminue sensiblement dans les débris végétaux et les gains minéraux où elle varie entre 68% et 85% des traceurs résiduels stabilisés.

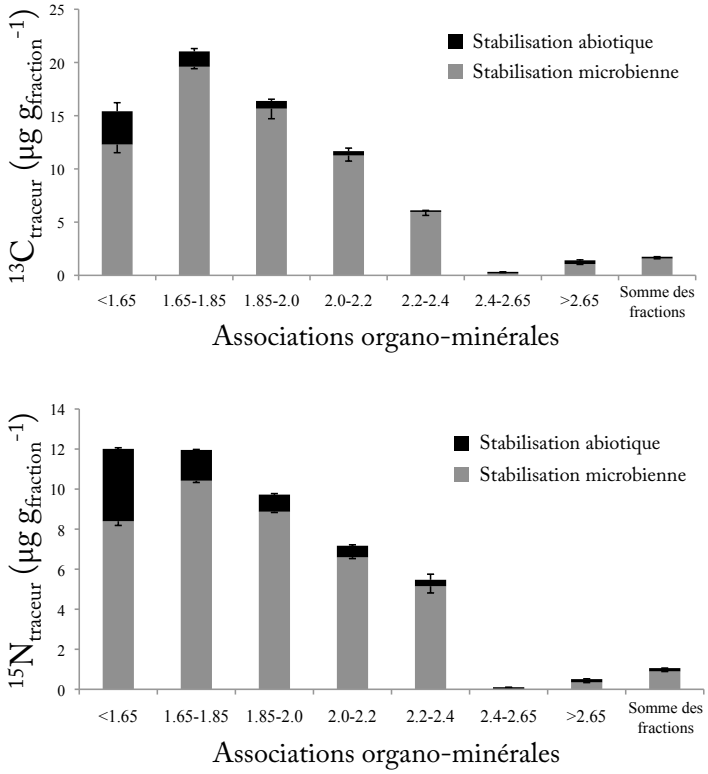

Figure 9: Stabilisation abiotique (noir) et microbienne (gris) des $^{15}N_{traceur}$ résiduels (bas) et $^{13}C_{traceur}$ résiduels (haut) dans différentes associations organo-minérales séquentiellement isolées par densité 8 heures après apport de glycine enrichie en ^{13}C et ^{15}N (n=3). La stabilisation abiotique a été quantifiée depuis le traitement stérile. La stabilisation microbienne a été estimée par différence entre le traitement non stérile et stérile. La somme des fractions représente la somme des traceurs de chaque fraction exprimée en µg.g_{soil}^{-1}. Les débris végétaux sont isolés <1.65 g.cm^{-3} ; les agrégats végétaux entre 1.65-1.85 g.cm^{-3} ; les agrégats microbiens entre 1.85-2.4 g.cm^{-3} ; les grains minéraux de faible et forte réactivité entre 2.4-2.65 g.cm^{-3} et >2.65 g.cm^{-3}, respectivement.

La stabilisation abiotique ne représente qu'une part marginale des traceurs stabilisés dans les associations organo-minérales (Figure 9). Les rapports $^{13}C_{traceur}$ résiduels/ $^{15}N_{traceur}$ résiduels mesurés dans les débris végétaux et les agrégats sont significativement inférieurs à celui de la glycine initialement appliquée (1.0<<1.7), alors que ceux mesurés dans les grains minéraux sont significativement supérieurs (2.2>>1.7 ; Figure 10). Ces traits sont similaires à ceux observés après incubation des feuilles $^{13}C^{15}N$ (Figure 8), suggérant que la glycine est stabilisée de manière similaire aux résidus de feuilles. Ces rapports indiquent également que la majorité des traceurs stabilisés par des processus abiotiques ne sont plus sous forme de glycine, mais sous forme produits de la lyse extracellulaire exercée par les enzymes libres du sol et/ ou,

dans une moindre mesure, les radicaux libres produits lors de la stérilisation (McNamara *et al.*, 2003). Les microorganismes du sol contrôlent directement et indirectement la stabilisation de la majorité des $^{15}N_{traceur}$ résiduels et $^{13}C_{traceur}$ résiduels dans tous les types d'associations organo-minérales. Les traceurs s'y trouvent donc principalement sous forme de produits microbiens résultant, pour l'essentiel, d'une biosynthèse intracellulaire (Geisseler *et al.*, 2009; Geisseler *et al.*, 2010; Knowles *et al.*, 2010).

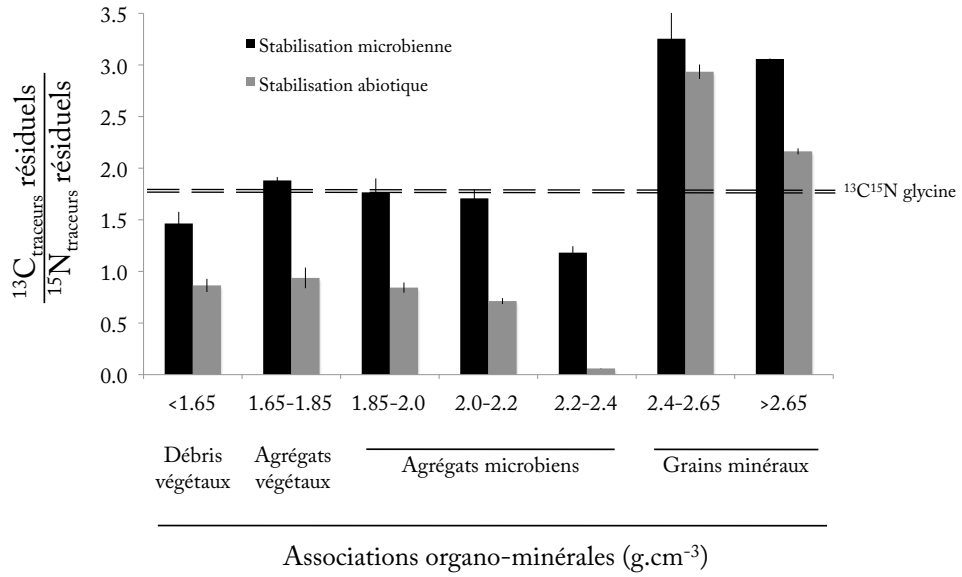

Figure 10: $^{13}C^{traceurs}$ résiduels/ $^{15}N_{traceurs}$ résiduels stabilisés via les processus microbiens (noir) et abiotiques (gris) dans différentes associations organo-minérales séquentiellement isolées par densité 8 heures après apport de glycine $^{13}C^{15}N$ (n=3). Les débris végétaux sont isolés <1.65 g.cm^{-3} ; les agrégats végétaux entre 1.65-1.85 g.cm^{-3} ; les agrégats microbiens entre 1.85-2.4 g.cm^{-3} ; les grains minéraux de faible et forte réactivité entre 2.4-2.65 g.cm^{-3} et >2.65 g.cm^{-3}, respectivement. La ligne discontinue indique le rapport mesuré sur la glycine $^{13}C^{15}N$ initialement appliquée.

La pertinence de l'utilisation de la glycine a été validée pour l'étude des processus de stabilisation microbiens : Ils contribuent directement à ≥87% de la stabilisation du C et N résiduels issus de glycine dans les agrégats et à ≥68% dans les débris végétaux et les grains minéraux. De plus, les rapports $^{13}C_{traceur}$ résiduels/$^{15}N_{traceur}$ résiduels indiquent que la stabilisation abiotique concerne principalement des produits de la lyse extracellulaire de la glycine, soit une contribution indirecte des microorganismes à la stabilisation.

3.3.2.2. Nature des produits microbiens stabilisés

3.3.2.2.1. Produits extracellulaires (Article VI)

La NanoSIMS permet l'étude de mécanismes fins à une échelle pertinente pour l'étude de la mise en place des associations organo-minérales. C'est pourquoi, les $^{15}N_{traceur}$ résiduels et $^{13}C_{traceur}$ résiduels dérivés de glycine $^{13}C^{15}N$ ont été imagés par NanoSIMS à la surface de différentes associations organo-minérales isolées par densité 8 heures après incubation au laboratoire. Les surfaces couvertes par les produits microbiens stabilisés et leurs C/N ont été investigués pour caractériser la distribution des produits microbiens et identifier les mécanismes de stabilisation avec les MOS sous-jacentes.

L'ensemble des $^{15}N_{traceur}$ résiduels et $^{13}C_{traceur}$ résiduels imagés par NanoSIMS couvrent 7.4 10^{-3} de la surface totale imagée contre une surface estimée à 1 10^{-8} pour les microorganismes du sol (Young and Crawford, 2004). Les traceurs occupent des surfaces plusieurs milliers de fois supérieures à celles occupées par les microorganismes du sol. Ces derniers se trouvant majoritairement sous forme de produits microbiens, ces observations indiquent que les traceurs se trouvent essentiellement sous forme de produits microbiens extracellulaires. Bien que la surface couverte par les microorganismes peut être sous estimée dans les conditions d'incubation extrêmement favorables à la croissance microbienne (Bowen and Rovira, 1976; Lee *et al.*, 2011; Murase *et al.*, 2012), aucune prolifération microbienne d'une telle ampleur n'a été reportée en un délai aussi bref (Darrah, 1991; Sato, 1987). De plus, aucune cellule microbienne n'a été formellement identifiée sur les particules de sol imagées. Compte tenu de la résolution spatiale de la NanoSIMS (<0.01µm²) et des caractéristiques morphologiques des cellules microbiennes (Chenu and Stotzky, 2002; Young, 2006), l'observation de cellules microbiennes aurait nécessité l'exploration d'au moins 10^6µm². Or, la surface totale imagée au cours de cette étude est seulement de 3796µm². Bien qu'improbable, il ne peut pas être exclu que les traceurs imagés en Figure 11b indiquent des cellules microbiennes : (1) ils se trouvent dans des zones compatibles en taille et en C/N (calibrés en Article III) avec des cellules microbiennes (Franklin and Mills, 2003; Nunan *et al.*, 2003; Young, 2006) ; (2) l'identification visuelle des cellules microbienne a été compromise par le fait que les images obtenues par microscopie électronique ont été acquises après l'analyse destructive par NanoSIMS.

a)

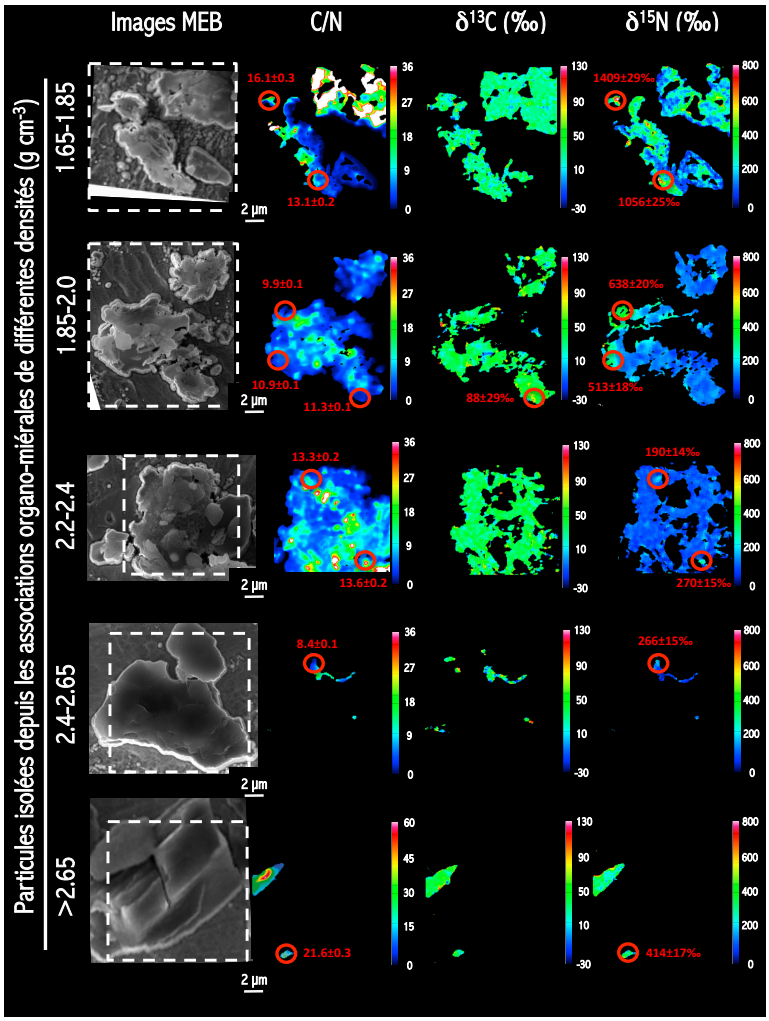

b)

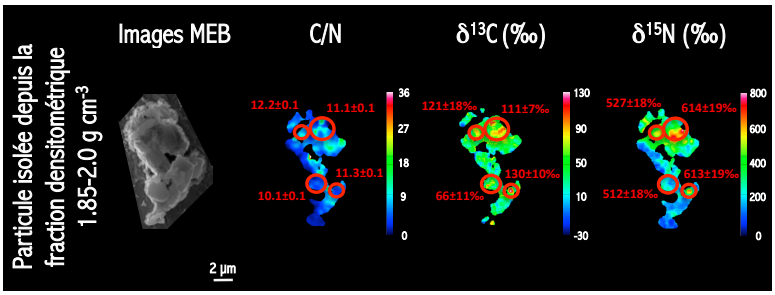

Figure 11: Images NanoSIMS des rapports C/N, des δ^{13}C (‰) et δ^{15}N (‰) – Article VI. Les traceurs sont déterminés en accord avec l'Eq. 2 et indiqués en rouge. Les agrégats végétaux sont isolés entre 1.65-1.85 g.cm^{-3} ; les agrégats microbiens entre 1.85-2.4 g.cm^{-3} ; les grains minéraux de faible et forte réactivité entre 2.4-2.65 g.cm^{-3} et >2.65 g.cm^{-3}, respectivement. MEB signifie microscope électronique à balayage ; les zones délimitées par des lignes blanches discontinues indiquent les zones imagées par NanoSIMS. Les C/N et

$\delta^{15}N$ sont calculés selon la méthode de la calibration interne ; les $\delta^{13}C$ par rapport au kérogène III (Article IV).

Les quantités de traceurs déterminées à l'échelle des fractions (Cf. Figure 9) sont fortement corrélées au taux de couverture par les MO des assemblages de sol (R≥0.85 ; Cf. Tableau 1), suggérant que traceurs et MO de surface des associations organo-minérales sont associées par les mêmes processus. Ceci est confirmé par les images NanoSIMS obtenues depuis le traitement non stérile (Figure 11a, b). Une fois les C/N déterminés par NanoSIMS calibrés (Article IV), l'analyse des C/N mesurés à l'emplacement exact les traceurs indiquent des valeurs généralement faibles, homogènes et comparables à celles des particules correspondantes (Figure 12). Les analogies entre les C/N des anomalies et les particules de sol entières confirment que les traceurs sont associés comme, et non par, les MOS de surface des associations organo-minérales. Les associations organo-minérales contenant la plus forte proportion de minéraux réactifs (section 3.1.) montrent un tout autre trait : 2 des 3 anomalies identifiées sur les grains minéraux contenant des minéraux de forte réactivité (>2.65 g.cm^{-3}) ont des C/N très différents de ceux des particules qui les hébergent. Ceci suggère que la réactivité des minéraux contrôle la stabilisation des traceurs.

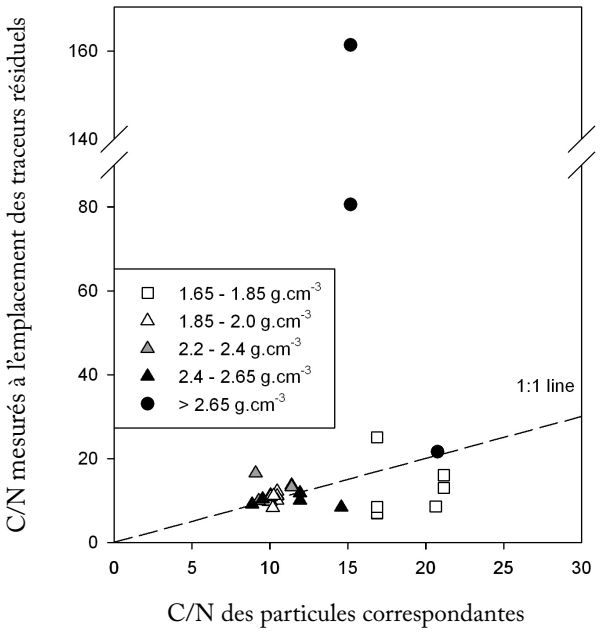

Figure 12: Comparaison des C/N mesurés à l'emplacement exact des traceurs résiduels et sur les particules correspondantes (Article VI). La ligne discontinue représente la ligne 1:1. Les agrégats végétaux sont isolés entre 1.65-1.85 g.cm^{-3} ; les agrégats microbiens entre 1.85-2.4 g.cm^{-3} ; les grains minéraux de faible et forte réactivité entre 2.4-2.65 g.cm^{-3} et >2.65 g.cm^{-3}, respectivement.

Les images NanoSIMS montrent que les produits microbiens observés sont extracellulaires. Ils s'associent aux différents assemblages organo-minéraux de manière similaire à la MO déjà associée, suggérant que les mêmes mécanismes assurent leur stabilisation - vraisemblablement la réactivité des minéraux sous-jacents. En raison du faible échantillonnage inhérent à l'imagerie NanoSIMS, aucune cellule microbienne n'a été formellement identifiée.

3.3.2.2.2. Biomasse microbienne (Article VII)

A l'instar des analyses NanoSIMS, les analyses LC-IRMS permettent d'étudier la formation des biomasses microbiennes grâce au suivi quantitatif des isotopes du carbone dans des composés spécifiques, les sucres aminés (Amelung *et al.*, 2008; Glaser, 2005). Contrairement à la NanoSIMS, les analyses LC-IRMS s'effectuent sur des échantillons représentatifs du sol étudié. Dans chaque type association organo-minérale, l'incorporation de $^{13}C_{traceur}$ issus $^{13}C^{15}N$-glycine et de $^{13}C^{15}N$-feuilles dans les biomarqueurs des biomasses bactérienne (acide muramique et galactosamine) et fongiques (glucosamine ; Cf. section 1.4.1.2.) a été étudiée après 12 semaines d'incubation au laboratoire par LC-IRMS. Un prélèvement intermédiaire a été effectué 7 jours après apport de la glycine.

Les trois sucres aminés dérivés de la glycine et des litières de feuilles sont produits en très faibles quantités comparables à celles reportées dans d'autres travaux (Amelung, 2003; Amelung *et al.*, 2001; Glaser and Gross, 2005). Ceci suggère que l'incorporation dans les biomasses microbiennes est faible, conformément à ce qui a été suggéré dans la section 3.3.2.2.1. Bien que les quantités de substrats initialement appliquées soient différentes, les proportions de glucosamine et de galactosamine nouvellement formées depuis les deux substrats sont similaires relativement au stock total des sucres aminés correspondant : ~1µg.$mg_{glucosamine}^{-1}$ et ~0.1µg.$mg_{galactosamine}^{-1}$, respectivement. En revanche, les proportions d'acide muramique nouvellement formées varient d'un ordre de grandeur selon le substrat originel : 1.2µg.$mg_{acide\ muramique}^{-1}$ sont produits après apport de feuilles contre 0.2µg.$mg_{acide\ muramique}^{-1}$ après apport de glycine. Ainsi, la production de biomasse fongique apparaît relativement favorisée par l'apport de glycine, contrairement à la production de biomasse bactérienne qui semble, quant à elle, favorisée en présence de fragments végétaux (Amelung *et al.*, 2001; Bossuyt *et al.*, 2001).

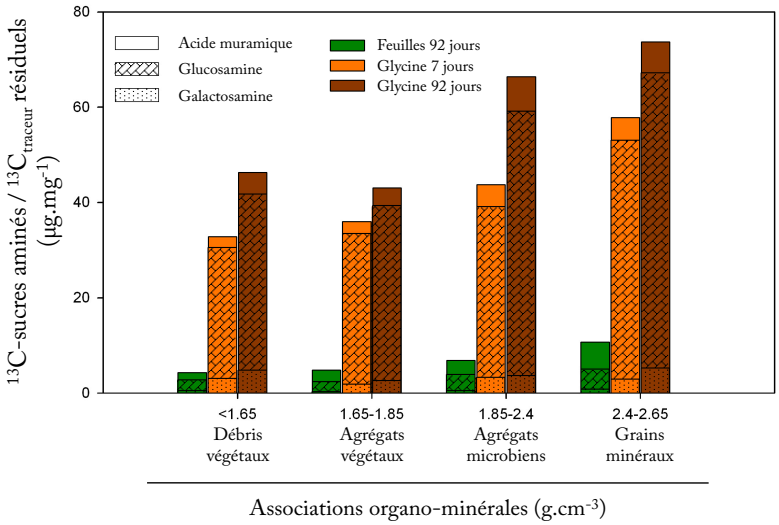

Figure 13: Proportions de $^{13}C_{traceur}$ dans les sucres aminés nouvellement formés (^{13}C-sucres aminés) relativement au $^{13}C_{traceur}$ résiduels trouvés dans les associations organo-minérales de sol ($^{13}C_{traceur}$ résiduels) isolées 7 jours (glycine) ou 12 semaines (feuilles de hêtre broyées et glycine) après apport de glycine ou de substrat (n=2). Les débris végétaux sont isolés <1.65 g.cm^{-3} ; les agrégats végétaux entre 1.65-1.85 g.cm^{-3} ; les agrégats microbiens entre 1.85-2.4 g.cm^{-3} ; les grains minéraux d >2.4 g.cm^{-3}.

Contrairement aux sucres aminés nouvellement formés depuis les feuilles et concentrés dans les débris végétaux (~50%), les sucres aminés nouvellement formés depuis la glycine se retrouvent, comme les sucres aminés totaux (R≥0.97), préférentiellement dans les agrégats microbiens (Tableau 2). Ces différences reflètent les différences d'accessibilité des substrats aux microorganismes du sol. La production de sucres aminés nouvellement formées depuis la glycine soluble varie peu entre 7 et 92 jours d'incubation, indiquant que se formation est rapide et vraisemblablement stable sur cette période. Bien que les sucres aminés nouvellement formés depuis la glycine et les litières de feuilles ne soient pas distribués de la même façon dans les associations organo-minérales (Tableau 2), les proportions de $^{13}C_{traceur}$ des sucres aminés nouvellement produits relativement au $^{13}C_{traceur}$ résiduel augmentent progressivement avec la densité des associations organo-minérales (Figure 13). Ce trait suggère une augmentation progressive de (i) la minéralisation du $^{13}C_{traceur}$ résiduel et/ ou (i) l'efficience de formation de nouveaux sucres aminés, depuis une cohorte donnée, des débris végétaux aux grains minéraux.
La même relation est observée avec les sucres aminés totaux relativement au C total de chaque fraction (R≥0.91 ; Figure 14). Considérant cette dernière comme l'état intégré des différentes cohortes successives au cours du temps, les contributions des biomasses microbiennes totales et fraichement produites aux C résiduels des cohortes dont elles sont issues augmentent avec la densité des associations organo-minérales. Les biomasses totales étant principalement constituées de biomasses

mortes (Amelung *et al.*, 2008), ces résultats indiquent que les biomasses microbiennes mortes et récemment produites se répartissent de manière similaire par rapport au C des cohortes dont elles sont issues.

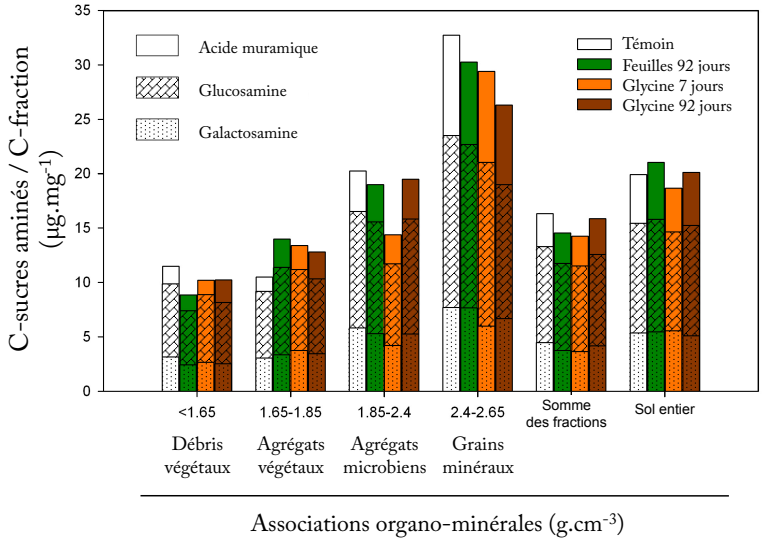

Figure 14: Proportions de C dans les sucres aminés totaux (C-sucres aminés) exprimées relativement au C trouvés dans les associations organo-minérales de sol (C-fraction) isolées 7 jours (glycine) ou 12 semaines (feuilles de hêtre broyées et glycine) après apport du substrat (n=2). Les débris végétaux sont isolés <1.65 g.cm^{-3} ; les agrégats végétaux entre 1.65-1.85 g.cm^{-3} ; les agrégats microbiens entre 1.85-2.4 g.cm^{-3} ; les grains minéraux d >2.4 g.cm^{-3}.

Les sucres aminés incorporent de faibles quantités de C dérivés de la glycine et des feuilles, suggérant une faible incorporation dans les biomasses microbiennes.
L'incorporation se fait dans des proportions différentes selon le substrat, suggérant que la production de biomasses fongiques est favorisée par la glycine et que les feuilles favorisent la production de biomasses bactériennes.
Quelque soit le substrat, l'incorporation dans les sucres aminés, relative au C résiduels des cohortes dont ils sont issus, augmente avec la densité des associations organo-minérales. Ceci suggère une augmentation progressive de (i) la minéralisation du $^{13}C_{traceur}$ résiduel et/ ou (i) l'efficience de formation de nouveaux sucres aminés, depuis une cohorte donnée, des débris végétaux aux grains minéraux. La même relation étant observée avec les sucres aminés totaux, ces résultats suggèrent que les biomasses microbiennes mortes et récemment produites sont distribuées de manière similaire par rapport au C des cohortes dont elles sont issues.

Tableau 2: Teneurs & distributions des sucres aminés nouvellement produits (n=2). $GalN_{tot}$: galactosamine nouvellement formée; $GluN_{tot}$: glucosamine nouvellement formée; $MurN_{tot}$: acide muramique nouvellement formé. Distribution (%) indique la distribution des sucres aminés ($\mu g/g_{sol}$) en fonction de la quantité totale recouvrée après séparation densitométrique (Somme des fractions). SD signifie déviation standard. Les valeurs sont arrondies à l'unité ou au centième.

Treatment	Incubation	Fraction		Galactosamine nouvellement produite						Glucosamine nouvellement produite						Acide muramique nouvellement produit					
	Jours	g/cm^{-3}	Composition	µg/ gsol	SD	Distribution (%)	SD	µg /mg fraction $GalN_{tot}$	SD	µg/ gsol	SD	Distribution (%)	SD	µg /mg fraction $GluN_{tot}$	SD	µg/ gsol	SD	Distribution (%)	SD	µg /mg fraction $MurN_{tot}$	SD
Feuilles de hêtre	92	Sol entier		0.05	0.01			0.12	0.03	0.48	0.02			0.69	0.03	0.39	0.05			1.19	0.17
		<1.65	Débris végétaux	0.03	0.00	62	7	0.40	0.04	0.11	0.01	50	3	0.77	0.05	0.07	0.01	38	3	1.78	0.14
		1.65-1.85	Agrégats végétaux	0.01	0.00	12	2	0.12	0.02	0.04	0.00	18	1	0.36	0.02	0.04	0.00	24	1	1.30	0.06
		1.85-2.4	Agrégats microbiens	0.01	0.00	16	3	0.07	0.01	0.05	0.00	22	2	0.24	0.02	0.04	0.01	22	3	0.63	0.10
		2.4-2.65	Grains minéraux	0.00	0.00	10	3	0.10	0.03	0.02	0.00	10	1	0.24	0.03	0.03	0.00	16	0	0.65	0.02
		Somme des fractions		0.04	0.01			0.18	0.03	0.21	0.02			0.40	0.03	0.17	0.01			1.01	0.08
Glycine	7	Sol entier		0.05	0.01			0.14	0.04	0.48	0.03			0.79	0.05	0.04	0.01			0.17	0.03
		<1.65	Débris végétaux	0.01	0.00	20	2	0.12	0.01	0.05	0.00	15	1	0.46	0.03	0.00	0.00	11	2	0.18	0.03
		1.65-1.85	Agrégats végétaux	0.00	0.00	14	4	0.09	0.03	0.07	0.00	19	1	0.75	0.03	0.00	0.00	14	5	0.19	0.07
		1.85-2.4	Agrégats microbiens	0.02	0.00	51	10	0.17	0.03	0.17	0.01	46	3	1.01	0.07	0.02	0.00	56	4	0.36	0.03
		2.4-2.65	Grains minéraux	0.00	0.00	15	1	0.12	0.01	0.08	0.01	21	3	0.84	0.10	0.01	0.00	19	0	0.14	0.00
		Somme des fractions		0.03	0.01			0.14	0.03	0.37	0.03			0.79	0.06	0.04	0.00			0.23	0.03
	92	Sol entier		0.05	0.01			0.15	0.04	0.46	0.05			0.68	0.07	0.06	0.01			0.21	0.03
		<1.65	Débris végétaux	0.01	0.00	24	11	0.15	0.07	0.06	0.00	14	1	0.52	0.04	0.01	0.00	15	3	0.17	0.04
		1.65-1.85	Agrégats végétaux	0.00	0.00	14	5	0.11	0.04	0.06	0.00	16	1	0.78	0.04	0.01	0.00	13	5	0.21	0.09
		1.85-2.4	Agrégats microbiens	0.01	0.00	44	10	0.13	0.03	0.21	0.00	53	1	0.97	0.02	0.03	0.00	58	8	0.37	0.05
		2.4-2.65	Grains minéraux	0.01	0.00	18	1	0.12	0.01	0.07	0.00	17	0	0.79	0.02	0.01	0.00	15	1	0.14	0.01
		Somme des fractions		0.03	0.01			0.13	0.03	0.40	0.01			0.81	0.03	0.04	0.01			0.25	0.04

4. Conclusions

Les objectifs initiaux de cette thèse étaient (i) l'approfondissement des devenirs du C et du N dérivés des litières de feuilles dans différentes associations organo-minérales des horizons de surface et (ii) la caractérisation du rôle qu'y jouent les microorganismes. Pour répondre à ces objectifs, des techniques de traçage isotopique ont été combinées à la séparation densitométrique des associations organo-minérales et investiguées à différentes échelles pour démontrer que :

(1) **Les transferts de C et N résiduels issus des feuilles dans les associations organo-minérales du sol sont similaires** (Article III). Ces transferts s'opèrent principalement via l'évolution des associations organo-minérales sous le contrôle de l'activité des microorganismes. La plupart des résidus de litières entrent dans le sol sous forme de débris végétaux, puis migrent vers les agrégats et, dans une moindre mesure, les grains minéraux. Parallèlement, l'N dérivé des litières apparaît de moins en moins disponible. Une décennie après la chute des litières, les débris végétaux représentent ~40% de l'N des feuilles contenu dans les 2,5 premiers centimètres de l'horion A, contre ~58% pour les agrégats. **Les agrégats apparaissent particulièrement pertinents pour la stabilisation décennale du C et du N à l'échelle décennale.** Une faible partie (~2%) se retrouve rapidement et vraisemblablement durablement stabilisée sur les grains minéraux (Article II). Des différences apparaissent cependant au sein des fractions avec la rétention préférentielle de l'N dans les agrégats et du C dans les grains minéraux (Article III) ;

(2) **La stabilisation des produits microbiens s'opère (i) directement par immobilisation dans la biomasse microbienne** (Article VII) et **(ii) indirectement via une abondante production extracellulaire** (Article VI). L'efficience de production des biomasses microbiennes est faible, mais croit avec la densité des associations organo-minérales. Les produits microbiens extracellulaires sont stabilisés à la surface des MO attachées aux assemblages de sol via des processus physico-chimiques. Ces processus semblent davantage liés à la réactivité des minéraux sous-jacents qu'à la composition des MO sur lesquels ils se fixent. L'ensemble de ces mécanismes conduit, à terme, à une contribution croissante des matériels microbiens dans les associations organo-minérales de densité croissante : débris végétaux, agrégats végétaux, agrégats microbiens et grains minéraux.

Les observations faites au cours de cette thèse peuvent être interprétées du point de vue de l'écologie des sols. L'occurrence des $^{13}C_{traceur}$ à la surface des associations organo-minérales, largement inférieure à celle des $^{15}N_{traceur}$ (Figure 11), peut s'expliquer par des notions simples d'écologie microbienne. En effet, les produits

microbiens extracellulaires riches en C, tels que les exopolysaccharides, sont susceptibles de développer des interactions électrostatiques avec des surfaces positivement chargées (Mikutta *et al.*, 2011). Ils se trouvent préférentiellement dans l'environnement immédiat des cellules microbiennes (Foster, 1988; Young *et al.*, 2008), dont l'observation est compromise par les contraintes d'échantillonnage inhérentes à l'imagerie NanoSIMS. Les produits microbiens riches en N, tels que les composés amides, se stabilisent par interaction avec les surfaces chargées négativement (Kleber *et al.*, 2007). L'occurrence des produits microbiens extracellulaires contenant le $^{15}N_{tracer}$ révélée par NanoSIMS, ainsi que l'absence de cellule dans leur environnement immédiat, semblent indiquer que les produits microbiens extracellulaires riches en N migrent plus que les produits microbiens extracellulaires riches en C.

La répartition spécifique des produits riches en C renseigne sur les habitats microbiens. La caractérisation de ces produits relativement rares par NanoSIMS nécessiterait l'analyse de grandes surfaces difficilement compatibles avec les contraintes techniques liées à cette technique de pointe. Le suivi de composés spécifiques par LC-IRMS permet quant à lui la caractérisation des habitats microbiens par comparaison des biomasses nouvellement formées produits depuis la glycine soluble et les litières de feuilles. Les composés spécifiques des biomasses microbiennes, les sucres aminés, nouvellement formés depuis la glycine ou les litières de feuilles sont distribués de manières très différentes au sein des associations organo-minérales (Tableau 2). La distribution des premiers est fortement corrélée à la distribution des sucres aminés totaux ($R \geq 0.97$), tous deux se trouvant préférentiellement dans les agrégats microbiens. En supposant que les biomasses microbiennes sessiles (isolées par densité) ne migrent pas après leur production, ceci indique que les microorganismes actifs se retrouvent préférentiellement dans les agrégats microbiens où leurs résidus s'accumulent pour former l'essentiel de la MO (Tableau 1). Cette répartition préférentielle permet d'expliquer pourquoi les processus de stabilisation microbiens dominent tout particulièrement ce type d'association organo-minérale (section 3.3.2.1.). Inversement, les biomasses microbiennes produites depuis les résidus de litières de feuilles sont préférentiellement retrouvées dans les débris végétaux eux-mêmes, dont on sait qu'ils sont colonisés par les microorganismes (section 3.1.). Sans surprise, les biomasses microbiennes sont donc produites là où la ressource se trouve (Chenu and Stotzky, 2002; Foster, 1988; Young *et al.*, 2008). Il en va de même pour les systèmes naturels où la majorité des biomasses microbiennes dérivent des litières végétales (Christensen, 2001). Les biomasses microbiennes étant préférentiellement retrouvées dans les agrégats microbiens (section 3.1.), les biomasses fraichement produites ne restent pas dans les débris végétaux mais semblent migrer progressivement vers les agrégats microbiens et les grains minéraux (Figure 14), vraisemblablement selon le modèle conceptuel précédemment exposé (3.2.2.). Ainsi, ces travaux mettent également en évidence :

(3) La distribution dynamique des microorganismes au sein les associations organo-minérales du sol (Article VI). Leur répartition est initialement guidée par la disponibilité de la ressource. A terme, agrégats et grains minéraux apparaissent comme des habitats préférentiels pour les bactéries et, dans une moindre mesure, pour les champignons. Ceci suggère un transfert des produits microbiens issus de la décomposition des feuilles expliqué par le modèle conceptuel exposé dans la section 3.2.2.

Ces travaux ont encore permis de :

(4) Préciser les domaines d'application des méthodes de fractionnement granulométrique et densitométrique (Article I). Alors que la première s'avère supérieure pour l'étude des MO particulaires, la seconde est plus pertinente pour l'étude des MO au sein des associations organo-minérales du sol. Le fractionnement densitométrique séquentiel sans sonication isole des compartiments écologiquement pertinents qui diffèrent de part leur structure physico-chimique et leur fonctionnement dynamique (Article II). La présence de structures agrégées ne permet pas d'utiliser le fractionnement densitométrique séquentiel sans sonication pour tester la théorie de l'empilement des MOS en couche à la surface des minéraux (Kleber *et al.*, 2007; Sollins *et al.*, 2006);

(5) Lever différents verrous méthodologiques pour :

(5.1) Le **couplage NanoSIMS/STXM-NEXAFS** pour déterminer la spéciation des MOS à l'emplacement exact d'un traceur isotopique (Article V). Techniquement délicate, cette combinaison de technique s'avère faisable et pertinente. Elle a permis la mise en évidence des transformations microbiennes subies par l'N dérivé des litières au cours de la première décennie après la chute des litières (section 3.3.1.) ;

(5.2) La **calibration de la NanoSIMS pour la détermination des rapports élémentaires et isotopiques** (Article IV). Jusqu'alors, la calibration desdits rapports s'effectuait à l'aide de standards organiques différant des MOS par la nature de leurs matrices, leurs homogénéités de formes et leurs compositions élémentaires et isotopiques. Bien que lourde dans sa mise en place, la calibration interne permet la détermination précise des rapports élémentaires et isotopiques. La calibration des C/N a notamment permis une meilleure identification des formes de MOS. La section 3.3.2.1 (Article VI) offre un exemple des avancées permises par le biais de cette méthode.

5. Perspectives

Ces recherches sont motivées *in fine* par la formulation de consignes de gestion amènes de maintenir ou d'accroitre (i) la capacité de stockage des sols en gaz à effet de serre et (ii) la mise en disponibilité de l'N pour la croissance arborée. Pour répondre à ces objectifs, une meilleure compréhension des mécanismes dynamiques de stabilisation et de déstabilisation des MOS est nécessaire. Il s'agit, entre autres, de :

(1) Identifier les devenirs des produits végétaux issus des litières. Les travaux menés au cours de cette thèse ont investigué la stabilisation des produits microbiens, mais la stabilisation des produits végétaux reste mal connue. Les mécanismes de stabilisation impliqués peuvent être étudiés, par exemple, à l'aide de biomarqueurs végétaux (carbohydrates, lignines, tanins, lipides, etc.).

(2) Caractériser les processus responsables des interactions organo-minérales. Leur étude à des échelles spatiales et temporelles pertinentes sont rares en dépit des récentes avancées technologiques permettant la caractérisation fine et simultanée des phases organique et minérale en association. L'étude réalisée sur les mécanismes de stabilisation médiés par les microorganismes met en évidence l'importance des interactions abiotiques dans la mise des interactions organo-minérales. Ces dernières restent faiblement décrites à des échelles pertinentes pour l'étude des mécanismes fins qui s'y jouent. La spéciation des MOS avec les minéraux de réactivité contrastée peut être étudiée, par exemple, par STXM-NEXAFS. Par ailleurs, la généricité des processus microbiens de stabilisation identifiés au cours de cette thèse reste à investiguer sur d'autres types de sol, dans d'autres des contextes pédo-climatiques différents.

(3) Identifier les communautés microbiennes dans les différents types d'association organo-minérales isolés par densité. Cette thèse a mis en évidence la rétention préférentielle de l'N dans les agrégats et du C dans les grains minéraux (Article III) et suggère un accroissement progressif de l'efficience d'incorporation du substrat par les microorganismes du sol, des débris végétaux aux grains minéraux (Article VI). Ces dernières peuvent potentiellement traduire la présence de communautés microbiennes différentes, inféodées à des types d'habitat qui leurs seraient spécifiques. Cette théorie peut être testée à l'aide de techniques telles que le DNA-SIP, RNA-SIP, etc.

(4) Quantifier les flux de déstabilisation et les temps moyens de résidence dans les associations organo-minérales. Les résultats obtenus au cours de cette thèse permettraient la modélisation des délais de transfert entre fractions. Le calcul des temps moyens de résidence des MOS dans les associations organo-minérales nécessiterait quant à lui la compréhension des mécanismes de déstabilisation. Ces derniers restent cependant à explorer aux pas de temps saisonnier, annuel et pluriannuel. Par exemple, les effets des évolutions conjointes des phases organique

(sujettes à décomposition) et minérale (sujettes à dissolution) sur la déstabilisation des MOS restent inconnus. La compréhension des mécanismes de déstabilisation, nécessaire à l'obtention des temps moyens de résidence, s'avère indispensable pour, à terme, formuler des consignes de gestion assurant une disponibilité accrue de l'N lors de la saison de végétation et réduite en dehors.

Références

Aita C, Recous S, Angers DA (1997). Short-term kinetics of residual wheat straw C and N under field conditions: Characterization by (CN)-C-13-N-15 tracing and soil particle size fractionation. *European Journal of Soil Science* **48:** 283-294.

Amelung W (2003). Nitrogen biomarkers and their fate in soil. *Journal of Plant Nutrition and Soil Science-Zeitschrift Fur Pflanzenernahrung Und Bodenkunde* **166:** 677-686.

Amelung W, Brodowski S, Sandhage-Hofmann A, Bol R (2008). Combining biomarker with stable isotope analyses for assessing the transformation and turnover of soil organic matter. *Advances in Agronomy, Vol 100* **100:** 155-250.

Amelung W, Miltner A, Zhang X, Zech W (2001). Fate of microbial residues during litter decomposition as affected by minerals. *Soil Science* **166:** 598-606.

Andrianarisoa KS, Zeller B, Dupouey JL, Dambrine E (2009). Comparing indicators of N status of 50 beech stands (Fagus sylvatica L.) in northeastern France. *Forest Ecology and Management* **257:** 2241-2253.

Angers DA, Recous S, Aita C (1997). Fate of carbon and nitrogen in water-stable aggregates during decomposition of (CN)-C-13-N-15-labelled wheat straw in situ. *European Journal of Soil Science* **48:** 295-300.

Appuhn A, Joergensen RG (2006). Microbial colonisation of roots as a function of plant species. *Soil Biology & Biochemistry* **38:** 1040-1051.

Baisden WT, Amundson R, Cook AC, Brenner DL (2002). Turnover and storage of C and N in five density fractions from California annual grassland surface soils. *Global Biogeochemical Cycles* **16**.

Balesdent J, Girardin C, Mariotti A (1993). Site-related delta C-13 of tree leaves and soil prganic matter in a temperate forest. *Ecology* **74:** 1713-1721.

Balesdent J, Mariotti A (1996). *Measurement of soil organic matter turnover using 13C natural abundance*, 83-111pp.

Basile-Doelsch I, Amundson R, Stone WEE, Borschneck D, Bottero JY, Moustier S *et al* (2007). Mineral control of carbon pools in a volcanic soil horizon. *Geoderma* **137:** 477-489.

Basile-Doelsch I, Amundson R, Stone WEE, Masiello CA, Bottero JY, Colin F *et al* (2005). Mineralogical control of organic carbon dynamics in a volcanic ash soil on La Reunion. *European Journal of Soil Science* **56:** 689-703.

Berns AE, Philipp H, Narres HD, Burauel P, Vereecken H, Tappe W (2008). Effect of gamma-sterilization and autoclaving on soil organic matter structure as studied by solid state NMR, UV and fluorescence spectroscopy. *European Journal of Soil Science* **59:** 540-550.

Bertrand R, Lenoir J, Piedallu C, Riofrio-Dillon G, de Ruffray P, Vidal C *et al* (2011). Changes in plant community composition lag behind climate warming in lowland forests. *Nature* **479:** 517-520.

Bird JA, Kleber M, Torn MS (2008). C-13 and N-15 stabilization dynamics in soil organic matter fractions during needle and fine root decomposition. *Organic Geochemistry* **39:** 465-477.

Bird JA, Torn MS (2006). Fine roots vs. Needles: A comparison of (13)C and (15)N dynamics in a ponderosa pine forest soil. *Biogeochemistry* **79:** 361-382.

Bird JA, van Kessel C, Horwath WR (2003). Stabilization of C-13-carbon and immobilization of N-15-nitrogen from rice straw in humic fractions. *Soil Science Society of America Journal* **67:** 806-816.

Blakemore LC, Searle PL, Daly BK (1987). Methods for chemical analysis of soils. *Bureau Scientific Report 80, Lower Hutt, New Zealand*.

Bodé S, Denef K, Boeckx P (2009). Development and evaluation of a high-performance liquid chromatography/isotope ratio mass spectrometry methodology for delta C-13 analyses of amino sugars in soil. *Rapid Communications in Mass Spectrometry* **23:** 2519-2526.

Bol R, Poirier N, Balesdent J, Gleixner G (2009). Molecular turnover time of soil organic matter in particle-size fractions of an arable soil. *Rapid Communications in Mass Spectrometry* **23:** 2551-2558.

Bolan NS, Adriano DC, Kunhikrishnan A, James T, McDowell R, Senesi N (2011). Dissolved organic matter: biogeochemistry, dynamics and environmental significance in soils. In: Sparks DL (ed). *Advances in Agronomy, Vol 110*. pp 1-75.

Bossuyt H, Denef K, Six J, Frey SD, Merckx R, Paustian K (2001). Influence of microbial populations and residue quality on aggregate stability. *Applied Soil Ecology* **16:** 195-208.

Bowen GD, Rovira AD (1976). MIicrobial colonization of plant roots. *Annual Review of Phytopathology* **14:** 121-144.

Brandes JA, Lee C, Wakeham S, Peterson M, Jacobsen C, Wirick S *et al* (2004). Examining marine particulate organic matter at sub-micron scales using scanning transmission X-ray microscopy and carbon X-ray absorption near edge structure spectroscopy. *Marine Chemistry* **92:** 107-121.

Campbell JL, Rustad LE, Boyer EW, Christopher SF, Driscoll CT, Fernandez IJ *et al* (2009). Consequences of climate change for biogeochemical cycling in forests of northern North America. *Canadian Journal of Forest Research-Revue Canadienne De Recherche Forestiere* **39:** 264-284.

Chan CS, Fakra SC, Edwards DC, Emerson D, Banfield JF (2009). Iron oxyhydroxide mineralization on microbial extracellular polysaccharides. *Geochimica Et Cosmochimica Acta* **73:** 3807-3818.

Chapman SK, Langley JA, Hart SC, Koch GW (2006). Plants actively control nitrogen cycling: uncorking the microbial bottleneck. *New Phytologist* **169:** 27-34.

Chenu C, Plante AF (2006). Clay-sized organo-mineral complexes in a cultivation chronosequence: revisiting the concept of the 'primary organo-mineral complex'. *European Journal of Soil Science* **57:** 596-607.

Chenu C, Stotzky G (2002). Interactions between micro-organisms ans soil particles: an overview. In: Huang PM, Bollag, J.M., Senesi, N. (ed). *Interactions between soil particles and microorganisms*. John Wiley and Sons: Chichester, UK. pp 3-40.

Christensen BT (2001). Physical fractionation of soil and structural and functional complexity in organic matter turnover. *European Journal of Soil Science* **52:** 345-353.

Courtillot V, Gallet Y, Le Mouel JL, Fluteau F, Genevey A (2007). Are there connections between the Earth's magnetic field and climate? *Earth and Planetary Science Letters* **253:** 328-339.

Craig H (1957). Isotopic standards for carbon and oxygen correction factors for mass spectrometric analysis of carbon dioxide. *Geochimica Et Cosmochimica Acta* **12:** 133-149.

d'Annuzio R, Zeller B, Nicolas M, Dhôte JF, Saint-André L (2008). Decomposition of European beech (Fagus sylvatica) litter: Combining quality theory and 15N labelling experiments. *Soil Biology & Biochemistry* **40:** 322-333.

Darrah PR (1991). Models of the rhizosphere - part. II: a quasi three dimensional simulation of the microbial-population dynamics around a growing root releasing soluble exudates. *Plant and Soil* **138:** 147-158.

De Gryze S, Six J, Merckx R (2006). Quantifying water-stable soil aggregate turnover and its implication for soil organic matter dynamics in a model study. *European Journal of Soil Science* **57:** 693-707.

Derrien D, Amelung W (2011). Computing the mean residence time of soil carbon fractions using stable isotopes: impacts of model framework. *European Journal of Soil Science* **62:** 237-252.

Derrien D, Marol C, Balabane M, Balesdent J (2006). The turnover of carbohydrate carbon in a cultivated soil estimated by (13)C natural abundances. *European Journal of Soil Science* **57:** 547-557.

Dijkstra P, Ishizu A, Doucett R, Hart SC, Schwartz E, Menyailo OV *et al* (2006). C-13 and N-15 natural abundance of the soil microbial biomass. *Soil Biology & Biochemistry* **38:** 3257-3266.

Ekschmitt K, Kandeler E, Poll C, Brune A, Buscot F, Friedrich M *et al* (2008). Soil-carbon preservation through habitat constraints and biological limitations on decomposer activity. *Journal of Plant Nutrition and Soil Science-Zeitschrift Fur Pflanzenernahrung Und Bodenkunde* **171:** 27-35.

Eusterhues K, Rumpel C, Kogel-Knabner I (2005). Organo-mineral associations in sandy acid forest soils: importance of specific surface area, iron oxides and micropores. *European Journal of Soil Science* **56:** 753-763.

Fahey TJ, Yavitt JB, Sherman RE, Groffman PM, Fisk MC, Maerz JC (2011). Transport of Carbon and Nitrogen Between Litter and Soil Organic Matter in a Northern Hardwood Forest. *Ecosystems* **14:** 326-340.

FAO (2011). State of Europe's Forests - Status and Trends in Sustainable Forset Management in Europe.

Foster RC (1988). Microenvironments of soil-microorganisms. *Biology and Fertility of Soils* **6:** 189-203.

Franklin RB, Mills AL (2003). Multi-scale variation in spatial heterogeneity for microbial community structure in an eastern Virginia agricultural field. *Fems Microbiology Ecology* **44:** 335-346.

Galloway JN, Dentener FJ, Capone DG, Boyer EW, Howarth RW, Seitzinger SP *et al* (2004). Nitrogen cycles: past, present, and future. *Biogeochemistry* **70:** 153-226.

Gardenas AI, Agren GI, Bird JA, Clarholm M, Hallin S, Ineson P *et al* (2011). Knowledge gaps in soil carbon and nitrogen interactions - From molecular to global scale. *Soil Biology & Biochemistry* **43:** 702-717.

Geisseler D, Horwath WR, Doane TA (2009). Significance of organic nitrogen uptake from plant residues by soil microorganisms as affected by carbon and nitrogen availability. *Soil Biology & Biochemistry* **41:** 1281-1288.

Geisseler D, Horwath WR, Joergensen RG, Ludwig B (2010). Pathways of nitrogen utilization by soil microorganisms - A review. *Soil Biology & Biochemistry* **42:** 2058-2067.

Glaser B (2005). Compound-specific stable-isotope (delta C-13) analysis in soil science. *Journal of Plant Nutrition and Soil Science-Zeitschrift Fur Pflanzenernahrung Und Bodenkunde* **168:** 633-648.

Glaser B, Gross S (2005). Compound-specific delta C-13 analysis of individual amino sugars - a tool to quantify timing and amount of soil microbial residue stabilization. *Rapid Communications in Mass Spectrometry* **19:** 1409-1416.

Glaser B, Turrion MB, Alef K (2004). Amino sugars and muramic acid - biomarkers for soil microbial community structure analysis. *Soil Biology & Biochemistry* **36:** 399-407.

Golchin A, Oades JM, Skjemstad JO, Clarke P (1994). Study of free and ocluded particulate organic matter in soils by solid-state C-13 CP/MAS NMR-spectrometry and scanning electron microscopy. *Australian Journal of Soil Research* **32:** 285-309.

Grandy AS, Neff JC (2008). Molecular C Dynamics Downstream: The Biochemical Decomposition Sequence and its impact on Soil Organic Matter Structure and Function. *Science of the Total Environment* **404:** 297-307.

Gregorich EG, Janzen HH (1996). Storage of soil carbon in the light fraction and macroorganic matter. In: Stewart MRCBA (ed). *Structure and Organic Matter Storage in Agricultural Soils* CRC Lewis Publishers: Boca Raton, FL.

Gruber N, Galloway JN (2008). An Earth-system perspective of the global nitrogen cycle. *Nature* **451:** 293-296.

Guggenberger G, Frey SD, Six J, Paustian K, Elliott ET (1999). Bacterial and fungal cell-wall residues in conventional and no-tillage agroecosystems. *Soil Science Society of America Journal* **63:** 1188-1198.

Guggenberger G, Kaiser K (2003). Dissolved organic matter in soil: challenging the paradigm of sorptive preservation. *Geoderma* **113:** 293-310.

He H, Zhang W, Zhang X, Xie H, Zhuang J (2011). Temporal responses of soil microorganisms to substrate addition as indicated by amino sugar differentiation. *Soil Biology & Biochemistry* **43:** 1155-1161.

Heijden Gvd, Legout A, Nicolas M, Ulrich E, Johnson DW, Dambrine E (2011). Long-term sustainability of forest ecosystems on sandstone in the Vosges Mountains (France) facing atmospheric deposition and silvicultural change. *Forest Ecology and Management* **261:** 730-740.

Holmgren GGS (1967). A rapid citrate and dithionite extractable iron procedure. *Proceedings-Soil Science Society of America* **31:** 210-211.

Holub SM, Lajtha K (2004). The fate and retention of organic and inorganic N-15-nitrogen in an old-growth forest soil in western Oregon. *Ecosystems* **7:** 368-380.

IPCC. (2007). *Contribution of working group to the fourth assessment report of intergovernmental panel on climate change*. S. Solomon DQ, M. Manning, Z. Chen, M.Marquis, K.B. Averyt, M. Tignor, and H.L. Miller (ed.): Cambridge, UK.

Janssens IA, Dieleman W, Luyssaert S, Subke JA, Reichstein M, Ceulemans R *et al* (2010). Reduction of forest soil respiration in response to nitrogen deposition. *Nature geoscience* **3:** 315-322.

Jonard M, Legout A, Nicolas M, Dambrine E, Nys C, Ulrich E *et al* (2012). Deterioration of Norway spruce vitality despite a sharp decline in acid deposition: a long-term integrated perspective. *Global Change Biology* **18:** 711-725.

Jones DL, Murphy DV (2007). Microbial response time to sugar and amino acid additions to soil. *Soil Biology & Biochemistry* **39:** 2178-2182.

Kaiser K, Eusterhues K, Rumpel C, Guggenberger G, Kogel-Knabner I (2002). Stabilization of organic matter by soil minerals - investigations of density and particle-size fractions from two acid forest soils. *Journal of Plant Nutrition and Soil Science-Zeitschrift Fur Pflanzenernahrung Und Bodenkunde* **165:** 451-459.

Kaiser K, Guggenberger G (2007). Distribution of hydrous aluminium and iron over density fractions depends on organic matter load and ultrasonic dispersion. *Geoderma* **140:** 140-146.

Keiluweit M, Nico PS, Johnson MG, Kleber M (2010). Dynamic Molecular Structure of Plant Biomass-Derived Black Carbon (Biochar). *Environmental Science & Technology* **44:** 1247-1253.

Kinyangi J, Solomon D, Liang BI, Lerotic M, Wirick S, Lehmann J (2006). Nanoscale biogeocomplexity of the organomineral assemblage in soil: Application of STXM microscopy and C 1s-NEXAFS spectroscopy. *Soil Science Society of America Journal* **70:** 1708-1718.

Kleber M (2010). What is recalcitrant soil organic matter? *Environmental Chemistry* **7:** 320-332.

Kleber M, Mikutta R, Torn MS, Jahn R (2005). Poorly crystalline mineral phases protect organic matter in acid subsoil horizons. *European Journal of Soil Science* **56:** 717-725.

Kleber M, Sollins P, Sutton R (2007). A conceptual model of organo-mineral interactions in soils: self-assembly of organic molecular fragments into zonal structures on mineral surfaces. *Biogeochemistry* **85:** 9-24.

Knowles TDJ, Chadwick DR, Bol R, Evershed RP (2010). Tracing the rate and extent of N and C flow from (13)C,(15)N-glycine and glutamate into individual de novo synthesised soil amino acids. *Organic Geochemistry* **41:** 1259-1268.

Koegel-Knabner I (2002). The macromolecular organic composition of plant and microbial residues as inputs to soil organic matter. *Soil Biology & Biochemistry* **34:** 139-162.

Koegel-Knabner I, Guggenberger G, Kleber M, Kandeler E, Kalbitz K, Scheu S *et al* (2008). Organo-mineral associations in temperate soils: Integrating biology, mineralogy, and organic matter chemistry. *Journal of Plant Nutrition and Soil Science-Zeitschrift Fur Pflanzenernahrung Und Bodenkunde* **171:** 61-82.

Kogel-Knabner I, Ekschmitt K, Flessa H, Guggenberger G, Matzner E, Marschner B *et al* (2008a). An integrative approach of organic matter stabilization in temperate soils: Linking chemistry, physics, and biology. *Journal of Plant Nutrition and Soil Science* **171:** 5-13.

Kogel-Knabner I, Guggenberger G, Kleber M, Kandeler E, Kalbitz K, Scheu S *et al* (2008b). Organo-mineral associations in temperate soils: Integrating biology,

mineralogy, and organic matter chemistry. *Journal of Plant Nutrition and Soil Science-Zeitschrift Fur Pflanzenernahrung Und Bodenkunde* **171:** 61-82.

Kogel-Knabner I, Kleber M (2011). Mineralogical, Physicochemical, and Microbiological Controls on Soil Organic Matter Stabilization and Turnover. In: 2nd ed./ Pan Ming Huang YL, Malcolm E. Sumner (ed). *Handbook of Soil Sciences: Resource Management and Environmental Impacts, Second Edition*. CRC London.

Kramer MG, Lajtha K, Thomas G, Sollins P (2009). Contamination effects on soil density fractions from high N or C content sodium polytungstate. *Biogeochemistry* **92:** 177-181.

Lajtha K, Crow SE, Yano Y, Kaushal SS, Sulzman E, Sollins P *et al* (2005). Detrital controls on soil solution N and dissolved organic matter in soils: a field experiment. *Biogeochemistry* **76:** 261-281.

Lee CG, Watanabe T, Sato Y, Murase J, Asakawa S, Kimura M (2011). Bacterial populations assimilating carbon from (13)C-labeled plant residue in soil: Analysis by a DNA-SIP approach. *Soil Biology & Biochemistry* **43:** 814-822.

Legout A, Walter C, Nys C (2008). Spatial variability of nutrient stocks in the humus and soils of a forest massif (Fougères, France). *Ann. For. Sci.* **65:** 1-10.

Lehman J, Kinyangi J, Solomon D (2007). Organic matter stabilization in soil microaggregates: implications from spatial heterogeneity of organic carbon contents and carbon forms. *Biogeochemistry* **85:** 45-57.

Lehman J, Solomon D, Kinyangi J, Dathe L, Wirick S, Jacobsen C (2008). Spatial complexity of soil organic matter forms at nanometer scales. *Nature geoscience* **1:** 238-242.

Liang C, Read HW, Balser TC (2009). Reliability of Muramic Acid as a Bacterial Biomarker is Influenced by Methodological Artifacts from Streptomycin. *Microbial Ecology* **57:** 494-500.

Liang C, Zhang XD, Balser TC (2007). Net microbial amino sugar accumulation process in soil as influenced by different plant material inputs. *Biology and Fertility of Soils* **44:** 1-7.

Mambelli S, Bird JA, Gleixner G, Dawson TE, Torn MS (2011). Relative contribution of foliar and fine root pine litter to the molecular composition of soil organic matter after in situ degradation. *Organic Geochemistry* **42:** 1099-1108.

Mariotti A (1983). Atmospheric nitrogen is a reliable standard for natural 15N abundance measurements. *Nature* **303:** 685-687.

Marschner B, Brodowski S, Dreves A, Gleixner G, Gude A, Grootes PM *et al* (2008). How relevant is recalcitrance for the stabilization of organic matter in soils? *Journal of Plant Nutrition and Soil Science-Zeitschrift Fur Pflanzenernahrung Und Bodenkunde* **171:** 91-110.

Matzner E (ed.) (2004) *Biogeochemistry of forested catchments in a changing environment*. Springer: Berlin, 498pp.

McNamara NP, Black HIJ, Beresford NA, Parekh NR (2003). Effects of acute gamma irradiation on chemical, physical and biological properties of soils. *Applied Soil Ecology* **24:** 117-132.

Mikutta R, Kaiser K, Doerr N, Vollmer A, Chadwick OA, Chorover J *et al* (2010). Mineralogical impact on organic nitrogen across a long-term soil chronosequence (0.3-4100 kyr). *Geochimica Et Cosmochimica Acta* **74:** 2142-2164.

Mikutta R, Kleber M, Torn MS, Jahn R (2006). Stabilization of soil organic matter: Association with minerals or chemical recalcitrance? *Biogeochemistry* **77:** 25-56.

Mikutta R, Schaumann GE, Gildemeister D, Bonneville S, Kramer MG, Chorover J *et al* (2009). Biogeochemistry of mineral-organic associations across a long-term mineralogical soil gradient (0.3-4100 kyr), Hawaiian Islands. *Geochimica Et Cosmochimica Acta* **73:** 2034-2060.

Mikutta R, Zang U, Chorover J, Haumaier L, Kalbitz K (2011). Stabilization of extracellular polymeric substances (Bacillus subtilis) by adsorption to and coprecipitation with Al forms. *Geochimica Et Cosmochimica Acta* **75:** 3135-3154.

Murase J, Shibata M, Lee CG, Watanabe T, Asakawa S, Kimura M (2012). Incorporation of plant residue-derived carbon into the microeukaryotic community in a rice field soil revealed by DNA stable-isotope probing. *FEMS Microbiology Ecology* **79:** 371-379.

Nicolas M, Ranger J (2009). Wood for energy: intensified harvests can lead to soil impoverishment in extensively managed forests. *Pollution atmosphérique***:** 47-54.

Nunan N, Wu KJ, Young IM, Crawford JW, Ritz K (2003). Spatial distribution of bacterial communities and their relationships with the micro-architecture of soil. *FEMS Microbiology Ecology* **44:** 203-215.

Nys C. (1998). *Programme "Hêtraie de basse altitude", Vol. 3*. Ecofor G (ed.). INRA de Nancy: Nancy.

Oades JM (1993). The role of biology in the formation, stabilization and degradation of soil structure. *Geoderma* **56:** 377-400.

Oades JM, Waters AG (1991). Aggregate hierarchy in soils. *Australian Journal of Soil Research* **29:** 815-828.

Plante AF, McGill WB (2002). Soil aggregate dynamics and the retention of organic matter in laboratory-incubated soil with differing simulated tillage frequencies. *Soil & Tillage Research* **66:** 79-92.

Post WM, Emanuel WR, Zinke PJ, Stangenberger AG (1982). Soil Carbon Pools and World Life Zones. *Nature* **298:** 156-159.

Post WM, Pastor J, Zinke PJ, Stangenberger AG (1984). Global patterns of soil nitrogen storage. *Nature* **317:** 613-616.

Prior CA, Baisden WT, Bruhn F, Neff JC (2007). Using a soil chronosequence to identify soil fractions for understanding and modeling soil carbon dynamics in New Zealand. *Radiocarbon* **49:** 1093-1102.

Puech J. (2009). *Mise en valeur de la forêt française et développement de la filière bois*: Paris.

Ravel B, Newville M (2005). ATHENA, ARTEMIS, HEPHAESTUS: data analysis for X-ray absorption spectroscopy using IFEFFIT. *Journal of Synchrotron Radiation* **12:** 537-541.

Rennenberg H, Dannenmann M, Gessler A, Kreuzwieser J, Simon J, Papen H (2009). Nitrogen balance in forest soils: nutritional limitation of plants under climate change stresses. *Plant Biology* **11:** 4-23.

Rillig MC, Caldwell BA, Wosten HAB, Sollins P (2007). Role of proteins in soil carbon and nitrogen storage: controls on persistence. *Biogeochemistry* **85:** 25-44.

Rovira P, Vallejo VR (2003). Physical protection and biochemical quality of organic matter in Mediterranean calcareous forest soils: a density fractionation approach. *Soil Biology & Biochemistry* **35:** 245-261.

Sato K (1987). Effect of increasing penachlorophenol (PCP) concentrations on bacterial-populations in glycine-percolated soils. *Biology and Fertility of Soils* **5:** 1-5.

Schimel JP, Bennett J (2004). Nitrogen mineralization: Challenges of a changing paradigm. *Ecology* **85:** 591-602.

Schmidt MWI, Torn MS, Abiven S, Dittmar T, Guggenberger G, Janssens IA *et al* (2011). Persistence of soil organic matter as an ecosystem property. *Nature* **478:** 49-56.

Six J, Feller C, Denef K, Ogle SM, Sa JCD, Albrecht A (2002). Soil organic matter, biota and aggregation in temperate and tropical soils - Effects of no-tillage. *Agronomie* **22:** 755-775.

Smucker AJM, Park E-J, Dorner J, Horn R (2007). Soil micropore development and contributions to soluble carbon transport within macroaggregates. *Vadose Zone Journal* **6:** 282-290.

Sollins P, Homann P, Caldwell BA (1996). Stabilization and destabilization of soil organic matter: Mechanisms and controls. *Geoderma* **74:** 65-105.

Sollins P, Kramer MG, Swanston C, Lajtha K, Filley T, Aufdenkampe AK *et al* (2009). Sequential density fractionation across soils of contrasting mineralogy: evidence for both microbial- and mineral-controlled soil organic matter stabilization. *Biogeochemistry* **96:** 209-231.

Sollins P, Swanston C, Kleber M, Filley T, Kramer M, Crow S *et al* (2006). Organic C and N stabilization in a forest soil: Evidence from sequential density fractionation. *Soil Biology & Biochemistry* **38:** 3313-3324.

Sollins P, Swanston C, Kramer M (2007). Stabilization and destabilization of soil organic matter - a new focus. *Biogeochemistry* **85:** 1-7.

Swanston C, Homann PS, Caldwell BA, Myrold DD, Ganio L, Sollins P (2004). Long-term effects of elevated nitrogen on forest soil organic matter stability. *Biogeochemistry* **70:** 227-250.

Torn MS, Swanston C, Trumbore S (2009). Storage and turnover of organic matter in soil. In: Senesi N, Xing B and Huang PM (eds). *Biophysico-chemical processes involving natural non-living organic matter in environmental systems*. Wiley J snd Sons Inc.

Trinsoutrot I, Recous S, Mary B, Nicolardota B (2000). C and N fluxes of decomposing C-13 and N-15 Brassica napus L.: effects of residue composition and N content. *Soil Biology & Biochemistry* **32:** 1717-1730.

Trumbore S (2009). Radiocarbon and Soil Carbon Dynamics. *Annual Review of Earth and Planetary Sciences*. pp 47-66.

van Hees PAW, Jones DL, Finlay R, Godbold DL, Lundstomd US (2005). The carbon we do not see - the impact of low molecular weight compounds on carbon dynamics and respiration in forest soils: a review. *Soil Biology & Biochemistry* **37:** 1-13.

von Lützow M, Koegel-Knabner I, Ekschmitt K, Flessa H, Guggenberger G, Matzner E *et al* (2007). SOM fractionation methods: Relevance to functional pools and to stabilization mechanisms. *Soil Biology & Biochemistry* **39:** 2183-2207.

von Lützow M, Kogel-Knabner I, Ekschmitt K, Matzner E, Guggenberger G, Marschner B *et al* (2006). Stabilization of organic matter in temperate soils: mechanisms and their relevance under different soil conditions - a review. *European Journal of Soil Science* **57:** 426-445.

von Lützow M, Kogel-Knabner I, Ludwig B, Matzner E, Flessa H, Ekschmitt K *et al* (2008). Stabilization mechanisms of organic matter in four temperate soils: Development and application of a conceptual model. *Journal of Plant Nutrition and Soil Science-Zeitschrift Fur Pflanzenernahrung Und Bodenkunde* **171:** 111-124.

Wagai R, Mayer LM (2007). Sorptive stabilization of organic matter in soils by hydrous iron oxides. *Geochimica Et Cosmochimica Acta* **71:** 25-35.

Wagai R, Mayer LM, Kitayama K (2009). Extent and nature of organic coverage of soil mineral surfaces assessed by a gas sorption approach. *Geoderma* **149:** 152-160.

Watteau F, Villemin G, Burtin G, Jocteur-Monrozier L (2006). Root impact on the stability and types of micro-aggregates in silty soil under maize. *European Journal of Soil Science* **57:** 247-257.

Young IM, Crawford JW (2004). Interactions and self-organization in the soil-microbe complex. *Science* **304:** 1634-1637.

Young IM, Crawford JW, Nunan N, Otten W, Spiers A (2008). Microbial distribution in soils: physics and scaling. *Advances in Agronomy* **100:** 81-121.

Young KD (2006). The selective value of bacterial shape. *Microbiology and Molecular Biology Reviews* **70:** 660-+.

Zeller B, Colin-Belgrand M, Dambrine E, Martin F (1998). N-15 partitioning and production of N-15-labelled litter in beech trees following [N-15] urea spray. *Annales Des Sciences Forestieres* **55:** 375-383.

Zeller B, Colin-Belgrand M, Dambrine E, Martin F (2001). Fate of nitrogen released from N-15-labeled litter in European beech forests. *Tree Physiology* **21:** 153-162.

Zeller B, Colin-Belgrand M, Dambrine E, Martin F, Bottner P (2000). Decomposition of N-15-labelled beech litter and fate of nitrogen derived from litter in a beech forest. *Oecologia* **123:** 550-559.

Zeller B, Dambrine E (2011). Coarse particulate organic matter is the primary source of mineral N in the topsoil of three beech forests. *Soil Biology & Biochemistry* **43:** 542-550.

Remerciements

Alors que je m'apprête à tourner une page sur une expérience riche en rencontres et en enseignements, je tiens à en remercier les différents acteurs pour m'avoir instruit, conseillé, guidé et épaulé. Merci à :

Tous ceux sans qui ce travail n'aurait pas pu se faire, financeurs (Région Lorraine & l'INRA-EFPA) et encadrants. Je tiens à témoigner ma plus vive reconnaissance au pétillant Etienne Dambrine pour m'avoir fait confiance, à la brillante Delphine Derrien pour son dynamisme et sa patience & à l'excellent Bernd Zeller pour ses bons conseils & sa constante bonne humeur. Merci mille fois de m'avoir tant appris !

Claire Chenu, Wulf Amelung, Isabelle Basile-Doelsch & Manuel Nicolas pour avoir accepté d'évaluer ce travail en dépit de leurs emplois du temps chargés.

Tous les encadrant informels & collaborateurs qui m'ont également beaucoup appris : Elizabeth Brewer, Kate Lajtha, Nicolas Angeli, Pascal Boeckx, Samuel Bodé, Markus Kleber, Peter Nico, Alain Plante & Laurent Remusat. Vous m'avez tous profondément marqué. Je remercie tout particulièrement Nicolas Angeli & Laurent Remusat pour tout ce qu'ils m'ont appris et pour les bons moments passés et à venir !

Tous ceux qui m'ont soutenu, d'une manière ou d'une autre, et qui ont largement contribué à ce que ce travail aboutisse : Séverine Boiry, Alexandra Corado, Jacqueline Noël, Jacqueline Marchand, Isabelle Martin, Pascal Bonnaud, Jérôme Demaison, Christian Hossan & José Vincente. Mille mercis à Louisette Gelhaye pour son aide précieuse et tous les bons moments passés autour des paillasses de Nancy et de Corvallis.

Toute la formidable unité BEF pour les discussions enrichissantes et bons moments passés autour du légendaire café de Nathalie. Je vous suis tous reconnaissant pour avoir fait de cette thèse une expérience inoubliable !

Aux 'jeunes' de Nancy à Corvallis, en passant par Fumay, Gand, Montpellier, Paris, Québec, Taintrux & Toulouse pour tous ces petits riens et bons moments que nous avons partagé et que je ne saurais oublier.

Ma famille pour son soutien sans faille & sa bienveillance qui ont su oublier bien des absences.

Aure-Amélie pour tout ce qu'elle est.

Articles

I

Density Fractions versus Size Separates: Does Physical Fractionation Isolate Functional Soil Compartments?

Christophe Moni [a,c*], Delphine Derrien [b], Pierre-Joseph Hatton [b], Bernd Zeller [b], Markus Kleber [a]

[a] Department of Crop and Soil Science, Oregon State University, 97331 Corvallis, OR, USA

[b] INRA-Nancy, Biogéochimie des Ecosystemes Forestiers, 54280 Champenoux, France

[c] Norwegian Institute for Agricultural and Environmental Research, 1432 Ås, Norway

* Corresponding author: christophe.moni@bioforsk.no

Submitted to *Biogeosciences*

Abstract

Physical fractionation is a widely used methodology to study soil organic matter (SOM) dynamics, but concerns have been raised that the available fractionation methods do not well describe functional SOM pools. We also test if examine the question whether physical fractionation techniques isolate ecologically meaningful, functionally relevant soil compartments. In this study we explore whether the kind of information that aggregate density fractionation (ADF) and particle size-density fractionation (PSDF) yield on soil OM dynamics is method-specific, similar, or complimentary. We do so by following the incorporation of a ^{15}N label into mineral soils of two European beech forests a decade after its application as ^{15}N labelled litter.

Both density- and size– based fractionation methods suggested that OM became increasingly associated with the mineral phase as decomposition progressed, within aggregates and onto mineral surfaces. Our results suggest that physical fractionation methods do isolate ecologically relevant functional soil subunits. However, scientists investigating specific aspects of OM dynamics are pointed towards ADF when adsorption and aggregation processes are of interest, whereas PSDF is the superior tool to research the fate of particulate organic matter (POM).

Some methodological caveats were observed mainly for the PSDF procedure, the most important one being that fine fractions isolated after sonication can not be linked to any defined decomposition pathway or stabilisation process. This also implies that historical assumptions about the "adsorbed" state of carbon associated with fine fractions need to be re-evaluated. Finally, this work demonstrates that establishing a comprehensive picture of whole soil OM dynamics requires a combination of both methodologies and we offer a suggestion for an efficient combination of the density and size-based approaches.

Keywords

Nitrogen; ^{15}N; Soil organic matter dynamics; Density fractionation; Size fractionation; Aggregate; Methods comparison.

1. Introduction

Mineral soil is a complex mixture of mineral and organic materials attached to each other by a variety of mechanisms. Soil process research has addressed the resulting mechanistic and structural complexity through the development of a large number of physical fractionation protocols (Balesdent et al., 1991; Christensen, 1992; Golchin et al., 1994b; Six et al., 2000b). These methods are based on the premise that the association of soil particles and their spatial arrangement play a key role in soil organic matter (SOM) dynamics, because bioaccessibility and bioavailability are prerequisites for decomposition (Balesdent, 1996; Gregorich et al., 2006; von Lützow et al., 2007). Protocols involve various degrees of soil **dispersion**, followed by density and/or size **separation** to isolate pools of SOM based on their size and degree of organo-mineral interaction (Torn et al., 2009).

1.1. Soil dispersion

Several procedures generating different levels of soil disaggregation ranging from moderate to strong are currently used. Moderate dispersion treatments include: various types of shaking with or without glass beads, mild sonication, slacking, disruption with a jet of water, blade mixing, and wet sieving (e.g. Billings et al., 2005; Huygens et al., 2005; Kong et al:, 2005; Shang and Tiessen, 2000; Six et al., 2002). Strong dispersion treatments include chemical dispersion with sodium hexametaphosphate and high-energy sonication treatments (e.g. Lehman et al., 2001; Sohi et al., 2001). Depending on whether a strong or a moderate dispersion treatment is being used we will refer to a **particle** or an **aggregate fractionation** procedure, respectively. **Particle fractionation** theoretically aims at isolating non-aggregated particles but appears biased when considering small-size fractions resistant to disaggregation (Chenu and Plante, 2006). On the contrary, **aggregate fractionation** does not yield only aggregates but rather a mixture of aggregated and non-aggregated particles. It is therefore important to realise that the terms **particles** and **aggregates,** traditionally used in many previous studies, are often misleading. With this realisation in mind, the philosophy behind each procedure can be expressed as follows: (1) **Particle fractionations** are based on the idea that equivalent soil particles are the seat of equivalent OM dynamic controlling processes. This type of procedure puts principally the accent on adsorption mechanisms. (2) **Aggregate fractionation** procedures are based on the assumption that soil structure is a major control on SOM turnover through physical protection. The emphasis of aggregate fractionations is on the isolation of ecologically meaningful subunits of the soil structure.

1.2. Separation into fractions

The two major separation principles are based on the physical categories "size" and "density", both pertaining to individual particles and aggregated structures. Size separation mostly relies on wet sieving for soil subunits coarser than 20µm, and sedimentation for finer soil subunits. The sedimentation method is based on Stokes'

law, but the conditions for its validity, which are a spherical shape of particles/aggregates and homogenous particle/aggregate density, are never realised in soil systems. The consequence is an inherent, yet unknown degree of experimental error which effectively turns the sedimentation approach into some kind of density-size separation method as opposed to a physically rigorous size separation.

Density separation is usually performed through floatation or swirling decantation procedures. Floatation can be performed on water to isolate intact plant remnants with a density >1 $g.cm^{-3}$, or in dense liquids, such as Ludox (i.e. colloidal silica), NaI or Sodium Polytungstate (SPT) to separate aggregates or particles composed of minerals that vary in density. SPT-solutions are the most common separation liquids, because SPT is non-toxic and allows to create solutions as dense as 2.8 $g\ cm^{-3}$. However, SPT is known to solubilise a certain proportion of C which may redistribute across fractions or become lost with the supernatant (Chenu and Plante 2006; Crow et al., 2007; Six et al., 1999b; Virto et al., 2008). The swirling decantation procedure takes place in water and is used to separate mostly organic from mostly mineral soil subunits. This last method combines floatation and sedimentation and therefore is different from the water floatation methods presented above (See section ***2.2.1*** for a brief description of the method)

Over the last three decades, depending on the functional soil compartments tracked, various procedures of density/size separations involving one or several dispersion steps, have been performed. A quick overview of the main types of fractionation procedures is given below (See also Fig. 1). In an attempt at organising information for the readers convenience, terms in bold characters and followed by an asterisk are further defined in Table 1.

Table 1: Definitions

'True' aggregate fraction:	Fraction that contains only aggregates, opposed to non-fully dispersed fractions including a mixture of aggregates, POM and fully dispersed mineral particles, which are sometimes referred as aggregates fraction.
Single step fractionation procedure:	Fractionation procedure that involves a single dispersion step followed by a separation step that could include a size, a density or a size-density separation.
Multiple step fractionation procedure:	Fractionation procedure that involves the redispersion of fractions obtained from a single step fractionation procedure. The redispersion can only occur on aggregate fractions.
Composite fractions:	Soil fractions made of heterogeneous elements aggregated or not. These heterogeneous elements can be fully dispersed mineral particles, POM, oxide concretions, black carbon.
Functional soil Compartment (FSC):	Represents an extra level of organisation gathering groups of physical fractions in which the majority of constitutive elements (i.e. particles or aggregates) undergo the same combination of decomposition processes

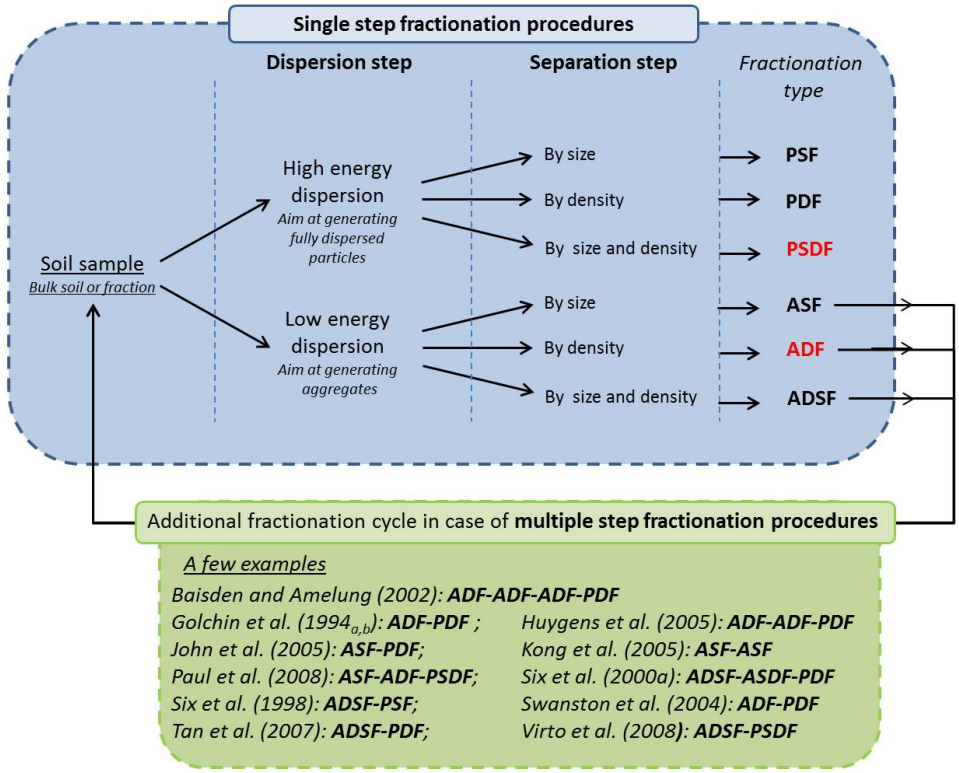

Figure 1: Flow chart to illustrate methodological differences between soil fractionation procedures. PDF = Particle density fractionation; PSF = Particle size fractionation; ADF = aggregate density fractionation; ASF = aggregate size fractionation; PSDF = Particle size density fractionation and ASDF = aggregate size density fractionation. ADF and PSDF are highlighted in red because they were chosen for this study.

1.3. A comprehensive inventory of fractionation procedures

Particle density fractionation (PDF) has been carried out to separate free OM and different types of mineral fractions. The idea behind this approach was that i) the association or the absence of associations with the mineral phase control OM dynamics (e.g. Rumpel et al., 2000; Swanston et al., 2002; Whalen et al., 2000), and that ii) the mineralogy of the minerals within the size fractions is distinct and of variable effect on the stability of the adsorbed SOM. Recent examples include the study of mineral-specific associations with organic matter and mineral-specific bonding mechanisms (e.g. (Basile-Doelsch et al., 2007; Basile-Doelsch et al., 2009).

Particle size fractionation (PSF) (e.g. Amelung et al., 1999; Jimenez et al., 2011; Rumpel et al., 2000; Sa et al., 2001; Schmidt et al., 1999b; Solomon et al., 2002; Solomon et al., 2000) was based on the assumption that particle sizes reflect the state of decomposition of associated SOM as decay induces fragmentation. Yet, coarse fractions that include both relatively fresh plant debris (particulate organic matter, POM), as well as more processed and protected OM bound to coarse mineral grains were too heterogeneous to correspond closely to the functional pools

used by SOM turnover models. As further described below, this problem was on occasion addressed by combining the particle-size and the particle-density fractionation procedures in what we designate a **particle size-density fractionation (PSDF)** scheme.

Particle size-density fractionation (PSDF) In addition to the size separation, a density separation which removed POM of low density was performed on coarse fractions. This density separation step has been performed using both H_2O as a separation liquid (e.g. Balesdent, 1996; Balesdent et al., 1998; Balesdent et al., 1991; Derrien et al., 2006) and flotation in dense liquids (e.g Kapkiyai et al., 1999; Sohi et al., 2001).

Aggregate density fractionation (ADF) (e.g. Arnarson and Keil, 2001; Billings, 2006; Bock and Mayer, 2000; Castanha et al., 2008; Crow et al., 2007; Echeverria et al., 2004) was initially developed to isolate **true aggregate fractions*** of intermediate density from fully dispersed particles that could be either dense\mineral or light\organic. **True aggregate fractions*** were also separated by density in an attempt to separate aggregates of different properties that control soil microbial activity, such as the ratio between organic matter and mineral phase or the importance of aggregates trapped porosity (e.g. Arnarson and Keil, 2001; Hatton et al., 2012). Sollins et al. (2006) also performed a sequential ADF but aimed at isolating particles and not aggregates.

Aggregate size fractionation (ASF) (e.g. Bayer et al., 2000; Billings, 2006; Jimenez et al., 2011; John et al., 2005; Moni et al., 2010; Ranjard et al., 2000) relies on the idea that OC acts as a glue in aggregates and that aggregate size is directly related to the state of decomposition of the organic carbon. Yet, ASF fractionation does not enable to isolate **true aggregate fractions** but rather a mixture of POM, fully dispersed particles and aggregates which renders a robust interpretation difficult. Several studies proposed ways to correct results in a way that would allow to estimate the **true aggregate** characteristics (e.g. Balabane and Plante, 2004; Moni et al., 2010).

Aggregate size-density fractionation (ASDF) (e.g. Cayet and Lichtfouse, 2001; Lehmann et al., 2001; Magid et al., 2010; Nelson et al., 1994; Römkens et al., 1999; Shang and Tiessen, 2000) relies on the same ideas as the **ASF** but a density separation is performed together with the size separation to ensure that only **true aggregates** are separated by size. Yet these fractionation schemes are often incomplete since only a few studies seek to cleanse the **true aggregate fraction** from POM and fully dispersed mineral particle simultaneously.

Because the above mentioned fractionation procedures all involve just a single dispersion step, we call them **single step fractionation procedure**s*. Yet, **single step fractionation procedure**s* were also successively combined to give rise to **multiple step fractionation procedures*** (Fig. 1). Those involve the successive redispersion\separation of aggregate fractions obtained from a **single step fractionation procedure*** and were used to investigate the internal architecture of soil

aggregates (e.g. Baisden et al., 2002; Golchin et al., 1995a; Golchin et al., 1994a, 1995b; Huygens et al., 2005; John et al., 2005; Kong et al., 2005; Paul et al., 2008; Six et al., 2000a; Six et al., 1998; Swanston et al., 2005; Tan et al., 2007; Virto et al., 2008). Multiple step procedures are largely inspired from the aggregate hierarchy concept (Oades, 1984; Oades and Waters, 1991; Tisdall and Oades, 1982), which posits that large, fast cycling aggregates are made of small slow cycling aggregates and that this aggregate organisation controls SOM dynamics in soil. **Multiple step fractionation procedures*** are the most informative fractionation procedures available to date, at the cost of being extremely time consuming and prone to generate propagated measurement errors.

1.4. Objectives of the study

With all this variety of fractionation protocols, and the scepticism prevailing with regard to the general usefulness of the fractionation approach (von Lützow et al., 2007), the fundamental question emerges which soil functions or soil process regimes are best represented by a given physical fraction scheme.

This study aims at evaluating the specificity and relevance of the information provided by size and density fractionations for the research question of nitrogen transfer from the litter layer into the underlying mineral soil after a decade of litter decay. By checking the progress of a ^{15}N label through physical fractions we can estimate to which extent a given physical fraction was involved in the turnover of organic matter in general and organic N in particular. We test the hypothesis that physical fractions may allow the observer to identify functional subunits of the soil fabric and the associated process dynamics of OM turnover.

The fractionation procedures selected for this study include an aggregate density fractionation (ADF), a fairly new procedure that has shown promise as a means to isolate ecologically meaningful aggregate structures (Sollins et al. 2006), while traditional particle size-density fractionation (PSDF) was selected because it can be considered as one of the most detailed and widely established fractionation procedures. The fractions obtained were characterised by a suite of analytical techniques with emphasis on parameters that would be informative of the intensity of N turnover.

Our strategy to draw inference involved two steps. First, principle component analysis (PCA) was used to reduce the set of organic matter related data (including C and N contents, C/N ratio, $\delta^{13}C$) to two independent variables or principal components (PC) that account for the majority of the data variability. The second step consisted of resolving the plane defined by the two principal components into contour maps of ^{15}N label incorporation among physical fractions from both fractionation procedures. By doing this, dynamics of litter derived N transformation can be visualized as trajectories in the PCA plane.

2. Materials and methods

2.1. Experimental design

A detailed description of soil sites and sampling procedures was given by Hatton et al. (2012). Briefly, soils were collected from long-term field experiments located at Ebrach (Germany, 49°52' N, 10°27' E) and Fougères (France, 48°23' N, 1°8' W) (Table 2). Both sites represent managed beech forests (Fagus sylvatica L.). According to the FAO classification (IUSS Working Group WRB, 2006), Ebrach is an acidic dystric Cambisol with a sandy loam texture while Fougères keyed out as acidic glossalbic Cambisol with a silty loam texture.

Table 2: Basic soil properties of the 0-2.5 horizon

C	N	pH_{H2O}	CEC_e†	Base saturation†	Years after the ^{15}N pulse	Remaining ^{15}N tracer	Texture (%)		
$mg.g^{-1}$	$mg.g^{-1}$		$mmol.kg^{-1}$	%	yr	%	Sand	Silt	Clay
Ebrach: *dystric Cambisol*									
45.9	2.0	3.9	87.8	34.5	12	11	76.2	19.0	4.8
Fougères: *glossalbic Cambisol*									
79.5	4.7	3.8	87	26	8	15	2.5	85.5	12.0

Data from Hatton *et al.* (2011) †= values from depth 0-5cm

At both sites, the label was applied as a single pulse of highly ^{15}N-enriched beech litter. The litters were obtained by foliar application of urea to ten year old beech trees in another forest (Zeller et al., 1998). In February 1996 at Ebrach and in February 2000 at Fougères, undecomposed litters were removed and replaced by the labeled beech leaves in an amount equal to the respective mean annual leaf litter input and covered with a 2-cm mesh nylon net (Zeller et al., 2001).

Twelve years (November 2007) and eight years (January 2008) after tracer application, labeled and control soils were collected at Ebrach and Fougères, respectively. The A-horizon was collected in triplicate and sieved to pass 2 mm. Observable roots were removed. Replicates were stored at +4°C. Soil moisture was measured at 105°C. The first 2.5 cm were investigated in this study as most of the litter-derived ^{15}N was concentrated here (Hatton et al., 2012).

2.2. Description of fractionation protocols

We compared two **single step fractionation procedures** that differ in the number of fractions generated, in the intensity of the dispersion step and in the type of separation used. Particle size-density fractionation (PSDF) uses high-energy ultrasonic dispersion, wet sieving, sedimentation and density separation in water to separate different size classes of organic and mineral fractions, while aggregate density fractionation (ADF) employs a low-energy dispersion step and uses a salt solution diluted to various densities to separate out fractions of varying density.

2.2.1. Particle size-density fractionation (PSDF)

We followed a method originally proposed by Balesdent et al. (1991) and sequentially isolated the following size fractions: >2000, 2000-630, 630-200, 200-63, 63-20, 20-6, 6-2, 2-0.2, 0.2-0.035, and <0.035µm (see Fig. 2). The procedure entails the suspension of aggregates > 63 µm without breaking POM using mechanical shaking with glass beads (Balesdent et al., 1998) followed by the complete dispersion of <63 µm micro-aggregates using ultrasound. Briefly, deionised water (360 ml) was added to ~50 g of air-dried bulk soil, and shaken overnight with 20 glass beads (diameter = 5mm). The fractions >63 µm were recovered by wet sieving, whereas the fraction < 63 µm was sonified using conditions calibrated to obtain a clay-sized fraction equivalent in proportion to that achieved during standard particle size analyses (Balesdent et al., 1998; Schmidt et al., 1999a). The input of energy delivered by the ultrasonic probe to the soil suspension [soil mass (g) to water volume (ml) ratio of 1:10] was fixed at 320 J/ml delivered over a 20 min period of time. An ice bath was used to limit temperature increase and to avoid reduction of cavitation during sonication (Roscoe et al., 2000). The 63-20µm fraction was then recovered by wet sieving, whereas all fractions <20µm were separated by sequential sedimentation performed either under normal gravity for fractions >2µm or under increased gravity for fractions <2µm. Assuming an average particle density of 2.44 g cm^{-3}, sedimentation times were determined according to Stokes' law under normal gravity, and according to an adapted version under centrifugation (Poppe et al., 1988). Fractions coarser than 6µm were further separated by density in water into a dense fraction mostly mineral and a lighter fraction mostly organic, using a method similar to gold panning and sometimes referred to as the swirling decantation method (e.g.Shang and Tiessen, 2000). Repeatedly, soil fractions immersed in water were gently swirled in a beaker to achieve preferential resuspension of light organic particles as opposed to denser particles. Subsequently, the upper part of the beaker containing POM was poured away into another beaker. The full PSDF-procedure yields a total of 16 fractions: 6 coarse fractions denser than water, 6 coarse fractions lighter than previous fractions and 4 fine fractions (Fig. 2). Coarse dense fractions were oven dried at 105°C, whereas coarse light and fine fractions were freeze-dried.

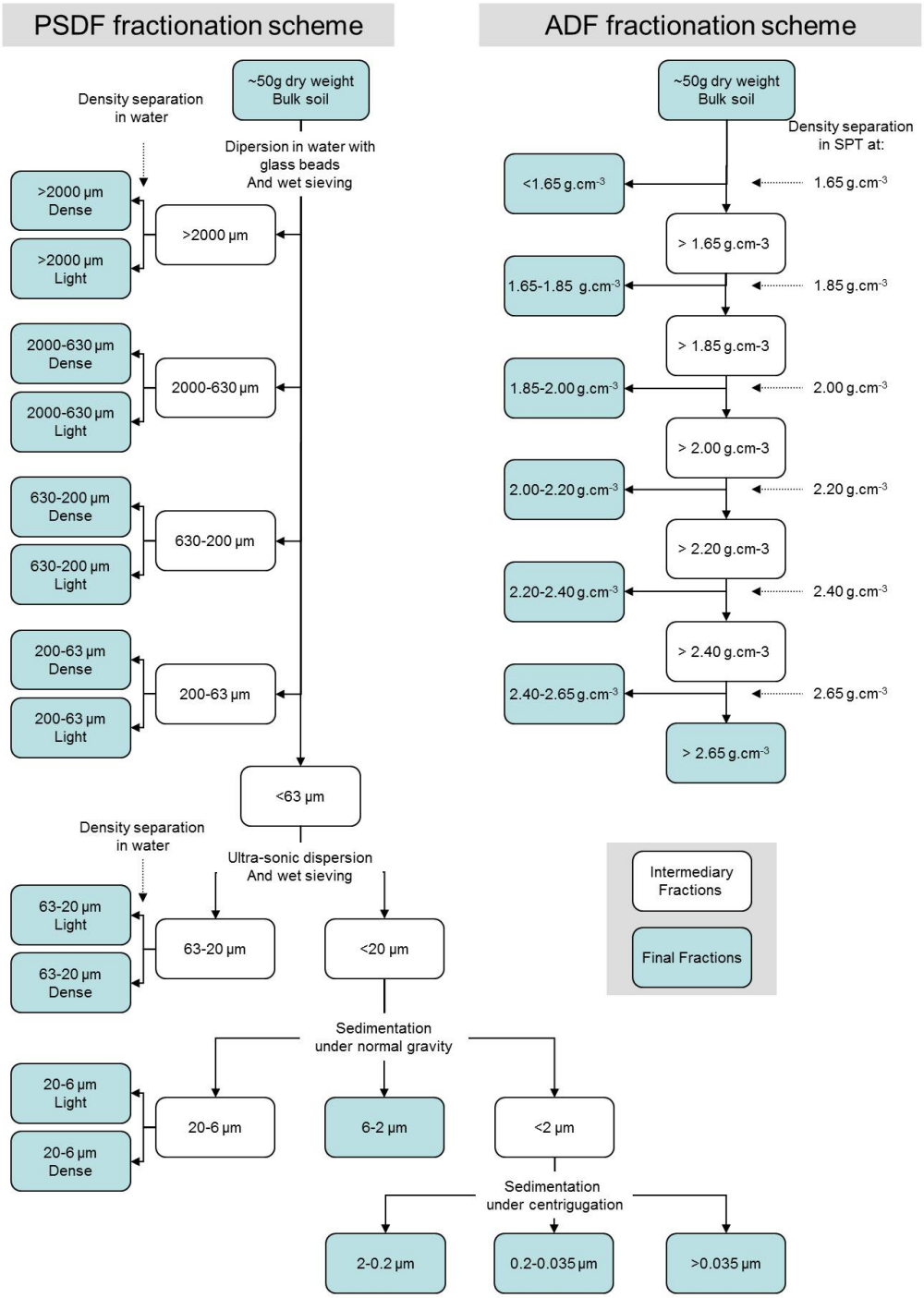

Figure 2: PSDF and ADF Fractionation schemes

2.2.2. Aggregate density fractionation (ADF)

Aggregate density fractionation was performed as described by Sollins et al. (2006) to isolate different soil fractions by flotation on sodium polytungstate solutions (SPT) of varying density. Seven density fractions were isolated: <1.65; 1.65-1.85; 1.85-2.0; 2.0-2.2; 2.2-2.4; 2.4-2.65 and >2.65 $g.cm^{-3}$. For more details about the procedure, see Hatton et al. (2012) or Fig. 2.

2.3. Characterization of physical fractions

The seven aggregate fractions generated by the ADF procedure are labeled A1-A7 in Fig. 3 and 4.

The PSDF procedure generates 16 fractions falling in three categories which we designate as follows:

1) fractions > 6 µm and with a mineral content that renders their density greater than that of water are labeled "coarse dense" (designated P7-P12 in Fig. 3 and 4);

2) fractions > 6 µm whose mineral content is low enough to allow them to float on water are labeled "coarse light" (labeled P1-P6 in Fig.3 and 4);

3) fractions < 6 µm are labeled as "fine" (P13-P16 in Fig. 3 and 4).

2.3.1. Physical appearance

All fractions were examined with a stereomicroscope. For PSDF, fractions were directly observed after drying, whereas fractions recovered by ADF were observed after dispersion in water. Aliquots were immersed in Petri dishes (ø: 4cm) filled with deionised water. Petri dishes were gently hand shaken to check for the presence of different density phases. Visual description was performed under a range of magnifications starting from 6× to 50×. Samples were checked for: recognizable organic debris, black carbon, aggregates, non-aggregated mineral particles (including oxides and concretions).

2.3.2. Organic matter

Total C, total N, $\delta^{15}N$ and $\delta^{13}C$ were determined in triplicate using a 20-20 coupled continuous flow elemental analyzer - isotope ratio mass spectrometer (EA-IRMS; PDZ Europa Ltd., Crewe, Cheshire, England). The degree of microbial processing was determined using $\delta^{13}C$, $\delta^{15}N$ and C:N values as proxies (Baisden et al., 2002).

2.3.3. ^{15}N Tracer

In bulk soil and isolated fractions, the ^{15}N tracer enrichment [excess ^{15}N; $E^{15}N(\%)$] was quantified as a proportion of total N as follows:

$$E^{15}N(\%) = (A^{15}N(\%)_{labelled_plot} - A^{15}N(\%)_{control_plot}) \qquad (A)$$

where $A^{15}N(\%)_{labelled_plot}$ and $A^{15}N(\%)_{control_plot}$ are the abundances of the ^{15}N isotope, expressed in percent of total N, in labelled and reference plots.

2.3.4. Statistics

Total C, total N, $\delta^{15}N$ and $\delta^{13}C$ data are presented as means of three replicates with their standard deviations.

2.3.5. Principal component analysis

Fractionation procedures were compared through standardized principal component analysis (PCA). The procedure reduces the overall variability in the data from the fractions by derivation of a small number of linear combinations of the original variables, called the principal components. The results of a PCA are usually discussed in terms of component scores and loadings (Shaw, 2003). Scores represent the coordinates of fractions in the new space defined by the principal components, while loadings represent the correlation between the principal components and the original variables. To perform the PCA, we combined the following original variables: C, N, C/N ratio, $A^{13}C$ (%) measured on all the fractions isolated from Ebrach and Fougères, including both labelled and control treatments. Since we did not want to separate our fractions on the basis of the ^{15}N labeling, $A^{15}N$ (%) was excluded from multivariate analyses. This way of representation constitutes a convenient way of assessing the level of similarity between fractions at a glance. Fractions whose positions are close together in the PCA plane share overall characteristics without being necessarily equivalent, i.e. an aggregate fraction can display the same carbon content as a fraction encompassing a mixture of fully dispersed mineral particles and POM.

Visualization of the label incorporation within fractions was performed by applying a contour map representing the excess of ^{15}N ($E^{15}N$) in the plane defined by the main PCs behind related scatter plots. Interpolated contour maps were obtained by kriging using a default linear variogram (slope=1, nugget effects =0) using the software "Surfer", version 7.02. Here the goal was to provide an easy way to visualize a three dimensional data set.

3. Results

3.1. Recoveries

Mass losses in the course of the fractionation process were characterised by calculating mass budgets as well as C and N recovery rates. For both fractionation procedures mass losses never exceeded 2%. Carbon and nitrogen recovery rates averaged 91.4±2.6% for ADF and 91.7±7.2% for PSDF and were similar to recovery values presented by other studies (Balabane and Plante, 2004; Balesdent et al., 1998; Schmidt et al., 2000; Schmidt and Kogel-Knabner, 2002; Schöning and Kögel-Knabner, 2006).

Table 3 : Visual description of fractions

Fractions Names	**Ebrach:** *dystric Cambisol*					**Fougères:** *glossalbic Cambisol*				
	Mineral phase		Organic phase			Mineral phase		Organic phase		
	Quartz, Feldspar	Concretions/ oxides	POM	Aggregates	Black carbon	Quartz, Feldspar	Concretions/ oxides	POM	Aggregates	Black carbon
Particle Size Density Fractionation (PSDF)										
Coarse dense										
>2000 µm		100%				99%	+++			+
2000-630 µm	50%	50%			+	99%	++			+
630-200 µm	99%		+		+	99%	++	+		+
200-63 µm	99%		+		+	99%	+	+		+
63-20 µm	99%		++		+	99%		++		+
20-6 µm	99%		++		+	99%		++		+
Coarse light										
>2000 µm			99%		+			99%		+
2000-630 µm			99%		+			99%		+
630-200 µm	+		99%		+	+		99%		+
200-63 µm	+		99%		+	+		99%		+
63-20 µm	++		99%		+	++		99%		+
20-6 µm	++		99%		+	++		99%		+
Fine fractions	Stereomicroscope insufficient resolution					Stereomicroscope insufficient resolution				
<6 µm	2 distinct phases : a dark light organic and a dense clear mineral					2 distinct phases : a dark light organic and a dense clear mineral				
Aggregates Density Fractionation (ADF)										
Density Fractions										
<1.65 g.cm^{-3}	+		99%		+	+		99%		+
1.65-1.85 g.cm^{-3}	10%		+++	89%	+	10%		+++	89%	+
1.85-2.0 g.cm^{-3}	16%		++	83%	+	16%		++	83%	+
2.0-2.2 g.cm^{-3}	26%		+	73%	+	21%		+	78%	+
2.2-2.4 g.cm^{-3}	40%		+	59%	+	35%		+	64%	+
2.4-2.65 g.cm^{-3}	99%	+	+			99%	+	+		
>2.65 g.cm^{-3}	80%	20%	+			80%	20%	+		

+, ++, +++ the fraction element is present as trace of increasing importance

Fractions susceptible to be composite in term of OM

Fractions **composite*** in term of OM

3.2. Physical appearance of isolated fractions

Microscopic observations of separates from Fougères and Ebrach are summarized in Table 3.

For ADF, the fraction <1.65 g.cm^{-3} was composed of free plant debris with minor encrustations of mineral grains. Fractions from 1.65 to 2.4 g cm^{-3} mostly consisted of aggregates whose content of non-aggregated mineral particles (determined after mild grinding and resuspension in water) increased with increasing density, from 10% to 60% of observed items.

Traces of charcoal (i.e. about 3% of items) were identified in every fraction below a density of 2.4 g.cm^{-3}. Fractions > 2.4 g.cm^{-3} were mostly composed of non-aggregated mineral particles. Brown to red colored oxides and concretions were nearly exclusively observed in fractions > 2.65 g.cm^{-3} and accounted for about 10% of the material there.

For the PSDF, coarse dense fractions were almost exclusively composed of non-aggregated mineral particles, whereas coarse light fractions were almost exclusively composed of POM. The purity of these mineral and organic fractions slightly decreased with decreasing particle size, which illustrates that it became increasingly difficult to separate organic and mineral phases by density in water as particle size approached colloidal dimensions. Oxide concretions were observed in varying proportions in coarse dense fractions. Representing in mass up to <1% and nearly 100% of the >2000 μm fractions at Fougère and Ebrach, respectively, their abundance decreased quickly with decreasing fraction size. A few particles of charcoal were identified in all coarse fractions (i.e. >6 μm). Visual description of fine fractions was beyond the resolution of the stereomicroscope, yet it was still possible to see that the fine fractions were composed of two phases, a black one and white one with black fractions likely corresponding to low density materials and white ones to minerals.

3.3. Organic matter

For both fractionation procedures, fractions isolated from labeled and control soils had comparable C and N concentrations and C/N ratio and similar $\delta^{13}C$ values (Fig. 3).

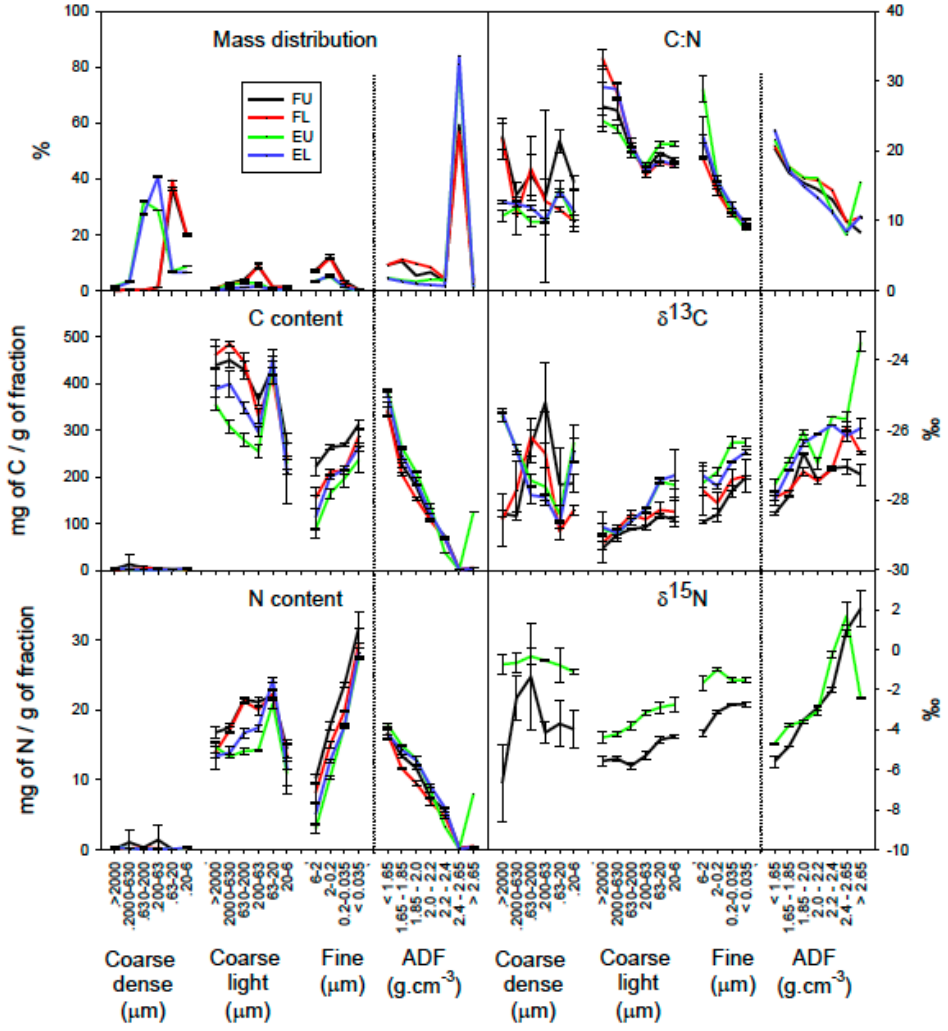

Figure 3: Chemical characteristics of PSDF and ADF fractions isolated from Ebrach and Fougères labelled and unlabelled soils (EL, EU, FL, and FU respectively). Mass distribution, C and N contents, C/N ratio, as well as, $\delta^{13}C$ and $\delta^{15}N$ natural abundances.

3.4. Dry mass, total C, N

Dry mass peaked in fraction 2.4-2.65 $g.cm^{-3}$ recovered from ADF with about 58% of total soil mass in this fraction at Fougères and 83% at Ebrach. These values were equivalent to the mass percentage of the coarse dense fractions isolated by PSDF in both soils. Mass proportions in other fractions isolated by ADF or PSDF ranged from 1 and 10% of dry weight. Soil mass distributions among fractions were similar between labeled and control soils (Fig. 3).

For both Ebrach and Fougères samples, C and N content of ADF fractions dropped by an order of magnitude from the lightest fraction to the two densest fractions. Some PSDF fractions exhibited some similarities with ADF fractions. Coarse dense fractions were as depleted in C and N as the ADF fractions denser than 2.4 $g.cm^{-3}$. Coarse light fractions had on average the same C and N concentrations as the lightest ADF fractions. Their C content slightly decreased with decreasing particle size with the exception of the 63-20µm fractions that reached a local maximum, while their N contents slightly peaked in the 63-20µm fractions. Within fine fractions, C and N increased with decreasing particle size.

3.5. Indicators for microbial processing: C/N ratio, natural abundance in ^{13}C and ^{15}N

Within ADF fractions, C/N ratios decreased and natural abundance of ^{13}C and ^{15}N increased with increasing density from plant-like to microbe-like values (in Fig. 3; C:N ratios from 21±1 to 11±3; $\delta^{13}C$ from -28.0±0.3‰ to -25.8±1.7‰ and natural $\delta^{15}N$ from -3.4±0.6‰ to -0.1±3.2‰). Within the organic rich fractions generated by PSDF, i.e. coarse light and fine fractions, the same trend was observed with decreasing particle size, (C/N ratios from 28±4 to 9.4±4, $\delta^{13}C$ from -29.1±0.3‰ to -26.9±0.5‰ and natural $\delta^{15}N$ from -3.3±0.8‰ to -1.4±0.9‰). In the coarse dense fractions generated by PSDF, no clear trend could be observed when size decreased: C/N ratios ranged between 9.5 and 22, $\delta^{13}C$ between -29‰ and -25‰, and natural $\delta^{15}N$ between -7‰ and 0‰.

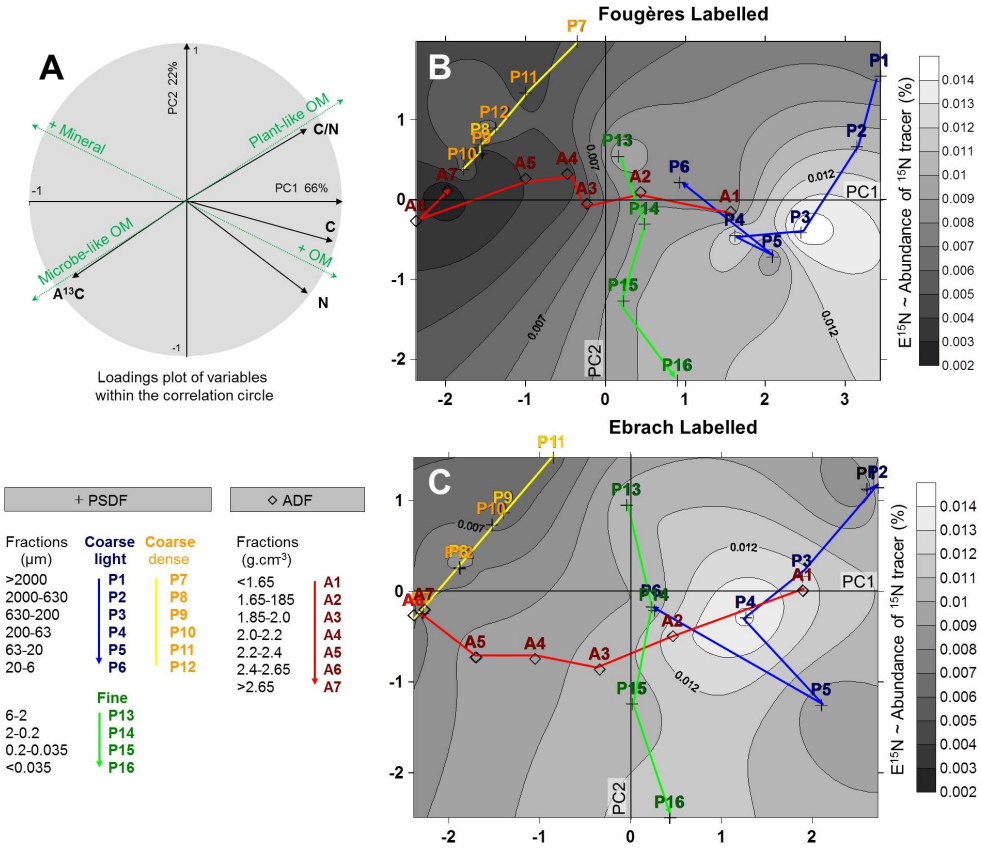

Blue trajectory: Particulate organic material with hyperbolic gradient from plant like over more microbial characteristics. High variation of the OM content after P4 observed for both soils is probably an artefact of the ultrasonic dispersion.
Yellow trajectory : Mineral material depleted in OM. Absence of trend within the trajectory due to decreasing accuracy of C/N and $A^{13}C$ measurements at low OM content. High degree of similarity between soils
Green trajectory : clay (very fine silt) associated organic matter, increasing microbial character and increasing OM content with decreasing size, high degree of similarity between soils
Red trajectory : Mineral-organic matter mix, strong and unidirectional gradients for C/N, C, N, OM in both soils from purely organic material A1 to purely mineral material A6 and A7, but decidedly more microbial character in the Ebrach soil

Figure 4: Principal component analyses (PCA). PCA was performed for both sites independently on fractions isolated from labelled and unlabelled soil samples. Fractions were discriminated as a function of their C and N content, C/N ratio and the abundance of ^{13}C, $A^{13}C$. A) Correlation circle between the new components and the original variables. B) Fougères and C) Ebrach score plots for labelled soil fractions only (unlabelled plot are very similar). Visualization of ^{15}N tracer abundance (See equation A) within fractions was performed by applying the relevant contour map as a background image. Interpolated contour maps were obtained by kriging using a default linear variogram (slope=1, nuggets effects =0) using the software "Surfer v. 7.02). Fractions are grouped for similarity based on their level of affiliation with one of four clearly discernible trajectories (indicated by line style) within the PCA plane. A synthetized representation of the PCA results as well as its visual interpretation is given in Figs. 5 and 6.

3.6. Principal component analysis

3.6.1.Gradients within the PCA plane

The two first principal components (PC) accounted for 88% of the total variance in the samples (Fig. 4 and Table 4, PC1 66%, PC2: 22%). With respect to component loadings (Table 4), two gradients set at ~45° from the PC1 and PC2 were identified (Fig. 4A). The first gradient was characterised by a decreasing C/N ratio and increasing $\delta^{13}C$, and represented the degree of OM microbial processing from a plant-like to a microbe-like pool of OM. The second gradient follows increasing levels of C and N content and corresponds to the gradient of OM content within fractions.

Table 4: Eigenvalues and percentage of explained variance for the fraction datasets on OM quality

	PC1	PC 2
Eigenvalues	2.645	0.893
Variance (%)	66.13	22.32

Correlation coefficients (loading) between the original reduced data and the two first components

	PC1	PC2
C	0.948	-0.265
N	0.787	-0.599
C/N ratio	0.770	0.465
$A^{13}C$	-0.731	-0.497

PC: principal component.

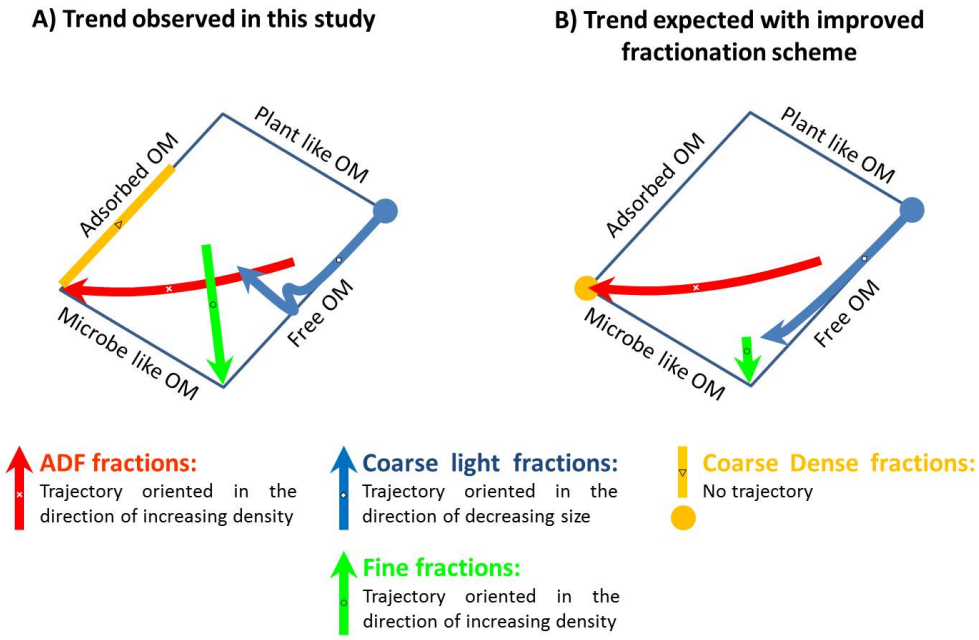

Figure 5: Schematic representation of A) the PCA results and B) the change that could be expected in the PCA plan after application of the improved PSDF fractionation procedure suggested for future work in Fig. 6.

3.6.2.Plot of the isolated fractions in the PCA plane

Coordinates of the isolated fractions in the plane defined by the two first components PC1 and PC2 were similar for both control and the label treatments. Therefore only fractions isolated from labeled plots are displayed in Fig. 4 (Fougères on panel B and Ebrach on panel C). A schematic interpretation of fraction distribution in the PCA plane is given in Fig. 5A.

In the PCA plane, fractions are separated along the two previously identified gradients according to their OM characteristics. Their geometric arrangement can be interpreted as indicating their proximity to either a plant or a microbe-like state of OM and between a more organic-poor and a more organic rich state. These four different states can be represented as the four sides of a parallelogram delimiting a space where all possible OM combinations may be observed (Figs. 5A). Consequently, fractions located within this space are characterized by intermediary carbon content and must be interpreted as **composite fractions*** (defined as fractions neither purely organic nor purely mineral made of heterogeneous elements that may be aggregated or not).

3.7 ^{15}N tracer distribution in soil fractions a decade after litter application

The ^{15}N tracer was applied as a pulse of labelled litter on the top of the forest humus layer. Its release into the first centimetres of mineral soil took several years as shown by Zeller and Dambrine (2011). After a decade, it was mainly located in the **two lightest ADF** fractions or in the **coarse light fractions isolated by PSDF**, revealing that these fractions acted as recipient of litter residues at the decadal-timescale (Fig. 4), and how N cycling differed across fractions.

4. Discussion

4.1 Process dynamics as inferred from the combination of fractionation procedures

The numerous trajectories and trends revealed by the principal component analysis are explained in Figure 6 in a step-by-step fashion.

Fractions isolated from the ADF spread only along PC1 crossing the composite domain (see Figs. 4, 5A) from the pole of unaltered fresh OM to the pole of adsorbed microbial derived OM. This indicated that with increasing density the level of microbial processing increased and the OM content decreased, and confirms the aggregated nature of mid-density fractions (Fig. 5).

Fractions isolated from the PSDF followed a fundamentally different pattern and were discriminated according to both principal components. Figs. 3 and 4 shows that the three groups of PSDF fractions (i.e. coarse-dense, coarse-light and fine-fractions) were well separated.

Coarse light fractions (upper right hand corner, Figs. 4, 5A) were characterised by high positive scores on PC1 and PC2 that decreased with decreasing fraction size. Fractions > 63µm (P1, P2, P3 and P4) are on the gradient of increasing degree of OM microbial processing when they get finer. The application of ultrasound dispersion to particles less than 63 µm induced an increase of OM content from P4 to P5 (see also Fig. 6 step 4). This process may have removed mineral matter loosely attached to organic 63-20 µm particles or may have redistributed OM from finer fractions, although several authors demonstrated ultrasonic dispersion has minor effects on OM redistribution within fine fractions (Morra et al., 1991; Oorts et al., 2005; Schmidt et al., 1999a; Yang et al., 2009). The next finer coarse light fractions (20-6 µm, P6) show less OM and more mineral matter. This increase of mineral matter from P5 to P6 was also evident from visual observation and is likely to result from an imperfect separation of organic matter from mineral particles during suspension in water (see also Fig. 6 step 3). In theory, had the dispersion and the separation of organic and mineral phases been ideal, coarse light fractions should have been restricted to the pole of pure OM and evolved from a plant like to a more microbe like signature without intruding the composite domain.

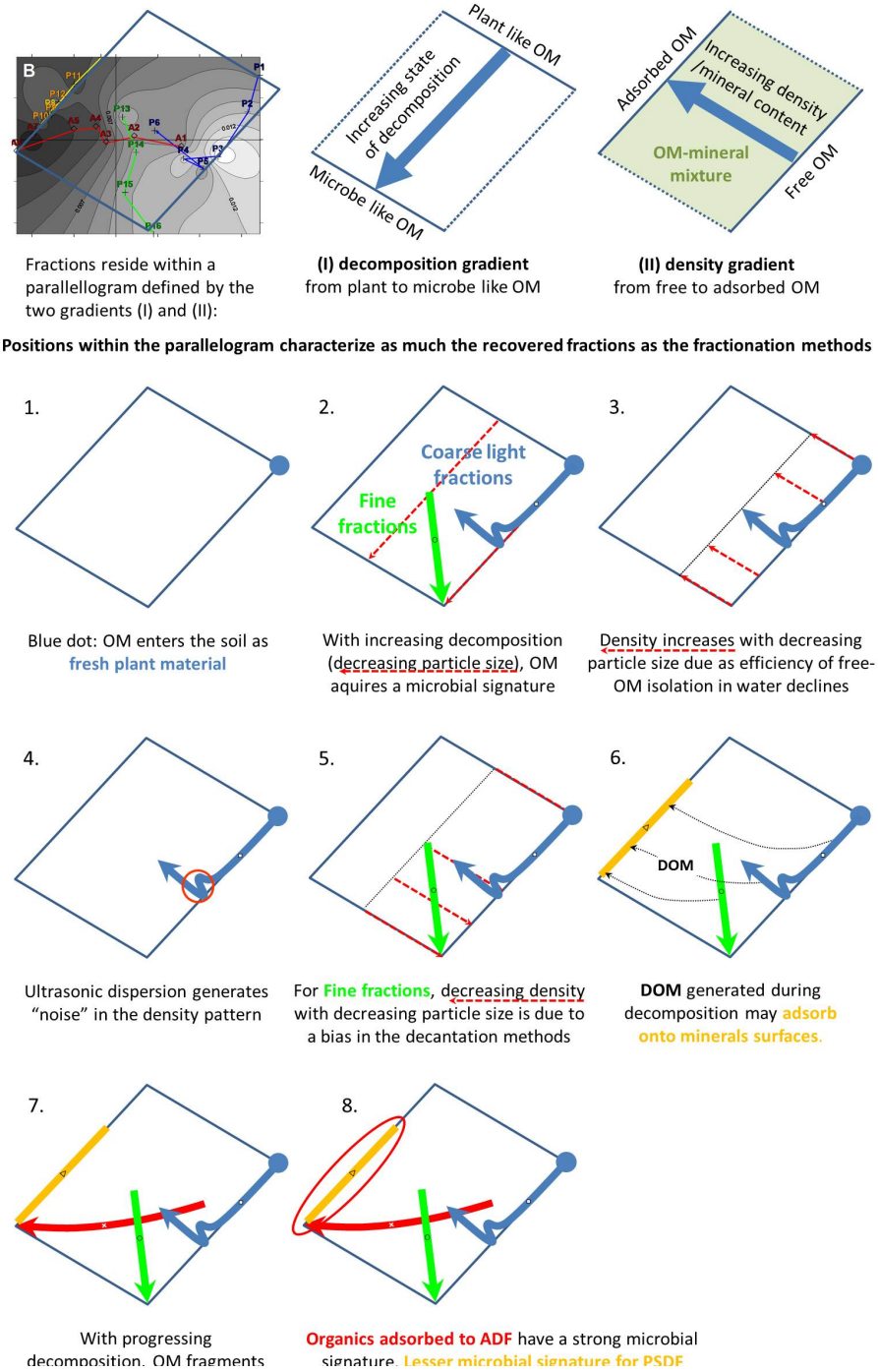

Figure 6: Interpretative schemes of the PCA analysis presented Fig. 4. Meanings of arrows are described in Fig. 5. The green zone in the upper right scheme represents a zone where fractions must be composite* (i.e. made of heterogeneous elements aggregated or not). Thin dashed red arrows highlight the component of OM processing that is being discussed.

Coarse dense fractions (upper left hand corner, Figs. 4, 5A) were characterised by high negative scores on PC1 and high positive scores on PC2. They were almost exclusively composed by non-aggregated mineral particles, had very low OM content and differed mainly from each other by the degree to which OM has undergone microbial processing, which explains why they were aligned parallel to the plant-microbe gradient on the adsorbed OM pole (Figs. 4, 5A). However, decreasing particle size was not equivocally related to increasing degree of microbial alteration. This could in theory result from a lack of analytical sensitivity at low OM contents, but visual observations also suggested that some black carbon particle may have interfered with the detection of consistent change related to decreasing particle size. There have been reports of high density for black carbon particles (up to 2.4 $g.cm^{-3}$ according to Glaser et al. (2000), which would clearly make it impossible to segregate dense black carbon from mineral matter of similar density. Moreover, the imperfection of the density separation in water might be responsible for a contamination of the mineral phase by organic materials, negligible in terms of overall mass but significant in terms of OM content (see also Fig. 6 step 8).

Fine fractions (Aligned with PC2 in the centre. Figs. 4, 5A) were parallel with the PC2 axis and are characterised by PC2 scores that decreased with decreasing size of particles, indicating that OM content and the level of microbial processing increased with decreasing particle size (from P13 going to P16). The fact that fine fractions are located in the composite domain (see also Fig. 6 upper part) confirms that they combine all small-scale organic or mineral debris that are generated by the ultra-sonic dispersion. Increasing OM content with decreasing particle size may be explained by (i) a lower efficiency of ultrasonic dispersion to detach OM patches from small clay particles than from larger silt particles as suggested by Chenu and Plante (2006), (ii) the accumulation of colloidal OM released by the previous dispersion of coarser aggregates or (iii) may result from variations in settling velocities as a result of small variations in density. The unavoidable violation of the conditions for the application of Stokes law (spherical shape, uniform density) will have introduced an error and will have enhanced the organic content of fine fractions as the speed of sedimentation of light organic-rich particles is slower than the one of heavy mineral grains, for a given diameter (see also Fig. 5 step 2). Although the (P16) fraction <0.035µm was relatively depleted in mineral matter, its carbon content suggests that it might not be completely mineral free. Therefore P16 might not qualify as dissolved organic matter (DOM).

4.2. ^{15}N tracer distribution and evaluation of the turnover of processes captured by physical fractions

The superimposition of the ^{15}N excess map to the PCA plane provides several insights in the contrasted N cycling processes captured by individual fractions (Fig. 4).

Of particular interest are the coarse light PSDF fractions from P1 to P4 that displayed contrasting levels of ^{15}N incorporation. As they plot on the pole of pure

OM, they keyed out as a functionally homogeneous group especially relevant to capture such processes that are directly related to decomposer activity and can be considered as controlling N cycling, with no influence from the mineral phases. Thus the maximum of ^{15}N tracer was located within the 630-200µm fraction (P3) at Fougères but within the 200-63 µm fraction (P4) at Ebrach. This indicates that, independent from the time elapsed since tracer application; the mesofauna fragmentation and microbial transformation of the labelled litter was more advanced at Ebrach than at Fougères.

Contrastingly, **mineral-rich fractions** that are the coarse dense PSDF fractions and the ADF fractions above 1.85 $g.cm^{-3}$, incorporated very little tracer-N a decade after its application. This shows that they correspond to reservoirs of older organic N in forest soil. They either cycled nitrogen very slowly, or did not come into contact with the label on a decadal time scale, possibly because the label was preferentially retained in the OM rich fractions. A distinction must be done between these mineral-rich fractions isolated either by size or density regarding their relevance to N cycling processes though. Coarse dense PSDF fractions consisting of individual grains coated with adsorbed OM exhibited no real difference in term of ^{15}N tracer incorporation. This might be due to a level of tracer close to the detection limit of the instrument, or to the fact that size separation of coarse dense fractions was neither able nor expected to separate defined mineralogical fractions that would have influenced the nitrogen dynamic. More interestingly, the (low) level of tracer incorporation in ADF fractions progressively decreased as density increased. These fractions thus appear to be particularly promising as tools for the investigation of time-dependent N sequestration mechanisms (See Hatton et al., 2012 for example).

The absence of contrast in tracer enrichment in the finest fractions isolated by PSDF probably resulted from the incomplete dispersion and separation procedure. This confirmed the methodological artefacts already revealed by the location of the fraction in the PCA plane and clearly demonstrated that fine particle size fractions can not be treated as functional soil compartments regarding N and OM cycling. They constitute a heterogeneous mixture of debris and leftovers of both mineral and organic sorts and cannot be expected to exist as an identifiable fraction in natural soil.

4.3 Derivation of functional soil compartments (FSC's) among physical fractions

These observations on OM characteristics and N cycling can be synthesized to identify **functional soil compartments (FSC)***, which we define as groups of fractions for which organic matter transformation and decomposition processes are controlled by fundamentally different process regimes (Table 5). In other words, FSC's* represent an extra level of organisation, encompassing physical fractions in which the majority of constitutive elements (i.e. particles or aggregates) undergo the same combination of decomposition processes.

Table 5: identification of functional soil compartment* (FSC's) among physical fractions

Soil subunit	Represented by	FSC?	Associated processes and their timescale	Remarks
Particulate organic matter (POM)	PSDF: (P1 to P6) and ADF: (A1)	Yes	Progressive processing by mesofauna, provides adhesive nuclei for aggregate formation Year to decade	POM fractions isolated by PSDF represent a decomposition gradient that can be seen as representing the litter - soil organic matter transition. ADF with only one fraction can not characterize the dynamics in this cohort. Changes in this fraction are independent from interactions with minerals.
Aggregated stuctures	ADF : (A2 to A5)	Yes	Physical isolation of substrate from decomposition actors and factors within defined micro-environments (i.e. microbes, O_2 and H_2O supply, etc) Several decades	ADF is effective at isolating functional microstructures. The biogeochemical stability of individual aggregates, the proportion of mineral materials and the microbial characteristics increase with increasing aggregate density.
Coarse mineral grain coated with OM	PSDF: (P7 to P12) and ADF: (A6 to A7)	Yes	All processes that are controlled by surface chemistry, including adsorption, electron transfer, catalytic effects. Involved dissolved organic matter generated in any stage of the dynamics Several decades	Organic matter associated with the mineral grains isolated by ADF had a greater microbial character than such as was isolated by PSDF.
Residuals	PSDF: (P13 to P16)	No	Does not represent specific soil process	These fractions represent a mixture of mineral and organic materials that 1) were incompletely dispersed, that 2) could not be separated by density in water and that 3) could not be properly separated by size using the single density assumption of Stoke's law. These materials were not necessarily joined or even co-localized in soil.

PSDF = Particle size density fractionation, ADF = Aggregate density fractionation

We identified three groups of physical fractions that could be regarded as FSC*. They are listed below and on Figs. 4 and 5.

1. Free particulate organic matter (POM), where litter derived-N resides for about one decade in forest ecosystems (A1, P1-6)
2. Non-aggregated mineral particles with adsorbed organic matter, location of N cycling processes occurring on timescale longer than decades (A6-A7, P7-P12)
3. Aggregates, also determining N dynamics on pluridecadal time scales in soil (A2-A5)

4.4. PSDF versus ADF procedures: recommendations

In addition to our goal of investigating the general usefulness of soil fractionation for the isolation of ecologically relevant soil subunits, we examined how the process of soil fractionation can be economised such that only meaningful fractions are being

retrieved. Below we offer some considerations to help with the choice of fractionation procedure.

As revealed previously, both ADF and PSDF successfully isolate the functional soil compartment POM and non-aggregated mineral particles coated with OM. To help with the decision for any of the two, we recommend favouring the fractionation procedure that better mimics the natural processes. PDSF is better suited than ADF to investigate the dynamic of POM, as POM sizes are directly related to the natural fragmentation that occurs with the decomposition process. In the case of mineral particles associated with adsorbed carbon, ADF isolated fewer of these fractions (i.e. A6 and A7) than PSDF (i.e. P7-P12). Yet, since the mineralogy and the subsequent adsorption capacity of a particle are more directly linked to its density than to its size, the ADF must be considered to be more appropriate for the investigation of the dynamics of adsorbed OM than the PSDF. Finally, only ADF enables the study of aggregates.

As a conclusion, the two fractionation methods can not be considered alternatives; they must be seen as complementary. However, we recognized 4 major methodological issues of the PSDF procedure which need to be considered when data are interpreted:

1) Density separation in water as performed in PSDF is not designed to achieve strict separation of the mineral and organic phases and therefore generates slight impurities. Coarse dense and coarse light fractions were slightly polluted with residual POM and black carbon in one case, as well as mineral grains in the other case. In the case of coarse light fractions the OC pollution was negligible, though (See also Fig. 6 steps 3 and 8).
2) There is an absence of good separation within the fine fractions, which are obviously composed of phases with contrasting density in contradiction with the sedimentation separation methods which require a unique density for all particles (Stokes' Law) (See also Fig. 6 step 5).
3) Separating coarse dense fractions by size was not very informative.
4) Ultrasonic dispersion at the energy level chosen for this work (i.e. 320 J/ml delivered over a 20 min period of time) does not achieve complete dispersion at submicron scales, and was responsible for slight redistributions in the finest coarse light fractions (i.e. P5, P6) (See also Fig. 6 step 4).

In response to this situation, we propose a PSDF fractionation protocol that reduces the creation of ecologically irrelevant fractions. To do so, we recommend separating the mineral from the organic phases directly after the dispersion procedures, prior to size separations by wet sieving and sedimentation. To avoid interference of dense organic phases (some forms of charcoal) we suggest to adjust the density of the separating liquid to 2.4 $g.cm^{-3}$ (using a solution of sodium polytungstate) to exclude all residual POM as well as a maximum of black carbon particles from the mineral phase. Finally, we propose to abandon the size separation of the mineral fraction (d

> 2.4 g.cm^{-3}). In oxide rich soils, these fractions could eventually be pooled and further separated by density at 2.65 g.cm^{-3} to obtain reactive and less reactive mineral fractions (Fig. 7). Ultrasonication, although unable to achieve complete dispersion at the submicron scale is still extremely efficient at larger size scales and should be kept for that reason. Finally, the size separation of light fraction <20 µm would be performed after density exclusion of dense fractions to limit the effects of varying particle density during sedimentation. The characteristics of the fractions recovered with this new procedure are displayed in Fig. 5B.

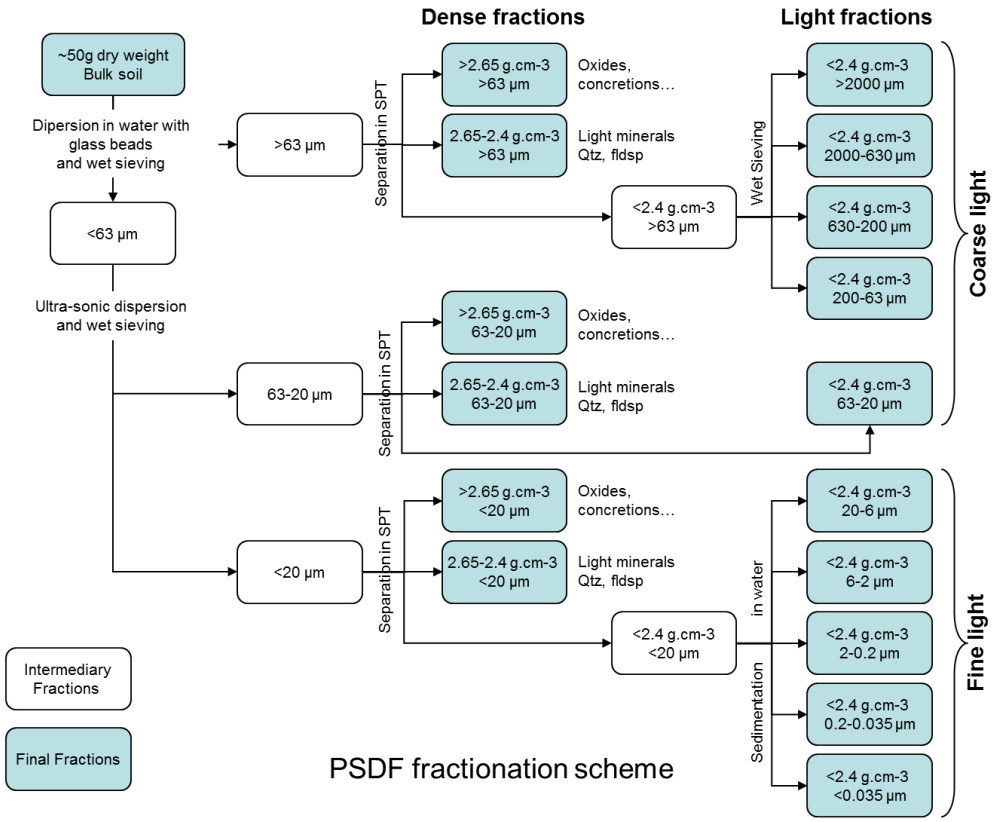

Figure 7: Suggestion for the improvement of the PSDF fractionation scheme

Most contemporary PSDF procedures opt for a separation of the organic phase at ~1.6-1.8 g.cm^{-3} after various degrees of dispersion (e.g. Bruun et al., 2008; Magid et al., 2010; Paul et al., 2008; Shang and Tiessen, 2000; Sohi et al., 2001). In theory this standard method allows the separation of the organic from the mineral phase in most soils, however if applied in soils that contain substantial amounts of black carbon particles and pedogenic oxides, it will not be possible to isolate confounding effects of charcoal when interpreting the fractionation data.

All these issues are resolved with the proposed fractionation procedure (Fig. 7) while keeping the advantages of the old methods.

5. Conclusions

1) We set out to test whether physical fractionation would allow us to identify functional subunits of the soil fabric and their associated process dynamics. We demonstrated how physical fractions can be separated into well-defined functional categories (Table 5) and we showed that both fractionation procedures brought complementary information about SOM dynamics. PSDF fractionation was more adapted to the investigation of the natural fragmentation of POM at decadal time scale whereas ADF was more adapted to the study of adsorption and aggregations at pluridecadal time scale. This suggests that SOM dynamics cannot be fully understood when using a unique single step fractionation procedure.

2) We evidenced a few defects in the PSDF procedure that might be wide spread among similar procedures, the most important one being that fine fractions isolated after sonication can not be linked to any defined decomposition pathway or stabilisation process. An improved PSDF fractionation procedure was proposed to address most of the methodological issues observed.

3) Our work demonstrated that it is fundamentally possible to use physical fractionation for the purpose of isolating organic matter of progressing decomposition stage from soils. This applies to organic matter associated with minerals as well as to particulate organic matter. Figure 7 illustrates how this purpose can be achieved through the application of an optimised, combined fractionation scheme.

Acknowledgments

This work was financially supported by Department of Crop and Soil Science, Oregon State University start-up funds to M.K. and by the Institut National de la Recherche Agronomique (INRA-EFPA) and the Région Lorraine (grant 12000162A). The authors are grateful to Rocky Yarwood of the OSU/CSS Stable Isotope Research Unit (SIRU) who performed stable isotope analyses and to Jade Salleles who kindly accepted to give constructive comments on earlier versions of the manuscripts.

References

Amelung, W., Bol, R., Friedrich, C., 1999. Natural C-13 abundance: A tool to trace the incorporation of dung-derived carbon into soil particle-size fractions. Rapid Communication in Mass Spectrometry 13, 1291-1294.

Arnarson, T.S., Keil, R.G., 2001. Organic-mineral interactions in marine sediments studied using density fractionation and X-ray photoelectron spectroscopy. Organic Geochemistry 32, 1401-1415.

Baisden, W.T., Amundson, R., Cook, A.C., Brenner, D.L., 2002. Turnover and storage of C and N in five density fractions from California annual grassland surface soils. Global Biogeochemical Cycles 16.

Balabane, M., Plante, A.F., 2004. Aggregation and carbon storage in silty soil using physical fractionation techniques. European Journal of Soil Science 55, 415-427.

Balesdent, J., 1996. The significance of organic separates to carbon dynamics and its modelling in some cultivated soils. European Journal of Soil Science 47, 485-493.

Balesdent, J., Besnard, E., Arrouays, D., Chenu, C., 1998. The dynamics of carbon in particle-size fractions of soil in a forest-cultivation sequence. Plant And Soil 201, 49-57.

Balesdent, J., Petraud, J.-P., Feller, C., 1991. Effets des ultrasons sur la distribution granulometrique des maitres organiques des sols. Science du Sol 29, 95-106.

Basile-Doelsch, I., Amundson, R., Stone, W.E.E., Borschneck, D., Bottero, J.Y., Moustier, S., Masin, F., Colin, F., 2007. Mineral control of carbon pools in a volcanic soil horizon. Geoderma 137, 477-489.

Basile-Doelsch, I., Brun, T., Borschneck, D., Masion, A., Marol, C., Balesdent, J., 2009. Effect of landuse on organic matter stabilized in organomineral complexes: A study combining density fractionation, mineralogy and delta(13)C. Geoderma 151, 77-86.

Bayer, C., Martin-Neto, L., Mielniczuk, J., Ceretta, C.A., 2000. Effect of no-till cropping systems on soil organic matter in a sandy clay loam Acrisol from Southern Brazil monitored by electron spin resonance and nuclear magnetic resonance. Soil & Tillage Research 53, 95-104.

Billings, S.A., 2006. Soil organic matter dynamics and land use change at a grassland/forest ecotone. Soil Biology & Biochemistry 38, 2934-2943.

Bock, M.J., Mayer, L.M., 2000. Mesodensity organo-clay associations in a near-shore sediment. Marine Geology 163, 65-75.

Bruun, S., Thomsen, I.K., Christensen, B.T., Jensen, L.S., 2008. In search of stable soil organic carbon fractions: a comparison of methods applied to soils labelled with C-14 for 40 days or 40 years. European Journal of Soil Science 59, 247-256.

Castanha, C., Trumbore, S., Amundson, R., 2008. Methods of separating soil carbon pools affect the chemistry and turnover time of isolated fractions. Radiocarbon 50, 83-97.

Cayet, C., Lichtfouse, E., 2001. delta C-13 of plant-derived n-alkanes in soil particle-size fractions. Organic Geochemistry 32, 253-258.

Chenu, C., Plante, A.F., 2006. Clay-sized organo-mineral complexes in a cultivation chronosequence: revisiting the concept of the 'primary organo-mineral complex'. European Journal of Soil Science 57, 596-607.

Christensen, B.T., 1992. Physical fractionation of soil and organic matter in primary particle size and density separates. Advances in Soil Science 20, 1-90.

Crow, S.E., Swanston, C.W., Lajtha, K., Brooks, J.R., Keirstead, H., 2007. Density fractionation of forest soils: methodological questions and interpretation of incubation results and turnover time in an ecosystem context. Biogeochemistry 85, 69-90.

Derrien, D., Marol, C., Balabane, M., Balesdent, J., 2006. The turnoverof carbohydrate carbon in a cultivated soil

estimated by13Cnatural abundances. Euroean Journal of Soil Science 57, 547-557.

Echeverria, M.E., Markewitz, D., Morris, L.A., Hendrick, R.L., 2004. Soil organic matter fractions under managed pine plantations of the southeastern USA. Soil Science Society of America Journal 68, 950-958.

Glaser, B., Balashov, E., Haumaier, L., Guggenberger, G., Zech, W., 2000. Black carbon in density fractions of anthropogenic soils of the Brazilian Amazon region. Organic Geochemistry 31, 669-678.

Golchin, A., Clarke, P., Oades, J.M., Skjemstad, J.O., 1995a. The Effects of Cultivation on the Composition of Organic-Matter and Structural Stability of Soils. Australian Journal of Soil Research 33, 975-993.

Golchin, A., Oades, J.M., Skjemstad, J.O., Clarke, P., 1994a. Study of Free and Occluded Particulate Organic-Matter in Soils by Solid-State C-13 Cp/Mas Nmr-Spectroscopy and Scanning Electron-Microscopy. Australian Journal of Soil Research 32, 285-309.

Golchin, A., Oades, J.M., Skjemstad, J.O., Clarke, P., 1994b. Study of free and occluded particulate organic matter in soils by solid state 13C CP/MAS NMR Spectroscopy and Scanning Electron Microscopy. Australian Journal of Soil Research 32, 285-309.

Golchin, A., Oades, J.M., Skjemstad, J.O., Clarke, P., 1995b. Structural and Dynamic Properties of Soil Organic-Matter as Reflected by C-13 Natural-Abundance, Pyrolysis Mass-Spectrometry and Solid-State C-13 Nmr-Spectroscopy in Density Fractions of an Oxisol under Forest and Pasture. Australian Journal of Soil Research 33, 59-76.

Gregorich, E.G., Beare, M.H., Mckim, U.F., Skjemstad, J.O., 2006. Chemical and biological characteristics of physically uncomplexed organic matter. Soil Science Society of America Journal 70, 975-985.

Hatton, P.-J., Kleber, M., Zeller, B., Moni, C., Plante, A.F., Townsend, K., Gelhaye, L., Lajtha, K., Derrien, D., 2012. Transfer of litter-derived N to

soil mineral-organic associations: Evidence from decadal 15N tracer experiments. Organic Geochemistry In press, corrected proof.

Huygens, D., Boeckx, P., Van Cleemput, O., Oyarzun, C., Godoy, R., 2005. Aggregate and soil organic carbon dynamics in South Chilean Andisols. Biogeosciences 2, 159-174.

Jimenez, J.J., Lorenz, K., Lal, R., 2011. Organic carbon and nitrogen in soil particle-size aggregates under dry tropical forests from Guanacaste, Costa Rica - Implications for within-site soil organic carbon stabilization. Catena 86, 178-191.

John, B., Flessa, H., Yamashita, T., Ludwig, B., 2005. Storage of organic carbon in aggregate and density fractions of silty soils under different types of land use. Geoderma 128, 63-79.

Kapkiyai, J.J., Woomer, P.L., Karanja, N.K., Qureshi, J.N., Smithson, P.C., 1999. Soil organic matter and nutrient dynamics in a Kenyan nitisol under long-term fertilizer and organic input management. Soil Biology & Biochemistry 31, 1773-1782.

Kong, A.Y.Y., Six, J., Bryant, D.C., Denison, R.F., van Kessel, C., 2005. The relationship between carbon input, aggregation, and soil organic carbon stabilization in sustainable cropping systems. Soil Science Society of America Journal 69, 1078-1085.

Lehmann, J., Cravo, M.D., Zech, W., 2001. Organic matter stabilization in a Xanthic Ferralsol of the central Amazon as affected by single trees: chemical characterization of density, aggregate, and particle size fractions. Geoderma 99, 147-168.

Magid, J., De Nowina, K.R., Lindedam, J., Andren, O., 2010. Organic matter in size-density fractions after 16-50 years of grass ley, cereal cropping and organic amendments. European Journal of Soil Science 61, 539-550.

Moni, C., Chenu, C., Rumpel, C., Virto, I., Chabbi, A., 2010. Relative importance of sorption versus aggregation for organic matter storage in subsoil horizons of two contrasting soils. European Journal of Soil Science 61, 958-969.

Morra, M.J., Blank, R.R., Freeborn, L.L., Shafii, B., 1991. Size Fractionation of Soil Organo-Mineral Complexes Using Ultrasonic Dispersion. Soil Science 152, 294-303.

Nelson, P.N., Dictor, M.C., Soulas, G., 1994. Availability of Organic-Carbon in Soluble and Particle-Size Fractions from a Soil-Profile. Soil Biology & Biochemistry 26, 1549-1555.

Oades, J.M., 1984. Soil Organic-Matter and Structural Stability - Mechanisms and Implications for Management. Plant And Soil 76, 319-337.

Oades, J.M., Waters, A.G., 1991. Aggregate Hierarchy in Soils. Australian Journal of Soil Research 29, 815-828.

Oorts, K., Vanlauwe, B., Recous, S., Merckx, R., 2005. Redistribution of particulate organic matter during ultrasonic dispersion of highly weathered soils. European Journal of Soil Science 56, 77-91.

Paul, S., Veldkamp, E., Flessa, H., 2008. Soil organic carbon in density fractions of tropical soils under forest - pasture - secondary forest land use changes. European Journal of Soil Science 59, 359-371.

Poppe, L.J., Fredericks, J.J., Hathaway, J.C., 1988. A Computer-Program to Calculate Centrifugation Parameters for Sedimentation Analyses. Computers & Geosciences 14, 541-545.

Ranjard, L., Nazaret, S., Poly, F., Combrisson, J., Richaume, A., Gourbiere, F., Thioulouse, J., 2000. Heterogeneous cell density and genetic structure of bacterial pools associated with various soil microenvironments as determined by enumeration and DNA fingerprinting approach (RISA). Microbial Ecology 39, 263-272.

Romkens, P.F.A.M., van der Plicht, J., Hassink, J., 1999. Soil organic matter dynamics after the conversion of arable land to pasture. Biology and Fertility of Soils 28, 277-284.

Roscoe, R., Buurman, P., Velthorst, E.J., 2000. Disruption of soil aggregates by varied amounts of ultrasonic energy in fractionation of organic matter of a clay Latosol: carbon, nitrogen and delta C-13 distribution in particle-size fractions. European Journal of Soil Science 51, 445-454.

Rumpel, C., Kogel-Knabner, I., Knicker, H., Huttl, R.F., 2000. Composition and distribution of organic matter in physical fractions of a rehabilitated mine soil rich in lignite-derived carbon. Geoderma 98, 177-192.

Sa, J.C.D., Dick, W.A., Cerri, C.C., Lal, R., Venske, S.P., Piccolo, M.C., Feigl, B.E., 2001. Organic matter dynamics and carbon sequestration rates for a tillage chronosequence in a Brazilian Oxisol. Soil Science Society of America Journal 65, 1486-1499.

Schmidt, M.W.I., Knicker, H., Kogel-Knabner, I., 2000. Organic matter accumulating in Aeh and Bh horizons of a Podzol - chemical characterization in primary organo-mineral associations. Organic Geochemistry 31, 727-734.

Schmidt, M.W.I., Kogel-Knabner, I., 2002. Organic matter in particle-size fractions from A and B horizons of a Haplic Alisol. European Journal of Soil Science 53, 383-391.

Schmidt, M.W.I., Kogel-Knabner, I., Rumpel, C., 1999a. Evaluation of an ultrasonic dispersion procedure to isolate primary organomineral complexes from soils European Journal of Soil Science 50, 87-94.

Schmidt, M.W.I., Rumpel, C., Kogel-Knabner, I., 1999b. Particle size fractionation of soil containing coal and combusted particles. European Journal of Soil Science 50, 515-522.

Schoening, I., Kogel-Knabner, I., 2006. Chemical composition of young and old carbon pools throughout Cambisol and Luvisol profiles under forests. Soil Biology & Biochemistry 38, 2411-2424.

Shang, C., Tiessen, H., 2000. Carbon turnover and carbon-13 natural abundance in organo-mineral fractions of a tropical dry forest soil under cultivation. Soil Science Society of America Journal 64, 2149-2155.

Shaw, P.J.A., 2003. Multivariate statistics for the environmental sciences. Arnold ; Distributed in the United States by Oxford University Press, London; New York, ix, 233 p. pp.

Six, J., Elliott, E.T., Paustian, K., 2000a. Soil macroaggregate turnover and microaggregate formation: a mechanism for C sequestration under no-tillage agriculture. Soil Biology & Biochemistry 32, 2099-2103.

Six, J., Elliott, E.T., Paustian, K., Doran, J.W., 1998. Aggregation and soil organic matter accumulation in cultivated and native grassland soils. Soil Science Society of America Journal 62, 1367-1377.

Six, J., Paustian, K., Elliott, E.T., Combrink, C., 2000b. Soil structure and organic matter: I. Distribution of aggregate-size classes and aggregate-associated carbon. Soil Science Society of America Journal 64, 681-689.

Six, J., Schultz, P.A., Jastrow, J.D., Merckx, R., 1999. Aggregate and soil organic matter dynamics under conventional and no-till systems. Soil Science Society of America Journal 63, 1350-1358.

Sohi, S.P., Mahieu, N., Arah, J.R.M., Powlson, D.S., Madari, B., Gaunt, J.L., 2001. A procedure for isolating soil organic matter fractions suitable for modeling. Soil Science Society of America Journal 65, 1121-1128.

Sollins, P., Swanston, C., Kleber, M., Filley, T., Kramer, M., Crow, S., Caldwell, B.A., Lajtha, K., Bowden, R., 2006. Organic C and N stabilization in a forest soil: Evidence from sequential density fractionation. Soil Biology & Biochemistry 38, 3313-3324.

Solomon, D., Fritzsche, F., Lehmann, J., Tekalign, M., Zech, W., 2002. Soil organic matter dynamics in the subhumid agroecosystems of the Ethiopian highlands: Evidence from natural C-13 abundance and particle-size fractionation. Soil Science Society of America Journal 66, 969-978.

Solomon, D., Lehmann, J., Zech, W., 2000. Land use effects on soil organic matter properties of chromic luvisols in semi-arid northern Tanzania: carbon, nitrogen, lignin and carbohydrates. Agriculture Ecosystems & Environment 78, 203-213.

Swanston, C.W., Caldwell, B.A., Homann, P.S., Ganio, L., Sollins, P., 2002. Carbon dynamics during a long-term incubation of separate and recombined density fractions from seven forest soils. Soil Biology & Biochemistry 34, 1121-1130.

Swanston, C.W., Torn, M.S., Hanson, P.J., Southon, J.R., Garten, C.T., Hanlon, E.M., Ganio, L., 2005. Initial characterization of processes of soil carbon stabilization using forest stand-level radiocarbon enrichment. Geoderma 128, 52-62.

Tan, Z., Lal, R., Owens, L., Izaurralde, R.C., 2007. Distribution of light and heavy fractions of soil organic carbon as related to land use and tillage practice. Soil & Tillage Research 92, 53-59.

Tisdall, J.M., Oades, J.M., 1982. Organic-Matter and Water-Stable Aggregates in Soils. Journal of Soil Science 33, 141-163.

Torn, M.S., Swanston, C.W., Castanha, C., Trumbore, S.E., 2009. Storage and turnover of organic matter in soil, In: Senesi, N., Xing, B., Huang, P.M. (Eds.), Biophysico-Chemical Processes Involving Natural Nonliving Organic Matter in Environmental Systems. John Wiley & Sons, Inc, Hoboken, New Jersey, pp. 219-272.

Virto, I., Barre, P., Chenu, C., 2008. Microaggregation and organic matter storage at the silt-size scale. Geoderma 146, 326-335.

von Lutzow, M., Kogel-Knabner, I., Ekschmittb, K., Flessa, H., Guggenberger, G., Matzner, E., Marschner, B., 2007. SOM fractionation methods: Relevance to functional pools and to stabilization mechanisms. Soil Biology & Biochemistry 39, 2183-2207.

Whalen, J.K., Bottomley, P.J., Myrold, D.D., 2000. Carbon and nitrogen mineralization from light- and heavy-fraction additions to soil. Soil Biology & Biochemistry 32, 1345-1352.

Yang, X.M., Drury, C.F., Reynolds, W.D., MacTavish, D.C., 2009. Use of sonication to determine the size distributions of soil particles and organic matter. Canadian Journal of Soil Science 89, 413-419.

Zeller, B., Colin-Belgrand, M., Dambrine, E., Martin, F., 1998. N-15 partitioning and production of N-15-labelled litter in beech trees following [N-15]urea spray. Annales Des Sciences Forestieres 55, 375-383.

Zeller, B., Colin-Belgrand, M., Dambrine, E., Martin, F., 2001. Fate of nitrogen released from N-15-labeled litter in European beech forests. Tree Physiology 21, 153-162.

Zeller, B., Dambrine, E., 2011. Coarse particulate organic matter is the primary source of mineral N in the topsoil of three beech forests. Soil Biology & Biochemistry 43, 542-550.

II

Transfer of litter-derived N to soil mineral-organic associations: Evidence from decadal N-15 tracer experiments

Pierre-Joseph Hatton [a,b], Markus Kleber [b], Bernd Zeller [a], Christophe Moni [b], Alain F. Plante [c], Kimberly Townsend [b], Louisette Gelhaye [a], Kate Lajtha [d], Delphine Derrien [a*]

[a] INRA-Nancy, Biogéochimie des Ecosystemes Forestiers, 54280 Champenoux, France

[b] Department of Crop and Soil Science, Oregon State University, 97331 Corvallis, OR, USA

[c] University of Pennsylvania, Department of Earth and Environmental Science, 19104-6316 Philadelphia, PA, USA

[d] Department of Botany and Plant Pathology, Oregon State University, 97331 Corvallis, OR, USA

* Corresponding author: delphine.derrien@nancy.inra.fr

Published in *Organic Geochemistry* **42** (2012) : 1489-1501 [DOI]

Organic Geochemistry 42 (2012) 1489–1501

Contents lists available at ScienceDirect

Organic Geochemistry

journal homepage: www.elsevier.com/locate/orggeochem

Transfer of litter-derived N to soil mineral–organic associations: Evidence from decadal ^{15}N tracer experiments

Pierre-Joseph Hatton [a,b], Markus Kleber [b], Bernd Zeller [a], Christophe Moni [b], Alain F. Plante [c], Kimberly Townsend [d], Louisette Gelhaye [a], Kate Lajtha [d], Delphine Derrien [a,*]

[a] INRA, Centre de Nancy, UR 1138 Biogéochimie des Ecosystèmes Forestiers, 54280 Champenoux, France
[b] Oregon State University, Department of Crop and Soil Science, Corvallis, OR 97331, USA
[c] University of Pennsylvania, Department of Earth and Environmental Science, Philadelphia, PA 19104-6316, USA
[d] Oregon State University, Department of Botany and Plant Pathology, Corvallis, OR 97331, USA

ARTICLE INFO

Article history:
Received 10 March 2010
Received in revised form 23 March 2011
Accepted 1 May 2011
Available online 15 May 2011

ABSTRACT

Mineral–organic associations act as mediators of litter-derived N flow to the mineral soil, but the time scales and pathways involved are not well known. To close that gap, we took advantage of decade old ^{15}N litter labeling experiments conducted in two European forests. We fractionated surface soils by density with limited disaggregating treatment and investigated organic matter (OM) characteristics using $\delta^{13}C$, $\delta^{15}N$ and the *C*/*N* ratio. Mineral properties were studied by X-ray diffraction and selective dissolution of pedogenic oxides.

Three types of associations were isolated: plant debris with few trapped minerals (<1.65 g/cm^3), aggregates dominated by phyllosilicates (1.65–2.4 g/cm^3), and single mineral grains and pedogenic oxides with little OM (>2.4 g/cm^3). A small proportion of ^{15}N tracer was rapidly attached to single mineral grains, while most of it moved from plant debris to aggregates of low density and progressively to aggregates of higher density that contain a more microbially processed OM. After a decade, 60% of the ^{15}N tracer found in the investigated horizon was retained in aggregates, while plant debris still contained 40% of the tracer.

We present a conceptual model of OM and N flow through soil mineral–organic associations, which accounts for changes in density, dynamics and chemistry of the isolated structures. It suggests that microbial reworking of OM entrapped within aggregates (1.65–2.4 g/cm^3) causes the gradient of aggregate packing and, further on, controls the flow of litter-derived N through aggregates. For associations with denser material (>2.4 g/cm^3), mineralogy determines the density of the association, the type of patchy OM attached to mineral surfaces and controls the extent of litter-derived N incorporation.

© 2011 Elsevier Ltd. All rights reserved.

1. Introduction

The supply of plant-available nitrogen (N) to non-fertilized terrigenous ecosystems is thought to be controlled largely by the depolymerization and mineralization of organic N stored in litter and soil organic matter (SOM) (Schimel and Bennett, 2004). During microbial decomposition of litter in forest soils, amino acids, NH_4^+ and NO_3^- are produced. Both organic and inorganic forms of N are plant-available (Häussling et al., 1991; Schimel and Bennett, 2004; Chapman et al., 2006), but are simultaneously subject to microbial immobilization and to stabilization through sorption and the formation of mineral–organic associations. This association of organic N with minerals may be an important mechanism to preserve N in forest soils over decades to centuries. However, the pathways of N incorporation into mineral–organic associations and the extent of protection that they may experience within these associations still require investigation.

There have been many studies of the fate of N in soils using relatively high levels of either labeled or unlabeled inorganic N fertilizer. However, such studies often use unrealistic addition rates of N, which can both put soils and the microbial community into a state of disequilibrium, as well as cause changes in osmotic potential that would greatly affect soil responses. Moreover, experiments using inorganic N are not well adapted to exploring the fate of litter-derived N in non-fertilized soils. To date, few studies have used ^{15}N labeled litter, in spite of the fact that it is a sensitive tool (Zeller et al., 2000; Blumfield et al., 2004; Tonon et al., 2007; d'Annunzio et al., 2008).

* Corresponding author.
E-mail addresses: Pierre-joseph.hatton@nancy.inra.fr (P.-J. Hatton), markus.kleber@oregonstate.edu (M. Kleber), zeller@nancy.inra.fr (B. Zeller), Christophe.Moni@oregonstate.edu (C. Moni), aplante@sas.upenn.edu (A.F. Plante), Zoeykim@aol.com (K. Townsend), lgelhaye@nancy.inra.fr (L. Gelhaye), lajthak@science.oregonstate.edu (K. Lajtha), delphine.derrien@nancy.inra.fr (D. Derrien).

0146-6380/$ - see front matter © 2011 Elsevier Ltd. All rights reserved.
doi:10.1016/j.orggeochem.2011.05.002

Experiments conducted by Zeller et al. (1998, 2000, 2001) in two European forests showed that a large amount of the N released from beech leaf litter was retained as organic N in the soil. Only 2% of the litter-derived N had been taken up by trees after 4 years and 25% after 8 years (Fig. 1); whereas the rest was distributed as organic N within the top few centimetres of the soil profile (Matzner, 2004). This observation led us to hypothesize that interactions of organic N with the mineral matrix may be responsible for the high retention of N in soil.

Mineral–organic associations involve occlusion of N-organic compounds into aggregates at the micrometer scale and interactions with mineral surfaces at the nanometre scale (Jastrow, 1996; Chenu and Plante, 2006; Lehmann et al., 2007). They are believed to slow decomposition and mineralization processes by making organic materials inaccessible to decomposers (Torn et al., 1997, 2005; Mikutta et al., 2007; Kögel-Knabner et al., 2008). Mineral–organic matter interactions are known to depend on the surface chemistry of the minerals involved (Kleber et al., 2005) and on the chemical nature of the organic matter (OM) involved. Nitrogen rich microbial products appear to have a particularly high affinity for mineral surfaces (Guggenberger et al., 1994, 1999; Guggenberger and Zech, 1999; Miltner and Zech, 1998; Omoike and Chorover, 2006; Gougeon et al., 2003; Mikutta et al., 2009). Although the transformation of OM appears critical for the association with minerals and for the fate of N in soils, the extent to which the composition of the mineral matrix or the chemistry of OM constrains the dynamics of N association with minerals over the years following litterfall is not well known.

Density fractionation is a procedure that has recently become popular as a means to isolate and investigate mineral–organic associations. Traditional density fractionation methods employ disaggregating treatments, such as sonication, to allow individual mineral grains to settle according to their specific density (Baisden et al., 2002; Castanha et al., 2008; Basile-Doelsch et al., 2009; Plante et al., 2010). A few studies have employed a different option involving minimum energy inputs with the intention of avoiding aggregate disruption (Golchin et al., 1994; Sollins et al., 2006, 2009; Prior et al., 2007). When no disaggregating treatment is applied, the specific densities of the embedded mineral grains, the mineral to organic ratio and the volume of voids within the aggregate determine the density of individual mineral–organic associations. This approach treats density isolates as functional soil subunits and therefore is thought to isolate associations that are more ecologically relevant than those obtained by traditional, more disruptive techniques. The procedure is able to isolate fractions with distinct carbon (C), N, lignin phenol and isotopic compositions indicating trends in the chemistry of mineral-associated OM with increasing density (Golchin et al., 1994; Sollins et al., 2006, 2009; Prior et al., 2007). It further demonstrates mineralogical changes among density fractions and shows that rates of incorporation of ^{14}C from thermonuclear bomb testing vary among density fractions (Swanston et al., 2004; Sollins et al., 2006, 2009; Prior et al., 2007; Torn et al., 2009). Such varying rates of ^{14}C incorporation have often been interpreted as longer mean residence time in higher density fractions, but it is not known whether organic N is directly coupled to organic C and benefits from the same degree of protection in these increasingly protective mineral–organic associations. Additionally, the previous studies all tracked the bomb ^{14}C signal to infer turnover dynamics at the timescale of half a century. The focus of our work is on N, which is likely decoupled from C during OM decay, and on the decadal timescale when initial processes of mineral–organic interactions are expected to occur. In temperate ecosystems and at this early phase of decomposition, a significant proportion of plant residues is available to microbes as coarse decomposable fragments (Balesdent, 1998; Sandermann and Amundson, 2005), with potentially meaningful consequences for the formation of mineral–organic associations.

Here, we investigate the pathways of litter-derived N through various types of mineral–organic associations over the first decade following litterfall (i) to determine its dynamics of incorporation within Mineral–organic associations over time, (ii) to investigate the role of microbial transformations of mineral-associated OM for its dynamics and (iii) to assess the extent of protection of litter-derived N within mineral–organic associations. Our experimental approach was to track a cohort of litter-derived ^{15}N tracer in decadal experiments conducted in two European forests, Ebrach (Germany) and Fougères (France), on its way through operationally defined mineral–organic associations. Mineral–organic associations were isolated from the 0–2.5 cm depth horizon 4 and 12 years after label application at Ebrach and after 8 years at Fougères, using sequential density fractionation with no sonication. The degree of microbial processing of OM was investigated using the *C*/*N* ratio and the natural abundances of $\delta^{13}C$ and $\delta^{15}N$ (determined in control treatments), whereas minerals were characterized by X-ray diffraction and acid oxalate extraction. The accessibility of litter-derived ^{15}N tracer to decomposers with mineral–organic associations was quantified at Ebrach by potential net mineralization. Assuming density fractions represent ecologically meaningful soil isolates, we expected the tracer distribution to depend on the presence of reactive minerals such as pedogenic oxides and to be a function of the density of the isolated fractions.

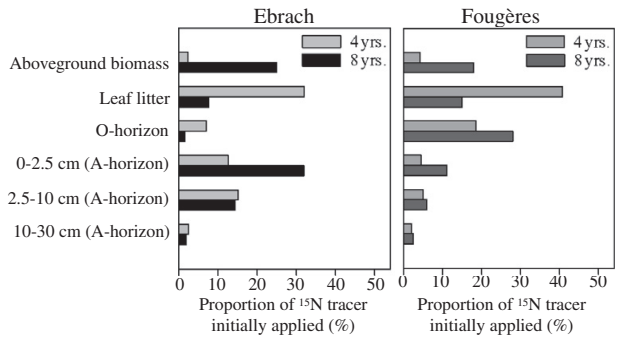

Fig. 1. Distributions of ^{15}N tracer derived from a labeled beech litter in the various compartments of the ecosystem of Ebrach and Fougères, as a function of time. The ^{15}N tracer in the above ground biomass consists of the label recovered in biomass of the tree growing close to the place where the labeled litter was deposited, and the cumulative amount of ^{15}N tracer exported in its leaves.

2. Materials and methods

2.1. Sites

Soils were collected from long term field experiments located at Ebrach (Germany, 49°52′N, 10°27′E) and Fougères (France, 48°23′N, 1°8′W) (Table 1). Both sites have been forested for centuries. At present, they consist of even aged beech forests (*Fagus sylvatica* L.). Fougères is at an elevation of 150 m above sea level and has a temperate oceanic climate with mean annual temperature of 12.9 °C and mean annual precipitation of 870 mm. The soil is an acidic (pH_{H20} = 3.8) glossalbic Cambisol (WRB, 2006) developed from sandy granitic bedrock (Vire type) covered by thick non-carbonated aeolian loam. It was fertilized in April 1973 with 150 kg P_2O_5/ha, 150 kg K_2O/ha and 1500 kg CaO/ha and in May 1973 and 1974 with 100 kg N/ha (Nys, 1998; Legout et al., 2008). The 90 year old beech stand is interspersed with few oak trees (*Quercus robur* L.) and a dense understory dominated by common ivy (*Hedera helix* L.). Ebrach is 400 m above sea level and is characterized by a temperate continental climate with a mean annual temperature of 7.5 °C and 750 mm of mean annual precipitation. The soil is an acidic (pH_{H20} = 3.9) dystric Cambisol (WRB, 2006) developed from Triassic sandstones from the upper Keuper period (Kaiser et al., 2002). The 21 year old beech stand is dense without understory vegetation (Zeller et al., 2001).

2.2. ^{15}N labeling and sample collection

At both sites, the label was applied as a single pulse of ^{15}N enriched beech litter obtained by foliar application of urea to young beech trees growing at Puvenelle forest, France (Zeller et al., 1998). In February 1996 at Ebrach and in February 2000 at Fougères, original undecomposed litters were removed and replaced by the labeled beech leaves in an amount equal to the respective mean annual leaf litter input and covered with a 2 cm mesh nylon net (Zeller et al., 2001). Thus, at Ebrach, three plots of 1 m^2 received 250 g of ^{15}N labeled litter (at 2.5 At^{15}N%; Table 1). At Fougères, three plots of 5 m^2 received 270 g of ^{15}N labeled litter per square meter (at 2.1 At^{15}N%; Table 1). Leaves shed by the tree growing on the labeled plot at the Ebrach site were collected and removed each fall to avoid ^{15}N return to soil via litterfall and to ensure the integrity of the ^{15}N pulse. Litterfall from the surrounding, unlabeled trees was permitted to ensure a constant above ground input during the time of the experiment. At Fougères, the height of the trees (25 m) made litter collection difficult, but patterns of wind dispersal of litter were determined to be such that litter return to the soil surface was negligible.

Table 1
Basic properties of Ebrach and Fougères from Legout et al. (2008), Matzner (2004) and Nys (1998). SOM = soil organic matter.

	Ebrach	Fougères
Mean annual temperature (°C)	7.9	12.9
Mean annual precipitation (mm year^{-1})	750	868
pH_{H20}	3.9	3.8
Clay (%)	14[a]	22[a]
Effective CEC (mmol kg^{-1})	87.8[a]	87[a]
Base saturation (%)	34.5[a]	26[a]
C_{soil} (mg g^{-1}_{soil})	45.9	79.5
N_{soil} (mg g^{-1}_{soil})	2.0	4.7
C/N_{soil}	23	16.8
$C_{leaf\ litter}$ (mg $g^{-1}_{leaf\ litter}$)	484	477
$N_{leaf\ litter}$ (mg $g^{-1}_{leaf\ litter}$)	8.4	9.1
$C/N_{leaf\ litter}$	52	58

[a] Values from depth 0–5 cm.

Soils were collected 4 and 12 years after tracer application at Ebrach and after 8 years at Fougères. The first 2.5 cm of the A horizon were sampled and sieved to pass 2 mm. Observable roots were removed. Soils were stored at + 4 °C. Soil moisture was measured at + 105 °C.

2.3. Isolation of mineral–organic associations

Mineral–organic associations were isolated from the top 2.5 cm of the A horizon, where most of the litter derived ^{15}N was concentrated (Fig. 1), by sequential density fractionation. We followed the method described by Sollins et al. (2006) and sequentially isolated seven density fractions: <1.65; 1.65–1.85; 1.85–2.0; 2.0–2.2; 2.2–2.4; 2.4–2.65 and >2.65 g/cm^3. As suggested by Kramer et al. (2009), we used sodium polytungstate (SPT) with a low N concentration (<0.001%) to reduce potential external ^{15}N contamination. Moist bulk soil samples were suspended in SPT solutions (1/3 soil/SPT ratio) in 175 ml polycarbonate centrifuge tubes and shaken initially for 2 h on a shaker table, before being centrifuged at a relative centrifugal force of 2560*g* in a swinging bucket rotor for 10 min. Density of the supernatant was checked using a 10 ml volumetric flask combined with a precision balance. After adjusting density to target cutoffs (±0.01 g/cm^3), floaters and supernatant were aspirated down to the pellet using a vacuum system. SPT solution adjusted to the next higher density in the sequence was then added to the remaining soil pellet, shaken for 1 h and the same procedure repeated again. The SPT was removed from the isolated fractions using deionized water. The lightest fraction was filtered (Whatman GF/F 0.7 μm particle retention) and subsequent ones were rinsed several times in polycarbonate centrifuge bottles until a density <1.01 g/cm^3 was obtained. Once well cleaned, sequentially isolated fractions were observed for physical appearance, put in pre-weighted tins and oven dried for 2 days at + 55 °C. Dried fractions were then weighed (±0.01 g) and ground with a mortar and pestle to fine powder before further analyses. All values are reported on an oven dried basis.

2.4. Structure and composition of mineral–organic associations

2.4.1. Physical appearance

Density fractions were visually observed with a stereo microscope. Aliquots were immersed in Petri dishes (ø: 4 cm) filled with deionized water. Petri dishes were gently hand shaken to check for the presence of different density phases. Visual description was performed under a range of magnifications starting from 6× to 50×. Samples were checked for recognizable organic debris, black carbon, aggregates, individual mineral particles (including oxides and concretions) and experimental artifacts such as pieces of filter fiber.

2.4.2. Organic matter

Total C, total N, $\delta^{15}N$ and $\delta^{13}C$ were determined in triplicate using a 20–20 coupled continuous flow elemental analyzer-isotope ratio mass spectrometer (EA-IRMS; PDZ Europa Ltd., Crewe, Cheshire, England). The degree of microbial processing was determined using $\delta^{13}C$, $\delta^{15}N$ and *C*/*N* values as proxies (Baisden et al., 2002). As these indicators are insufficient indicators individually (Bird et al., 2003; Kramer et al., 2003; Dijkstra et al., 2006, 2008; Huygens et al., 2008), we considered the simultaneous enrichments of $\delta^{13}C$ and $\delta^{15}N$ and the decline in the *C*/*N* ratio as an indication of an increasing microbial character of OM.

2.4.3. Mineralogy

Mineralogy of the fractions was investigated in samples from the unlabeled control plots. Oxalate extractable iron (Fe), aluminium (Al) and silica (Si) were determined according to Blakemore

et al. (1987) by shaking 1 g of soil for 4 h in the dark in 100 ml of extracting solution (mixture of ammonium oxalate and oxalic acid, 0.2 M with respect to oxalate, with proportions adjusted to give pH 3). Fe, Al and Si concentrations in the supernatant were determined by inductively coupled plasma atomic emission spectrometry (ICP-AES).

Total "free" oxides were determined by the modified Holmgren procedure (Holmgren, 1967). Fine ground soil (0.5 g) was placed in a 250 ml polypropylene bottle. Sodium citrate (50 ml 0.3 M $Na_3C_6H_5O_7 \cdot 2\ H_2O$) and 1 g of sodium dithionite ($Na_2S_2O_4$) were added and the suspension shaken for 16 h, the samples were flocculated with 0.1 M $MgSO_4$, centrifuged and the supernatant decanted. Fe, Al and Si concentrations in the supernatant were determined by ICP-AES.

Bulk mineralogy was assessed by X-ray diffraction (XRD). An aliquot (1.5 g) of soil was hand ground using mortar and pestle to a mean particle size <200 μm. Ground samples were back loaded into a 2.5 cm diameter circular cavity holder and run on a PANanalyticalX'Pert Pro Instrument using Co Kα radiation at 40 kV and 40 mA. Diffraction patterns were recorded by step scanning from 3–80° 2θ, with the sample spinning at 2 revolutions/s. Phase identification and peak area determinations were done using the X'pert High Score plus software.

2.5. Tracking N derived from leaf litter

The stable isotope of nitrogen (^{15}N) was used to trace litter-derived N. The concentration of ^{15}N derived from the labeled litter ($^{15}N_{tracer}$) was computed as follows:

$$^{15}N_{tracer} = \frac{(A^{15}N(\%)_{labeled} - A^{15}N(\%)_{control})}{100} \times N_{labeled} \quad (1)$$

where $A^{15}N(\%)_{labeled}$ and $A^{15}N(\%)_{control}$ are the abundances of the ^{15}N isotope, expressed in percent, in labeled and control plots and $N_{labeled}$ is the amount of N in the labeled plot. This equation was applied at the scale of bulk soil and of density fractions.

An indicator of litter-derived N retention (*litter-derived N retention*$_{fraction(i)}$) was computed to compare the contribution of any fraction to total ^{15}N tracer derived from the labeled leaf litter, with total soil N:

$$\textit{Litter-derived N retention}_{fraction(i)} = \frac{^{15}N_{tracer_fraction(i)} / \sum_{i<1.65}^{i>2.65} {}^{15}N_{tracer_fraction(i)}}{N_{fraction(i)} / \sum_{i<1.65}^{i>2.65} N_{fraction(i)}} \quad (2)$$

$N_{fraction(i)}$ and $^{15}N_{tracer_fraction(i)}$ stand for the concentration of N and $^{15}N_{tracer}$ in the individual fraction i.

2.6. N and ^{15}N tracer accessibility to decomposers

The accessibility of N and ^{15}N tracer to decomposers was measured at Ebrach 4 and 12 years after litter application by potential net mineralization, which is defined as the amount of inorganic N and ^{15}N tracer accumulated over 42 days of soil incubation in the laboratory (1/5 soil/air ratio; 60% water holding capacity; 20 °C; dark). After 42 days, 20 g of sieved soil samples were shaken in 100 ml of 1 M KCl for 1 h. Extracts were then analyzed for NO_3^- and NH_4^+ by continuous flow colorimetry (TRAACS, Bran and Luebbe). The ^{15}N tracer was measured in triplicate by EA-IRMS (Delta S, ThermoFinnigan, Bremen, Germany).

2.7. Recovery rates

Weighed C, N and $^{15}N_{tracer}$ concentrations were summed across all density fractions and compared to bulk soil concentration to determine C, N and $^{15}N_{tracer}$ recoveries, as reported in following equation:

$$X_{recovery} = \frac{\sum_{i<1.65}^{i>2.65} X_{fraction(i)} \times m_{fraction(i)}}{X_{bulk_soil} \times m_{bulk_soil}} \quad (3)$$

where $X_{recovery}$ represents the recovery of C, N or ^{15}N-tracer, where $X_{fraction(i)}$ and X_{bulk_soil} represent the concentration of this element in the fraction i and in the bulk soil, and where $m_{fraction(i)}$ and m_{bulk_soil} are masses of the fraction i and of bulk soil.

2.8. Statistics

Data are presented as means of three replicates with their standard errors. Comparisons between N and ^{15}N tracer distributions within density fractions were performed using a Student's t-test, after confirming normal distributions and homogeneity of variances. Distributions were considered significantly different when the probability associated with the test was <0.05.

3. Results

3.1. Structure and composition of mineral–organic associations

3.1.1. Physical appearance

Microscopic observations confirmed that the physical appearance of the same density fractions did not vary much between the Ebrach and Fougères sites. The fraction <1.65 g/cm^3 was dominated by free plant debris with minor encrustations of mineral grains. Few microscopic glass fiber filter fragments were found in this fraction but represented a negligible mass proportion. Fractions 1.65–2.4 g/cm^3 mainly contained small size aggregates (<1 mm) mixed with very few mineral grains. About 3% of items in each fraction <2.4 g/cm^3 were visually identified as charcoal. Charred particles were not observed in denser fractions. Fractions >2.4 g/cm^3 were largely composed of individual mineral grains. Brown to red colored oxides and concretions were nearly exclusively observed in fractions >2.65 g/cm^3 and accounted for less than 10% of the material.

3.1.2. Organic matter

3.1.2.1. Dry weight, total C and N. Recoveries for mass, total C and total N were computed to assess losses due to the fractionation method and to check procedural accuracy. Light microscopy and XRD were used to confirm that dried fractions were free of residual tungsten compounds, thereby confirming that residual tungsten salts did not bias recovered masses. Mass recovery was almost total for all fractionated samples (Table 2) thanks to the application of a technique with minimum energy input. Recoveries rates were 93% and 89% of total soil C, and 93% and 91% of total soil N, at Ebrach and Fougères, respectively (Table 2). No significant differences between the distributions of soil mass, total C and total N were observed at Ebrach 4 and 12 years after labeling. Dry weight strongly peaked in fraction 2.4–2.65 g/cm^3 with about 83% of total soil mass in this fraction at Ebrach and 58% at Fougères. Mass proportions in other fractions ranged from 1–10% of dry weight. Good agreement of soil mass distributions was also found between labeled and control soils (Table 2), and isolated fractions from labeled and control soils had comparable C and N concentrations (Table 2, Fig. 2). Although fractions <1.85 g/cm^3 comprised only a small proportion of total soil weight, they accounted for most of soil OM at both sites. Together they contained 64% and 61% of the total C as well as 69% and 68% of the total N at Ebrach and Fougères, respectively. Carbon and N concentrations decreased from the lightest fraction to the fraction 2.2–2.4 g/cm^3 in both sites. In both sites, C and N concentrations dropped by one order of magnitude in the fraction

Table 2
Fraction weights, total C, total N and ^{15}N tracer in sequentially isolated density fractions and bulk soil. Means and standard errors of concentrations, distributions and recoveries values are computed from three replicates, potential net mineralization for N and ^{15}N tracer under controlled conditions (20 °C, 60% WHC, 42 days) are expressed in percent of total N and ^{15}N tracer, respectively (n = 6).

Soil fractions	Control					Labeled								
	Mass	Carbon		Nitrogen		Mass	Carbon		Nitrogen		^{15}N tracer			
	% of bulk soil	mg $g^{-1}_{fraction}$	% of total C	mg $g^{-1}_{fraction}$	% of total N	% of bulk soil	mg $g^{-1}_{fraction}$	% of total C	mg $g^{-1}_{fraction}$	% of total N	g $g^{-1}_{fraction}$	% of total tracer	g $g^{-1}_{fraction}$	% of total tracer
EBRACH											4 years after labelling		12 years after labelling	
Bulk soil	100	48.1 2.6	100	2.6 0.1	100	100	36.2 16.8	100	2.2 1.0	100	0.11 0.01	100	0.25 0.02	100
Density fractions														
<1.65	4.6	386 3.7	41 0.4	18 0.2	34 0.4	4.3	378 7.6	48 1.0	16.5 0.6	37 1.2	1.48 0.07	57 2.6	2.06 0.21	41 4.2
1.65–1.85	3.8	263 2.8	22 0.2	15 0.1	22 0.1	3.3	247 10.3	24 1.0	14.3 0.7	25 1.2	1.09 0.02	22 0.4	1.82 0.17	28 2.7
1.85–2.0	3.2	210 1.8	16 0.1	13 0.0	17 0.1	2.4	191 7.3	14 0.5	12.8 0.5	17 0.7	0.65 0.01	9 0.2	1.34 0.08	15 0.9
2.0–2.2	4.0	137 5.3	13 0.5	8.5 0.3	14 0.5	2.1	122 1.0	7.7 0.1	9.1 0.2	10 0.2	0.47 0.03	6.3 0.3	0.87 0.02	8.6 0.2
2.2–2.4	3.8	38 0.4	3.2 0.0	3.3 0.0	5.0 0.1	1.7	68 1.2	3.5 0.1	6.0 0.1	5.5 0.1	0.23 0.01	2.0 0.1	0.57 0.01	4.5 0.1
2.4–2.65	80.9	0.8 0.1	1.6 0.1	0.1 0.0	3.5 0.3	83.9	0.9 0.0	2.4 0.1	0.1 0.0	5.0 0.1	0.00 0.00	3.0 0.2	0.01 0.00	2.7 0.1
>2.65	1.1	125 0.3	3.1 0.0	8.0 0.0	3.5 0.0	1.1	3.8 0.1	0.1 0.0	0.4 0.0	0.2 0.0	0.01 0.00	0.1 0.0	0.03 0.00	0.2 0.0
Recovery (%)	101.1	88.4		91.2			98.6	92.8		87.0	98.1		87.0	
Potential net mineralization										0.8 0.1		2.5 0.1		0.5 0.1
FOUGÈRES											8 years after labelling			
Bulk soil	100	84 4.8	100	4.7 0.3	100	100	87.4 15.0	100	5.0 1.0	100	0.35 0.01	100		
Density fractions														
<1.65	9.2	341 9.1	41 1.1	16.7 0.3	35 0.7	9.2	344 16.3	38 1.8	16.6 0.8	33 1.5	1.38 0.30	39 2.5		
1.65–1.85	10.5	226 5.2	31 0.7	13.4 0.3	31 0.8	11.1	206 4.1	28 0.6	11.6 0.2	28 0.5	1.00 0.08	34 3.2		
1.85–2.0	5.4	181 1.2	13 0.1	11.7 0.2	14 0.2	9.7	153 4.8	18 0.6	9.5 0.4	20 0.7	0.55 0.13	16 1.1		
2.0–2.2	6.6	108 0.3	9 0.0	7.5 0.1	11 0.1	8.4	107 4.4	11 0.5	6.8 0.4	12 0.6	0.29 0.12	7.6 3.2		
2.2–2.4	3.3	72 1.4	3.1 0.0	5.6 0.2	4.1 0.2	4.3	67 1.6	3.5 0.1	4.7 0.2	4.4 0.2	0.19 0.06	2.5 0.5		
2.4–2.65	59.3	2.3 0.4	1.8 0.3	0.3 0.0	3.1 0.5	56.6	1.2 0.3	1.1 0.2	0.2 0.0	2.0 1.5	0.01 0.01	1.0 0.2		
>2.65	3.6	3.1 0.0	0.1 0.0	0.4 0.1	0.3 0.0	2.5	5.1 0.1	0.2 0.0	0.5 0.0	0.3 1.5	0.01 0.01	0.1 0.0		
Recovery (%)	97.9	92.8		95.2		101.7	92.3		91.7		91.1			

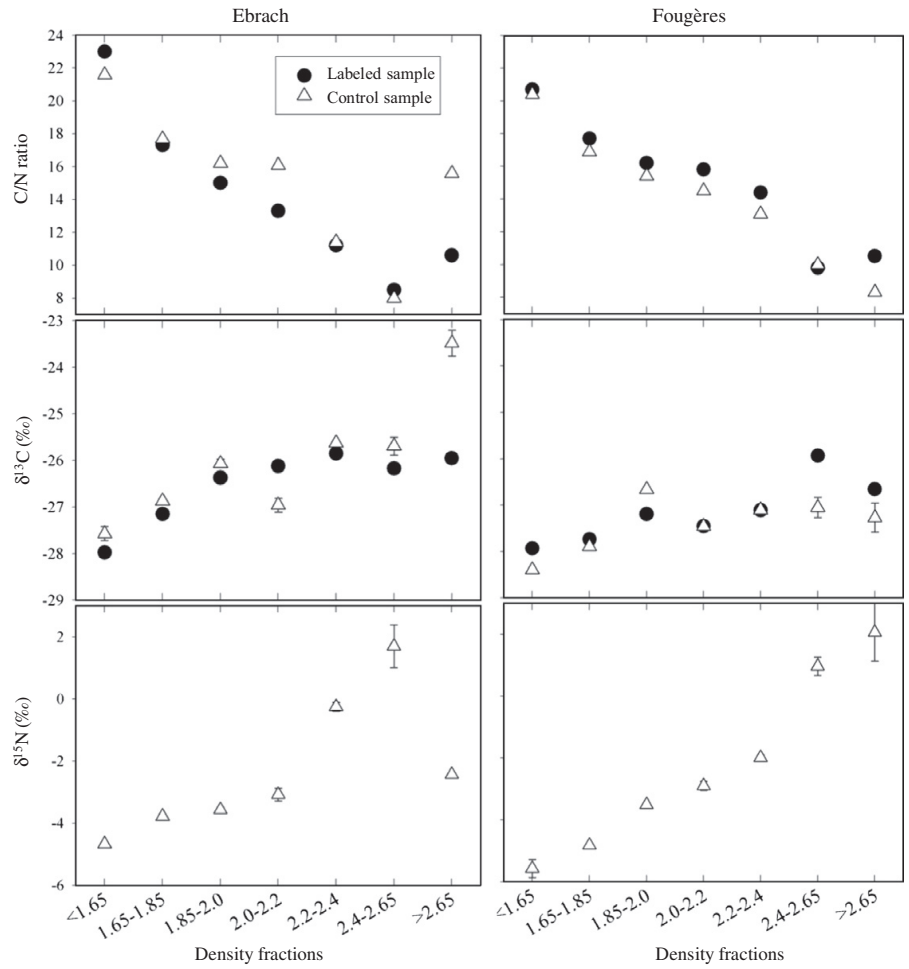

Fig. 2. Indicators of OM decomposition in sequentially isolated density fractions of Ebrach and Fougères ($n = 3$). Filled symbols represent labeled treatments, open symbols represent the controls.

2.4–2.65 g/cm^3, which comprised the bulk of soil mass. The densest fraction (>2.65 g/cm^3) exhibited concentrations in C and N similar to the fraction 2.4–2.65 g/cm^3. Two exceptions appeared in this consistent pattern between soils and treatments (Table 2), both at Ebrach. The densest fraction of the control sample contained about 30 times more C and N than the densest fractions of the Ebrach labeled treatment. Carbon and N concentrations in the fraction 2.2–2.4 g/cm^3 of the control were about half of those in the labeled treatment.

3.1.2.2. Indicators of decomposition. Isolated fractions from labeled and control soils exhibited similar patterns. *C*/*N* ratios decreased and natural abundances in ^{15}N increased with increasing density, from plant-like to microbe-like values (*C*/*N* from 23 to 8 and δ^{15}N from ca −6‰ to +2‰). The densest fraction from the Ebrach control plot did not follow this pattern and exhibited a more plant-like signature. In both sites, δ^{13}C values increased from ca. −28.4‰ to ca. −26.0‰ across the three lightest fractions, leveled off in the fraction 2.4–2.65 g/cm^3, and finally tended to slightly decrease (Fig. 2). The δ^{13}C value of the densest fraction at Ebrach control treatment was significantly enriched compared with the other samples. The simultaneous changes in the *C*/*N*, δ^{13}C and δ^{15}N values indicate that fractions 1.65–2.65 g/cm^3 contain increasingly microbially processed OM, whereas fractions denser than 2.65 g/cm^3 consist of OM of mixed origin.

3.1.3. Mineralogy

3.1.3.1. X-ray diffraction. In both soils, XRD scans can be grouped into three distinct categories (Fig. 3):

Fractions <2.4 g/cm^3 showed evidence for the presence of phyllosilicates, mainly visible through the {02, 11} and {13, 20} *hk* reflections. The signals from the *hkl* 0 0 1 refracting planes appeared to be obscured by an amorphous hump between 6° and 10° 2Θ, which is particularly strong in the two lightest fractions in both soils. While this broad feature disappeared after the first two light fractions in the Fougères fractions, it persisted throughout all the five lighter fractions at Ebrach. The major difference in phyllosilicate mineralogy between the two soils appeared to be the lack of a kaolinite peak at Ebrach while this feature can be readily observed at Fougères.

Fractions 2.4–2.6 g/cm^3 appeared to be very similar between the two soils in that they represented the maximum of alkali feld-

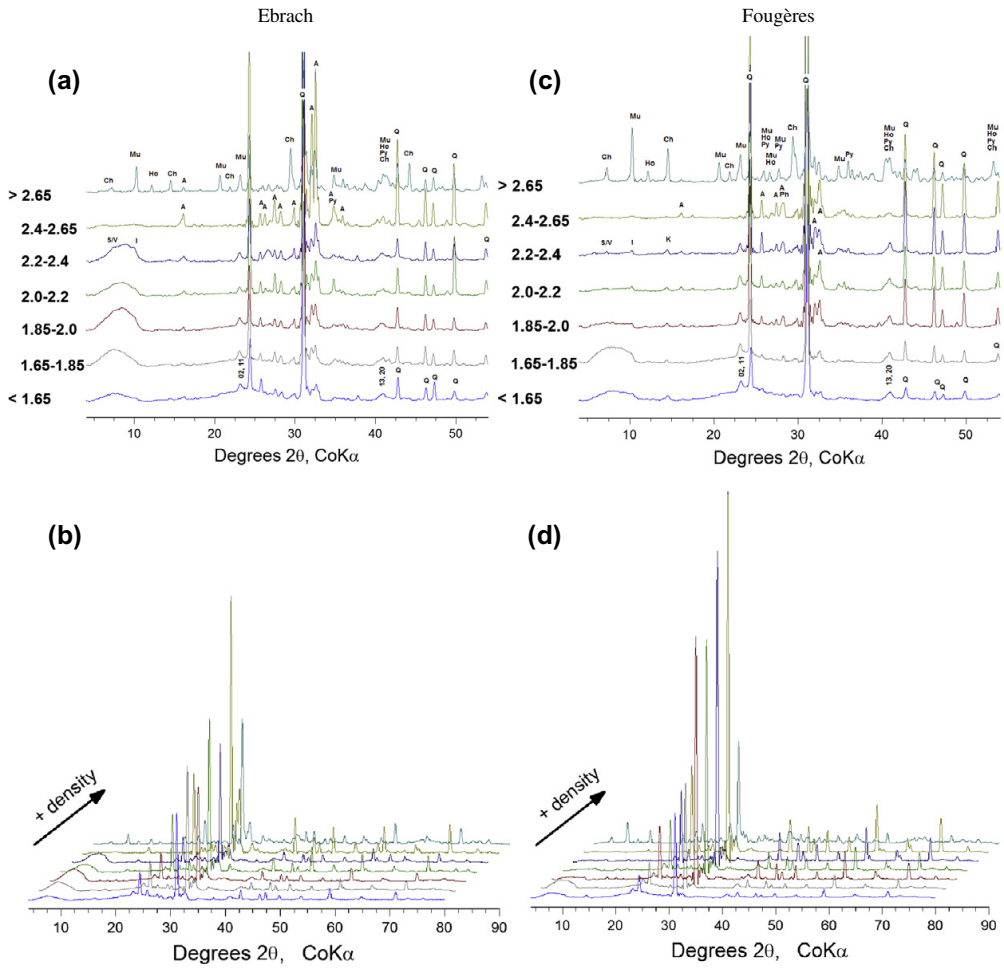

Fig. 3. XRD analysis (cobalt radiation) of sequentially isolated density fractions (g/cm^3). (a) XRD spectra of density fraction from Ebrach. A = alkali feldspar, Q = quartz, Ch = chlorite, Mu = muscovite, Ho = hornblende, Py = pyroxene, S/V smectite/vermiculite, K = kaolinite, I = illite. The (02, 11) and (13, 20) signals are hk reflections of phyllosilicates. (b) Change of signal intensity as a function of fraction density at Ebrach. Density increases with distance from *X*-axis. Peak assignments as indicated in (a). (c) XRD analysis (cobalt radiation) of density fractions (g/cm^3) from Fougères. A = alkali feldspar, Q = quartz, Ch = chlorite, Mu = muscovite, Ho = hornblende, Py = pyroxene, S/V = smectite/vermiculite, K = kaolinite, I = illite. The [02, 11}; and [3, 20} signals are hk reflections of phyllosilicates. (d) Change of signal intensity as a function of fraction density at Fougères. Density increases with distance from *X*-axis. Peak assignments as indicated in Fig. 3b.

spar (2.5–2.6 g/cm^3) signals as well as the highest quartz signal intensity (Fig. 3: Fougères d, Ebrach b). A difference between the two sets of density fractions were the lower relative intensities of quartz signals at Ebrach, possibly indicating a more advanced stage of pedogenesis at the warmer and moister Fougères site with concomitant enrichment of resistant quartz grains.

Fractions > 2.65 g/cm^3 showed the presence of chlorite (approximate density 2.6–3.4 g/cm^3), muscovite (2.8–2.9 g/cm^3) and pyroxene (3.2–3.6 g/cm^3). A significant contribution of quartz (2.65 g/cm^3) was also apparent in this fraction.

3.1.3.2. Selective dissolution of pedogenic oxides. In both soils, absolute values of poorly crystalline pedogenic oxides were well below the taxonomic reactivity threshold of 20 mg/g ($Al_o + 0.5Fe_o$) that defines soil horizons whose properties are controlled by poorly crystalline minerals (Shoji et al., 1996). When examining a metric for weathering intensity (the Fe_o/Fe_d activity ratio indicates the relative proportion of total iron oxides that can be considered poorly crystalline, Table 3), we observed a clear trend towards more unweathered minerals with increasing density in the Fougères soil but not at Ebrach, where pedogenic Fe oxides had similar activity ratios in all density fractions.

In all 14 fractions investigated, C/Fe_d ratios (w/w) were much in excess of the sorptive threshold of about 0.2 that indicates the maximum sorptive capacity of Fe oxides according to Kaiser et al. (2007) and Wagai and Mayer (2007). This leads us to infer that even in the high density, strongly mineral enriched fractions of the Fougères and Ebrach topsoils, pedogenic oxides were not controlling OM contents.

3.2. Labeled litter-derived ^{15}N: location and accessibility

^{15}N tracer provides a snapshot of the state of a single cohort of litter-derived N, whereas the bulk N is the integrated state of N from the succeeding litter-derived N inputs over time. As a consequence, differences in $^{15}N_{tracer}$ and total N distributions, expressed

Table 3
Contents of metallic elements in sequentially isolated fractions after oxalate and dithionite extractions. Dithionite extractions reveal both crystalline and poorly crystalline oxides, whereas oxalate extracts only give poorly crystalline oxides. The Fe activity ratio (Fe_o/Fe_d) indicates the relative proportion of poorly crystalline oxides. $Al_o + 0.5Fe_d$ distinguishes subtypes of andic properties in andic taxonomy. C/Fe_d describes the sorptive capacity of iron oxides.

Study sites	Density fractions	Fe_d	Al_o	Fe_o	Mn_o	Fe_o/Fe_d	$Al_o+0.5Fe_o$	C/Fe_d
			$mg.g_{fraction}^{-1}$					
Ebrach	<1.65	1.47	0.71	1.28	0.49	0.87	1.3	259.1
	1.65-1.85	2.18	0.71	1.63	0.19	0.75	1.5	117.1
	1.85-2.0	1.57	0.89	1.82	0.19	1.16	1.8	127.7
	2.0-2.2	1.51	0.45	0.83	0.16	0.55	0.9	85.7
	2.2-2.4	1.91	0.62	0.97	0.35	0.51	1.1	27.6
	2.4-2.65	0.24	0.09	0.18	0.06	0.75	0.2	3.7
	>2.65	5.33	1.07	3.47	5.07	0.65	2.8	12.1
Fougères	<1.65	4.53	2.49	4.18	0.06	0.92	4.6	75.5
	1.65-1.85	5.34	0.91	4.18	0.04	0.78	3.0	40.4
	1.85-2.0	4.48	0.68	3.72	0.03	0.83	2.5	37.3
	2.0-2.2	5.74	0.74	4.14	0.04	0.72	2.8	18.8
	2.2-2.4	4.65	0.53	3.01	0.03	0.65	2.0	15.0
	2.4-2.65	0.77	0.11	0.34	0.01	0.44	0.3	2.5
	>2.65	4.85	0.30	1.61	0.11	0.33	1.1	0.9

by the *litter-derived N retention* factor (Eq. (2)), indicate where the litter-derived N cohort is preferentially incorporated or retained over time (Fig. 4).

In both soils, the annual amount of litter-derived N represents approximately 0.4% of the total N in the observed horizons. Assuming steady state, the turnover times in these two forest soils are in the range of 250 years. A decade after litter application, the ^{15}N tracer can then be considered as a marker of young litter-derived N.

3.2.1. Ebrach

Four, 8 and 12 years after the labeled litter addition, 13%, 32% and 15% of the ^{15}N tracer initially applied as labeled litter were found in the first 2.5 cm of the A horizon (see Fig. 1 for 4 and 8 years). Recovery rates of the ^{15}N tracer after density fractionation were 98% and 87% after 4 and 12 years. The ^{15}N tracer decreased with increasing fraction density and somewhat more regularly after 12 years than after 4 years. Four years after litter application, 57% and 40% of the label was found in fractions <1.65 g/cm^3 and in fractions 1.65–2.4 g/cm^3, respectively, while this relation had reverted to 41% of the label in fractions <1.65 g/cm^3 and 56% in fractions 1.65–2.4 g/cm^3 after 12 years. This indicates that the label moved from fractions <1.65 g/cm^3 to fractions 1.65–2.4 g/cm^3. Fractions >2.4 g/cm^3 only account for a small, but stable part of litter-derived N incorporation, even though significant differences appeared in the last density fraction between the two dates.

Fig. 4 shows the extent to which the patterns of bulk N and ^{15}N distributions differed over time and informs on the state of the tracer cohort. Twelve years after litter application, the proportion of ^{15}N tracer equaled the proportion of total N in fractions 1.65–2.0 g/cm^3, while fractions 2.0–2.4 g/cm^3 contributed statistically less in ^{15}N tracer compared to total N. This indicates that the 1.65–2.0 g/cm^3 fractions incorporated litter-derived N more rapidly than the 2.0–2.4 g/cm^3 fractions. Indicators of litter-derived N retention illustrate the enrichment of fractions 1.65–2.0 g/cm^3

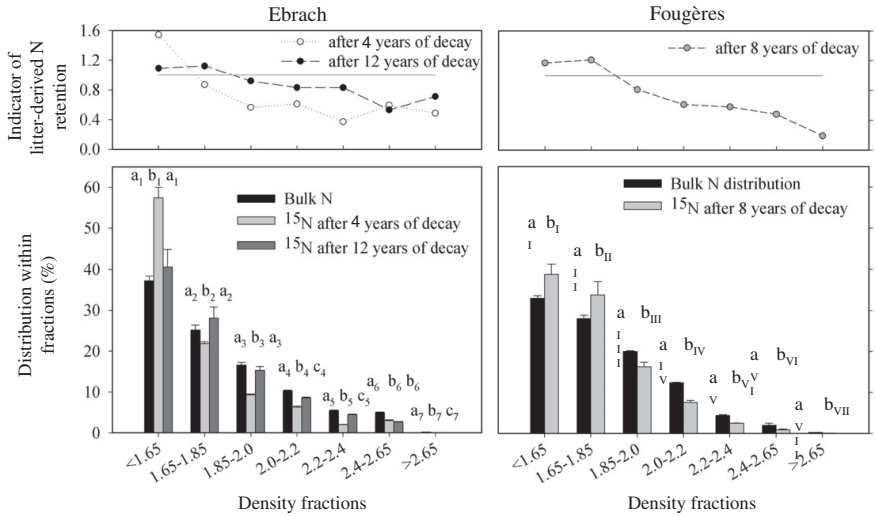

Fig. 4. Bulk N and ^{15}N tracer distributions through the sequence of density fractions at Ebrach and Fougères. Dark bars represent the bulk N and light ones the ^{15}N tracer ($n = 3$). Indicators of litter-derived N retention are defined as the proportion of tracer divided by the proportion of total N (Eq. (2)). Values above 1 signify a preferential incorporation and values below 1 signify a relative depletion in ^{15}N tracer, a, b and c represent statistical differences (t-test at 95%): two identical letters indicate that the marked distributions are equivalent, while two different letters indicate that the two distributions are different.

in ^{15}N tracer over the course of the experiment and the depletion in fractions 2.0–2.4 g/cm^3. Altogether, the comparison of ^{15}N tracer and total N revealed time lags for the tracer to enter mineral–organic associations of density 1.65–2.4 g/cm^3 within the same soil horizon.

In parallel, the potential net mineralization of the ^{15}N tracer represented 2.5% of the total ^{15}N tracer 4 years after litter application, while only 0.8% of the bulk N was mineralized (Table 2). Twelve years after litter application, the part of bulk N that has been mineralized did not vary, but the fraction of ^{15}N tracer mineralized significantly decreased, to only account for 0.5% of the total tracer found in the investigated soil horizon. This indicates that litter-derived N becomes less accessible to decomposers with time.

3.2.2. Fougères

Eight years after labeling, 11% of the total ^{15}N tracer applied as labeled litter was found in the sampled horizon (Fig. 1). Recovery rates after density fractionation for the ^{15}N tracer were comparable to the recoveries measured at Ebrach (Table 2).

The amount of ^{15}N tracer decreased with increasing fraction density in a way very similar to what was observed at Ebrach 12 years after litter application (Fig. 4). Fractions <1.65 g/cm^3 contained 39% of the label, while fractions 1.65–2.4 g/cm^3 comprised 60%. The amount of tracer found in fractions >2.4 g/cm^3 was negligible. After 8 years, the distribution of ^{15}N tracer was shifted towards the fractions with densities <1.85 g/cm^3 compared to the distribution of bulk N as revealed by the indicator of litter-derived N retention.

4. Discussion

4.1. Assignment of different density fractions to mineral–organic association types

Materials isolated at a density <1.65 g/cm^3 consist of coarse plant fragments with traces of trapped minerals. The plant debris nature of the fraction <1.65 g/cm^3 was confirmed by visual observations and isotopic patterns from both sites. *C*/*N* ratios lower than those of unaltered beech leaves (Table 1) suggested that plant debris in the lightest fractions were already affected by decay and colonized by microorganisms (Rovira and Vallejo, 2003; Derrien et al., 2006; Watteau et al., 2006; Zeller and Dambrine, 2011). Visual examination, XRD analyses and acid oxalate extraction indicated that the mineral components in this fraction consisted of trapped individual quartz and feldspar grains, some phyllosilicates and non-crystalline oxides precipitated on OM.

Microscopic observations indicated that materials with a density between 1.65 g/cm^3 and 2.4 g/cm^3 consist of OM sorbed or entrapped within microaggregates. XRD scans did not reveal much change in the composition of the mineral phase in this density region dominated by phyllosilicates. Carbon and nitrogen contents revealed that the increase in density results from the increasing contribution of minerals over organic materials. The indicators of microbial transformation indicated that the properties of mineral associated OM change from plant-like to microbial-like with increasing density, which is consistent with previous observations (Golchin et al., 1994; Prior et al., 2007; Sollins et al., 2006, 2009). Increasing contributions of adhesive microbial metabolites can be expected to influence aggregate density by forming more densely packed and less porous aggregates, as illustrated in the aggregate compartment of Fig. 5.

Visual characterization indicated that materials isolated in fractions >2.4 g/cm^3 mainly consist of single mineral grains with little OM attached. XRD and acid oxalate analyses revealed two distinct types of mineral–organic associations. The fractions 2.4–2.65 g/cm^3 consist of well crystallized primary minerals, mainly quartz and alkali feldspars, known to have a low OM binding potential (Basile-Doelsch et al., 2005, 2007). The indicators of microbial decomposition revealed microbial characteristics in the small amount of OM attached to minerals, suggesting that microbial fragments or extracellular products sustain the association between the two phases. This could be explained either by adhesive properties of microbial products or by an active attachment of microbial cells. Quartz and feldspars dominated fractions >2.65 g/cm^3, but more reactive minerals were also found. These reactive minerals consisted of iron-containing mafic minerals, concretions of pedogenic oxides and some admixtures of felsic primary minerals partially covered by oxide coatings. (Felsic is a term used to refer to silicate minerals enriched in the lighter elements such as oxygen, aluminium, sodium and potassium; mafic is an adjective describing silicate minerals rich in magnesium and iron.) Organic matter properties in this fraction were less indicative of microbial processing, suggesting that organic materials interact with the mineral surfaces regardless of their plant or microbial origin. This could result from either the strong sorptive capacities of hydroxylated oxide surfaces or the cementing effects of oxide concretions.

Overall, the relatively gentle nature of the separation process also preserves microaggregates from disruption, suggesting that the relative proportions of particulate organic debris in the lighter fractions and single mineral grains in denser fractions are not artificially increased (Kaiser and Guggenberger, 2007; Castanha et al., 2008; Wagai et al., 2009; Wilson et al., 2009).

4.2. Dynamics of N transfer through time and space

Earlier results published by Zeller et al. (2000) showed that ^{15}N tracer losses from labeled leaf litters were correlated to litter mass loss, and that incorporation of litter-derived N into the bulk mineral soil is initially delayed until faunal activity in the O horizon has modified litter materials in a way that they are able to cross a mobility threshold. In this study, we observed that, after a decade, most of the litter-derived N had left the O horizon and had either migrated to deeper soil depths or been reincorporated by the vegetation (Fig. 1). Still, a relatively large proportion of the litter-derived N was retained in the thin layer of mineral soil immediately adjacent to the O horizon.

In the 0–2.5 cm depth layer, tracing of the ^{15}N label indicated that most of the litter-derived N enters mineral soil as plant fragments and, over the years, moves from plant debris to aggregates during the first decade after litterfall.

After a decade, plant debris still contains a considerable amount of litter-derived N (~40%), but most of the label has moved into aggregates (~60%); from aggregates of low density (1.65–2.0 g/cm^3) to aggregates of higher density (2.0–2.4 g/cm^3) that contain a more microbially processed OM. Because our investigations did not reveal much change in the mineral composition, the stage of microbial transformation of occluded OM and the aggregate porosity appeared as the most significant factors constraining the dynamics of N association with aggregates.

With little litter-derived N incorporated over the course of the experiment, single mineral grains did not appear to be quantitatively important for the retention of litter-derived N. However, their levels of incorporation remained somewhat constant, suggesting that litter-derived N was quickly attached and efficiently retained or actively replaced. This leads us to suggest that litter-derived N is adsorbed by reactive mineral surfaces that are specific to dense minerals. Those mineral surfaces could stabilize the pulse of soluble small labeled organic compounds and mineral $^{15}NH_4^+$ that is released during the initial phase of litter breakdown.

In parallel to the progressive association of litter to minerals, assessments of net mineralization revealed that litter becomes less

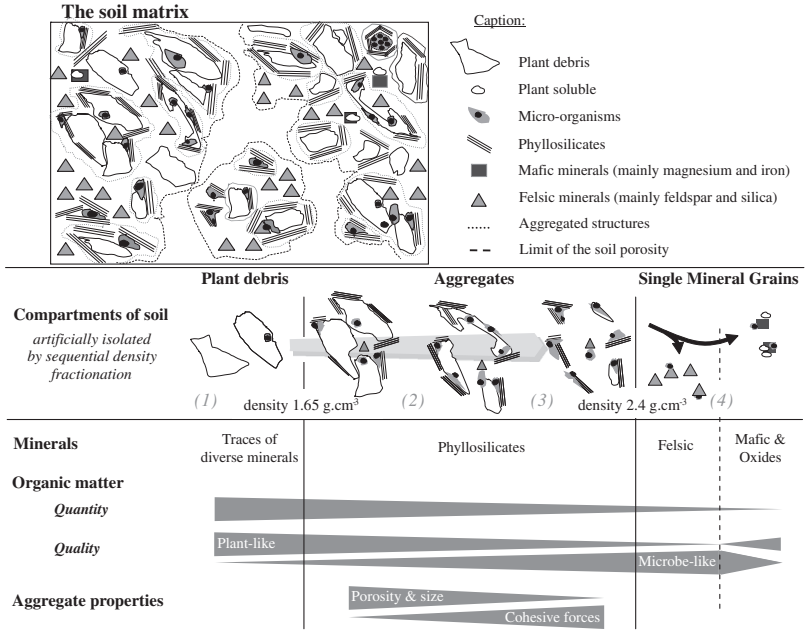

Fig. 5. Conceptual model relating properties of mineral–organic associations to their density and illustrating how these properties control the distribution of ^{15}N tracer derived from a leaf litter in the various associations a decade after application. (1) Plant fragments enter the soil as plant debris that are progressively decomposed and incorporated into aggregates. The aggregate compartment contains an illustration of change in density induced by transformation of the OM entrapped in the aggregate over time. (2) During decomposition the mineralization and transformation of the occluded plant material into microbial metabolites eventually causes the disintegration of the low density aggregate. (3) The released smaller aggregates are tight associations between microbial OM and mineral particles. They consequently exhibit a higher proportion of mineral materials and a lower proportion of pores, which progressively elevates the density of the resulting microaggregate compared to the source aggregate. (4) Single mineral grains with little OM attached composed the densest fractions. Felsic minerals are coated with microbial OM; mafic primary minerals and pedogenic oxides adsorb OM independently of their plant or microbial origin via their hydroxylated surfaces. Felsic is a term used to refer to silicate minerals enriched in the lighter elements such as oxygen, aluminium, sodium and potassium; mafic is an adjective describing silicate minerals enriched in magnesium and iron.

accessible to decomposers. This may suggest that mineral–organic associations efficiently protect litter-derived N from microbial activity.

The patterns of tracer distribution did not vary much between the Ebrach and Fougères sites, 12 and 8 years after litter application, respectively, although they are different soils with contrasted structures, bedrock and OM composition, developed under different climatic conditions. This suggests that litter-derived N follows the same pathways in two different European forested sites. We can therefore expect that the pathways of litter-derived N, which we observed in our soils, may be generalized for temperate soils that evolved under a similar weathering regime. As the duration of the experiment was longer at Ebrach than at Fougères, and as litter-derived N mean residence time is shorter at Ebrach than at Fougères (2.78 years versus 3.45 years) (Zeller et al., 2000; d'Annunzio et al., 2008), we expected the decomposition of the labeled litter to be at a less advanced stage at Fougères than at Ebrach. The comparison of the indicators of litter-derived N retention (Eq. (2), Fig. 4), which allows for a more direct account of the tracer distribution, reveals slight differences. Aggregates of high density (2.0–2.4 g/cm^3) isolated at Fougères were depleted in ^{15}N tracer compared to what was observed at Ebrach. This further supports the assumption that the extent of OM decay is a major factor controlling interaction between OM and minerals into aggregated structures.

Finally, the present study demonstrated time lags for the transfer of litter-derived N from organic to mineral layers of the soil (vertical delays, Fig. 1) and from plant debris to mineral–organic associations (horizontal delays, Fig. 4). These time lags could explain the delayed responses previously observed in ecological processes (Dörr et al., 2010). Moreover, litter-derived N cannot come in contact with occluded surfaces, which induces a spatial heterogeneity of litter-derived N localization through soil microstructures. Time lags and spatial heterogeneity prevent the accurate calculation of mean residence times of litter-derived N in density fractions (Derrien and Amelung, 2011).

4.3. Conceptual model of OM and N flow through soil mineral–organic associations

Soil is a structured natural body where organic and mineral phases are intimately associated in dynamic aggregates of various sizes, forming an interconnected fabric (Fig. 5). Any attempt to describe the flux of N or C from surface litters into the mineral soil must therefore account for the fact that decomposing OM will continuously be incorporated into and released from dynamic mineral–organic associations, especially in the biologically active topsoil. We propose here a conceptual model describing the time dependent dynamics of litter-derived N incorporation into the structural elements of mineral soil. We postulate that physicochemical properties of mineral–organic associations isolated by density fractionation explain the dynamics of litter-derived N through the density sequence.

4.3.1. Determinants for initial interaction of litter-derived components with mineral particles

When litter decays over time and is increasingly processed by decomposers, litter-derived components become associated with

minerals, and so become incorporated into fractions >1.65 g/cm^3. We distinguish between three mechanisms for the incorporation of litter-derived compounds into associations with abiotic soil constituents: (i) incorporation by entering the aggregate structures through natural pores, (ii) sorptive interactions of small mobile compounds (soluble molecules and nutrients like NH_4^+) with any responsive surface and (iii) associations that are created in the course of aggregate turnover and recombination by decomposers. In the following passages we discuss potential controls on each of the proposed mechanisms of OM-aggregate interaction, especially how the intensity of each mechanism may change over time and how the parameters controlling interactions are also responsible for the density of the mineral–organic associations in which the litter material is finally retained.

As decomposition proceeds, plant debris is broken down into smaller pieces by the macro- and microfauna. Smaller compounds are progressively produced, enabling the incorporation into the pore system of aggregates (Smucker et al., 2007). Amphiphilic molecular size fragments or NH_4^+ released towards the end of the decomposition chain are highly mobile and may penetrate the pore systems of aggregates but also engage in sorptive interactions with suitable and accessible mineral surfaces.

Litter-derived material may also become incorporated into some newly formed aggregates due to decomposer action promoting aggregate breakdown and formation. The probability of an aggregate to be broken down partly depends on the nature of the occluded OM (Oades and Waters, 1991; Christensen, 2001; Plante and McGill, 2002; de Gryze et al., 2006). For example, associations between adhesive microbial products and minerals (isolated in aggregates of high densities) are thought to be bound by stronger forces than associations between hydrophobic plant materials and mineral particles (aggregates of low densities). This would render plant material rich aggregates more susceptible to physical disruption (de Gryze et al., 2006). As a result, the free plant material has a greater probability to be recombined with some components originating from plant aggregates than with components derived from an aggregate dominated by microbial metabolites.

4.3.2. Transfer of litter-derived components from low density aggregates into high density aggregates as a consequence of progressive OM decay

Over time, decomposition of litter residues occluded in aggregates impacts the density of the mineral–organic association in two ways. It causes a decline in the proportion of unaltered, low density plant material entrapped in aggregates (Table 2), thereby increasing overall aggregate density (Oades and Waters, 1991; Golchin et al., 1994; Six et al., 2002). Concomitantly, the macroscopic structure of plant debris eventually breaks apart, causing the disintegration of the aggregate. At the same time, there is a production of microbial metabolites and their subsequent deposition on mineral particles in mineral–organic contact zones (Fig. 5, aggregate compartment). The released smaller fragments of the original aggregate are tight associations between microbial OM and mineral particles and consequently show a high proportion of mineral materials and a low proportion of pores. This renders them denser than their precursors and elevates the resulting microaggregate density into the higher range of aggregate density.

5. Conclusions

We posit that our investigations of the pathways of labeled litter-derived N from the organic surface horizon to mineral–organic associations over a decade closed a gap between short term laboratory and field investigations of bomb derived ^{14}C abundance. Specifically, we showed that:

- Sequential density fractionation without sonication isolates mineral–organic associations that differ in their physico-chemical properties and dynamics of litter-derived N incorporation. Because of the presence of aggregated structures, this method cannot be considered as a peeling off of organic layers of different composition as proposed by Sollins et al. (2006, 2009), but is better seen as a means to separate soil microstructures with distinct structural and functional properties. This means that the multilayer model for the nanoscale arrangement of organic molecules on mineral surfaces (Kleber et al., 2007) is not suited to interpret the features and properties of the much larger, micron-sized aggregated structures in density fractions.
- A small proportion of the litter-derived N rapidly comes in association with single mineral particles. Most decaying plant residues enter the soil as coarse fragments, then pass through aggregates of low density and through aggregates of progressively higher density that contain OM in an increasingly microbially-processed state. Exceptions are soluble compounds, which can theoretically come in direct contact with all porous soil structures. The progression from plant debris to aggregates induces increasing time lags prior to N reaching the dense mineral–organic associations and, in turn, partly explains why such a large amount of ^{15}N tracer is still found in the first 2.5 cm of the two studied forest mineral soils a decade after application.
- Litter-derived N is increasingly protected from decomposition during the first decade of litter decay. The pattern of label incorporation suggests that mineral–organic associations mediate the retention and flow of litter-derived N through the soil system.

Acknowledgements

This work was financially supported by Oregon State University, Department of Crop and Soil Science and Subsurface Biosphere Initiative start-up funds (M.K.), the Institut National de la Recherche Agronomique (INRA-EFPA) and the Région Lorraine. We are grateful to the reviewers and the editor for constructive comments and suggestions that significantly improved the manuscript. We are also indebted to Jennifer Parke (OSU, Department of Crop and Soil Science) for access to her microscopy equipment, Rocky Yarwood (OSU, Department of Crop and Soil Science) and Christian Hossan (INRA, Plateau Technique d'Ecologie Fonctionnelle) who performed stable isotope analyses, Tim Teague (UC Berkeley) who provided access to and helped with XRD analysis, Sarah Fay and Elizabeth Brewer for discussions and help in the laboratory.

References

Baisden, W.T., Amundson, R., Cook, A.C., Brenner, D.L., 2002. Turnover and storage of C and N in five density fractions from California annual grassland surface soils. Global Biogeochemical Cycles 16, 1117.

Balesdent, J., 1998. Analysis of soil organic matter dynamics using carbon isotopes. Cahiers Agricultures 7, 201–206.

Basile-Doelsch, I., Amundson, R., Stone, W.E.E., Masiello, C.A., Bottero, J.Y., Colin, F., Masin, F., Borschneck, D., Meunier, J.D., 2005. Mineralogical control of organic carbon dynamics in a volcanic ash soil on La Reunion. European Journal of Soil Science 56, 689–703.

Basile-Doelsch, I., Amundson, R., Stone, W.E.E., Borschneck, D., Bottero, J.Y., Moustier, S., Masin, F., Colin, F., 2007. Mineral control of carbon pools in a volcanic soil horizon. Geoderma 137, 477–489.

Basile-Doelsch, I., Brun, T., Borschneck, D., Masion, A., Marol, C., Balesdent, J., 2009. Effect of landuse on organic matter stabilized in organomineral complexes: a study combining density fractionation, mineralogy and delta C-13. Geoderma 151, 77–86.

Bird, J.A., van Kessel, C., Horwath, W.R., 2003. Stabilization of C-13-carbon and immobilization of N-15-nitrogen from rice straw in humic fractions. Soil Science Society of America Journal 67, 806–816.

Blakemore, L.C., Searle, P.L., Daly, B.K., 1987. Methods for chemical analysis of soils. New Zealand Soil Bureau Scientific Report 80, Lower Hutt, 10A, pp. 103.

Blumfield, T.J., Xu, Z.H., Mathers, N.J., Saffigna, P.G., 2004. Decomposition of nitrogen-15 labelled hoop pine harvest residues in subtropical Australia. Soil Science Society of America Journal 68, 1757–1761.

Castanha, C., Trumbore, S., Amundson, R., 2008. Methods of separating soil carbon pools affect the chemistry and turnover time of isolated fractions. Radiocarbon 50, 83–97.

Chapman, S.K., Langley, J.A., Hart, S.C., Koch, G.W., 2006. Plants actively control nitrogen cycling: uncorking the microbial bottleneck. New Phytologist 169, 27–34.

Chenu, C., Plante, A.F., 2006. Clay-sized organo-mineral complexes in a cultivation chronosequence: revisiting the concept of the 'primary organo-mineral complex'. European Journal of Soil Science 57, 596–607.

Christensen, B.T., 2001. Physical fractionation of soil and structural and functional complexity in organic matter turnover. European Journal of Soil Science 52, 345–353.

d'Annunzio, R., Zeller, B., Nicolas, M., Dhôte, J.F., Saint-André, L., 2008. Decomposition of European beech (*Fagus sylvatica* L.) litter: combining quality theory and 15N labelling experiments. Soil Biology & Biochemistry 40, 322–333.

de Gryze, S., Jassogne, L., Six, J., Bossuyt, H., Wevers, M., Merckx, R., 2006. Pore structure changes during decomposition of fresh residue: X-ray tomography analyses. Geoderma 134, 82–96.

Derrien, D., Marol, C., Balabane, M., Balesdent, J., 2006. The turnover of carbohydrate carbon in a cultivated soil estimated by ^{13}C natural abundances. European Journal of Soil Science 57, 547–557.

Derrien, D., Amelung, W., 2011. Computing mean residence time of soil carbon fractions using stable isotopes: impacts of the model framework. European Journal of Soil Science 62, 237–252.

Dijkstra, P., Ishizu, A., Doucett, R.R., Hart, S.C., Schwartz, E., Menyailo, O.V., A, H.B., 2006. 13C and 15N natural abundance of the soil microbial biomass. Soil Biology & Biochemistry 38, 3257–3266.

Dijkstra, P., LaViolette, C.M., Coyle, J.S., Doucett, R.R., Schwartz, E., Hart, S.C., A, H.B., 2008. N-15 enrichment as an integrator of the effects of C and N on microbial metabolism and ecosystem function. Ecology Letters 11, 389–397.

Dörr, N., Kaiser, K., Mikutta, R., Guggenberger, G., 2010. Slow response of soil organic matter to the reduction in atmospheric nitrogen deposition in a Norway spruce forest. Global Change Biology 16, 2990–3003.

Golchin, A., Oades, J.M., Skjemstad, J.O., Clarke, P., 1994. Study of free and occluded particulate organic matter in soils by solid-state C-13 CP/MAS NMR-spectrometry and scanning electron microscopy. Australian Journal of Soil Research 32, 285–309.

Gougeon, W.D., Soulard, M., Reinholdt, M., Miehe-Brendle, J., Chezeau, J.M., Le Dred, R., Marchal, R., Jeandet, P., 2003. Polypeptide adsorption on a synthetic montmorillonite: a combined solid-state NMR spectroscopy, X-ray diffraction, thermal analysis and N-2 adsorption study. European Journal of Inorganic Chemistry 7, 1366–1372.

Guggenberger, G., Frey, S.D., Six, J., Paustian, K., Elliott, E.T., 1999. Bacterial and fungal cell-wall residues in conventional and no-tillage agroecosystems. Soil Science Society of America Journal 63, 1188–1198.

Guggenberger, G., Zech, W., 1999. Soil organic matter composition under primary forest, pasture, and secondary forest succession, Region Huetar Norte, Costa Rica. Forest Ecology and Management 124, 93–104.

Guggenberger, G., Zech, W., Schulten, H.R., 1994. Formation and mobilization pathways of dissolved organic matter – evidence from chemical structural studies of organic matter fractions in acid forest floor solutions. Organic Geochemistry 21, 51–66.

Häussling, M., George, E., Lorenz, K., Kreutzer, K., Marschner, H., 1991. Einfluss von saurer Beregnung auf Wachstum von Lang-wurzeln und pH-Werte in der Rhizosphäre von Fichten im Versuch Höglwald. Forstliche Wissenschaftliches Forschung 39, 44–48.

Holmgren, G.G.S., 1967. A rapid citrate and dithionite extractable iron procedure. Proceedings-Soil Science Society of America 31, 210–211.

Huygens, D., Denef, K., Vandeweyer, R., Godoy, R., Van Cleemput, O., Boeckx, P., 2008. Do nitrogen isotope patterns reflect microbial colonization of soil organic matter fractions. Biology and Fertility of Soils 44, 955–964.

Jastrow, J.D., 1996. Soil aggregate formation and the accrual of particulate and mineral-associated organic matter. Soil Biology & Biochemistry 28, 665–676.

Kaiser, K., Eusterhues, K., Rumpel, C., Guggenberger, G., Kogel-Knabner, I., 2002. Stabilization of organic matter by soil minerals – investigations of density and particle-size fractions from two acid forest soils. Journal of Plant Nutrition and Soil Science-Zeitschrift Fur Pflanzenernahrung Und Bodenkunde 165, 451–459.

Kaiser, K., Guggenberger, G., 2007. Distribution of hydrous aluminium and iron over density fractions depends on organic matter load and ultrasonic dispersion. Geoderma 140, 140–146.

Kaiser, K., Mikutta, R., Guggenberger, G., 2007. Increased stability of organic matter sorbed to ferrihydrite and goethite on aging. Soil Science Society of America Journal 71, 711–719.

Kleber, M., Mikutta, R., Torn, M.S., Jahn, R., 2005. Poorly crystalline mineral phases protect organic matter in acid subsoil horizons. European Journal of Soil Science 56, 717–725.

Kleber, M., Sollins, P., Sutton, R., 2007. A conceptual model of organo-mineral interactions in soils: self-assembly of organic molecular fragments into zonal structures on mineral surfaces. Biogeochemistry 85, 9–24.

Koegel-Knabner, I., Guggenberger, G., Kleber, M., Kandeler, E., Kalbitz, K., Scheu, S., Eusterhues, K., Leinweber, P., 2008. Organo-mineral associations in temperate soils: Integrating biology, mineralogy, and organic matter chemistry. Journal of Plant Nutrition and Soil Science-Zeitschrift Fur Pflanzenernahrung Und Bodenkunde 171, 61–82.

Kramer, M.G., Lajtha, K., Thomas, G., Sollins, P., 2009. Contamination effects on soil density fractions from high N or C content sodium polytungstate. Biogeochemistry 92, 177–181.

Kramer, M.G., Sollins, P., Sletten, R.S., Swart, P.K., 2003. N isotope fractionation and measures of organic matter alteration during decomposition. Ecology 84, 2021–2025.

Legout, A., Walter, C., Nys, C., 2008. Spatial variability of nutrient stocks in the humus and soils of a forest massif (Fougères, France). Annals of Forest Science 65, 1–10.

Lehmann, J., Kinyangi, J., Solomon, D., 2007. Organic matter stabilization in soil microaggregates: implications from spatial heterogeneity of organic carbon contents and carbon forms. Biogeochemistry 85, 45–57.

Matzner, E., 2004. Biogeochemistry of forested catchments in a changing environment. Ecological Studies, vol. 172. Springer, Berlin, pp. 498.

Mikutta, R., Mikutta, C., Kalbitz, K., Scheel, T., Kaiser, K., Jahn, R., 2007. Biodegradation of forest floor organic matter bound to minerals via different binding mechanisms. Geochimica et Cosmochimica Acta 71, 2569–2590.

Mikutta, R., Schaumann, G.E., Gildemeister, D., Bonneville, S., Kramer, M.G., Chorover, J., Chadwick, O.A., Guggenberger, G., 2009. Biogeochemistry of mineral-organic associations across a long-term mineralogical soil gradient (0.3–4100 kyr), Hawaiian Islands. Geochimica et Cosmochimica Acta 73, 2034–2060.

Miltner, A., Zech, W., 1998. Beech leaf litter lignin degradation and transformation as influenced by mineral phases. Organic Geochemistry 28, 457–463.

Nys, C., 1998. Gestion durable de la fertilité de l'écosystème hêtraie acidiphile de basse altitude. In: Ecofor, G. (Ed.), Programme "Hêtraie de basse altitude", 3. INRA de Nancy, Nancy.

Oades, J.M., Waters, A.G., 1991. Aggregate hierarchy in soils. Australian Journal of Soil Research 29, 815–828.

Omoike, A., Chorover, J., 2006. Adsorption to goethite of extracellular polymeric substances from *Bacillus subtilis*. Geochimica et Cosmochimica Acta 70, 827–838.

Plante, A.F., Virto, I., Malhi, S.S., 2010. Pedogenic, mineralogical and land-usecontrols on organic carbon stabilization in two contrasting soils. Canadian Journal of Soil Science 90, 5–26.

Plante, A.F., McGill, W.B., 2002. Soil aggregate dynamics and the retention of organic matter in laboratory-incubated soil with differing simulated tillage frequencies. Soil & Tillage Research 66, 79–92.

Prior, C.A., Baisden, W.T., Bruhn, F., Neff, J.C., 2007. Using a soil chronosequence to identify soil fractions for understanding and modeling soil carbon dynamics in New Zealand. Radiocarbon 49, 1093–1102.

Rovira, P., Vallejo, V.R., 2003. Physical protection and biochemical quality of organic matter in Mediterranean calcareous forest soils: a density fractionation approach. Soil Biology & Biochemistry 35, 245–261.

Sandermann, J., Amundson, R., 2005. Biogeochemistry of decomposition and detrital processing. In: Schlesinger, H.D. (Ed.), Biogeochemistry. Elsevier, Amsterdam, pp. 249–316.

Schimel, J.P., Bennett, J., 2004. Nitrogen mineralization: Challenges of a changing paradigm. Ecology 85, 591–602.

Shoji, S., Nanzyo, M., Dahlgren, R.A., Quantin, P., 1996. Evaluation and proposed revisions of criteria for andosols in the world reference base for soil resources. Soil Science 161, 604–615.

Six, J., Feller, C., Denef, K., Ogle, S.M., Sa, J.C.D., Albrecht, A., 2002. Soil organic matter, biota and aggregation in temperate and tropical soils – effects of no-tillage. Agronomie 22, 755–775.

Smucker, A.J.M., Park, E.-J., Dorner, J., Horn, R., 2007. Soil micropore development and contributions to soluble carbon transport within macroaggregates. Vadose Zone Journal 6, 282–290.

Sollins, P., Kramer, M.G., Swanston, C., Lajtha, K., Filley, T., Aufdenkampe, A.K., Wagai, R., Bowden, R.D., 2009. Sequential density fractionation across soils of contrasting mineralogy: evidence for both microbial- and mineral-controlled soil organic matter stabilization. Biogeochemistry 96, 209–231.

Sollins, P., Swanston, C., Kleber, M., Filley, T., Kramer, M., Crow, S., Caldwell, B.A., Lajtha, K., Bowden, R., 2006. Organic C and N stabilization in a forest soil: evidence from sequential density fractionation. Soil Biology & Biochemistry 38, 3313–3324.

Swanston, C., Homann, P.S., Caldwell, B.A., Myrold, D.D., Ganio, L., Sollins, P., 2004. Long-term effects of elevated nitrogen on forest soil organic matter stability. Biogeochemistry 70, 227–250.

Tonon, G., Ciavatta, C., Solimando, D., Gioacchini, P., Tagliavini, M., 2007. Fate of N-15 derived from soil decomposition of abscised leaves and pruning wood from apple (Malusdomestica) trees. Soil Science and Plant Nutrition 53, 78–85.

Torn, M.S., Swanston, C., Trumbore, S., 2009. Storage and turnover of organic matter in soil. In: Senesi, N., Xing, B., Huang, P.M. (Eds.), Biophysico-Chemical Processes Involving Natural Non-living Organic Matter in Environmental Systems. Wiley and Sons Inc.

Torn, M.S., Trumbore, S.E., Chadwick, O.A., Vitousek, P.M., Hendricks, D.M., 1997. Mineral control of soil organic carbon storage and turnover. Nature 389, 170–173.

Torn, M.S., Vitousek, P.M., Trumbore, S.E., 2005. The influence of nutrient availability on soil organic matter turnover estimated by incubations and radiocarbon modeling. Ecosystems 8, 352–372.

Wagai, R., Mayer, L.M., 2007. Sorptive stabilization of organic matter in soils by hydrous iron oxides. Geochimica et Cosmochimica Acta 71 (1), 25–35.

Wagai, R., Mayer, L.M., Kitayama, K., 2009. Extent and nature of organic coverage of soil mineral surfaces assessed by a gas sorption approach. Geoderma 149, 152–160.

Watteau, F., Villemin, G., Burtin, G., Jocteur-Monrozier, L., 2006. Root impact on the stability and types of micro-aggregates in silty soil under maize. European Journal of Soil Science 57, 247–257.
Wilson, G.W.T., Rice, C.W., Rillig, M.C., Springer, A., Hartnett, D.C., 2009. Soil aggregation and carbon sequestration are tightly correlated with the abundance of arbuscular mycorrhizal fungi: results from long-term field experiments. Ecology Letters 12, 452–461.
Zeller, B., Colin-Belgrand, M., Dambrine, E., Martin, F., 1998. N-15 partitioning and production of N-15-labelled litter in beech trees following [N-15] urea spray. Annales Des Sciences Forestieres 55, 375–383.
Zeller, B., Colin-Belgrand, M., Dambrine, E., Martin, F., 2001. Fate of nitrogen from 15N-labelled litter in European beech forests. Tree Physiology 21, 153–162.
Zeller, B., Colin-Belgrand, M., Dambrine, E., Martin, F., Bottner, P., 2000. Decomposition of N-15-labelled beech litter and fate of nitrogen derived from litter in a beech forest. Oecologia 123, 550–559.
Zeller, B., Dambrine, E., 2011. Coarse particulate organic matter is the primary source of mineral N in the topsoil of three beech forests. Soil Biology and Biochemistry 43, 542–550.

III

Flows of leaf litter-derived C and N through density-isolated soil organo-mineral associations

Pierre-Joseph Hatton [a]*, Bernd Zeller [a], Laurent Remusat [b], Séverine Boiry [c], Delphine Derrien [a]

[a] INRA-Nancy, Biogéochimie des Ecosystemes Forestiers, 54280 Champenoux, France

[b] Laboratoire de Minéralogie et Cosmochimie du Muséum, UMR 7202 CNRS/MNHN, Muséum National d'Histoire Naturelle, case postale 52, 57 rue Cuvier, 75231 Paris Cedex 05, France

[c] CEA Cadarache, DEVM, Groupe de Recherches Appliquées en Phytotechnologie, Saint-Paul-les-Durance F-13108, France.

* Corresponding author: pierre-joseph.hatton@nancy.inra.fr

Short communication in prep. for *Biogeochemistry*

Abstract
We captured the transfers of $^{13}C^{15}N$ beech leaf fragments through density-isolated soil organo-mineral associations over a year of laboratory incubation. Although there was more residual $^{15}N_{tracer}$ than $^{13}C_{tracer}$, their distributions and kinetics were similar. They both moved from plant debris to aggregates and, to a lesser extent, mineral grains. This indicates that our previously published conceptual model for litter-N flows through density-isolated soil organo-mineral associations also applies for litter-C. $^{13}C_{tracer}/^{15}N_{tracer}$ revealed patterns that were invisible at the fraction-scale, indicative of the fine-scale partitioning of microbial activities with an increasing $^{15}N_{tracer}$ immobilization in aggregates of increasing density and a clear $^{13}C_{tracer}$ accumulation in mineral grains. These fine-scale discrepancies further indicate that density fractions physically isolated contrasted microbial activities along with changes in soil organo-mineral structure.

Keywords
Soil organic matter/ $^{13}C^{15}N$/ density fraction /leaf/ dynamic/ transfer

Manuscript
Forest soils receive significant amounts of organic matter (OM) via leaf litters (Zeller et al. 2000). Most of these inputs are rapidly lost by the soil system via mineralization, but a small fraction gets stabilized for longer period of time and accumulates over the years in organo-mineral assemblages to finally account for 60% to 90% of soil carbon (C) and nitrogen (N) (Basile-Doelsch et al. 2007; Hatton et al. 2012b; Mikutta et al. 2009; Sollins et al. 2009; Sollins et al. 2006). Physical fractionation procedures have been operationally defined to study soil OM dynamics through time and space (von Lützow et al. 2007). Recently, Moni et al. (2012) demonstrated that sequential density fractionation should be preferred to particle-size fractionation for studying mineral-attached OM. By using this method, we earlier tracked the incorporation of a ^{15}N label over a decade after its application as ^{15}N-beech leaf litter into density-isolated soil organo-mineral associations isolated from a forest surface soil (Hatton et al. 2012b). We conceptualized the flow of residual litter-derived organic nitrogen through aggregates of increasing density as controlled by the microbial reworking of OM, while both microbial transformations and mineral reactivity would control the flow of residual litter-N through mineral grains (Figure 1).

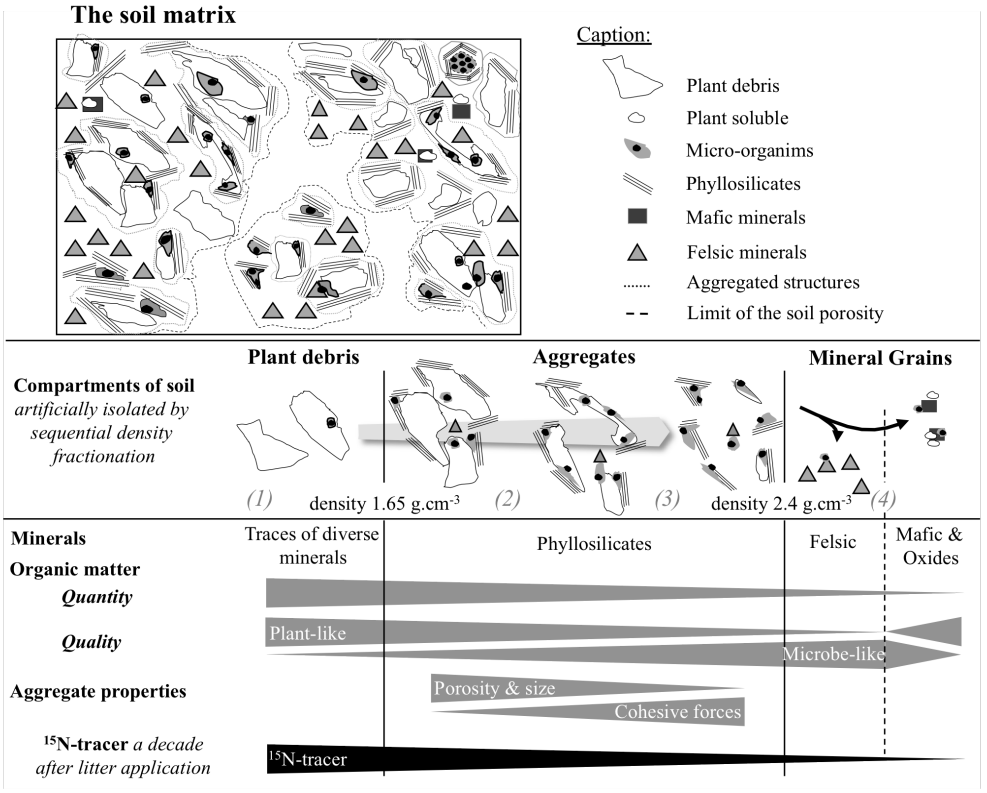

Figure 1: Simplified conceptual model relating properties of mineral–organic associations to their density and illustrating how these properties control the distribution of 15N tracer derived from a leaf litter in the various organo-mineral associations a decade after application (reprinted from (Hatton et al. 2012b). (1) Leaf litter enters the soil as plant debris progressively decomposed and incorporated into aggregates. Microbial transformations eventually cause the disintegration of (2) low density aggregate into (3) smaller aggregates richer in microbial OM with a higher proportion of mineral materials and a lower proportion of pores. (4) Mineral grains with little OM attached composed the densest fractions. Felsic minerals are coated with microbial OM; mafic primary minerals and pedogenic oxides adsorb OM independently of their plant or microbial origin via their hydroxylated surfaces.

Previous studies showed that litter-derived C and N are rapidly decoupled through processes such as C mineralization and microbial N immobilization (Bird et al. 2008; Bird & Torn 2006; Fahey et al. 2011; Trinsoutrot et al. 2000). However, short-term distributions and kinetics of residual litter-C and –N through particle-size and water-stable aggregate fractions have been showed to remain similar (Aita et al. 1997; Angers et al. 1997), suggesting that residual litter-C and –N similarly flow through the soil system. Based upon these findings, we hypothesized that residual litter-C and –N similarly flows through density-isolated organo-mineral associations.

This study aims at capturing the flows of C and N deriving from leaf litters through distinct soil organo-mineral associations to test the Hatton's model for litter-C (Hatton et al. 2012b). The same surface soil than previously studied (0-2.5cm depth) was collected in November 2009 (Ebrach, 49°52'N, 10°27'E), mixed and sieved to pass a 2mm sieve. Observable roots were removed. The soil was pre incubated for 15 days at 20°C (dark; 1:3 soil to air ratio) prior amendment with finely ground $^{13}C^{15}N$ beech leaves (3.27-8.10% excess) obtained at the CEA Cadarache (France) from 10 year-old trees grown in a chamber. $^{13}CO_2$ was provided continuously from April to May and as pulse from June to September. ^{15}N-urea was regularly vaporized from April to September (Zeller et al. 1998). NanoSIMS images showed that leaves are homogeneously labeled (Figure 2): ^{13}C and ^{15}N isotopes were distributed similarly to their counterpart ^{12}C and ^{14}N. $^{13}C^{15}N$ leaf fragments were added in proportions similar to mean annual N inputs: $15\mu g_N.g_{soil}^{-1}$, what corresponded to $1.1mg_C.g_{soil}^{-1}$. Amended soils were thoroughly homogenised prior incubation at 20°C (dark; 1:3 soil to air ratio; 50% water holding capacity). Samples were regularly aerated and collected after 42, 92, 184 and 365 days and frozen at -20°C.

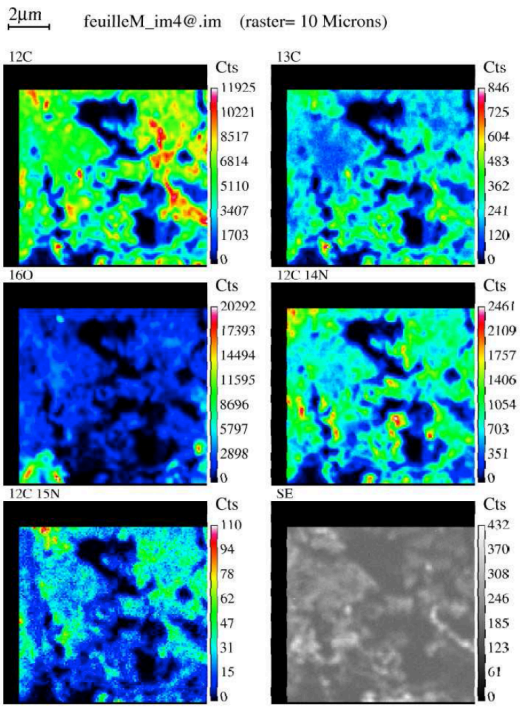

Figure 2: NanoSIMS images of $^{13}C^{15}N$ senescent beech leaves mounted onto a gold foil. NanoSIMS images were acquired using a Cs+ primary ion beam (1.5pA) of a NanoSIMS 50 (Cameca) at the LMCM, Museum National d'Histoire Naturelle of Paris, France. Images and data were processed using the L'IMAGE® software (developed by L. Nittler, Carnegie Institution, Washington DC, USA) accordingly to Remusat et al. (2012). Cts: counts; SE secondary ions.

Soil organo-mineral associations were sequentially isolated by density according to Hatton et al. (2012b). Plant debris were isolated <1.65 g cm-3; plant aggregates between 1.65-1.85 g cm-3; microbial aggregates between 1.85-2.4 g cm-3; mineral grains >2.4 g cm-3. Composition in ^{12}C, ^{13}C, ^{14}N and ^{15}N was determined in triplicates using an elemental analyzer (CE instruments, NA 1500 type II) coupled to isotope ratio mass spectrometery (Finnigan, Delta S) at the Technical Platform of Functional Ecology (OC 081), INRA-Nancy, France. Quantities of ^{13}C and ^{15}N tracers were calculated as proportions of C and N by subtracting the abundances in ^{13}C and ^{15}N isotopes of the labeled and reference treatments (Hatton et al. 2012b). Comparisons between tracer distributions were performed using Student's *t*-tests with a statistical significance threshold at $p<.05$, after confirming normal distributions and homogeneity of variances.

Table 1: Dry weight, C and N properties of different soil fractions isolated from a surface soil before beech leaf litter amendment (control) and after 42, 92, 184 and 365 days of laboratory incubation (n=3). SD means standard deviation. The composition of the density fractions is from Hatton et al. (2012b). Carbon and nitrogen distributions through the set of density fractions are expressed as percent of total recovered after density fractionation (*Sum of fractions*).

Treatment	Incubation	Fraction			Carbon				Nitrogen			
	days	Density (g cm^{-3})	Composition	Dry weight (%)	mg g^{-1}soil	SD	Distribution (%)	SD	mg g^{-1}soil	SD	Distribution (%)	SD
Control	0	Bulk soil			27.2	0.5			1.66	0.04		
		<1.65	Plant debris	2.1	8.0	0.1	34	0	0.31	0.01	23	1
		1.65-1.85	Plant aggregates	1.1	5.5	0.0	23	0	0.25	0.02	19	1
		1.85-2.4	Microbial aggregates	10.2	7.8	0.4	33	1	0.60	0.01	45	1
		>2.4	Mineral grains	86.8	2.5	0.0	10	0	0.19	0.02	14	2
		Sum of fractions		100.3	23.8	0.4			1.35	0.03		
Beech leaf litter addition	42	Bulk soil			27.0	0.3			1.58	0.19		
	92	Bulk soil			27.2	0.4			1.64	0.07		
		<1.65	Plant debris	3.5	11.1	0.1	42	0	0.36	0.01	25	1
		1.65-1.85	Plant aggregates	1.9	5.3	0.1	20	0	0.30	0.01	21	0
		1.85-2.4	Microbial aggregates	9.3	7.3	0.1	28	0	0.61	0.02	42	1
		>2.4	Mineral grains	85.1	2.4	0.1	9	0	0.19	0.01	13	1
		Sum of fractions		99.8	26.2	0.2			1.46	0.02		
	184	Bulk soil			27.1	1.5			1.59	0.02		
		<1.65	Plant debris	3.4	10.4	0.1	41	0	0.33	0.00	24	0
		1.65-1.85	Plant aggregates	2.0	5.4	0.0	21	0	0.27	0.00	20	0
		1.85-2.4	Microbial aggregates	9.6	6.7	0.5	26	2	0.55	0.02	41	2
		>2.4	Mineral grains	86.3	2.7	0.0	11	0	0.19	0.01	14	1
		Sum of fractions		101.4	25.2	0.5			1.33	0.02		
	365	Bulk soil			27.0	1.2			1.58	0.01		
		<1.65	Plant debris	2.5	9.6	0.0	39	0	0.31	0.01	24	1
		1.65-1.85	Plant aggregates	1.7	4.9	0.1	20	0	0.24	0.01	18	1
		1.85-2.4	Microbial aggregates	6.9	7.1	0.4	29	2	0.56	0.01	44	1
		>2.4	Mineral grains	88.5	3.1	0.1	13	0	0.19	0.01	14	1
		Sum of fractions		99.6	24.7	0.4			1.29	0.02		

Soil fractions isolated from control and treatments overtime were globally comparable (Table 1). Recovery rates after density fractionation were 100±0%, 92±4% and 81±4% of total dry weight, C and N for both control and treatments overtime. Plant debris only accounted for 2.9±0.7% of the total soil mass. Unsurprisingly, C and N contents measured from the soils amended with leaf litters were higher than in the control and regularly decreased overtime as reported by Aïta et al. (1997) and Trinsoutrot et al. (2000). Plant aggregates accounted for 1.7±0.4%, 21±1% and 20±2% of total soil mass, C and N, against 9±1%, 29±2% and 43±2% for microbial aggregates. Mineral grains represented more than 85% of total soil weight, but only accounted for about 11±1% and 13±1% of total C and N.

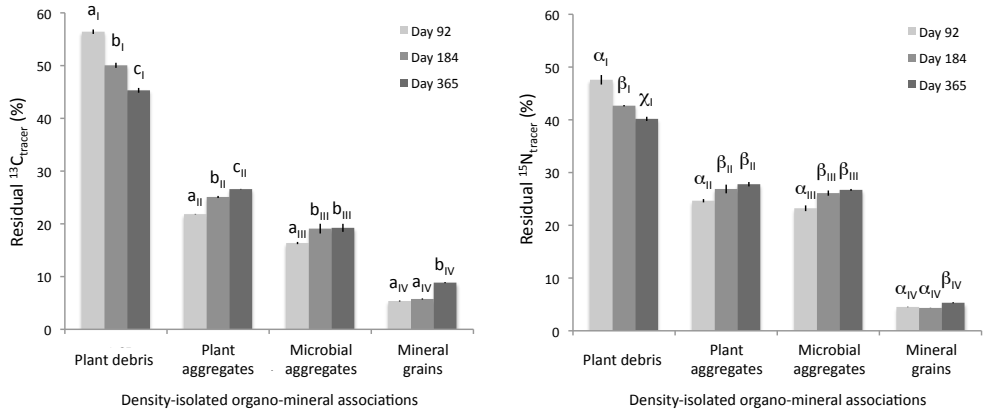

Figure 3: Distributions of residual $^{13}C_{tracer}$ (left) and $^{15}N_{tracer}$ (right) through density-isolated soil organo-mineral associations after 92, 184 and 365 days of laboratory incubation (n=3). Tracer distributions through the set of density fractions are expressed as percent of total recovered after density fractionation. Letters represent statistical differences (*t*-test; 95% confidence level): identical letters indicate a statistical equivalence, while different letters indicate a significant difference. The composition of the density fractions is from Hatton et al. (2012b): plant debris were isolated <1.65 g cm-3, plant aggregates between 1.65-1.85 g cm-3, mineral aggregates between 1.85-2.4 g cm-3 and mineral grains >2.4 g cm-3.

$^{13}C_{tracer}$ recovered from the initially applied regularly decreased overtime, while no significant losses of $^{15}N_{tracer}$ were observed (Table 2). Despite there was more residual $^{15}N_{tracer}$ than $^{13}C_{tracer}$, Figure 3 shows that they share similar distributions and kinetics throughout the density fractions. Both tracers decreased with increasing fraction density. Although plant debris remained the largest pools of residual litter-^{13}C and -^{15}N at all sampling dates, the residual tracers found in plant debris significantly decreased overtime. Concomitantly, residual tracers statistically increased in all denser fractions overtime. Residual tracers found in aggregates increased overtime from 38% to 48% and 48 to 55% of residual ^{13}C and ^{15}N tracers, while only small amounts were rapidly and increasingly attached to mineral grains overtime (Table 2). As earlier showed with other fractionation procedures (Aita et al. 1997; Angers et al. 1997), our results indicate that residual litter-^{13}C and -^{15}N progressively moved from plant debris to aggregates and, to a lesser extent, mineral grains. Time lags for litter-

^{13}C and -^{15}N transfers tended to increase with organo-mineral density. Overall, these results validate the Hatton's model for the transfer of both litter-derived C and N through density-isolated organo-mineral associations (Hatton et al. 2012b).

Much less residual $^{15}N_{tracer}$ was found in plant debris after 92 days of incubation than after 4 years in the field (Hatton et al. 2012b), while $^{15}N_{tracer}$ distributions found after one year of incubation were very similar to what was observed after 12 years under natural conditions. This reveals that relatively large proportions of tracers were rapidly found in association with aggregates and, to a lesser extent, mineral grains when using ground materials. This illustrates how the lab incubation of ground materials accelerated the transfers of litter-derived materials in soils, notably by skipping the processes of litter fragmentation and enhancing the microorganisms' activities through a more favourable temperature (20°C in lab instead of a mean annual temperature of 7.5°C in the field).

Table 2: Beech leaf litter $^{13}C_{tracer}$ and $^{15}N_{tracer}$ through soil fractions after 42, 92, 184 and 365 days of laboratory incubation (n=3). SD means standard deviation. The composition of the density fractions is from Hatton et al. (2012b).

Treatment	Incubation	Fraction		$^{13}C_{tracer}$		$^{15}N_{tracer}$		$^{13}C_{tracer}$ / $^{15}N_{tracer}$	
	days	Density (g cm^{-3})	Composition	µg g^{-1}soil	SD	µg g^{-1}soil	SD	Mean	SD
Beech leaf litter addition	42	Bulk soil		41.3	1.4	1.25	0.03	33	1
	92	Bulk soil		35.4	1.2	1.25	0.02	28	1
		<1.65	Plant debris	19.3	0.1	0.51	0.01	38	0
		1.65-1.85	Plant aggregates	7.5	0.0	0.26	0.00	28	0
		1.85-2.4	Micobial aggregates	5.6	0.1	0.25	0.01	22	0
		>2.4	Mineral grains	1.8	0.0	0.05	0.00	38	0
		Sum of fractions		34.1	0.2	1.07	0.01	32	0
	184	Bulk soil		31.5	1.8	1.25	0.02	25	2
		<1.65	Plant debris	15.6	0.2	0.45	0.00	35	0
		1.65-1.85	Plant aggregates	7.8	0.1	0.28	0.01	28	0
		1.85-2.4	Micobial aggregates	6.0	0.3	0.27	0.01	22	0
		>2.4	Mineral grains	1.8	0.0	0.05	0.00	40	0
		Sum of fractions		31.2	0.3	1.05	0.01	30	0
	365	Bulk soil		30.3	1.7	1.25	0.02	24	2
		<1.65	Plant debris	13.1	0.1	0.42	0.00	32	0
		1.65-1.85	Plant aggregates	7.7	0.0	0.29	0.00	27	0
		1.85-2.4	Micobial aggregates	5.6	0.2	0.28	0.00	20	0
		>2.4	Mineral grains	2.6	0.0	0.06	0.00	47	0
		Sum of fractions		29.0	0.3	1.04	0.01	28	0

Although residual $^{13}C_{tracer}$ and $^{15}N_{tracer}$ distributions were globally similar at the fraction-scale, $^{13}C_{tracer}$/$^{15}N_{tracer}$ revealed finer-scale decoupling indicative of contrasted microbial activities between aggregates and mineral grains (Table 2). Aggregates became progressively richer in $^{15}N_{tracer}$ than in $^{13}C_{tracer}$ with time and density, while mineral grains became progressively richer in 13Ctracer. Indeed, their $^{13}C_{tracer}$/$^{15}N_{tracer}$ were significantly higher than for the leaf fragments initially applied (36) and

regularly increased overtime from 38 to 47. This not only reveals that two contrasted mechanisms of attachment operate in aggregates and mineral grains, but also indicates that microorganisms have transformed the leaf fragments. Hatton et al. (2012c) reported similar transformations after glycine additions and showed that tracers were spatially decoupled at a nano-scale as a result of microbial transformations. The extent of decoupling increased along with aggregate density, where microorganisms have been showed to increasingly contribute to SOM stabilization (Hatton et al. 2012c). This in agreement with observations by Trinsoutrot et al. (2000) to suggest that microorganisms are responsive for $^{15}N_{tracer}$ immobilization in aggregates. Conversely, the accumulation of $^{13}C_{tracer}$-rich compounds in mineral grains reveals the spatial partitioning of different microbial activities that may be related to preferential habitats for soil microorganisms (Hatton et al. 2012a; Hatton et al. 2012c). Overall our results confirmed that density fractionation isolates ecologically contrasted soil organo-mineral associations from which ecological interpretations can be derived. They further provide converging evidences supporting earlier thoughts that the stage of microbial transformation of the soil OM is a key controlling factor constraining the dynamics of litter-derived materials association with soil organo-mineral associations (Sollins et al., 2009; Hatton et al., 2012b).

By studying ^{13}C and ^{15}N dynamics through soil organo-mineral associations, we showed that residual litter-$^{13}C_{tracer}$ and –$^{15}N_{tracer}$ were similarly transferred from plant debris to aggregates and, to a lesser extent, mineral grains. Such observations validate the Hatton's model for the transfer of both litter-derived C and N through density-isolated organo-mineral associations (Hatton et al. 2012b). Further on, $^{13}C_{tracer}/^{15}N_{tracer}$ revealed finer-scale decoupling between residual ^{13}C and ^{15}N tracers supporting earlier observations that two contrasted mechanisms of attachment operate in aggregates and mineral grains in link with contrasted microbial activities (Hatton et al. 2012c). Overall, microbial transformations appeared as key-controlling factors for transfers between ecologically contrasted soil entities.

Acknowledgments

The Institut National de la Recherche Agronomique (INRA-EFPA) and the Région Lorraine (grants #12000292 and #12000184) have financially supported this work. We are in debt to Christian Hossan (PTEF, INRA) for EA-IRMS analyses.

References

Aita C, Recous S & Angers DA (1997) Short-term kinetics of residual wheat straw C and N under field conditions: Characterization by (CN)-C-13-N-15 tracing and soil particle size fractionation. European Journal of Soil Science 48: 283-294

Angers DA, Recous S & Aita C (1997) Fate of carbon and nitrogen in water-stable aggregates during decomposition of (CN)-C-13-N-15-labelled wheat straw in situ. European Journal of Soil Science 48: 295-300

Basile-Doelsch I, Amundson R, Stone WEE, Borschneck D, Bottero JY, Moustier S, Masin F & Colin F (2007) Mineral control of carbon pools in a volcanic soil horizon. Geoderma 137: 477-489

Bird JA, Kleber M & Torn MS (2008) C-13 and N-15 stabilization dynamics in soil organic matter fractions during needle and fine root decomposition. Organic Geochemistry 39: 465-477

Bird JA & Torn MS (2006) Fine roots vs. Needles: A comparison of (13)C and (15)N dynamics in a ponderosa pine forest soil. Biogeochemistry 79: 361-382

Fahey TJ, Yavitt JB, Sherman RE, Groffman PM, Fisk MC & Maerz JC (2011) Transport of Carbon and Nitrogen Between Litter and Soil Organic Matter in a Northern Hardwood Forest. Ecosystems 14: 326-340

Hatton P-J, Bode S, Boeckx P, Zeller B, Gelhaye L, Boiry S & Derrien D (2012a) Contribution of dead and fresh bacterial and fungal biomasses to soil organo-mineral associations In Prep. For Soil Biology and Biochemistry:

Hatton P-J, Kleber M, Zeller B, Moni C, Plante AF, Townsend K, Gelhaye L, Lajtha K & Derrien D (2012b) Transfer of litter-derived N to soil mineral-organic associations: Evidence from decadal N-15 tracer experiments. Organic Geochemistry 42: 1489-1501

Hatton P-J, Remusat L, Zeller B, Brewer E & Derrien D (2012c) Influence of microbial processes on soil organo-mineral associations. *In prep.*

Mikutta R, Schaumann GE, Gildemeister D, Bonneville S, Kramer MG, Chorover J, Chadwick OA & Guggenberger G (2009) Biogeochemistry of mineral-organic associations across a long-term mineralogical soil gradient (0.3-4100 kyr), Hawaiian Islands. Geochimica Et Cosmochimica Acta 73: 2034-2060

Moni C, Derrien D, Hatton P-J, Zeller B & Kleber M (2012) Density Fractions versus Size Separates: Does Physical Fractionation Isolate Functional Compartments? In Prep. For Soil Biology and Biochemistry:

Remusat L, Hatton P-J, Nico PS, Zeller B, Kleber M & Derrien D (2012) NanoSIMS study of organic matter associated with soil aggregates: advantages, limitations and combination with STXM. Environmental Science & Technology 46: 3943-3949

Sollins P, Kramer MG, Swanston C, Lajtha K, Filley T, Aufdenkampe AK, Wagai R & Bowden RD (2009) Sequential density fractionation across soils of contrasting mineralogy: evidence for both microbial- and mineral-controlled soil organic matter stabilization. Biogeochemistry 96: 209-231

Sollins P, Swanston C, Kleber M, Filley T, Kramer M, Crow S, Caldwell BA, Lajtha K & Bowden R (2006) Organic C and N stabilization in a forest soil: Evidence from sequential density fractionation. Soil Biology & Biochemistry 38: 3313-3324

Trinsoutrot I, Recous S, Mary B & Nicolardota B (2000) C and N fluxes of decomposing C-13 and N-15 Brassica napus L.: effects of residue composition and N content. Soil Biology & Biochemistry 32: 1717-1730

von Lützow M, Koegel-Knabner I, Ekschmitt K, Flessa H, Guggenberger G, Matzner E & Marschner B (2007) SOM fractionation methods: Relevance to functional pools and to stabilization mechanisms. Soil Biology & Biochemistry 39: 2183-2207

Zeller B, Colin-Belgrand M, Dambrine E & Martin F (1998) N-15 partitioning and production of N-15-labelled litter in beech trees following [N-15] urea spray. Annales Des Sciences Forestieres 55: 375-383

Zeller B, Colin-Belgrand M, Dambrine E, Martin F & Bottner P (2000) Decomposition of N-15-labelled beech litter and fate of nitrogen derived from litter in a beech forest. Oecologia 123: 550-559

A multi-scale approach to determine accurate and isotopic ratios by nano-scale secondary ion mass spectrometry imaging

IV

Pierre-Joseph Hatton [a]*, Laurent Remusat [b], Bernd Zeller [a], Delphine Derrien [a]

[a] INRA-Nancy, Biogéochimie des Ecosystemes Forestiers, 54280 Champenoux, France

[b] Laboratoire de Minéralogie et Cosmochimie du Muséum, UMR 7202 CNRS/MNHN, Muséum National d'Histoire Naturelle, case postale 52, 57 rue Cuvier, 75231 Paris Cedex 05, France

* Corresponding author: pierre-joseph.hatton@nancy.inra.fr

Published in *Rapid Communication in Mass Spectrometry* **26** (2012) : 1363-1371 [DOI]

Research Article

Rapid Communications in Mass Spectrometry

Received: 20 January 2012 Revised: 7 March 2012 Accepted: 8 March 2012 Published online in Wiley Online Library

Rapid Commun. Mass Spectrom. **2012**, *26*, 1363–1371
(wileyonlinelibrary.com) DOI: 10.1002/rcm.6228

A multi-scale approach to determine accurate elemental and isotopic ratios by nano-scale secondary ion mass spectrometry imaging

Pierre-Joseph Hatton[1]*, Laurent Remusat[2], Bernd Zeller[1] and Delphine Derrien[1]

[1]INRA, Laboratoire de Biogéochimie des Ecosystèmes Forestiers, UR 1138, INRA Nancy, 54280 Champenoux, France
[2]Laboratoire de Minéralogie et Cosmochimie du Muséum, UMR 7202 CNRS/MNHN, Muséum National d'Histoire Naturelle, case postale 52, 57 rue Cuvier, 75231 Paris Cedex 05, France

RATIONALE: Nano-scale secondary ion mass spectrometry (NanoSIMS) is still hampered by a lack of appropriate calibration method for the quantification of elemental and isotopic ratios in heterogeneous materials such as soil samples. The potential of ^{13}C-^{15}N-labeled density fractions of soil to calibrate the C/N, $^{13}C/^{12}C$ and $^{15}N/^{14}N$ ratios provided by NanoSIMS was evaluated.
METHODS: The spatial organization of soil particles found at the macro- and micro-scales were compared. The C/N, $^{13}C/^{12}C$ and $^{15}N/^{14}N$ ratios measured at the macroscopic scale from different density fractions using an elemental analyzer coupled to an isotope ratio mass spectrometer (EA/IRMS) were compared with the corresponding micro-scale NanoSIMS measurements. When the macro- and micro-scales patterns were similar, macroscopic scale measurements obtained by EA/IRMS and the corresponding NanoSIMS C/N and $^{15}N/^{14}N$ ratios averaged per fraction were used to obtain correction equations. The correction method using the internal calibration procedure was compared with the traditional one using a single organic standard.
RESULTS: It was demonstrated that the correction method using an internal calibration procedure was applicable for NanoSIMS images acquired on more than 500 μm^2 per fraction and provided more accurate C/N and $^{15}N/^{14}N$ ratios than the traditional correction method.
CONCLUSIONS: As long as the NanoSIMS sampling was representative of the macroscopic properties, the correction method using an internal calibration procedure allowed better quantification of the isotope tracers and characterization of the C/N ratios. This method not only produced qualitative images, but also accurate quantitative parameters from which ecological interpretations can be derived. Copyright © 2012 John Wiley & Sons, Ltd.

Knowledge of the distribution of organic materials in the soil matrix is mandatory to understand the processes that rule the quantity, quality and turnover of organic matter attached to minerals.[1,2] By using ion microprobes instruments based on secondary ion mass spectrometry, Cliff and co-workers[3–5] and Madsen and colleagues[6–8] revealed process heterogeneities in soil systems that were invisible at the macroscopic scale and pointed out the necessity to explore the conditions controlling processes at the scale of tens to hundreds of microns. However, until recently, such fine-scale characterization of organo-mineral assemblages has been hampered by the lack of an appropriate standardization method.

Nano-scale secondary ion mass spectrometry (NanoSIMS) is the most recent generation of ion probes used to tackle this scientific challenge: it can generate quantitative maps of elements and isotopes from the outer hundreds nm of a sample with a lateral spatial resolution below 100 nm. This technique has been used to study the surface distribution and composition of organic and inorganic materials in many fields of research such as cosmochemistry, biology, biogeochemistry, semiconductor and surface-science.[9–12] In soil systems, the conjunction of stable isotope labeling and NanoSIMS has also been used to track isotope tracers, to locate microorganisms,[13] to study nutrient uptake in the rhizosphere,[14] and to study the fate of amino acids through several structures of soil.[15] However, instrumental fractionation, contrasting ionizing properties[16] and the high heterogeneity of the soil matrix – resulting from the high complexity of both organic materials and minerals that are assembled in many different combinations – induce significant bias in the determination of elemental ratios that prevents them from being used for ecological purposes. Carbon-to-nitrogen (C/N) ratios directly obtained by NanoSIMS are not accurate and, although highly valuable, they cannot be used to study the chemical forms in which the isotopic tracer is found. To overcome such a limitation, Remusat and co-authors[17] characterized the molecular composition of isotopically labeled organic matter localized using NanoSIMS with additional scanning transmission X-ray microscopy (STXM) coupled to near edge X-ray absorption fine structure spectroscopy (NEXAFS). They demonstrated that this combination of

* *Correspondence to:* P.-J. Hatton, INRA, Laboratoire de Biogéochimie des Ecosystèmes Forestiers, UR 1138, INRA Nancy, 54280 Champenoux, France.
E-mail: Pierre-Joseph.Hatton@nancy.inra.fr

Copyright © 2012 John Wiley & Sons, Ltd.

techniques promised great advances in the understanding of the processes that rule organic matter dynamics, but also pointed out how challenging it might be. As an alternative, the NanoSIMS determination of accurate C/N ratios would provide a less precise but much simpler characterization of the organic matter forms in which the label ends up.

Obtaining accurate quantitative information on elemental and isotopic compositions with NanoSIMS is still a problem. Usually, the raw data are corrected using terrestrial standards, such as graphite or kerogen. However, they are quite different from soil samples in several aspects: (1) their matrix is purely organic, contrary to organo-mineral soil particles, and (2) they are homogeneous whereas soil is highly heterogeneous. These two facts can induce different matrix effects and different ion yields. In addition, (3) their elemental and isotopic compositions are often not comparable with what is found in mineral-organic soils. These differences may significantly bias the accuracy of the measured elemental and isotopic ratios. A large set of standards of comparable material types,[18] e.g. organic, mineral or organo-mineral assemblages, with similar elemental and isotopic compositions[11] would ideally be required for the calibration of the NanoSIMS results, but these are not yet available.

In this paper, we describe a multi-scale approach that overcomes the bias resulting from the complexity of the soil samples matrix. We used the opportunity offered by a panel of ^{13}C-^{15}N labeled soil fractions that differ in structure and composition[19] to provide the means for an internal calibration of NanoSIMS results. We consider that a similar range of heterogeneity for elemental and isotopic ratios is displayed at the macroscopic scale between several density fractions and at the micro-scale within few (or even a single) soil particle(s) of a given density fraction. Thus, the density fractions would be composed of several types of soil particles that cover a large range of elemental and isotopic ratios and the proportion of each type would, in turn, explain the difference between the fractions (Fig. 1). To calibrate the NanoSIMS measurements, we further assume that a set of NanoSIMS images acquired on an aliquot of each fraction completely spans the range of the nano-scale variability and that the average value obtained on this set of images is representative of macroscopic measurements. To test the hypothesis supporting this NanoSIMS correction method, we compare (1) the aggregated or non-aggregated organization of soil particles found at the macro- and micro-scales and (2) the C/N, $^{13}C/^{12}C$ and $^{15}N/^{14}N$ ratios measured at the macroscopic scale from different density fractions using an elemental analyzer coupled to isotope ratio mass spectrometry (EA/IRMS) with the corresponding micro-scale NanoSIMS measurements obtained for each fraction. When the macro- and micro-scale patterns are similar, we compute a correction equation for the NanoSIMS data by fitting elemental and isotopic ratios determined by NanoSIMS with data measured by EA/IRMS. We compare the correction method using the internal calibration procedure with that using a single standard (here the type III kerogen) and finally present its application for investigating nano-scale elemental and isotopic heterogeneity.

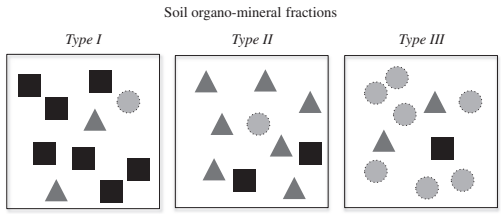

Figure 1. The soil organo-mineral fractions separated by density are heterogeneous at the nanometre scale. They are made of various types of microstructures that cover a large range of elemental and isotopic ratios. We consider that (1) a similar range of heterogeneity for elemental and isotopic ratios is displayed at the macroscopic scale between several density fractions and at the micro-scale within few (or even a single) soil particle(s) of a given density fraction; (2) the type of microstructure that dominates a given fraction defines its chemical composition at the macroscopic scale. Geometric forms represent different types of soil microstructures. Squares, triangles and circles dominate organo-mineral fractions of type I, II and III, respectively.

EXPERIMENTAL

Soil and labeling experiment

The soil is an acidic ($pH_{H2O} = 3.9$) dystric Cambisol (sand: 80%; loam: 13%; clay: 7%) collected in November 2009 at Ebrach, Germany (49°52′N, 10°27′E). It has been described by Hatton and co-authors.[19] The first 2.5 cm of the A-horizon were sampled on a surface area of 2 m^2, mixed and sieved to pass 2 mm. Observable roots were removed. The collected soil has a total C content of 28.7 ± 0.5 mg.g^{-1} and a total N content of 1.85 ± 0.04 mg.g^{-1}.

The soils were pre-incubated for 2 weeks prior to being amended with 80 µg of uniformly ^{13}C-^{15}N-labeled glycine (98–99% excess; Sigma-Aldrich, Saint Quentin Fallavier, France) per gram of soil, which corresponds to the natural annual input in nitrogen. Glycine was added in solution to set the moisture content at half of the water-holding capacity (21%). The amended soil was thoroughly mixed by hand and sieved twice to ensure a homogeneous mixing. It was incubated in the dark at 20 °C for 8 h before freezing at −20 °C to stop the microbial activity. The moisture content was determined at 105 °C. All values are stated on an oven-dried basis.

Isolation of soil fractions

The soil was sequentially separated by density to isolate soil fractions that differ in structure, organic matter composition and dynamics. Based on a previous study in which we described a set of seven physically and functionally different density fractions isolated from the same soil,[19] we selected and isolated five fractions: 1.65–1.85; 1.85–2.0; 2.2–2.4; 2.4–2.65 and >2.65 g.cm^{-3}. Briefly, the 1.65–1.85 g.cm^{-3} fraction consisted of aggregates dominated by organic matter. The fractions between 1.85 and 2.4 g.cm^{-3} mainly consisted of aggregates dominated by phyllosilicates. The extent of microbial transformation of the mineral-associated organic matter increased with density. The 2.4–2.65 g.cm^{-3} fraction was dominated by quartz and feldspar covered by little microbial organic matter whereas the fraction >2.65 g.cm^{-3} was dominated by quartz and oxides covered by little plant and microbial organic materials. After being isolated and

 Copyright © 2012 John Wiley & Sons, Ltd.

rinsed, the density fractions were frozen at −20 °C and freeze-dried. The recovery rates after density fractionation were 99%, 76% and 68% of dry weight, total C and total N, respectively.

Nano-scale characterization

The nano-scale characterization referred to the submicron mapping of individual or clustered NanoSIMS pixels from maximum one individual soil particle. The NanoSIMS analyses were performed as follows.

An aliquot of each selected density fraction was deposited onto a clean gold foil without the use of any chemical or epoxy resin to avoid contamination. Soil particles adsorbed by electrostatic forces onto the holder were then coated with 20 nm of gold to ensure charge compensation. Images of mounted soil particles and corresponding data were acquired using a NanoSIMS 50 (Cameca, Gennevilliers, France) at the LMCM, Museum National d'Histoire Naturelle of Paris, France. Samples were first presputtered with a high Cs^+ current (120 pA) for 10 to 25 min (depending on the surface analyzed) to remove surface contamination and the gold coating, and to implant Cs^+ into the surface of the sample until a sputtering steady state was reached. Areas between 144 and 1600 μm^2 were then scanned with a low primary current of Cs^+ ions (1.5 pA) to ensure a spatial resolution of ca. 80 nm. The resolutions of the images were 128 × 128 pixels or 256 × 256 pixels wide with a raster speed of 2 ms.pixel^{-1}. Secondary ion images of $^{12}C^-$, $^{13}C^-$, $^{16}O^-$, $^{12}C^{14}N^-$ and $^{12}C^{15}N^-$ were simultaneously recorded with a high mass resolution to resolve potential mass interferences (10 000 mass resolving power for ^{26}CN). Forty to fifty frames of secondary ion images were accumulated per imaged areas. The $^{16}O^-$ maps were used as a proxy for mineral surfaces.[17] The instrumental stability for elemental and isotopic ratios was checked using an organic type III kerogen (reference standard) analyzed several times a day (n ≥2). The images and data were processed using the L'IMAGE® software (developed by L. Nittler, Carnegie Institution, Washington DC, USA) and corrected for detector dead time (44 ns, set electronically) and secondary ion images drift in X and Y positions.

Micro-scale characterization

The micro-scale characterization referred to the NanoSIMS and secondary electron mapping of soil particles from a given density fraction.

The NanoSIMS data were obtained as described above. The NanoSIMS data acquired from more than one NanoSIMS image were averaged considering all the measurements as a unique sampling. The aggregated or non-aggregated organization of the soil particles was assessed using the secondary electron detector of the NanoSIMS instrument and, when possible, environmental scanning electronic microscopy (SEM) at the LMCM. Individual particles were defined as nonaggregated, while assemblages of several individual particles were defined as aggregated.

Macro-scale characterization

The macro-scale characterization referred to EA-IRMS data and visual observations of the density fractions (≥1 mm). Total C, total N, $^{13}C/^{12}C$ and $^{15}N/^{14}N$ were measured in triplicate using an elemental analyzer (NA 1500 type II, CE Instruments, Rodano, Italy) coupled to a Finnigan, Delta S isotope ratio mass spectrometer (Thermo Scientific, Bremen, Germany) at the Technical Platform of Functional Ecology (OC 081) at INRA Forest Ecology and Ecophysiology Unit, INRA Nancy, France. $^{13}C/^{12}C$ and $^{15}N/^{14}N$ ratios were expressed as δ values relative to the Vienna PeeDee Belemnite (VPDB) standard[20] and the atmospheric N_2 standard,[21] respectively.

Soil fractions were visually checked for aggregated and non-aggregated particles using a polarizing microscope (Leica DM LP, Rueil-Malmaison, France) with low magnification ranges.[19]

Calculations

The C/N, $^{13}C/^{12}C$ and $^{15}N/^{14}N$ NanoSIMS ratios averaged per fraction were calculated using, for each ratio, the sum of counts (of $^{12}C^-$, $^{13}C^-$, etc…) of all the images of a given fraction. The error for each region of interest (ROI) was calculated by propagating errors on counting statistics and the uncertainty associated with the instrumental fractionation according to Remusat et *al*.[17]

Isotopic anomalies were defined as follows: the isotopic ratio must be three times its associated error above the isotopic composition of the whole image.[17]

$$R_{\text{anomaly}} > R_{\text{image}} + 3 \times \sigma_{\text{anomaly}} \quad (1)$$

where R_{anomaly} is the isotopic ratio of a ROI, R_{image} is the isotopic ratio of the whole image and σ_{anomaly} is the error associated with the R_{anomaly}. Isotopic anomalies are defined on ROI surfaces larger than 0.3 μm^2, i.e. about 30 times the surface corresponding to the spatial resolution (<100 nm).

Statistics

Comparison between NanoSIMS and EA/IRMS measurements was performed using Pearson correlation analysis. We considered that the average values from all NanoSIMS images acquired for a given fraction could be fitted to the EA/IRMS value of the corresponding fraction to obtain a correction equation when the Pearson correlation coefficient (R) was higher than 0.8.

For correction methods, the maximum deviation to reference EA/IRMS measurements was computed as follows:

$$\text{Maximum Deviation} = \max_i \left| \left(R_{\text{NanoSIMS corrected}} - R_{\text{EA-IRMS}} \right) / R_{\text{EA-IRMS}} \right| \quad (2)$$

where $R_{\text{EA-IRMS}}$ and $R_{\text{NanoSIMS corrected}}$ stand for the reference EA-IRMS ratios and the corresponding corrected NanoSIMS value, respectively; $\max_i$ is the maximum deviation determined from the corrected values ($_i$),

The error associated with elemental and isotopic ratios obtained by the correction method using the internal calibration procedure, $\sigma_{\text{RNanoSIMS corrected}}$, was computed as follows:

$$\sigma_{R_{\text{NanoSIMS corrected}}} = \frac{\text{Maximum Deviation}}{100} \times \left(R_{\text{NanoSIMS corrected}} + a \times \sigma R_{\text{NanoSIMS uncorrected}} \right) \quad (3)$$

where a is the slope of the calibration equation and $\sigma_{\text{RNanoSIMS uncorrected}}$ is the error associated with $R_{\text{NanoSIMS uncorrected}}$.

 Copyright © 2012 John Wiley & Sons, Ltd.

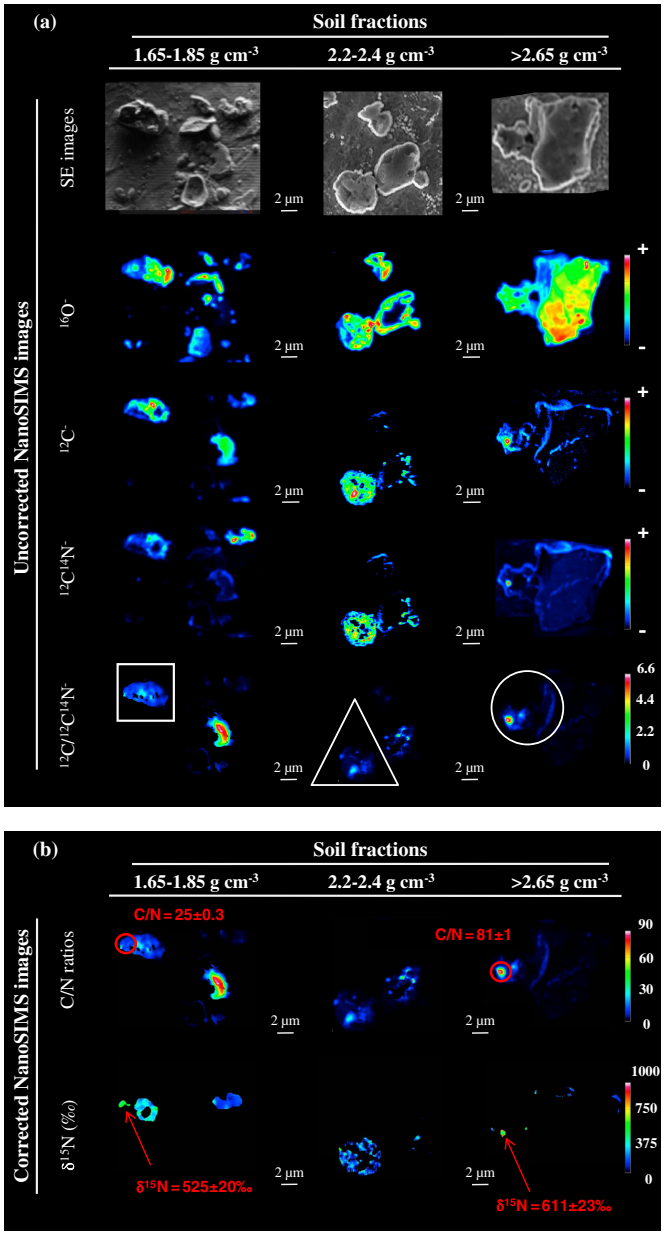

Figure 2. (a) NanoSIMS secondary electron (SE) images and the corresponding $^{16}O^-$, $^{12}C^-$, $^{12}C^{14}N^-$ and $^{12}C^-/^{12}C^{14}N^-$ images from three organo-mineral density fractions of soil. $^{12}C^-/^{12}C^{14}N^-$ images illustrate the high variability of mineral-associated organic materials through three different types of organo-mineral associations. Square, triangle and circle indicate areas representative of each soil fraction and refer to Fig. 1. (b) NanoSIMS images of C/N and $^{15}N/^{14}N$ ratios corrected using the internal calibration method. ^{15}N anomalies are circled in red in C/N maps and quantified in δ values (‰).

 Copyright © 2012 John Wiley & Sons, Ltd.

RESULTS AND DISCUSSION

Multi-scale analyses of heterogeneity

Nano-scale complexity

The NanoSIMS images showed that the organo-mineral assemblages were highly heterogeneous at the nano-scale with, for example, several types of organic materials covering a large range of C/N ratios (lower part of Fig. 2(a)). Nitrogen-rich regions represented in blue with uncorrected $^{12}C^-/^{12}C^{14}N^-$ ratios ≤1 were found throughout all the particles imaged without distinguishable spatial gradient. Nitrogen-poor regions represented in green, yellow and red with uncorrected $^{12}C^-/^{12}C^{14}N^-$ ratios >2 were much less abundant. They were found without apparent pattern of spatial distribution. Figure 2(a) shows two clear N-poor regions at the surface of particles isolated from the lightest (3.1 μm^2) and the densest fraction (0.3 μm^2). The average uncorrected $^{12}C^-/^{12}C^{14}N^-$ ratios measured on the whole images resulted from the relative proportions of each organic material. The C/N ratios of the soil particles reported in Fig. 2(a) were 0.84 for the NanoSIMS image of the 1.65–1.85 g.cm^{-3} fraction, 0.33 for the image of the 2.2–2.4 g.cm^{-3} fraction and 0.71 for the image of the fraction >2.65 g.cm^{-3}.

Comparison of micro- and macro-scale characterizations of the density fractions

Optical microscope observations indicated that the soil fractions <2.4 g.cm^{-3} were dominated by aggregated particles and that non-aggregated particles progressively became more abundant with increasing density (Fig. 3). In contrast, >99% of soil particles from the two fractions >2.4 g.cm^{-3} are non-aggregated particles (Table 1). Sizing down to the micro-scale, the secondary electron images indicated that the proportion of aggregated particles decreased with density from 99% in the lightest fraction to <1% in the densest fraction (Table 1). Despite small discrepancies between the observations

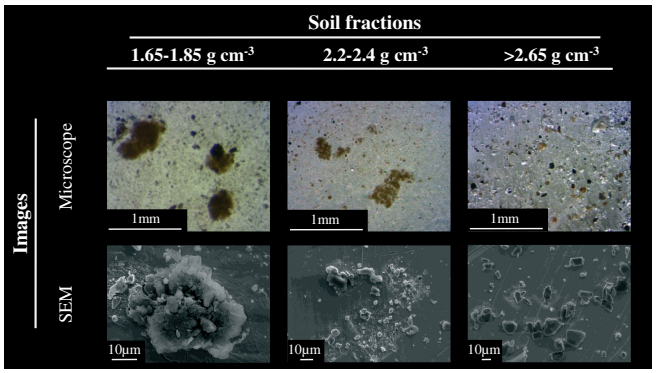

Figure 3. Aggregated or non-aggregated organization of soil particles isolated from three density fractions of soil observed at the macro-scale with a polarizing microscope and at the micro-scale using scanning electron microscopy (SEM).

Table 1. Aggregated or non-aggregated organization of soil particles isolated from five types of organo-mineral density fractions investigated at both the macro- and the micro-scales. Aggregated and non-aggregated particles are visually identified using a polarization microscope at the macro-scale and a scanning electron microscope or NanoSIMS at the micro-scale. At the micro-scale, the investigated surfaces are quantified by NanoSIMS using $^{16}O^-$ as proxy for the soil particles; proportions are computed from NanoSIMS images acquired in each fraction

Samples	Organization of the soil particules					
	At the macro-scale using a polarization microscope			At the micro-scale combining scanning electron microscopy and NanoSIMS 50		
Density fractions	Surface area	Aggregated	Non-aggregated	Surface area	Aggregated	Non-aggregated
g.cm^{-3}	cm^2	%	%	μm^2	%	%
1.65-1.85	9.2	89	11	1127	>99	<1
1.85-2.0	9.6	83	17	306	>99	<1
2.2-2.4	10.1	57	43	528	41	59
2.4-2.65	8.7	<1	>99	522	30	70
>2.65	10.5	<1	>99	1313	<1	>99

 Copyright © 2012 John Wiley & Sons, Ltd.

performed at the two scales, they both revealed a progressive shift in particle organization with increasing density, from aggregated organization in the light fractions to non-aggregated organization in the densest fractions

The carbon and nitrogen concentrations measured at the macroscopic scale decreased with increasing density until the densest fraction, in which they increased slightly. This was consistent with the NanoSIMS measurements averaged per fraction, revealing that the surface covered by organic materials decreased with increasing density (Table 2). The C/N ratios measured at the macroscopic scale by EA/IRMS decreased from 19.8 to 10.8 with increasing density until the density cut off at 2.4 g.cm^{-3}, and then slightly increased again to 14.0. The uncorrected $^{12}C^-/^{12}C^{14}N^-$ ratios obtained with NanoSIMS for the same fractions also decreased with fraction density. They were correlated to the larger scale measurements obtained by EA/IRMS (R = 0.85) and even more (R >0.99) when excluding the fraction 1.85–2.0 g.cm^{-3} that was less imaged than the other fractions (306 µm^2 – see Table 1). The uncorrected $^{12}C^-/^{12}C^{14}N^-$ ratios determined by NanoSIMS were much lower at between 0 and 1.1. This was attributed to the lower emissivity of C^- than of CN^-.[10,16] The NanoSIMS uncorrected $^{12}C^{15}N^-/^{12}C^{14}N^-$ ratios determined from the set of density fractions followed the same trend as the corresponding EA/IRMS measurements, with correlation coefficients of 0.76 and 0.84 when excluding the less imaged fraction (1.85-2.0 g.cm^{-3} - see Table 1). The $^{13}C/^{12}C$ ratios measured by EA/IRMS did not vary for the fractions <2.4 g.cm^{-3} where they were 1.100%, but increased slightly with increasing density in the two fractions >2.4 g.cm^{-3} (Table 2). The uncorrected $^{13}C^-/^{12}C^-$ ratios measured with NanoSIMS were not correlated with larger-scale EA/IRMS measurements (R = 0.15) and became weakly correlated when excluding the less imaged fraction (R = 0.57). This is probably due to (1) the small range of variations in the bulk $^{13}C/^{12}C$ variations among the different fractions compared with the uncertainty of the NanoSIMS measurement (Table 2) or the result of (2) the occurrence of small patches of the ^{13}C label too heterogeneously distributed to be confidently sampled by the set of images that we have acquired.

Our results showed that the particles organization, organic matter contents, C/N and $^{15}N/^{14}N$ ratios exhibited consistent patterns with increasing density at both macro- and micro-scales as long as the surface imaged exceeded 500 µm^2 (i.e. for the fractions 1.65–1.85 g.cm^{-3} and >2.2 g.cm^{-3}). This supported the hypothesis that the set of NanoSIMS images acquired on more than 500 µm^2 per fraction encompassed all the nano-scale heterogeneity and that the images were comparable with the larger-scale EA/IRMS measurements (Fig. 1), making the internal calibration relevant. Conversely, the $^{13}C^-/^{12}C^-$ ratios measured by NanoSIMS did not meet this requirement for applying the internal calibration method.

NanoSIMS data correction

The correction equations for the internal calibration method were obtained by fitting uncorrected $^{12}C^-/^{12}C^{14}N^-$ and $^{12}C^{15}N^-/^{12}C^{14}N^-$ ratios measured by NanoSIMS on more than 500 µm^2 per fraction to the corresponding reference EA/IRMS values. The correction equations for the classical method using a single standard, here a type III kerogen, were obtained by multiplying the uncorrected $^{12}C^-/^{12}C^{14}N^-$ and

Table 2. Elemental and isotopic compositions of five density fractions investigated at both the macro-scale by EA-IRMS (n = 3) and the micro-scale by NanoSIMS (>500 µm^2 per fraction). The NanoSIMS measurements are not corrected. Organic matter (OM) covering rates are measured by NanoSIMS using $^{16}O^-$ as a proxy for the soil particles and $^{12}C^-$ for OM. Isotopic ratios are also expressed as δ values relative to the VPDB and the atmospheric N_2 standard. *n.d.*: not determined; SD: standard deviation

Samples	Densities	Elemental and isotopic ratios																							
		At the macro-scale using EA-IRMS (n ≥ 3)											At the micro-scale using NanoSIMS 50 (>500 µm^2)												
		C		N		C/N		$^{13}C/^{12}C$		$\delta^{13}C$		$^{15}N/^{14}N$		$\delta^{15}N$		OM covering rate	$^{12}C^-/^{26}CN^-$		$^{13}C^-/^{12}C^-$		$\delta^{13}C$		$^{12}C^{15}N^-/^{12}C^{14}N^-$		$\delta^{15}N$	
	g.cm^{-3}	mg.g	SD	mg.g	SD		SD	%	SD	‰	SD	%	SD	‰	SD	%		SD	%	SD	‰	SD	%	SD	‰	SD
Kerogen III	*n.d.*	762.1	0.0	11.4	0.0	66.7	0.0	1.095	0.000	−25.2	0.1	0.369	0.000	3.7	0.2	100	4.75	0.00	1.092	0.000	−28.7	0.1	0.376	0.000	22.9	0.1
Soil fractions	1.65–1.85	227.1	0.3	11.5	0.3	19.8	0.4	1.099	0.000	−21.9	0.0	0.430	0.001	170.6	2.2	46	1.07	0.00	1.049	0.006	−66.7	5.7	0.458	0.002	247.0	6.5
	1.85–2.0	158.6	17.1	10.7	0.1	14.8	1.4	1.100	0.000	−20.9	0.1	0.423	0.001	149.6	2.5	57	0.31	0.00	1.068	0.006	−49.5	5.5	0.463	0.001	259.5	3.4
	2.2–2.4	83.1	0.3	7.7	0.2	10.9	0.2	1.099	0.002	−22.0	1.3	0.411	0.003	117.7	8.4	31	0.38	0.00	1.054	0.011	−62.3	9.8	0.390	0.001	60.5	4.0
	2.4–2.65	2.2	0.2	0.2	0.0	11.5	0.8	1.104	0.000	−17.2	0.2	0.400	0.002	89.3	6.1	16	0.41	0.00	1.043	0.020	−71.5	17.6	0.417	0.002	133.5	6.5
	>2.65	5.1	0.0	0.4	0.0	14.0	0.8	1.113	0.000	−9.3	0.4	0.454	0.004	234.5	11.2	2	0.61	0.01	1.061	0.026	−55.9	23.2	0.468	0.002	273.8	5.1

 Copyright © 2012 John Wiley & Sons, Ltd.

$^{12}C^{15}N^-/^{12}C^{14}N^-$ ratios measured by NanoSIMS by the ratio of EA/IRMS to reference NanoSIMS measurements from the standard. Table 3 reports the correction equations and the corresponding maximum deviations to reference EA-IRMS measurements (Eqn. (2)).

Evaluation of the correction methods

The maximum deviations (Eqn. (2)) associated with C/N and $^{15}N/^{14}N$ ratios corrected using the internal calibration method were 1.2% and 3.5%, respectively, in the composition ranges displayed in the soil samples used for the calibration (Table 3). The maximum deviations obtained with the type III kerogen correction were larger: 50.9% for the C/N ratios and 6.9% for the $^{15}N/^{14}N$ ratios.

The C/N ratios corrected with the type III kerogen were about five units lower than the reference EA/IRMS values (Fig. 4). The C/N ratios corrected with the internal calibration were in much better agreement with the EA/IRMS values (Fig. 4). The soil samples and the type III kerogen differed by their matrix, e.g. organo-mineral vs. purely organic. Earlier reports[11,16] suggested that the intimate interaction of organics and minerals affected the $^{12}C^-$ and $^{26}CN^-$ emissivities and the resulting elemental ratios. The underestimated values obtained with the type III kerogen correction might also be due to (1) the fact that the C/N ratio of the kerogen standard was not in the range commonly observed in soil but much higher, or (2), to a lesser extent, the contribution of a N-rich contaminant, such as adsorbed N_2 from the atmosphere, occurring at the surface of the samples. This contribution was taken into account by the internal calibration method.

The type III kerogen correction for $^{15}N/^{14}N$ ratios was, again, less accurate than the internal calibration correction (Fig. 4), but the maximum deviation of 6.9% indicated that the correction with the type III kerogen was more accurate for $^{15}N/^{14}N$ ratios than for C/N ratios. This might be explained by the similar emissivity of the $^{12}C^{14}N^-$ and $^{12}C^{15}N^-$ species and by the high levels of isotopic enrichment found through the panel of fractions.

Examples of applications

The correction equations were applied to the NanoSIMS images obtained to quantitatively evaluate the nano-scale elemental and isotopic heterogeneity of the organic forms found at the surface of the soil samples (Fig. 2(b)). Most of the organics appear in dark blue and show values of between 6 and 19. The few pale blue spots are indicative of material with a C/N ratio close to 30 whereas the C/N ratios of the two N-poor regions identified in yellow-red exhibit C/N values of 52.4 ± 0.6 and 80.5 ± 1.0. As the scale of investigation was between the molecular and the cellular scale, the

Table 3. Calibration equations for NanoSIMS determination of C/N and $^{15}N/^{14}N$ ratios and the corresponding maximum deviations to reference EA/IRMS values. Equations are the regression coordinates between the uncorrected NanoSIMS measurements and the reference EA/IRMS measurements. Uncorrected NanoSIMS values of a given region of interest are noted x, while the corresponding NanoSIMS values after correction are noted y. Maximum deviations are expressed in percentages

Correction method	Ratio	Calibration equation	Maximum deviation (%)
Internal calibration	C/N	$y = 12.759x + 6.151$	1.2
	$^{15}N/^{14}N$	$y = 0.5384x + 0.0019$	3.5
Type III kerogen	C/N	$y = 14.049x$	50.9
	$^{15}N/^{14}N$	$y = 0.9812x$	6.9

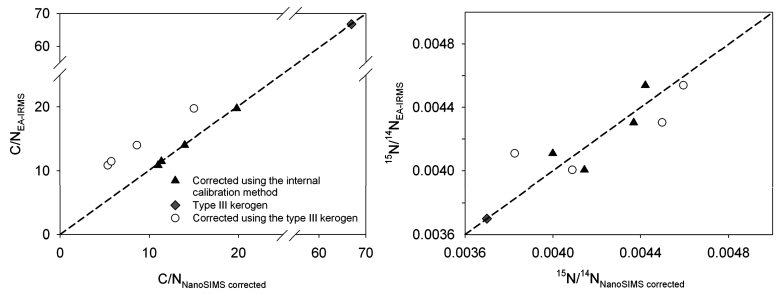

Figure 4. C/N and $^{15}N/^{14}N$ ratios obtained by NanoSIMS after correction with the organic type III kerogen and with the internal correction method compared with reference C/N and $^{15}N/^{14}N$ ratios obtained by EA-IRMS (n = 3). The dark triangles are the ratios of each organo-mineral density fraction corrected with the internal correction method; the light dots are the ratios of each organo-mineral density fraction corrected with the organic type III kerogen; the dashed line is the 1:1 line; the diamonds are the type III kerogen.

 Copyright © 2012 John Wiley & Sons, Ltd.

C/N ratios differentiated classes of compounds based on their relative richness in C compared with N. Thus, low C/N ratios indicated N-rich compounds, such as peptides, amino acids and amino sugars, whereas high C/N ratios indicated C-rich compounds, such as carbohydrates, lipids and phenolics. The NanoSIMS images showed that N-rich organic materials were much more abundant than the N-poor ones at the surface of the soil particles. They were both found throughout the surface of all soil particles with clear agglomeration sites, but without any apparent spatial gradient, as also shown by earlier NanoSIMS observations.[9,13,15,17] By applying the correction method based on an internal calibration procedure, it appeared that the predominant N-rich regions have C/N ratios <19, suggesting that amide-containing compounds dominated at the surface of the organo-mineral assemblages. In agreement with earlier STXM-NEXAFS studies,[17,22,23] these observations provided pieces of evidence that peptide-like compounds dominated the mineral-attached organic matter.[24–27]

The lower part of Fig. 2(b) points to two significant ^{15}N anomalies defined according to Eqn. (1) and illustrates how sparsely the label was spatially distributed throughout the soil particles. After correction of the NanoSIMS data, it was found that the spot of glycine-derived ^{15}N found in the 1.65–1.85 g.cm^{-3} fraction had a $\delta^{15}N$ value of 525 ± 20‰ and was located in a region with a C/N ratio of 25 ± 0.3. In the >2.65 g.cm^{-3} fraction, the $\delta^{15}N$ value of the label spot was 611 ± 23‰ and it was found in a region with a C/N ratio of 81 ± 1. This indicated that the ^{15}N tracer derived from the labeled glycine ended up in diverse soil organic matter forms and suggested that very different mechanisms were operative in the association of the newly incorporated N with organo-mineral assemblages in a very short timescale.

CONCLUSIONS AND RECOMMENDATIONS

Our results supported our initial assumption that the macro-scale differences found through the set of density fractions were also found when sizing down to the micro-scale within each individual density fractions. The consistency of the patterns in particles organization and in chemical composition displayed with increasing density between macro-scale measurements and averaged micrometric analyses improved when the surface investigated increased to better embrace the spatial and chemical complexity of the mineral-associated organic matter.

In the absence of elaborated organo-mineral standards that cover the range of elemental and isotopic ratios found in soils, our internal calibration correction based on the multi-scales approach provided more accurate C/N and $^{15}N/^{14}N$ ratios – in the composition ranges displayed in the soil samples used for the calibration – than the classical correction method using a single standard. By improving the determination of the C/N ratio, the internal calibration method provided much better identification of the organic matter forms within the soil matrix, possibly further improving the understanding of the processes that rule the stabilization of the soil organic matter.

Such an approach might be of primary interest for NanoSIMS users studying heterogeneous organo-mineral materials who wish to improve the quantitative determination of elemental and isotopic ratios at the nano-scale. The mandatory condition is that the investigated material exhibits some contrasted macroscopic features that could be also detected at the micro-scale by averaging a defined number of NanoSIMS images. The density fractionation separated organo-mineral associations in a way that is suitable for the internal calibration, but we expect other means of separating the fractions, such as the particle-size fractionation, to also meet these requirements.

Acknowledgements

The Institut National de la Recherche Agronomique (INRA-EFPA) and the Région Lorraine (grants #12000292 and #12000184) have financially supported this work. The National NanoSIMS Facility at the Museum National d'Histoire Naturelle was established by funds from the CNRS, Région Île de France, Ministère délégué à l'Enseignement supérieur et à la Recherche, and the Muséum itself. We are indebted to Aurélien Thomen (LMCM, MNHN) for scientific discussions, Fabrice Elegbede and Julien Sainte-Marie (BEF, INRA) for the mathematical discussions, Christian Hossan (PTEF, INRA) for EA-IRMS analyses, and Sylvain Pont (LMCM, MNHN) for SEM analyses.

REFERENCES

[1] I. M. Young, J. W. Crawford. Interactions and self-organization in the soil-microbe complex. *Science* **2004**, *304*, 1634.
[2] I. Koegel-Knabner, G. Guggenberger, M. Kleber, E. Kandeler, K. Kalbitz, S. Scheu, K. Eusterhues, P. Leinweber. Organo-mineral associations in temperate soils: integrating biology, mineralogy, and organic matter chemistry. *J. Plant Nutr. Soil Sci. - Zeitschrift Fur Pflanzenernahrung Und Bodenkunde* **2008**, *171*, 61.
[3] J. B. Cliff, P. J. Bottomley, D. J. Gaspar, D. D. Myrold. Nitrogen mineralization and assimilation at millimeter scales. *Soil Biol. Biochem.* **2007**, *39*, 823.
[4] J. B. Cliff, D. J. Gaspar, P. J. Bottomley, D. D. Myrold. Exploration of inorganic C and N assimilation by soil microbes with time-of-flight secondary ion mass spectrometry. *Appl. Environ. Microbiol.* **2002**, *68*, 4067.
[5] J. B. Cliff, D. J. Gaspar, P. J. Bottomley, D. D. Myrold. Peak fitting to resolve CN^- isotope ratios in biological and environmental samples using TOF-SIMS. *Appl. Surf. Sci.* **2004**, *231*, 912.
[6] S. Chandra, G. M. Pumphrey, J. M. Abraham, E. L. Madsen. Dynamic SIMS ion microscopy imaging of individual bacterial cells for studies of isotopically labeled molecules. *Appl. Surf. Sci.* **2008**, *255*, 847.
[7] C. M. DeRito, G. M. Pumphrey, E. L. Madsen. Use of field-based stable isotope probing to identify adapted populations and track carbon flow through a phenol-degrading soil microbial community. *Appl. Environ. Microbiol.* **2005**, *71*, 7858.
[8] G. M. Pumphrey, B. T. Hanson, S. Chandra, E. L. Madsen. Dynamic secondary ion mass spectrometry imaging of microbial populations utilizing C-labelled substrates in pure culture and in soil. *Environ. Microbiol.* **2009**, *11*, 220.
[9] A. M. Herrmann, K. Ritz, N. Nunan, P. L. Clode, J. Pett-Ridge, M. R. Kilburn, M. D.V. Murphy, A. G. O'Donnell, E. A. Stockdale. Nano-scale secondary ion mass spectrometry – a new analytical tool in biogeochemistry and soil ecology: A review article. *Soil Biol. Biochem.* **2007**, *39*, 1835.
[10] C. Lechene, F. Hillion, G. McMahon, D. Benson, A. M. Keinfeld, J. P. Kampf, D. Distel, Y. Luyten, J. Bonventre, D. Hentschel, K. M. Park, S. Ito, M. Schwark, G. Benichou, G. Slodzian.

 Copyright © 2012 John Wiley & Sons, Ltd.

High-resolution quantitative imaging of mammalian and bacterial cells using stable isotope mass spectrometry. *J. Biol.* **2006**, *5*, 20.

[11] V. J. Orphan, C. H. House. Geobiological investigations using secondary ion mass spectrometry: microanalysis of extant and paleo-microbial processes. *Geobiology* **2009**, *7*, 360.

[12] M. Wagner. Single-cell ecophysiology of microbes as revealed by Raman microspectroscopy or secondary ion mass spectrometry Imaging. *Annu. Rev. Microbiol.* **2009**, *63*, 411.

[13] A. M. Herrmann, P. L. Clode, I. R. Fletcher, N. Nunan, E. A. Stockdale, A. G. O'Donnell, D. V. Murphy. A novel method for the study of the biophysical interface in soils using nano-scale secondary ion mass spectrometry. *Rapid Commun. Mass Spectrom.* **2007**, *21*, 29.

[14] P. L. Clode, M. R. Kilburn, D. L. Jones, E. A. Stockdale, J. B. Cliff, A. M. Herrmann, D. V. Murphy. In situ mapping of nutrient uptake in the rhizosphere using nanoscale secondary ion mass spectrometry. *Plant Physiol.* **2009**, *151*, 1751.

[15] C. Mueller, A. Kölbl, C. Hoeschen, F. Hillion, K. Heister, A. M. Herrmann, I. Koegel-Knabner. Submicron scale imaging of soil organic matter dynamics using NanoSIMS – from single particles to intact aggregates. *Org. Geochem.* **2012**, *42*, 1476.

[16] G. McMahon, F. Saint-Cyr, C. Lechene, C. J. Unkefer. CN^- secondary ions form by recombination as demonstrated using multi-isotope mass spectrometry of ^{13}C- and ^{15}N-labeled polyglycine. *J. Am. Soc. Mass Spectrom.* **2006**, *17*, 1181.

[17] L. Remusat, P.-J. Hatton, P. S. Nico, B. Zeller, M. Kleber, D. Derrien. NanoSIMS study of organic matter associated with soil aggregates: advantages, limitations and combination with STXM. *Environ. Sci. Technol.* **2012**. Available: http://pubs.acs.org/doi/abs/10.1021/es203745k.

[18] M. L. Davission, P. K. Weber, J. Pett-Ridge, S. Singer. Development of standards for NanoSIMS analyses of biological materials. Lawrence Livermore National Laboratory (LLNL), Livermore, CA, **2008**. Available: http://www.osti.gov/energycitations/product.biblio.jsp?osti_id=945782.

[19] P.-J. Hatton, M. Kleber, B. Zeller, C. Moni, A. Plante, K. Townsend, L. Gelhaye, K. Lajtha, D. Derrien. Transfer of litter-derived N to soil mineral–organic associations: evidence from decadal ^{15}N tracer experiments. *Org. Geochem.* **2012**, *42*, 1489.

[20] H. Craig. Isotopic standards for carbon and oxygen correction factors for mass spectrometric analysis of carbon dioxide. *Geochim. Cosmochim. Acta* **1957**, *12*, 133.

[21] A. Mariotti. Atmospheric nitrogen is a reliable standard for natural 15N abundance measurements. *Nature* **1983**, *303*, 685.

[22] J. Lehman, J. Kinyangi, D. Solomon. Organic matter stabilization in soil microaggregates: implications from spatial heterogeneity of organic carbon contents and carbon forms. *Biogeochemistry* **2007**, *85*, 45.

[23] J. Lehman, D. Solomon, J. Kinyangi, L. Dathe, S. Wirick, C. Jacobsen. Spatial complexity of soil organic matter forms at nanometer scales. *Nat. Geosci.* **2008**, *1*, 238.

[24] M. Kleber, P. Sollins, R. Sutton. A conceptual model of organo-mineral interactions in soils: self-assembly of organic molecular fragments into zonal structures on mineral surfaces. *Biogeochemistry* **2007**, *85*, 9.

[25] M. C. Rillig, B. A. Caldwell, H. A. B. Wosten, P. Sollins. Role of proteins in soil carbon and nitrogen storage: controls on persistence. *Biogeochemistry* **2007**, *85*, 25.

[26] A. J. Simpson, M. J. Simpson, E. Smith, B. P. Kelleher. Microbially derived inputs to soil organic matter: are current estimates too low? *Environ. Sci. Technol.* **2007**, *41*, 8070.

[27] H. Knicker. Soil organic N – an under-rated player for C sequestration in soils? *Soil Biol. Biochem.* **2011**, *43*, 1118.

NanoSIMS study of organic matter associated with soil aggregates: advantages, limitations and combination with STXM

Laurent Remusat [a*], Pierre-Joseph Hatton [b], Peter S. Nico [c], Bernd Zeller [b], Markus Kleber [d], Delphine Derrien [b]

V

[a] Laboratoire de Mineralogie et Cosmochimie du Muséum, UMR 7202 CNRS/MNHN, Musé um National d'Histoire Naturelle, case postale 52, 57 rue Cuvier, 75231 Paris Cedex 05, France

[b] INRA-Nancy, Biogéochimie des Ecosystemes Forestiers, 54280 Champenoux, France

[c] Earth Sciences Division, Lawrence Berkeley National Laboratory, 94720 Berkeley, California, USA

[b] Department of Crop and Soil Science, Oregon State University, 97331 Corvallis, OR, USA

* Corresponding author: remusat@mnhn.fr

Published in *Environmental Science & Technology* **46** (2012) : 3943-3949 [DOI]

Environmental Science & Technology

Article

pubs.acs.org/est

NanoSIMS Study of Organic Matter Associated with Soil Aggregates: Advantages, Limitations, and Combination with STXM

Laurent Remusat,*[,†] Pierre-Joseph Hatton,[‡] Peter S. Nico,[§] Bernd Zeller,[‡] Markus Kleber,[∥] and Delphine Derrien[‡]

[†]Laboratoire de Minéralogie et Cosmochimie du Muséum, UMR 7202 CNRS/MNHN, Muséum National d'Histoire Naturelle, case postale 52, 57 rue Cuvier, 75231 Paris Cedex 05, France

[‡]INRA, Laboratoire de Biogéochimie des Ecosystèmes Forestiers, UR 1138, INRA Nancy, 54280 Champenoux, France

[§]Earth Sciences Division, Lawrence Berkeley National Laboratory, Berkeley, California 94720, United States

[∥]Department of Crop and Soil Science, Oregon State University, Corvallis, Oregon 97331, United States

Supporting Information

ABSTRACT: Direct observations of processes occurring at the mineral-organic interface are increasingly seen as relevant for the cycling of both natural soil organic matter and organic contaminants in soils and sediments. Advanced analytical tools with the capability to visualize and characterize organic matter at the submicrometer scale, such as Nano Secondary Ion Mass Spectrometry (NanoSIMS) and Scanning Transmission X-ray Microscopy (STXM) coupled to Near Edge X-ray Absorption Fine Structure Spectroscopy (NEXAFS), may be combined to locate and characterize mineral-associated organic matter. Taking advantage of samples collected from a decadal ^{15}N litter labeling experiment in a temperate forest, we demonstrate the potential of NanoSIMS to image intact soil particles and to detect spots of isotopic enrichment even at low levels of ^{15}N application. We show how microsites of isotopic enrichment detected by NanoSIMS can be speciated by STXM-NEXAFS performed on the same particle. Finally, by showing how ^{15}N enrichment at one microsite could be linked to the presence of microbial metabolites, we emphasize the potential of this combined imaging and spectroscopic approach to link microenvironment with geochemical process and/or location with ecological function.

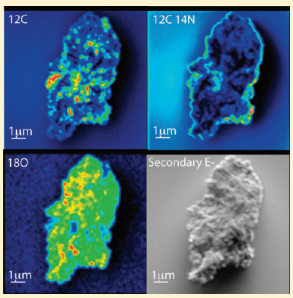

INTRODUCTION

The spatial distribution of organic matter (OM) within the soil matrix has major consequences for its accessibility to decomposers.[1] When mineral particles entrap or come in close association with OM, they build physical barriers that prevent decomposer organisms and exoenzymes from accessing OM and decrease the *in situ* supply of gas, water, and nutrients. A useful simplification divides the processes of mineral-organic interaction into two major categories. Organic matter can a) become occluded by aggregated soil structures and/or b) be engaged in fine scale interactions with mineral surfaces through the activity of microorganisms[2] and a variety of sorption mechanisms.[3,4] To date, investigations into the fate of mineral associated organic materials are restricted to procedures of bulk analysis performed on operationally defined physical fractions. They are expected to isolate mineral-organic associations of given characteristics, such as an increasing radiocarbon age and an increasing proportion of microbially processed organic matter in fractions of increasing density.[5−7] Nevertheless, all physical fractionation techniques in use today involve some level of interference with the spatial integrity of soil microenvironments, while there is an increasing awareness of a strong dependence of geochemical process intensity on the physical structure of the mineral matrix.

The development of micrometer to nanoscale techniques now opens the gate to elemental, isotopic, and molecular characterization at the required scale to shed new light on organo/mineral associations. Nano Secondary Ion Mass Spectrometry (NanoSIMS) provides elemental and isotopic maps of OM at the surface of mineral particles with a spatial resolution less than 100 nm[8−10] and permits tracking of isotopically labeled substrates added to the soil.[11−14] In contrast to bulk isotopic measurements by conventional techniques, NanoSIMS allows the visualization of the spread and dilution level of the label into the soil matrix. Previous NanoSIMS studies in soil science have been performed on samples embedded in epoxy and further polished to create surfaces without topography. However, studies on undisturbed microaggregates mounted without carbon-based chemicals are mandatory for applications that are focused on questions of OM turnover and contaminant degradation.

Scanning X-ray Transmission Microscopy in combination with Near Edge X-ray Absorption Fine Structure spectroscopy

Received: October 24, 2011
Revised: February 13, 2012
Accepted: February 24, 2012
Published: February 24, 2012

ACS Publications © 2012 American Chemical Society

(STXM/NEXAFS) can determine the speciation of OM at the nanoscale.[15−18] Because STXM and NanoSIMS operate at similar scales, they should theoretically provide complementary information about organic matter in soil microstructures, provided that samples have (i) intact spatial structure and are (ii) unaffected by embedding organic resins. Initial attempts toward this goal have recently been reported for tiny (micrometer-size) grains recovered from the coma of comet Wild 2 by the Stardust mission.[19] Our objective with this study is to demonstrate the potential and the limitation of NanoSIMS imaging for (1) tracking OM and labeled residues within soil microaggregates deposited on a clean surface, without any epoxy resin. We further use STXM/NEXAFS to (2) assess the nature of this labeled OM and (3) evaluate the information NanoSIMS can provide on the distribution of a ^{15}N-label within microaggregates. Our conceptual approach was to take advantage of the availability of physical soil separates collected from a forest soil in which ^{15}N-labeled litter had been applied 12 years before sampling.

EXPERIMENTAL METHODS

The soil was isolated from forest topsoil located at Ebrach in Germany (49°52′ N, 10°27′ E). It is classified (World Reference Base) as an acidic dystric Cambisol with a sandy loam texture.[20] ^{15}N labeled leaves were deposited 12 years before sampling (initial A^{15}N of incubated leaves was 2.48%, corresponding to δ^{15}N ≈ 5785‰ relative to the atmospheric N_2 standard). Physical fractions were obtained by density fractionation in order to isolate microaggregates. Organic matter within individual fractions was found to vary in the degree of microbial processing and carbon content:[21] microstructures from the 1.8−2.0 g cm^{-3} density fraction are more plant-like (C/N = 16, δ^{13}C = −27‰ relative to PDB) and contain 210 mg C/g of fraction, those found in the 2.2−2.4 g cm^{-3} density fractions show a more microbial-like signature (C/N = 11.5, δ^{13}C = −26‰) with a C content of 38 mg C/g of fraction. ^{15}N tracer applied a decade before sampling was found in both fractions: δ^{15}N values were 25.2 ± 0.5‰ in the 1.8−2.0 g cm^{-3} density and 25.6 ± 0.2‰ in the 2.2−2.4 g cm^{-3} density fraction, whereas δ^{15}N of unlabeled aggregates was −3.6 ± 0.1‰ in the lighter fraction and −0.3 ± 0.1‰ in the denser. More details and interpretation for the recovery of ^{15}N label in the microaggregates are available in ref 21.

An aliquot of each density fraction was deposited onto clean Si_3N_4 windows without the use of any fixative; particles are held in place by plain electrostatic forces. When samples were jointly studied with STXM-NEXAFS and NanoSIMS, they were first imaged by STXM-NEXAFS, because NanoSIMS beam damage is much more severe than that associated with STXM-NEXAFS.

STXM-NEXAFS analyses were performed at beamline 5.3.2 at the Advanced Light Source (ALS), Lawrence Berkeley National Laboratory, Berkeley, USA. Images were obtained by collecting stacks in the X-rays energy region of 278 to 330 eV for carbon NEXAFS and in the region of 390 to 440 eV for nitrogen NEXAFS. We omitted particles exhibiting an optical density greater than 2.0 at any energy between 278 eV and 290 eV, i.e. the main energy range of our carbon K-edge spectra. Those particles were considered to be nontransparent to X-rays, with an effective thickness larger than 150 nm; the thickness limit depends on energy and will be greater at higher energies. Data were processed with the software package aXis2000 to generate STXM images and NEXAFS spectra for selected regions of interest.[22]

NanoSIMS imaging was performed at MNHN Paris, France. Prior to NanoSIMS analysis, samples were gold coated (20 nm) to improve lateral charge compensation. Imaging was performed using a primary Cs^+ beam with a current set to 0.6 pA (using D1−3) to achieve an actual analytical spatial resolution of less than 100 nm. The primary beam stepped over the sample in a 256 × 256 pixel raster with a speed set at 2 ms/pixel. Secondary ions images of $^{12}C^-$, $^{13}C^-$, $^{18}O^-$, $^{26}CN^-$, and $^{27}CN^-$ were simultaneously collected by electron multipliers. The images cover areas from 64 to 225 μm^2. The secondary mass spectrometer was tuned for ∼6800 mass resolving power (Cameca definition for NanoSIMS) to resolve isobaric interferences (like at mass 27 between $^{12}C^{15}N$ and $^{13}C^{14}N$). Secondary electrons were also simultaneously collected in order to image the sample while we collect secondary ions. Several frames were collected and stacked to increase counting rate and reduce statistical error. Instrumental fractionation was corrected for isotopic ratios using terrestrial type III kerogen, an organic standard with properties similar to the unlabeled soil OM (δ^{15}N = 3.7 ± 0.2‰). Data were processed as quantitative isotopic ratio images and were corrected for instrumental bias including image drift from layer to layer (due to drift in the location of the ion beam from frame to frame). δ^{13}C maps did not reveal any significant enrichment over natural abundance, confirming that the method used in this study did not generate procedural isotope enrichment in our images. Prior to each image acquisition, the sample surface was presputtered using a high current beam (around 70 pA) to remove surface contamination and gold coating and to reach sputtering steady state. As a result, several 100s of nanometers are removed before the analysis. This means that a preexisting thin coating of the particle would be only visible at its edge, the center of the particle representing regions that are several 100s of nm below the surface of the microaggregates.

Detailed procedure for soil fractionation, sample preparation, technical settings for each technique, and statistics are described in the Supporting Information.

RESULTS AND DISCUSSION

1. NanoSIMS Investigation of Soil Microaggregates Deposited on a Si_3N_4 Window. Figure 1 shows a microaggregate of approximately 10 by 3 μm size that originated from a physical fraction dominated by plant-like organic materials.[21] In this image, ^{12}C and ^{26}CN are considered to represent OM, whereas ^{18}O signals are assigned to phyllosilicates, primary silicate minerals, or pedogenic oxides, ^{18}O yield being higher in mineral than in organic matrices. N is detected as the molecular CN^- ion due to much lower yield in N^- compared to CN^- under the Cs beam.[23,24] As expected the OM appears to be heterogeneously distributed: it occurs as a very thin coating or as patches in subsurface layers, possibly in protective pores. Nitrogen and carbon locations differ significantly, indicating a variable OM composition (see Figure S1). Carbon is distributed in patches all over the particle, while N is found in some patches and forms a discontinuous rim around the particle.

We need to consider possible sources of analytical bias to discuss the C and N distributions. Microaggregate roughness can be a potential source of bias because sample topography affects the NanoSIMS yield for $^{12}C^-$ and $^{26}CN^-$ ions,

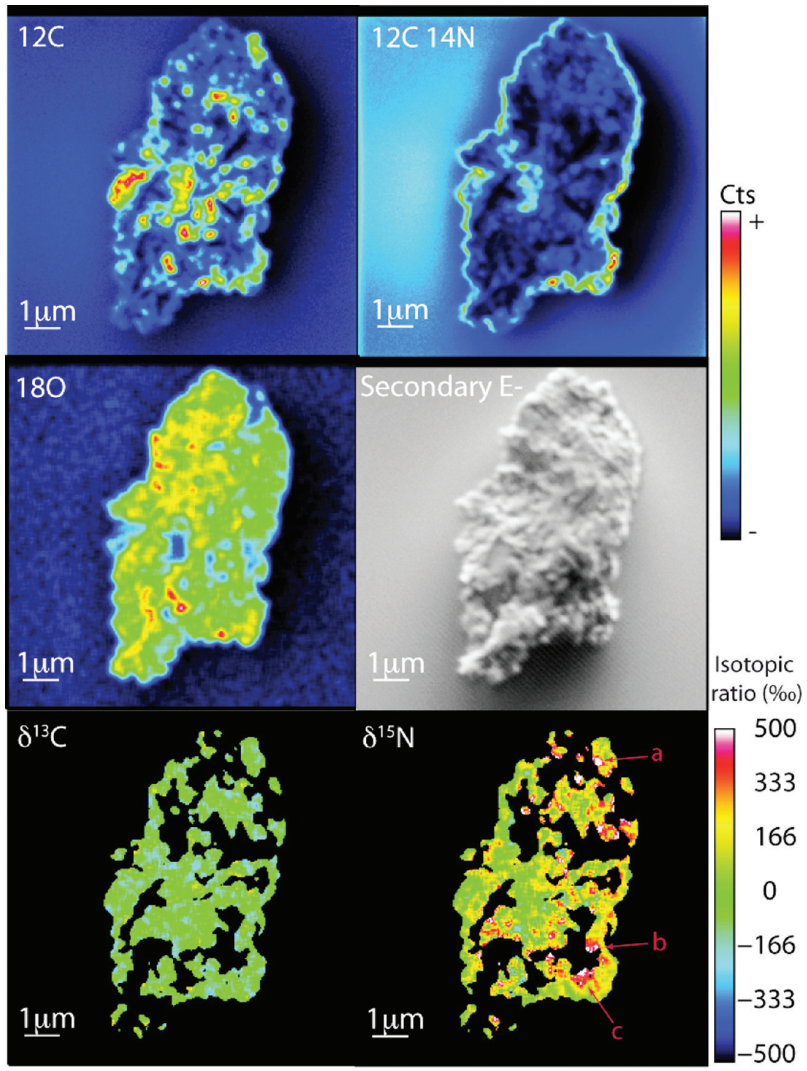

Figure 1. NanoSIMS images of a soil microaggregate, indicating the location of ^{12}C, ^{26}CN, and ^{18}O along the particle, whose shape is shown by secondary electrons. Maps of $\delta^{13}C$ and $\delta^{15}N$ are also represented. ^{15}N-rich hot spots can be distinguished with $\delta^{15}N$ significantly above the natural abundance; $\delta^{15}N = 573 \pm 175‰$, $382 \pm 85‰$, and $467 \pm 130‰$ (2 sigma errors) for a, b, and c, respectively. A mask was applied to these images by taking into account only the area of the particle with $^{12}C^-$ and $^{26}CN^-$ counts above an arbitrary threshold. Then, black regions correspond to the location of the Si_3N_4 window (on the sides) or to an area where we cannot get reliable data. δ(in ‰) = $(R_{sample}/R_{standard} - 1) \times 1000$. R stands for isotopic ratio.

preventing us from obtaining accurate C/N ratios.[25] However, on the X-Y profile (Figure S1) we find no correlation between the amplitude of secondary electrons (indicative of the topography) and $^{12}C^-$ and $^{26}CN^-$ signals. This allows us to exclude an influence of sample roughness on the distribution of N and C.

There is also the possibility that the $^{26}CN^-$ signal at the edges of the particle may be an artifact produced by the N-rich window. Scattering effects or wrong definition of the region of interest (ROI) may result in a fake rim. The X-Y profile through this particle (see Figure S1) proves that the $^{26}CN^-$ signal at the rim matches with the edge of the particle (indicated by the secondary electron signal) and that the CN^- signal is more intense at the particle rim than on the Si_3N_4 window. Scattering of the primary Cs beam[26,27] could skew the location of N rich areas in our configuration. When primary Cs ions hit the side of a particle, some may be deviated to the Si_3N_4 window and sputter it, potentially leading to of the appearance of a fake N-rich layer around the particle. This effect is nevertheless small if the particle is constituted by light

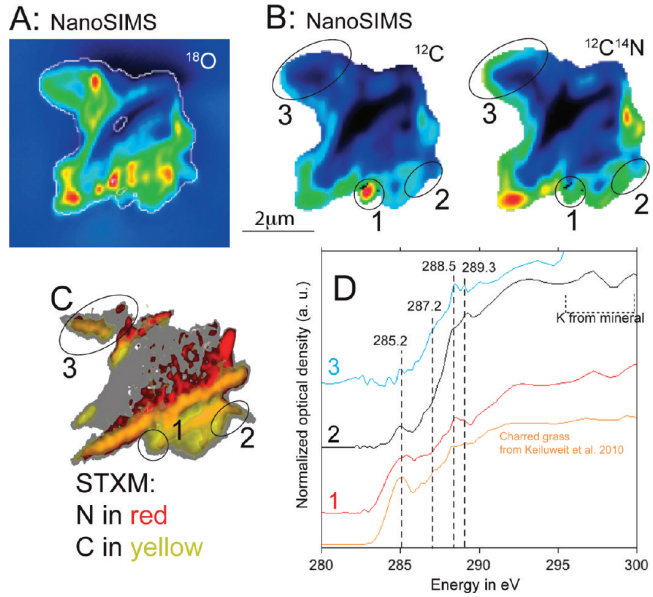

Figure 2. Example of the combined study of a soil aggregate by NanoSIMS (A and B) and STXM/NEXAFS (C and D). ^{18}O image (A) can be used to map the inorganic part of the whole particle. OM, represented by ^{12}C and ^{26}CN, occurs only as a rim around the particle (B). Color scale for A and B is similar to Figure 1. (C) is an image of C and N as revealed by STXM imaging, the regions where the sample was too thick to get NEXAFS spectra or was free of organic matter appear in gray. In (D), the carbon-NEXAFS spectra of the three areas defined in panels B and C are compared with a black carbon spectra obtained from ref 28. Area (1) is identified by C-NEXAFS as black carbon; this is consistent with a strong $^{12}C^-$ signal on the NanoSIMS image. See text for peak identification.

elements, inducing a small scattering effect because they absorb Cs ions more easily. We believe that we can rule out this effect here because 1) on the secondary electron image (Figure 1), the microaggregate is rather flat with a roughness smaller than its lateral extension, and it should not be thicker than a couple of micrometers and is composed of light elements (silicates and OM); such particles are not expected to induce significant scattering; 2) The $^{26}CN^-$ rich rim is discontinuous, like on the top side of the particle: the CN^- coating is absent, whereas the aspect of the particle is similar to other side regions; there is no reason scattering would not happen in this region in contrast to the rest of the edge of the particle, the primary beam in the NanoSIMS being quasi-perpendicular to the surface. On the other hand, it seems possible that an OM coating could have been cut off in some places during sample preparation. In addition, in another imaging study not involving STXM imaging, we have deposited similar soil microaggregates on cleaned N-free gold foil and the same N-rich rim could also be observed (see an example in Figure S2). Finally, redeposition of N-rich material around the particle during the Cs sputtering can be excluded here because it would occur outside the imaged area where the Cs beam does not raster.

We conclude that the observation of a N-rich coating, in this case, is not biased and reflects the actual occurrence of OM containing more N-rich moieties than most of the OM of this microaggregate. This N-rich OM also seems to occur in one area in the middle of grain in a pore (as revealed by a hole in $^{18}O^-$ image) that could have been connected to the outer part of the microaggregate. Clear determination of the origin of this OM is, however, hampered by the lack of information at the molecular scale.

2. NanoSIMS Characterization of OM Containing a ^{15}N Tracer. The amount of ^{15}N tracer was low in our samples collected from a decadal, in situ labeling experiment: the microaggregates contained about 10 $mg{\cdot}g^{-1}$ N, with ^{15}N representing only 0.3705% of the total N (very close to 0.3655%, the mean natural abundance of ^{15}N). Nevertheless, NanoSIMS successfully detected several cases of ^{15}N-enriched OM among 20 studied particles (Figure 1): the $\delta^{15}N$ map indicates three locations of ^{15}N rich organic materials (see the SI and Figure S3 for a description of the statistics used to identify ^{15}N-rich hotspots). In spite of the small size of these regions of interest (around 400 nm wide), the degree of isotopic enrichment is significant even when considerable natural variability is assumed, with $\delta^{15}N$ up to 500‰ whereas natural OM is around $\delta^{15}N = -2$‰. The occurrence of such enriched ^{15}N spots is not compatible with an intense microbial recycling of labeled residues over the 12 year incubation; an intense recycling would have diluted the isotopic signal and spread it over the soil components. As a result, the spots of ^{15}N-rich organic matter are either unaltered residues of the original labeled litter incubated for 12 years or stabilized products of the recycling of this litter. Unfortunately, C/N ratios determined by NanoSIMS in the course of this study are not accurate enough to distinguish between any of the two hypotheses.

A molecular investigation at a similar scale is desirable to assess the fate of the organic label in such a long-term experiment. Characterization at the molecular level is usually achieved by using NMR or GC-MS, but these techniques do

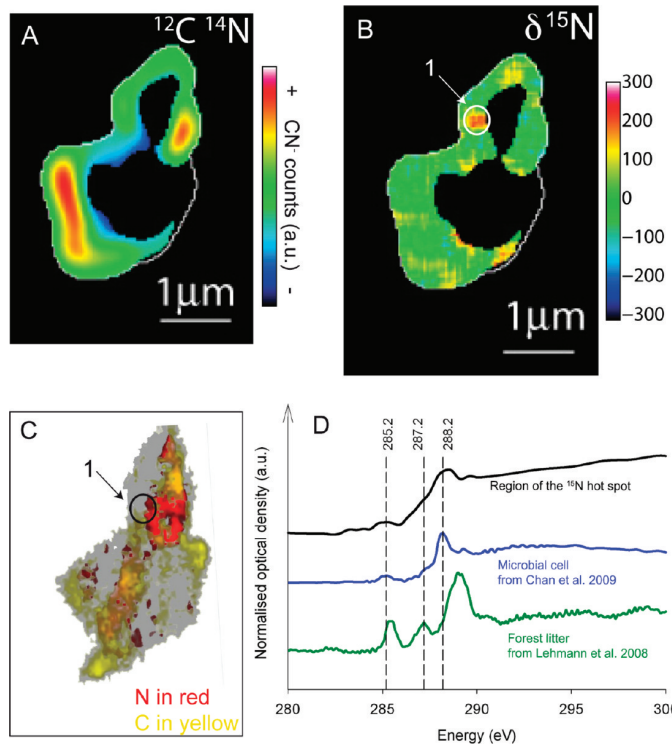

Figure 3. Joined NanoSIMS/STXM study of a soil aggregate with a ^{15}N hot spot. (A): ^{26}CN image. (B): $\delta^{15}N$ image of the same grain. A mask was applied on these images with a similar fashion as Figure 2. The point (1) indicates a ^{15}N-rich hot spot, $\delta^{15}N = 213 \pm 132‰$. STXM C and N imaging is reported in (C). Carbon-NEXAFS (panel D) shows that the litter-derived-^{15}N (region 1) would be involved in microbial OM as indicated by the comparison with forest litter from ref 30 and microbe cell from ref 31. See text for peak identification.

not provide information about the spatial distribution of molecular moieties at the micrometer scale.

3. Combined Investigation of Labeled Soil Microaggregates by STXM and NanoSIMS. Figure 2 shows images successively acquired on both STXM and NanoSIMS for a five micrometer-wide microaggregate from the fraction characterized by microbial organic matter.[21] On NanoSIMS images, OM appears only as a thick coating around a side of the particle (Figure 2B), while STXM mapping detects OM within a larger zone (Figure 2C). This illustrates that NanoSIMS and STXM do not image the sample in the same way. NanoSIMS, as a surface technique, can only probe the (sub)surface over a few tens of nm, whereas STXM is a transmission technique that averages information over the entire thickness of the sample. While OM located on the back of the sample will be invisible for NanoSIMS, it contributes to the signal obtained by STXM. For this reason, comparisons between STXM and NanoSIMS images need to account for the fact that the STXM/NEXAFS signal may indicate the presence of more organic species than are present in the thin surface layer probed by NanoSIMS. Only areas with concomitant NanoSIMS and STXM signals (like areas 1 and 2 in Figure 2) should be taken into account for joined interpretations. Area 1 is identified by both techniques as being composed of a type of OM that differs from the rest of the organic coating around the aggregate. On NanoSIMS images, this area appears to be very C-rich and could correspond to carbonized OM. The C-NEXAFS spectrum extracted for this area reveals a broad and strong absorption band around 285.2 eV produced by aromatic C and a second distinct peak at 288.5 eV in the carboxylic region. The dominance of the aromatic peak is suggestive of black carbon (BC), and, in fact the major features of this spectrum can be well reproduced by a 58% and 44% linear combination of two reference char spectra, Fescue grass charred at 300 and 700 °C respectively.[28] In the σ^* and postedge normalization range, >290.5 eV, the shape of the two spectra remain similar although the absolute intensity is different. As this range is very sensitive to normalization and thickness effects, the fact that the lower energy resonances can be well matched by sample BC spectra remains strong evidence for the carbon in the particle being derived from BC. In contrast, the rest of the OM of this particle, as sampled in areas 2 and 3, shows a smaller peak of aromatic material (285.2 eV) and noticeable resonances at 288.5 eV and 289.3 eV. The region 2 spectrum has the same overall shape of standard spectrum of Tall Fescue grass,[28] despite a slight shift to lower energy by 0.14 eV. Even without this shift, the very high degree of similarity implies a potential plant material origin of this spectrum. The region 3 spectrum shows the same features as the region 2 spectrum with additional intensity at 287.2 eV. Solomon et al.[16] assigned the 287.3 region to aliphatic carbon. Similarly, Brandes et al.[15] identified the aliphatic region as 287.1 to 287.4 eV. The

increased intensity in this region of the #3 spectrum indicates a greater concentration of aliphatic carbon.

Figure 3 shows the images we successively obtained by both techniques on a particle with a ^{15}N rich hot spot (Figure 3, region 1). This particle was from a density fraction enriched with microbial products.[21] The ^{15}N-rich hot spot has a $\delta^{15}N$ value of 213 ± 132‰ (2 sigma). According to NanoSIMS and STXM investigations, it is located in a N-poor region (see panels A and C). The feature in the C-NEXAFS spectrum extracted from this area has a relatively broad absorbance band, ranging from 287.8 eV to 288.9 ev, centered at 288.3 eV, and peaking at 288.5 eV. The 288.7 eV to 288.8 eV range is taken by Kinyangi et al.[17] to indicate carboxyl-C with amide type features resonating at the lower energy side of this range at 288.2.[29] The broad nature of this feature in the sample spectrum combined with the lack of large resonances in the aromatic (285.2 eV) region or other prominent features makes the most likely interpretation of this peak to be a mixture of carbon containing a large fraction of carboxylic/amide functional groups consistent with a mixture of proteins, amino-sugars, and acid containing polysaccharides. The ^{15}N rich hot spot is more consistent with microbial body material and/or exopolysaccacarides than it is with fresh plant litter material as seen in Figure 2 or in ref 30 (see the comparison in Figure 3). This is also supported by the comparison with data acquired on pure microbial cells.[31] These results are consistent with the hypothesis that the potential ^{15}N enrichment in this location originates from microbial metabolites produced from the decomposition of the ^{15}N-rich litter rather than a fragment of the litter itself.

It should be cautionary noted that fine scale mixing between several organic pools (like a little amount of labeled plant material embedded in a larger unlabeled blob of microbial material) may remain an issue. A greater number of observations at the nanoscale would help to establish a more robust assessment. If confirmed, such visual observations would represent a great step forward for the soil science community. They would illustrate that microbial processing of litter-^{15}N favors its retention in soil through to interactions with mineral surfaces and prevents it from being continuously cycled and eventually diluted, released, and lost as inorganic ^{15}N.

4. Technical Challenges To Combine STXM and NanoSIMS. Several technical constraints, sometimes hard to reconcile, arise if the exact same spot on a given specimen has to be examined with STXM and NanoSIMS.

1) The samples must be mounted in the same fashion for STXM and NanoSIMS analysis. Most STXM holders contain either N (Si_3N_4 window) or C (TEM Cu grid with C lacey) and may introduce unwanted bias for NanoSIMS N and C imaging (ion scattering, background contribution).
2) The regions of interest (ROI) have to be large enough (about 500 nm in diameter) to achieve decent counting statistics with NanoSIMS; this is easier to do for large particles. At the same time, particles have to be transparent to X-rays, i.e. with an effective thickness smaller than 150 nm, to be studied by STXM. Consequently, flat particles are the best targets for joint STXM/NanoSIMS studies − with resulting issues in terms of biased sample populations.
3) Charging of quartz grains during NanoSIMS imaging, in spite of gold coating, is an issue, resulting in a dramatic decrease of signal intensity. This is usually addressed by flooding the sample with electrons for charge compensation using a device called "electron gun". Because the electrons produced by the electron gun dazzle the detector for secondary electrons, the electron gun would have prevented us from acquiring the secondary electron images that were needed to overlap images obtained from STXM and NanoSIMS and to assess analytical bias. We decided to favor the secondary electron images and to mask, on our images, the very few regions showing obvious charging. As a consequence, there is no information at the location of charging, while the information for the rest of the image is deemed suitable for interpretation. When mineral grains are significantly coated by organic material, charging effects can be neglected (see Figure 1). As a result, only regions free of organic material appear to undergo charging; there is no significant loss of information about the OM at the surface of a microaggregate if charging obscures only the inorganic component.

5. Environmental Implications. Our study has demonstrated the feasibility of NanoSIMS investigations on isolated soil microstructures deposited on a clean surface. We have shown how NanoSIMS identifies organic and mineral components in microaggregates and detects the occurrence of local concentration of any isotopic label even in the case of weakly labeled samples. The observation of some label-rich hot spots in our long-term experiment shows that labeled organic matter in soil can be preserved over a long period.

STXM-NEXAFS combined with NanoSIMS generates more robust conclusions than NanoSIMS imaging alone. Joint STXM/NEXAFS analysis requires a significant amount of analytical time on both instruments. When implemented, the combination of methods offers a means to test hypothesis arising from bulk scale studies by visualizing the suspected process. The really unique set of results from such a combination, in addition to small-scale textural observation using SEM and TEM, opens a new window of opportunities for geochemical and ecological processes research at the submicrometer scale.

■ ASSOCIATED CONTENT

Supporting Information

Detailed information about the analytical parameters used for both STXM and NanoSIMS, sample preparation techniques, background information on the field study experiment, isotope reference standard analysis, and additional images. This material is available free of charge via the Internet at http://pubs.acs.org.

■ AUTHOR INFORMATION

Corresponding Author

*Phone: +33 1 40 79 81 42. Fax: +33 1 40 79 57 72. E-mail: remusat@mnhn.fr.

Notes

The authors declare no competing financial interest.

■ ACKNOWLEDGMENTS

This research was financially supported by the France-Berkeley Fund, DOE-BER-LBL Subsurface Science SFA, and LLNL LDRD #10ERD021. Johannes Lehmann, Alice Chan, Peter Weber, Jennifer Pett-Ridge, and Jean-Nicolas Audinot are

thanked for helpful discussion. We are also grateful to Sylvain Bernard for helpful advice and comments and David Kilcoyne for his support on the STXM beamline 5.3.2.2.Access to ALS beamline 5.3.2.2 was provided by the Office of Science, Office of Basic Energy Science (DE-AC02-05CH11231). The National NanoSIMS facility at the MNHN was established by funds from the CNRS , Région Ile de France, Ministère délégué à l'Enseignement supérieur et à la Recherche, and the MNHN. We also thank three anonymous reviewers for their comments that improved the manuscript.

REFERENCES

(1) Ekschmitt, K.; Kandeler, E.; Poll, C.; Brune, A.; Buscot, F.; Friedrich, M.; Gleixner, G.; Hartmann, A.; Kastner, M.; Marhan, S.; Miltner, A.; Scheu, S.; Wolters, V. Soil-carbon preservation through habitat constraints and biological limitations on decomposer activity. *J. Plant Nutr. Soil Sci.* **2008**, *171*, 27−35.

(2) Bos, R.; van der Mei, H. C.; Busscher, H. J. Physico-chemistry of initial microbial adhesive interactions - its mechanisms and methods for study. *FEMS Microbiol. Rev.* **1999**, *23* (2), 179−229.

(3) Lehmann, J.; Kinyangi, J.; Solomon, D. Organic matter stabilization in soil microaggregates: implications from spatial heterogeneity of organic carbon contents and carbon forms. *Biogeochemistry* **2007**, *85*, 45−57.

(4) Mikutta, R.; Kaiser, K.; Dörr, N.; Vollmer, A. C.; Chadwick, O. A.; Chorover, J.; Kramer, C.; Guggenberg, G. Mineralogical impact on organic nitrogen across a long-term soil chronosequence (0.3−4100 kyr). *Geochim. Cosmochim. Acta* **2010**, *74*, 2142−2164.

(5) Derrien, D.; Marol, C.; Balabane, M.; Balesdent, J. The turnover of carbohydrates in a cultivated soil estimated by 13C natural abundances. *Eur. J. Soil Sci.* **2006**, *57* (4), 547−557.

(6) von Lützow, M.; Kögel-Knabner, I.; Ekschmitt, K.; Flessa, H.; Guggenberg, G.; Matzner, E.; Marschner, B. SOM fractionation methods: Relevance to functional pools and stabilization mechanisms. *Soil Biol. Biochem.* **2007**, *39*, 2183−2207.

(7) Grandy, A. S.; Neff, J. C. Molecular C dynamics downstream: The biochemical decomposition sequence and its impact on soil organic matter structure and function. *Sci. Total Environ.* **2008**, *404* (2−3), 297−307.

(8) Lechene, C. P.; Luyten, Y.; McMahon, G.; Distel, D. L. Quantitative Imaging of Nitrogen Fixation by Individual Bacteria Within Animal Cells. *Science* **2007**, *317* (5844), 1563−1566.

(9) Herrmann, A. M.; Clode, P. L.; Fletcher, I. R.; Nunan, N.; Stockdale, E. A.; O'Donnel, A. G.; Murphy, D. V. A novel method for the study of the biophysical interface in soils using nano-scale secondary ion mass spectrometry. *Rapid Commun. Mass Spectrom.* **2007**, *21* (1), 29−34.

(10) Heister, K.; Höschen, C.; Pronk, G.; Mueller, C.; Kögel-Knabner, I. NanoSIMS as a tool for characterizing soil model compounds and organomineral associations in artificial soils. *J. Soils Sediments* **2012**, *12* (1), 35−47.

(11) Clode, P. L.; Kilburn, M. R.; Jones, D. L.; Stockdale, E. A.; Cliff, J. B.; Herrmann, A. M.; Murphy, D. V. In situ mapping of nutrient uptake in the rhizosphere using nanoscale sceondary ion mass spectrometry. *Plant Physiol.* **2009**, *151*, 1751−1757.

(12) Popa, R.; Weber, P. K.; Pett-Ridge, J.; Finzi, J. A.; Fallon, S. J.; Hutcheon, I. D.; Nealson, K. H.; Capone, D. G. Carbon and nitrogen fixation and metabolite exchange in and between individual cells of Anabaena oscillarioides. *ISME* **2007**, *1*, 354−360.

(13) Herrmann, A. M.; Ritz, K.; Nunan, N.; Clode, P. L.; Pett-Ridge, J.; Kilburn, M. R.; Murphy, D. V.; O'Donnell, A. G.; Stockdale, E. A. Nano-scale secondary ion mass spectrometry -- A new analytical tool in biogeochemistry and soil ecology: A review article. *Soil Biol. Biochem.* **2007**, *39* (8), 1835−1850.

(14) Mueller, C. W.; Kölbl, A.; Hoeschen, C.; Hillion, F.; Heister, K.; Herrmann, A. M.; Kögel-Knabner, I. Submicron scale imaging of soil organic matter dynamics using NanoSIMS - From single particles to intact aggregates. *Org. Geochem.* **2012**, *42* (12), 1476−1488.

(15) Brandes, J. A.; Lee, C.; Wakeham, S.; Peterson, M.; Jacobsen, C.; Wirick, S.; Cody, G. Examining marine particulate organic matter at sub-micron scales using scanning transmission X-ray microscopy and carbon X-ray absorption near edge structure spectroscopy. *Mar. Chem.* **2004**, *92*, 107−121.

(16) Solomon, D.; Lehmann, J.; Kinyangi, J.; Liang, B.; Heymann, K.; Dathe, L.; Hanley, K. Carbon (1s) NEXAFS spectroscopy of biogeochemically relevant reference organic compounds. *Soil Sci. Soc. Am. J.* **2009**, *73* (6), 1817−1830.

(17) Kinyangi, J.; Solomon, D.; Liang, B.; Lerotic, M.; Wirick, S.; Lehmann, J. Nanoscale biogeocomplexity of organnomineral assemblage in soil: Application of STXM microscopy and C 1s-NEXAFS spectroscopy. *Soil Sci. Soc. Am. J.* **2006**, *70*, 1708−1718.

(18) Bernard, S.; Benzerara, K.; Beyssac, O.; Brown, G. E.; Stamm, L. G.; Duringer, P. Ultrastructural and chemical study of modern and fossil sporoderms by Scanning Transmission X-ray Microscopy (STXM). *Rev. Palaeobot. Palynology* **2009**, *156* (1−2), 248−261.

(19) De Gregorio, B. T.; Stroud, R. M.; Nittler, L. R.; Alexander, C. M. O. D.; Kilcoyne, A. L. D.; Zega, T. J. Isotopic anomalies in organic nanoglobules from Comet 81P/Wild 2: Comparison to Murchison nanoglobules and isotopic anomalies induced in terrestrial organics by electron irradiation. *Geochim. Cosmochim. Acta* **2010**, *74* (15), 4454−4470.

(20) Zeller, B.; Colin-Belgrand, M.; Dambrine, E.; Martin, F. Fate of nitrogen released from 15N-labeled litter in European beech forests. *Tree Physiology* **2001**, *21* (2−3), 153−162.

(21) Hatton, P.-J.; Kleber, M.; Zeller, B.; Moni, C.; Plante, A.; Townsend, K.; Lajtha, K.; Derrien, D. Transfer of a ^{15}N litter label from the organic surface layer (O) to mineral-organic associations in the A-horizon: a decadal perspective. *Org. Geochem.* **2012**, *42* (12), 1489−1501.

(22) Hitchcock, A. P. *aXis2000. Analysis of X-ray Images and Spectra*; McMaster University: Hamilton, Ontario, Canada, 2006.

(23) McMahon, G.; Saint-Cyr, H. F.; Lechene, C.; Unkefer, C. J. CN- Secondary Ions Form by Recombination as Demonstrated Using Multi-Isotope Mass Spectrometry of 13C- and 15N-Labeled Polyglycine. *J. Am. Soc. Mass Spectrom.* **2006**, *17* (8), 1181−1187.

(24) Gnaser, H. Formation of metastable N2- and CO- anions in sputtering. *Phys. Rev. A* **1997**, *56* (4), R2518.

(25) Thomen, A.; Remusat, L.; Robert, F.; Meibom, A.; Mostefaoui, S., Chemical and Nitrogen Isotopic Composition of the Hotspots in Orgueil Insoluble Organic Matter. In *Lunar and Planetary Institute Science Conference*, **2010**; 2472.pdf.

(26) Luo, X. J.; Guillot, J.; Sanctuary, R.; Migeon, H. N., Topography artefacts in NanoSIMS 50 elemental images. In *7th European Workshop on Secondary Ion Mass Spectrometry*, Munster, **2010**; #20.

(27) Lee, J. L. S.; Gilmore, I. S.; Fletcher, I. W.; Seah, M. P. Topography and field effects in the quantitative analysis of conductive surfaces using ToF-SIMS. *Appl. Surf. Sci.* **2008**, *255* (4), 1560−1563.

(28) Keiluweit, M.; Nico, P.; Johnson, M. G.; Kleber, M. Dynamic molecular chemical strucutre of plant biomass-derived black carbon (biochar). *Environ. Sci. Technol.* **2010**, *44*, 1247−1253.

(29) Lawrence, J. R.; Swerhone, G. D. W.; Leppard, G. G.; Araki, T.; Zhang, X.; West, M. M.; Hitchcock, A. P. Scanning Transmission X-Ray, Laser Scanning, and Transmission Electron Microscopy Mapping of the Exopolymeric Matrix of Microbial Biofilms. *Appl. Environ. Microbiol.* **2003**, *69* (9), 5543−5554.

(30) Lehmann, J.; Solomon, D.; Kinyangi, J.; Dathe, L.; Wirick, S.; Jacobsen, C. Spatial complexity of soil organic matter forms at nanometre scales. *Nat. Geosci.* **2008**, *1*, 238−242.

(31) Chan, C. S.; Fakra, S. C.; Edwards, D. C.; Emerson, D.; Banfield, J. F. Iron oxyhydroxide mineralization on microbial extracellular polysaccharides. *Geochim. Cosmochim. Acta* **2009**, *73*, 3807−3818.

Supporting informations :

Soil sample preparation

The labeled forest soil sample was collected from an acidic dystric Cambisol with a sandy loam texture located at the Ebrach site in Germany (49°52' N, 10°27' E). It is a long-term labeling experiment conducted in situ. Site characteristics, labeling and sampling procedures are described in details Hatton et al. (2011). Shortly, the label was applied as a single pulse of highly 15N-enriched beech litter (δ15N≈5785‰) in February 1996, the label litter being obtained by two foliar applications of urea to young beech trees in another forest in 1994 and 1995 [1]. The soil sample was collected twelve years after tracer application, from the 0-2.5cm of the A-horizon, sieved to pass 2 mm and stored at +4°C. Following a method described by [2], it was further fractionated according to density using a sequential fractionation method in sodium polytungstate (SPT). Moist bulk soil samples were suspended in SPT solutions and shaken for 2 h, before being centrifuged at 2560g for 10 min. After adjusting density to target cutoffs (±0.01 g/cm3), the supernatant was aspirated using a vacuum system. The SPT solution was then adjusted to the next higher density in the sequence and the same procedure repeated again with the remaining soil pellet. The SPT was removed from the isolated fractions using deionized water and the fractions were oven dried for 2 days at + 55°C. Some particles from the 1.8-2.0 and 2.2-2.4 g.cm-3 density fractions have been imaged by both STXM-NEXAFS and NanoSIMS techniques. The organic matter in the first density fraction is expected to consist in plant residues aggregated with mineral particles whereas it has a dominant microbial signature in the heavier density fraction [3]. Samples were then mounted on standard Si3N4 windows (obtained from Silson Ltd., England) for STXM and NanoSIMS analysis. Prior to NanoSIMS analysis, the Si3N4 windows were gold coated (20 nm thick) to improve lateral dispersion of charges.

NanoSIMS settings

Isotopic and chemical images were acquired on the Cameca (Gennevilliers, France) NanoSIMS 50 installed at the Museum of Natural History (MNHN) in Paris, France. This instrument allows the simultaneous collection of 5 isotopes with a high spatial resolution and high mass resolution. A primary Cs+ beam was used, with a current set to 0.6 pA to achieve an actual analytical spatial resolution of less than 100 nm. The primary beam stepped over the sample in a 256 x 256 pixel raster with a speed set at 2 ms/pixel. Secondary ions images of 12C -,13C -, 18O -, 26CN – and 27CN – were simultaneously collected by electron multipliers with a dead time of 44 ns. Due to the poor yield of N- under the Cs+ primary beam, nitrogen is detected combined with C as the molecular ion CN- [4, 5]. The images cover areas from 64 to 225 μm^2. The secondary mass spectrometer was tuned for ~6800 mass resolving power (defined as the ratio ΔM/M) to resolve isobaric interferences (particularly at mass 27 between 12C15N and 13C14N). Samples were also imaged simultaneously by secondary electrons allowing us to have an electron image of the sample while we collect secondary ions. Several frames were collected and stacked to reach enough counting rate for descent statistics. Instrumental fractionations were corrected thanks to a terrestrial type 3 kerogen. Prior to each image, a high Cs+ current (around 70 pA) was used to presputter the surface of the sample in order to remove the gold coating and surface contaminants and to reach sputtering steady state.

Data were processed as quantitative isotopic ratio images using l'image software, developed by L. Nittler (Carnegie Institution of Washington), and were corrected for detector dead time and image drift from layer to layer (due to drift in the location of the ion beam from frame to frame).

Error calculations and statistics used

Errors reported in this study are based on counting statistics [6]. Assuming Poison counting statistics, the standard deviation (σion) for the number of ions in one pixel (or one region of interest) is given by σion=√N; N being the total ion counts collected at the location of this pixel (or region of interest). The standard deviation of any isotopic (or elemental) ratio is calculated by propagating the errors on each ion counts based on Taylor series expansion. During the session, the standard is measured several times. This allows us to determine an instrumental fractionation with an uncertainty. This uncertainty is based on the external reproducibility (achieved on the standard) that corresponds to the standard deviation of several measurements done at several locations. This uncertainty is propagated in the calculation of the final standard deviation

σratio of the isotopic ratio. The reported errors are 2 sigma errors (i.e. 2×σratio), corresponding to a 95% interval of confidence in a Gaussian distribution.
A significant isotopic anomaly is defined by a ratio RROI (that can be expressed in δ unit) significantly different than the average value, i.e. with an error σratio much smaller than the difference between these values. This means that we need to take in account not only the ratio or delta image (for instance figure 1) but also the image of the errors on this ratio. For an easier determination of isotopic anomalies (positive in the case of enrichments and negative in the case of depletion), we can define for each pixel a parameter Σpixel = |Rpixel-Rimage|/ σpixel. Rpixel is the ratio calculated for the considered pixel, Rimage is the same ratio calculated for the whole image and σpixel is the standard deviation of the ratio calculated for the considered pixel. Using the image of Σ (figure S3), it is easy to locate pixels with Rpixel>Rimage×3σpixel, which we considered as significantly above the average value and so corresponding to positive anomaly. As shown in figure S3, some pixels can exhibit a Σpixel>3, but if they do not define a region of interest (ROI) with a significant size (set arbitrary to 300nm, about three times the spatial resolution), they are rejected. All the hot spots that we have defined in this study had to fill two criteria that can be observed in figure S3: showing a hot spot larger than 300 nm in both the δ and the Σ images.

Synchrotron near edge X-ray absorption fine structure (NEXAFS) spectroscopy settings
Synchrotron X-ray spectromicroscopic analysis was conducted at scanning transmission X-ray microscope (STXM) endstation of beamline 5.3.2.2 of the Advanced Light Source of Lawrence Berkeley National Laboratory (beamline 5.3.2). Detailed operation principles of STXM/NEXAFS are published elsewhere [7-9] and will be described here only briefly. Except when mentioned, we disregarded particles with optical density greater than 2.0 at any energy between 278 eV and 290eV, i.e. the main energy range of our carbon K-edge spectra. This limited particle selection to those smaller than approximately five microns. We collected stacks in the region of 278 eV to 330 eV for carbon NEXAFS and in the region of 390 eV to 440 eV for nitrogen NEXAFS. NEXAFS stack alignment and analyses, alignment of background and edge maps of other elements were done using the Zimba alignment module of the software package aXis2000 [8]. Pre-edge subtraction and post-edge normalization was done using Athena [10-12]. Carbon spectra were smoothed using two iterations of the Athena interpolative smoothing algorithm.

References
1. Zeller, B.; Colin-Belgrand, M.; Dambrine, E.; Martin, F., N-15 partitioning and production of N-15-labelled litter in beech trees following [N-15] urea spray. Annales Des Sciences Forestieres 1998, 55, (3), 375-383.
2. Sollins, P.; Swanston, C.; Kleber, M.; Filley, T.; Kramer, M.; Crow, S.; Caldwell, B. A.; Lajtha, K.; Bowden, R., Organic C and N stabilization in a forest soil: Evidence from sequential density fractionation. Soil Biol. Biochem. 2006, 38, (11), 3313-3324.
3. Hatton, P.-J.; Kleber, M.; Zeller, B.; Moni, C.; Plante, A.; Townsend, K.; Lajtha, K.; Derrien, D., Transfer of a 15N litter label from the organic surface layer (O) to mineral-organic associations in the A-horizon: a decadal perspective. Org. Geochem. 2012, 42, 1489-1501.
4. Gnaser, H., Formation of metastable N2- and CO- anions in sputtering. Phys. Rev. A 1997, 56, (4), R2518.
5. McMahon, G.; Saint-Cyr, H. F.; Lechene, C.; Unkefer, C. J., CN- Secondary Ions Form by Recombination as Demonstrated Using Multi-Isotope Mass Spectrometry of 13C- and 15N-Labeled Polyglycine. J. Am. Soc. Mass Spectrom. 2006, 17, (8), 1181-1187.
6. Fitzsimons, I. C. W.; Harte, B.; Clark, R. M., SIMS stable isotope measurement: counting statistics and analytical precision. Mineral. Mag. 2000, 64, (1), 59-83.
7. Braun, A., Carbon speciation in airborne particulate matter with C (1s) NEXAFS spectroscopy. J. Environ. Monit. 2005, 7, (11), 1059-1065.
8. Hitchcock, A. P. aXis2000. Analysis of X-ray Images and Spectra, McMaster University, Hamilton, Ontario, Canada.: 2006.
9.Warwick, T.; Ade, H.; Kilcoyne, D.; Kritscher, M.; Tylisczcak, T.; Fakra, S.; Hitchcock, A.; Hitchcock, P.; Padmore, H., A new bend-magnet beamline for scanning transmission X-ray microscopy at the Advanced Light Source. J Synchrotron Radiat 2002, 9, 254-257.

10. Bargar, J. R.; Reitmeyer, R.; Davis, J. A., Spectroscopic confirmation of uranium(VI)-carbonato adsorption complexes on hematite. Environ. Sci. Technol. 1999, 33, (14), 2481-2484.
11. Newville, M., IFEFFIT: interactive EXAFS analysis and FEFF fitting. J. Synch. Rad. 2001, 8, 322-324.
12. Ravel, B.; Newville, M., ATHENA, ARTEMIS, HEPHAESTUS: data analysis for X-ray absorption spectroscopy using IFEFFIT. J. Synch. Rad. 2005, 12, 537-541.

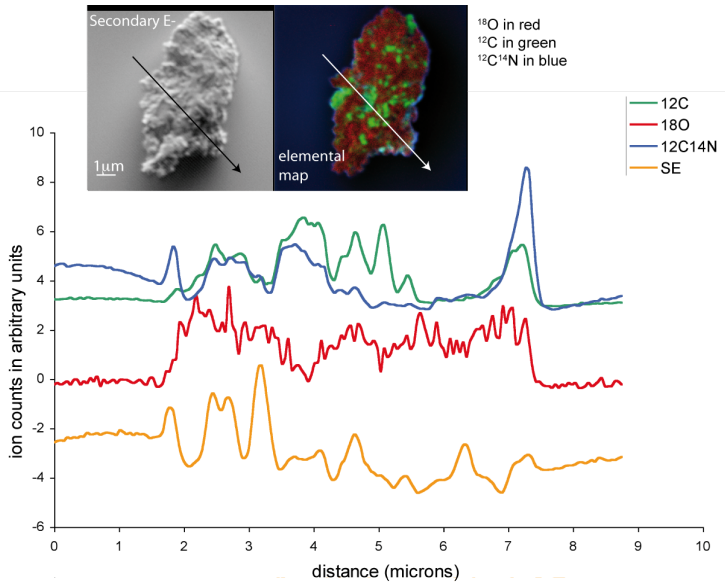

Figure S1: Line profiles through the particle imaged in figure 1 following the arrow. On this plot, we see the variations, along the particle, of the 12C, 26CN and 18O count rate, showing different distribution of these elements. O is related to inorganic mineral whereas C and CN indicate the location of organic material, but with variable composition. SE stands for secondary electrons, which reflects the particle topography.

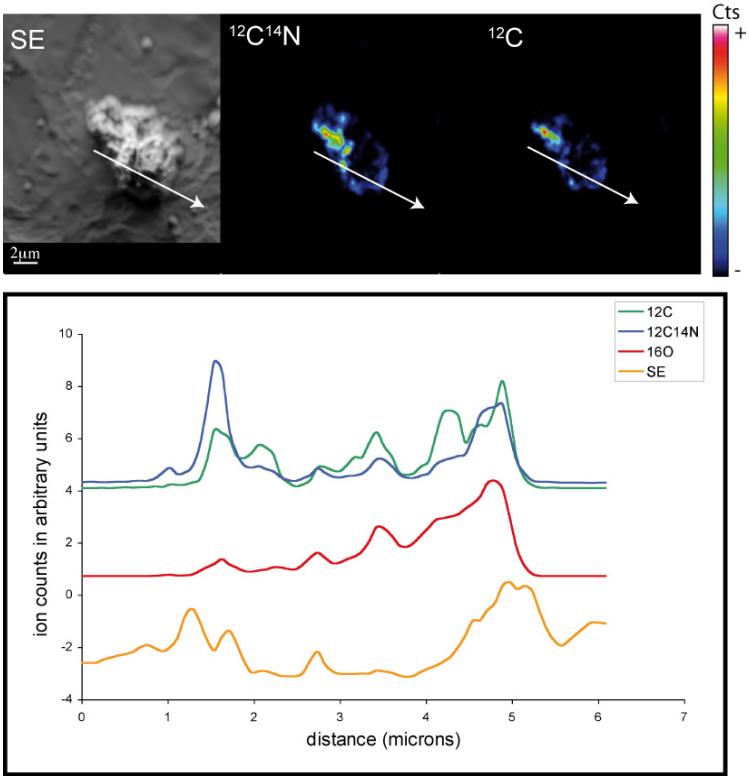

Figure S2: Line profiles through a microaggregate sitting on clean gold foil, from another study. The foil is N-free, so contribution from the background on the signal is excluded. We can see on this picture the same feature observed in figure 1 with a N-rich rim. The variable quality of the OM is also evidence by the comparison of linescans for C and CN.

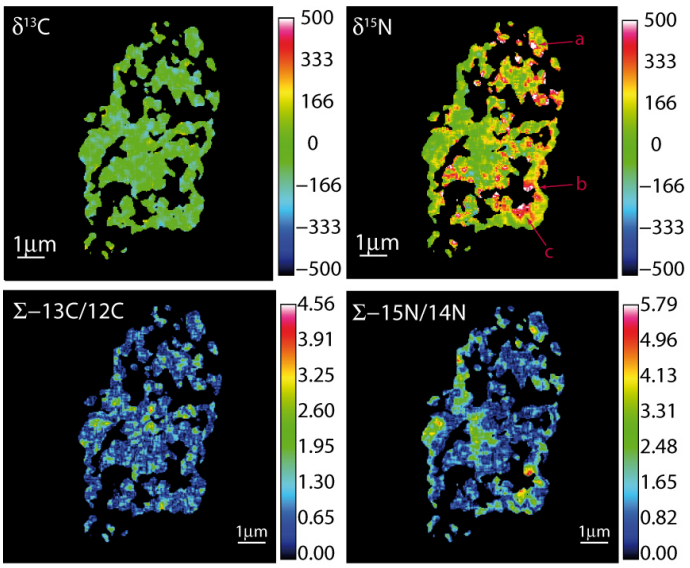

Figure S3: Isotopic ratio and corresponding Σ images for the particle of figure 1. On this picture we clearly see the benefit to use Σ to define ROI containing labeled material.

Formation of stable soil organic matter through microbial processes

Pierre-Joseph Hatton [a*], Laurent Remusat [b], Bernd Zeller [a], Elizabeth A. Brewer [c], Delphine Derrien [a]

[a] INRA-Nancy, Biogéochimie des Ecosystemes Forestiers, 54280 Champenoux, France

[b] Laboratoire de Minéralogie et Cosmochimie du Muséum, UMR 7202 CNRS/MNHN, Muséum National d'Histoire Naturelle, case postale 52, 57 rue Cuvier, 75231 Paris Cedex 05, France

[c] Department of Crop and Soil Science, Oregon State University, 97331 Corvallis, OR, USA

VI

* Corresponding author: pierre-joseph.hatton@nancy.inra.fr

In prep. for *Geochemica and Cosmochemica Acta*

Abstract

Soil microorganisms are increasingly seen as important drivers for the stable association of organic matter (OM) with soil assemblages, but the way they act remains largely misunderstood. Here, we investigate the attachment of fresh microbial products with several stable organo-mineral assemblages. A surface acidic Cambisol was amended with uniformly $^{13}C^{15}N$ labeled glycine and incubated for 8 hours with g-irradiated and non-sterile soils. Soil organo-mineral associations were jointly isolated by K_2SO_4 extraction and sequential density fractionation. Labels were tracked using elemental analyzer coupled to isotope ratio mass spectrometry and nano-scale secondary ions mass spectrometry (NanoSIMS). After 8 hours of incubation, 13% and 21% of the glycine ^{13}C and ^{15}N initially applied were associated to the soil, but only 7.0% and 7.2% withstood the density fractionation procedure and were considered as stabilised. Comparison between g-irradiated and non-sterile soils revealed that more than 90% and 85% of the stabilized glycine-derived ^{13}C and ^{15}N were found in microbial products, with a higher occurrence in aggregates than in plant debris and mineral grains. NanoSIMS images showed that these stabilized microbial products are principally not confined to the microbial cells, but evenly spread at the surface of the mineral-attached OM as extracellular products. Our results suggest that they are stabilized through physico-chemical interactions most likely mediated by the reactivity of the underlying minerals. However, their spatial distribution appears intimately related to soil ecological properties therein the preferential microbial habitats seem to lead to the specific partitioning of the microbial products throughout the entire soil matrix.

Keywords

Density/ Microorganism/ NanoSIMS/ Soil/ Stabilization/ $^{13}C^{15}N$

1. Introduction

Organic matter (OM) entering the soil system is principally fated to rapid mineralization through the activity of living organisms. A small proportion, however, remains for a longer period of time as a result of complex interactions with its environment (Schmidt *et al.*, 2011). Organo-mineral assemblages appear to be important in the processes that rule quantity, quality and turnover of OM (Koegel-Knabner *et al.*, 2008; Young and Crawford, 2004), but the mechanisms by which organic and minerals get associated remain poorly understood. Soil microorganisms are increasingly seen as important drivers for the build up of such interactions (Sollins *et al.*, 2009), but the way they act remains largely misunderstood.

In natural ecosystems, the initiation of stabilization processes expands over months to decades (Bird *et al.*, 2008; Hatton *et al.*, 2012b; Mueller *et al.*, 2009; Zeller *et al.*, 2001; Zeller *et al.*, 2000). As a result, chemically simple substrates have long been used to accelerate the processing of organics by microbes and investigate their effect (van Hees *et al.*, 2005). Previous works showed that microbial transformation of added amino acids occurs within few hours thanks to extremely rapid microbial responses (Jones and Murphy, 2007). Although the fates of these products have been investigated already (Andresen *et al.*, 2008; Derrien *et al.*, 2007; Jones and Hodge, 1999; Knowles *et al.*, 2010; Vieuble-Gonod *et al.*, 2006; Webster *et al.*, 1997), there is relatively little information on the extent to which microbially-processed materials contribute to the overall formation of organo-mineral associations.

The search for the drivers involved in the attachment of organics with stable organo-mineral associations is also a matter of spatial scale, so each technological progress refining the scale of investigation promises advances in their understanding (Herrmann *et al.*, 2007b; Young *et al.*, 2008). Lehman and co-authors (2006; 2007; 2008) were among the first to address spatial and chemical complexity of the soil mineral-associated OM at submicron scales. Using scanning transmission X-ray microscopy (STXM) coupled with near edge X-ray absorption fine structure spectroscopy (NEXAFS), they showed that microbial OM forms may dominate at soil surfaces. Remusat and colleagues (2012) combined STXM-NEXAFS with the nano-scale secondary ion mass spectrometry (NanoSIMS) for its ability to locate isotopically labeled substrates in soil (Herrmann *et al.*, 2007b). They demonstrated the strength of such a combination by elucidating the chemical composition of mineral-associated OM containing residues of ^{15}N-labeled beech litter, 12 years after application. Their work reveals that litter-derived ^{15}N may be found as microbial products, but also that this powerful combination of complementary techniques faces practical limitations, as it is not suited for the investigation of large number of samples. Thousands of μm^2 of soil surfaces have been examined by Herrmann *et al.* (2007a), Mueller *et al.* (2011) and Hatton *et al.* (2012c) using the NanoSIMS in conjunction with stable isotope labeling. The two latter groups imaged the rapid spatial decoupling of ^{13}C and ^{15}N deriving from $^{13}C^{15}N$ amino acids at the surface of

natural soil structures. This confirms that easily accessible substrates are rapidly utilized by living microorganisms under natural conditions (Jones and Murphy, 2007), as also observed in microbial cultures by Popa *et al* (2007) and Finzi-Hart *et al* (2009). However, the processes by which the microbially-processed materials become associated with soil organo-mineral assemblages remains poorly understood.

This study aims at capturing how microbial OM becomes associated with soil organo-mineral assemblages. To facilitate microbial processes, we incubated labile $^{13}C^{15}N$ glycine with a biologically active surface soil (Zeller and Dambrine, 2011). The amended soil was incubated for 8 hours in the laboratory. The amount of glycine ^{13}C and ^{15}N associated to the soil was determined after K_2SO_4 extraction. We used non-sterile and γ-irradiated modalities to verify our working hypothesis, that the glycine would be transformed into microbial products, and to further investigate how the microbial processing is a premise for association with protective organo-mineral assemblages. The amount of glycine ^{13}C and ^{15}N attached to the different types of soil organo-mineral associations was determined after density fractionation. Fractions were analyzed for C/N, $^{13}C/^{12}C$ and $^{15}N/^{14}N$ ratios using an elemental analyzer coupled with isotope ratio mass spectrometry (EA-IRMS). An aliquot of the five most contrasted organo-mineral density fractions was randomly isolated and examined by NanoSIMS to elucidate the spatial distribution of the glycine-derived ^{13}C and ^{15}N and the C/N ratios of the area in which they end up.

2. Material and methods

2.1. Soil

Site and soil were early described by Hatton *et al.* (2012b). Biologically very active (Zeller and Dambrine, 2011), the soil is an (pH_{H20}=3.9) dystric Cambisol (sand: 80%; loam: 13%; clay: 7%) collected in November 2009 at Ebrach (Germany; 49°52′N, 10°27′E) from a site forested for centuries and covered with an even-aged beech forest for the last 23 years. The first 2.5 cm of the A-horizon was sampled on a surface of 2 m^2, mixed and sieved to pass a 2mm sieve. Observable roots were removed. The moisture content was determined at 105°C.

2.2. Experimental setup

The soil was pre-incubated in the dark at 20°C for 15 days with a 1:3 soil to air ratio to reach a biological steady state before substrate addition. The soil was further treated under sterile and non-sterile conditions. Following McNamara *et al.* (2003), who demonstrated that the γ-irradiation should be preferred to other sterilization methods to preserve the soil physico-chemical properties, we sterilized our moist soils by γ-irradiation with a resultant dose of 40kGy (2kGy.h^{-1} for 20 hours; CEA of Cadarache, France). Comparison between the sterile and non-sterile treatments was assumed to inform on the degree of microbial processing of glycine by living microorganisms in non-sterile conditions (Berns *et al.*, 2008).

Sterile and non-sterile treatments were amended with 80µg.gsoil-1 of uniformly $^{13}C^{15}N$ glycine (98-99% excess; Sigma-Aldrich, France), which corresponded to 25.1 $\mu g^{13}C.g^{-1}_{soil}$ and 14.8 $\mu g^{15}N.g^{-1}_{soil}$. Glycine was added in solution to set the moisture content at half of the water holding capacity (21%). The amended soils were thoroughly mixed by hand and sieved twice to ensure homogeneity. Harvested soils were frozen at -20°C. The colonization of sterilized soil by microorganisms was avoided by working under sterilized conditions: use of UV irradiated materials, manipulation under laminar-flux hood and filtration of the labeled glycine using a syringe with a polycarbonate filter at 0.22µm to retain cell-size structures. Treatments were then incubated in the same conditions than the pre-incubation (20°C; dark; 1:3 soil to air ratio). The duration of the incubation was set to 8 hours to reduce the risks of contamination of the sterile treatment, which efficiency was checked for bacteria and fungi on PDA (potato dextrose agar) and TSB (tryptic soy broth) media (n=5, dilution factors: 1 and 10^{-2}).

2.3. Isolation of soil fractions

The soluble glycine residues were isolated using K_2SO_4 extraction: the incubated soil was shaken for 1 hour with 0.025M K_2SO_4 (1:5 soil to solution ratio) and filtered (Whatman N°2). Extracted soil and solution were frozen at -20°C before freeze-drying.

In parallel, the incubated soil was submitted to sequential density fractionation, as the procedure is able to isolate structurally and functionally different organo-mineral associations (Hatton *et al.*, 2012b). Mineral-attached OM isolated by this fractionation procedure is theoretically tightly bound since it withstands the high ionic force of the density liquid, sodium polytungstate (SPT0; TC-Tungsten, Germany). This procedure was performed according to Hatton *et al* (2012b) with a centrifugation kept <2000g to preserve microbial cells. Plant debris were isolated in the fraction <1.65 g cm^{-3}; plant aggregates in the fraction 1.65-1.85 g cm^{-3}; microbial aggregates in the fractions 1.85-2.0 g cm^{-3}, 2.0-2.2 g cm^{-3} and 2.2-2.4 g cm^{-3}; mineral grains with little OM attached in the fractions >2.4 g cm^{-3}. Plant aggregates consisted of poorly altered plant debris aggregated with phyllosilicates minerals. Fractions 1.85-2.4 g cm^{-3} were dominated by phyllosilicates. The mineral-associated OM was increasingly microbially-processed with increasing density. Fraction 2.4-2.65 g cm^{-3} was mainly made by quartz and feldspar covered by little microbial OM. Fraction >2.65 g cm^{-3} was dominated by quartz and oxides covered by little plant and microbial OM. After being isolated and properly rinsed, density fractions were frozen at -20°C and freeze-dried.

2.4. Quantitative determination of glycine-derived ^{13}C and ^{15}N

2.4.1. Macro-scale characterization

Soil fractions were analyzed in three replicates for C, N, $^{13}C/^{12}C$ and $^{15}N/^{14}N$ using an elemental analyzer (CE instruments, NA 1500 type II) coupled to an isotope ratio mass spectrometer (Finnigan, Delta S) at the Technical Platform of Functional

Ecology (OC 081) at INRA Forest Ecology and Ecophysiology Unit, INRA Nancy, France. For each fraction, the amount of ^{13}C tracer was computed as a proportion of C by subtracting the abundances in ^{13}C isotopes of the labeled and reference treatments. The amount of ^{15}N tracer was calculated accordingly. ^{13}C and ^{15}N enrichments were also expressed in δ units relative to the Vienna PeeDee Belemnite standard (Craig, 1957) and the atmospheric N_2 standard (Mariotti, 1983), respectively.

2.4.2. Submicron-scale characterization

NanoSIMS imaging was performed on five density fractions selected out of the seven for their contrasting physico-chemical properties: plant aggregates isolated at 1.65-1.85 g cm^{-3}; microbial aggregates isolated at 1.85-2.0 g cm^{-3} and 2.2-2.4 g cm^{-3}; mineral grains isolated at 2.4-2.65 g cm^{-3} and >2.65 g cm^{-3}. Aliquots of each fraction were deposited onto a clean gold foil and coated with 20 nm of gold to ensure charge compensation. A total of 25 particles of soil were analyzed using a NanoSIMS 50 (Cameca) at the LMCM, Museum d'Histoire Naturelle of Paris, France, according to Hatton *et al.* (2012c). Samples were presputtered with a Cs^+ current of 120pA for 10 to 25 minutes depending on the surface analyzed. Areas of 144 to 1600 μm^2 were scanned with a Cs^+ current of 1.5pA. Images were obtained at 128 x 128 pixels or 256 x 256 pixels wide with a raster speed of 2 ms.$pixel^{-1}$. Secondary ion images of $^{12}C^-$, $^{13}C^-$, $^{16}O^-$, $^{12}C^{14}N^-$ and $^{12}C^{15}N^-$ were simultaneously recorded with ca. 10,000 mass resolving power for ^{26}CN. Forty to fifty frames of secondary ion images were accumulated per imaged area. The instrumental stability was checked using an organic type III kerogen analyzed at least twice a day. NanoSIMS images were processed using the L'IMAGE® software (developed by L. Nittler, Carnegie Institution, Washington DC, USA) and corrected for detector dead time (44 ns, set electronically) and secondary ion images drift in X and Y positions. C/N and $^{15}N/^{14}N$ ratios were corrected using the internal calibration method developed on these samples, while $^{13}C/^{12}C$ ratios were corrected using the type III kerogen method (Hatton *et al.*, 2012c). $^{16}O^-$ and $^{12}C^-$ maps were used as proxies for particles and mineral-attached OM. The aggregated and non-aggregated organization of the soil particles were determined using the secondary electrons detector of the NanoSIMS or, when possible, the environmental scanning electronic microscope (SEM) of the LMCM, MNHN Paris, France. Isotopic anomalies are defined as three times above the isotopic composition of the image where they are found (Remusat *et al.*, 2012).

2.5. Statistics

The correlation between data was tested using Pearson correlation analysis. Further comparisons were performed using a Student's *t*-test once normal distributions and homogeneity of variances have been checked. Distributions were considered significantly different when the probability *p* associated to the test was <.05.

3. Results

3.1. Macroscopic measurements

3.1.1. Soluble and non-soluble K_2SO_4 fractions

Recovery rates after K_2SO_4 extraction were 97±5%, 101±3% and 99±2% for dry weight, total C and total N, respectively. 86±6% and 98±8% of the ^{13}C and ^{15}N initially applied were found eight hours after glycine additions. The fraction soluble to K_2SO_4 only represented 4±1% and 6±1% of the total C and N (Table 1), but contained 66% and 70% of the ^{13}C and ^{15}N initially applied. Its $^{13}C_{tracer}/^{15}N_{tracer}$ mass ratio of 1.8±0.2 was not statistically different from the one of the glycine initially applied ($^{13}C/^{15}N$=1.7). Contrastingly, the $^{13}C_{tracer}/^{15}N_{tracer}$ ratio of the K_2SO_4 extracted soil equalled 1.4±0.1, what is significantly lower than the one of the glycine initially applied.

3.1.2. Density fractions

Recovery rates after density fractionation were 99±3%, 76±5% and 68±4% of dry weight, total C and total N for both sterile and non-sterile treatments (Table 1). No significant differences between the distributions of soil mass ($R>0.99$), total C ($R=0.99$) and total N ($R>0.93$) were observed among the control, the sterile and non-sterile treatments. Dry weight strongly peaked in fraction 2.4-2.65 g cm^{-3} with 86% of the total soil dry weight. Other fractions represented 1% to 6% of the total soil dry weight. Density-isolated plant debris accounted for 2.8±0.7% of the total dry weight, aggregates (1.65-2.4 g cm^{-3}) for 7.7±0.6% and mineral grains with little OM (>2.4 g cm^{-3}) for 89.5±1.4%. Total C and total N both decreased from the lightest fraction to the fraction 2.2-2.4 g cm^{-3}, slightly increased in the fraction 2.4-2.65 g cm^{-3} and dropped by one order of magnitude in the densest fraction. Density-isolated plant debris (<1.65 g cm^{-3}) accounted for 41±7% and 26±6% of the total C and N, aggregates (1.65-2.4 g cm^{-3}) for 51±1% and 61±2% and mineral grains with little OM (>2.4 g cm^{-3}) for 8±1% and 13±1%. The similarities found between the two treatments for soil mass, C and N distributions indicated that the physico-chemical properties of the soil fractions were not affected much by γ-irradiation.

Quantities and distributions of ^{13}C and ^{15}N tracers differed between sterile and non-sterile treatments. Under sterile conditions, 0.68±0.03% and 1.11±0.01% of the ^{13}C and ^{15}N initially applied were recovered from density fractionation (Table 1). Table 1 shows that 42% and 50% of the associated glycine-derived ^{13}C and ^{15}N were found in plant debris (<1.65 g cm^{-3}), 30% and 40% in aggregates (1.65-2.4 g cm^{-3}) and 28% and 10% in mineral grains (>2.4 g cm^{-3}). The $^{13}C_{tracer}/^{15}N_{tracer}$ ratios measured in plant debris and aggregates were between 0.1 and 0.9, which is significantly lower than that of the glycine initially applied (*t*-test, $p<.05$). The $^{13}C_{tracer}/^{15}N_{tracer}$ ratios regularly decreased with aggregate density. The $^{13}C_{tracer}/^{15}N_{tracer}$ ratios of 2.2 and 2.9 measured in mineral grains, were significantly higher than the applied glycine (*t*-test, $p<.05$).

Under non-sterile conditions, 7.0±0.1% and 7.2±0.0% of the ^{13}C and ^{15}N initially applied were recovered from density fractionation (Table 1). 20% and 26% of the associated glycine-derived ^{13}C and ^{15}N were found in plant debris (<1.65 g cm^{-3}), 63% and 65% in aggregates (1.65-2.4 g cm^{-3}) and 17% and 9% in mineral grains (>2.4 g cm^{-3}). The $^{13}C_{tracer}/^{15}N_{tracer}$ ratios measured in aggregates decreased with increasing density from 1.8±0.0 to 1.1±0.1. They did not statistically differ from the glycine initially applied, except in the microbial aggregates of density 2.2-2.4 g cm^{-3} (*t*-test, p<.05). Plant debris showed a $^{13}C_{tracer}/^{15}N_{tracer}$ ratio of 1.3±0.1 significantly lower than the glycine (*t*-test, p<.05), whereas the $^{13}C_{tracer}/^{15}N_{tracer}$ ratio of ≥2.8 measured in mineral grains (>2.4 g cm^{-3}) was significantly higher (*t*-test, p<.05).

3.2. NanoSIMS analyses

Table 2 reports the characteristics of the soil particles imaged by NanoSIMS. The proportion of aggregated particles decreased with density from 99% in the lightest fractions to <1% in the densest fraction, as previously shown by Hatton *et al.* (2012c). Using $^{12}C^-$ as a proxy for OM, we observed that the surface area covered by OM decreased with increasing fraction density. Eighty-three percent of the total surfaces covered by $^{12}C^-$ were found on aggregated particles, against 17% on non-aggregated ones. The C/N ratios varied from 9.3±0.1 to 21.2±0.2 on aggregated soil particles and from 7.8±0.1 to 20.8±0.2 on non-aggregated soil particles. This indicates that OM forms found at the surface of all types organo-mineral assemblages are relatively rich in N. Figure 1 shows the predominance of relatively N-rich materials, but also the presence of sparser well-defined regions richer in C, which corroborated the observations of Lehman *et al.* (2008). Both C-rich and N-rich regions were found throughout the surface of soil particles isolated from all the density fractions imaged, and without any distinguishable spatial gradient.

Table 3 reports the characteristics of the ^{13}C and ^{15}N isotopic anomalies identified with NanoSIMS. Eight hours after the $^{13}C^{15}N$ glycine application, discrete ^{15}N and ^{13}C isotopic anomalies were found throughout the surface of soil particles. The ^{15}N anomalies were much more abundant than ^{13}C ones at the surface of the particles imaged: 28 ^{15}N anomalies were identified against only five for the ^{13}C (Figures 1 and 2). They were both found in clear agglomeration sites of 0.3µm² to 3.4µm² (median size = 0.6 µm²) and without any apparent spatial gradient. 82% of the surfaces covered by these glycine-derived tracers were found onto aggregated particles, against 18% onto non-aggregated ones. ^{15}N and ^{13}C isotopic anomalies were spatially decoupled except at four loci found at the surface of one micro-aggregated particle isolated from density fraction 1.85-2.0 g cm^{-3} (Figure 2). The glycine-derived ^{15}N covered 0.7% of the soil particle surfaces imaged and 3.0% of the surface covered by OM. Twenty-eight ^{15}N anomalies were spread across twelve particles varying on spatial organization and density (Table 3). Twenty were found onto particles lighter than 2.4 g cm^{-3}, and exhibited a micro-aggregated organization. Five ^{15}N anomalies were found on particles isolated from density 2.4-2.65 g cm^{-3}: two at the surface of a micro-aggregate and three at the surface of a non-aggregated particle. Finally, three ^{15}N anomalies were found in density fraction >2.65 g cm^{-3}, on

non-aggregated particles. In density fractions <2.65 g cm^{-3}, the ^{15}N anomalies showed low C/N ratios ranging from 7.0±0.1 to 25.1±0.3 with 95% comprised in between 7.0 and 16.5, without any differences between the C/N ratios of ^{15}N anomalies measured on aggregated and non-aggregated particles. Conversely, the three ^{15}N anomalies identified among the density fraction >2.65 g cm^{-3} were in areas with much more contrasted C/N ratios: 8.6±0.1, 21.6±0.3, 80.5±1.0 and 161.4±10.2.

The glycine-derived ^{13}C covered 0.1% of the surface of the soil particles imaged and 0.6% of the surface covered by OM. The five ^{13}C isotopic anomalies were found on two microaggregated particles isolated from the density fraction 1.85-2.0 g cm^{-3} (Table 3; Figure 2). They showed C/N ratios of between 10.1±0.1 and 12.2±0.1. No correlation was found between the size of the spots where glycine-derived ^{13}C and ^{15}N were found, their C/N ratios or their isotopic composition, indicating that the chemical composition of the sites of association were not related to size or isotopic composition.

Table 1: Dry weight, elemental and isotopic composition of soil fractions incubated for 8h with $^{13}C^{15}N$ labeled glycine (n=3). Dry weight and elemental composition were determined for both sterile and non-sterile treatments. The sterilization was obtained by g-irradiation (40kGy). The composition of the density fractions is from Hatton *et al.* (2012b). *SD* stands for standard deviation; – for non determined.

Soil fractions				Elemental composition				Isotopic composition																			
								Non sterile treatment										Sterile treatment									
Description	Composition	Dry weight		Carbon		Nitrogen		$^{13}C_{tracer}$				$^{15}N_{tracer}$				$^{13}C_{tracer}$/ $^{15}N_{tracer}$		$^{13}C_{tracer}$				$^{15}N_{tracer}$				$^{13}C_{tracer}$/ $^{15}N_{tracer}$	
		% of recovered	SD	mg.gsoil^{-1}	SD	mg.gsoil^{-1}	SD	µg.g$_{fraction}^{-1}$	SD	% initially applied	SD	µg.g$_{fraction}^{-1}$	SD	% initially applied	SD	Mean	SD	µg.g$_{fraction}^{-1}$	SD	% initially applied	SD	µg.g$_{fraction}^{-1}$	SD	% initially applied	SD	Mean	SD
Bulk soil	-	-	-	28.7	1	1.85	0	21.6	1.6	86.2	6	14.5	1.2	98	8	1.5	0.1	24.5	0.8	97.8	3.1	14.53	0.92	98.3	6.2	1.5	0.1
K_2SO_4 fractions																											
Soil extract	-	-	-	27.5	0	1.74	0	5.1	0.8	20.3	3	4.2	0.4	28.3	3	1.4	0.1	-	-	-	-	-	-	-	-	-	-
Soluble to K_2SO_4	-	-	-	1.2	0	0.11	0	16.5	0.2	65.9	1	10.3	0.3	69.7	2	1.8	0.2	-	-	-	-	-	-	-	-	-	-
Density fractions (g.cm^{-3})																											
<1.65	Plant debris	2.8	0.7	8.1	0.0	0.33	0.03	15.4	1.1	1.4	0.1	12.0	0.4	1.9	0.1	1.3	0.1	3.1	0.8	0.28	0.07	3.61	0.06	0.56	0.01	0.9	0.1
1.65-1.85	Plant aggregates	1.8	0.0	4.2	0.0	0.22	0.01	21.0	0.2	1.6	0.0	12.0	0.1	1.5	0.0	1.8	0.0	1.4	0.3	0.11	0.02	1.54	0.02	0.19	0.00	0.9	0.1
1.85-2.0	Microbial aggregates	1.9	0.1	3.2	0.3	0.21	0.00	16.4	1.6	1.3	0.1	9.7	0.0	1.3	0.0	1.7	0.2	0.7	0.2	0.06	0.01	0.86	0.05	0.12	0.01	0.8	0.0
2.0-2.2	Microbial aggregates	2.2	0.3	2.8	0.0	0.21	0.01	11.7	0.9	1.1	0.1	7.2	0.1	1.2	0.0	1.6	0.1	0.4	0.3	0.04	0.03	0.58	0.05	0.09	0.01	0.7	0.0
2.2-2.4	Microbial aggregates	1.7	0.2	1.5	0.0	0.13	0.01	6.1	0.8	0.4	0.1	5.5	0.5	0.7	0.1	1.1	0.1	0.0	0.0	0.00	0.00	0.32	0.28	0.04	0.03	0.1	0.0
2.4-2.65	Mineral grains	86.2	3.5	1.9	0.2	0.16	0.02	0.3	0.0	1.1	0.0	0.1	0.0	0.6	0.1	3.0	0.2	0.0	0.0	0.18	0.02	0.02	0.00	0.10	0.01	2.9	0.1
>2.65	Mineral grains	3.3	3.4	0.0	0.0	0.00	0.00	1.4	0.0	0.1	0.0	0.5	0.0	0.0	0.0	2.8	0.0	0.4	0.0	0.01	0.00	0.16	0.01	0.01	0.00	2.2	0.0
Sum of fractions	-			21.8	1.7	1.25	0.01	1.8	0.0	7.0	0.1	1.1	0.0	7.2	0.0	1.7	0.2	0.2	0.0	0.68	0.03	0.16	0.00	1.11	0.01	1.0	0.2

Table 2: Description of density-isolated soil particles imaged by NanoSIMS. The *aggregated* or non-aggregated organization of the soil particles was visually determined using secondary electrons images. The denomination of particles was the same as in Table 3. The C/N ratios and the $d^{15}N$ of the whole particle were obtained using the internal calibration method, while the $d^{13}C$ of the particle was determined using type III kerogen (Hatton *et al.*, 2012c). The surface area of each particle was computed using $^{16}O^-$ as a proxy; the organic matter (OM) covering rate of each soil particle was computed using $^{12}C^-$ as proxy for the mineral-attached OM.

Density fractions		Isotopic anomalies								
		^{13}C		^{15}N		C/N		Size		
g.cm^{-3}	Particles where anomalies are found	δ(‰)	SD	δ(‰)	SD		SD	µm^2	% of total surface imaged	% of total surface covered by OM
1.65-1.85	A_I			202	14	8.6	0.1	0.5	0.01	0.06
	A_{II}			1409	29	16.1	0.3	0.4	0.01	0.04
				1056	25	13.1	0.2	0.4	0.01	0.05
	A_{III}			525	20	25.1	0.3	0.9	0.02	0.10
				941	23	7.0	0.1	3.1	0.08	0.34
				1329	28	7.0	0.1	0.6	0.02	0.07
				833	22	8.5	0.1	0.5	0.01	0.06
1.85-2.0	B_I			202	14	9.8	0.1	0.6	0.02	0.07
	B_{II}	130	10	613	19	11.3	0.1	0.9	0.02	0.10
		121	18	527	18	12.2	0.1	0.4	0.01	0.04
		111	7	614	19	11.1	0.1	2.0	0.05	0.22
		66	11	512	18	10.1	0.1	1.2	0.03	0.13
	B_{III}	88	29			11.3	0.1	0.7	0.02	0.08
				513	18	9.9	0.1	2.8	0.07	0.31
				638	20	10.9	0.1	3.4	0.09	0.37
	B_{IV}			308	16	8.3	0.1	0.9	0.02	0.10
	B_V			290	15	11.2	0.1	0.9	0.02	0.10
2.2-2.4	C_{III}			148	14	16.6	0.2	0.4	0.01	0.04
	C_{IV}			270	15	13.6	0.2	0.4	0.01	0.04
				190	14	13.3	0.2	0.4	0.01	0.04
	C_V			202	14	9.9	0.1	0.6	0.02	0.07
2.4-2.65	D_I			226	15	10.3	0.1	0.9	0.02	0.09
	D_{II}			799	22	9.1	0.1	1.7	0.04	0.18
	D_{III}			266	15	8.4	0.1	0.4	0.01	0.05
	D_{IV}			187	14	10.0	0.1	1.0	0.03	0.11
				270	15	11.8	0.1	0.7	0.02	0.08
>2.65	E_{III}			611	23	80.5	6.0	0.3	0.01	0.04
				799	22	161.4	10.2	0.4	0.01	0.04
	E_V			414	17	21.6	0.3	0.6	0.02	0.07
Total										
	Non-aggregated	0		7				4.7	0.12	0.51
	Aggregated	1+4*		17+4*				23.5	0.62	2.56
	Sum	5		28				28.2	0.74	3.08

Table 3: Characterization of the ^{13}C and ^{15}N isotopic anomalies identified on particles characterized in Table 2. Their C/N ratios and the $d^{15}N$ were obtained using the internal calibration method (Hatton *et al.*, 2012c), while the $d^{13}C$ was determined using type III kerogen. The surface areas occupied by the isotopic anomalies are computed using $^{16}O^-$ and $^{12}C^-$ as proxies for soil particles and their mineral-attached OM, respectively. * indicates the sites where glycine-derived ^{13}C and ^{15}N were both found (See Figure 2).

Density fractions	Soil particles									
	Spatial organization	Denomination	^{13}C		^{15}N		C/N		Surface area	OM covering rate
g.cm^{-3}	*Aggregated* / Non-aggregated		δ(‰)	SD	δ(‰)	SD		SD	µm^2	% of surface area
1.65-1.85	*Aggregated*	A_I	-18	1	130	14	20.6	0.2	916	42
	Aggregated	A_{II}	-26	3	348	16	21.2	0.3	139	53
	Aggregated	A_{III}	-33	3	194	14	16.9	0.2	59	51
1.85-2.0	*Aggregated*	B_I	-31	3	111	13	9.9	0.1	77	46
	Aggregated	B_{II}	25	3	338	16	10.5	0.1	61	47
	Aggregated	B_{III}	-15	4	205	14	10.0	0.1	112	45
	Aggregated	B_{IV}	-31	10	239	15	10.2	0.1	33	36
	Aggregated	B_V	-17	13	178	14	10.2	0.1	23	32
2.2-2.4	Non-Aggregated	C_I	-14	14	111	13	8.0	0.1	151	9
	Non-Aggregated	C_{II}	-41	14	88	13	9.5	0.1	76	20
	Non-Aggregated	C_{III}	-21	13	89	13	9.1	0.1	71	21
	Aggregated	C_{IV}	-41	8	82	13	14.4	0.2	26	15
	Aggregated	C_V	-10	14	84	13	18.0	0.2	20	21
	Aggregated	C_{VI}	-18	3	108	13	11.4	0.1	143	38
	Aggregated	C_{VII}	-27	16	81	13	9.3	0.1	41	3
2.4-2.65	Non-Aggregated	D_I	-9	20	150	14	9.5	0.1	144	9
	Non-Aggregated	D_{II}	-17	19	332	16	8.9	0.1	96	14
	Non-Aggregated	D_{III}	-8	16	108	13	14.6	0.2	139	5
	Aggregated	D_{IV}	-36	4	102	13	11.9	0.1	143	52
>2.65	Non-Aggregated	E_I	2	14	324	16	10.1	0.1	260	5
	Non-Aggregated	E_{II}	0	17	183	14	7.8	0.1	339	12
	Non-Aggregated	E_{III}	-9	11	374	16	15.2	0.2	130	4
	Non-Aggregated	E_{IV}	-10	16	550	19	10.9	0.1	224	2
	Non-Aggregated	E_V	-20	7	256	15	20.8	0.3	258	8
	Non-Aggregated	E_{VI}	-26	15	522	18	15.3	0.2	115	5
Total	Non-Aggregated								2004	83
	Aggregated								1792	17

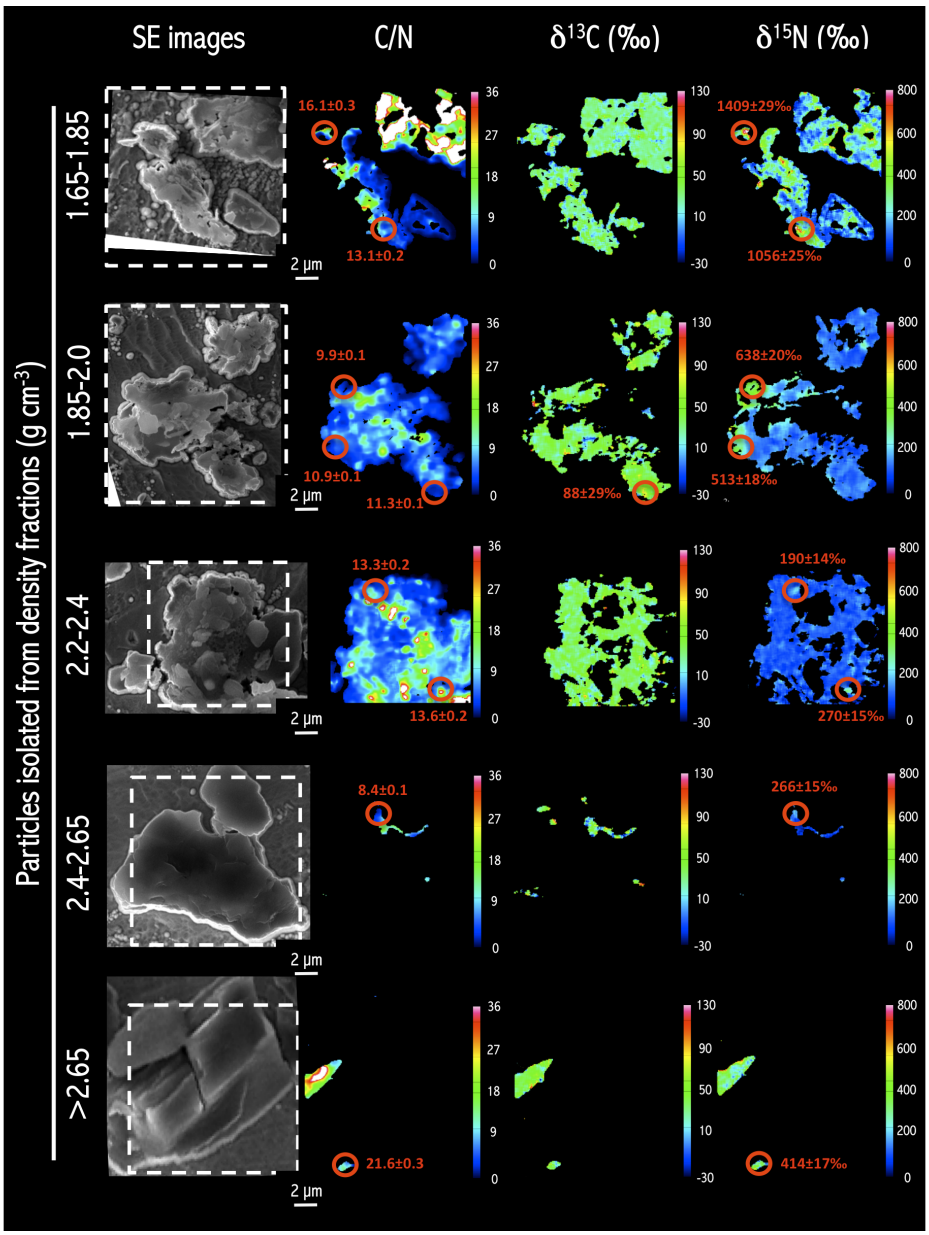

Figure 1: NanoSIMS images of isotopic anomalies identified at the surface of soil particles isolated from five contrasted density fractions. Soil particles were imaged by secondary electrons. The dashed line squares indicate what was imaged by NanoSIMS. The images are ordered by density and refer to *A*$_{II}$, *B*$_{III}$, *C*$_{IV}$, D$_{III}$ and E$_{V}$ in Table 2 and Table 3. The isotopic anomalies are circled in red: their C/N and d^{15}N values are obtained using the internal calibration method, whilst d^{13}C values are determined using type III kerogen (Hatton *et al.*, 2012c).

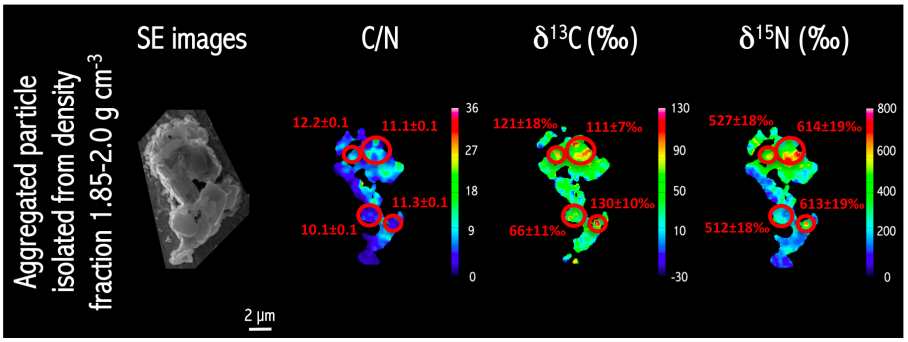

Figure 2: NanoSIMS images of spatially coupled ^{13}C ad ^{15}N coupled isotopic anomalies. The soil particle was imaged using secondary electrons and referred as B_{II} in Table 2 and Table 3. The isotopic anomalies are circled in red: their C/N and d^{15}N values were obtained using the internal calibration method, while d^{13}C values were determined using type III kerogen (Hatton *et al.*, 2012c).

4. Discussion

4.1. The extent of glycine ^{13}C and ^{15}N stabilization

Previous studies examined the fate of glycine within the soil matrix (Jones and Hodge, 1999; Vieuble-Gonod *et al.*, 2006; Webster *et al.*, 1997), but its partitioning through the soil OM pools remains not fully explored. Figure 3 distinguishes between (1) the soluble fraction corresponding to what was soluble to 0.025M K_2SO_4; (2) the fraction tightly attached to soil corresponding to what was recovered after density fractionation and (3) the fraction loosely attached to soil corresponds to the difference between the soil extracted with K_2SO_4 and the fraction tightly attached. Eight hours after $^{13}C^{15}N$ glycine addition, 7.0% and 7.2% of the glycine-derived ^{13}C and ^{15}N are already tightly attached to organo-mineral associations. Following Sollins *et al.* (2009; 2006), this fraction may be considered as more relevant in term of stabilization than the loosely attached glycine-derived ^{13}C and ^{15}N.

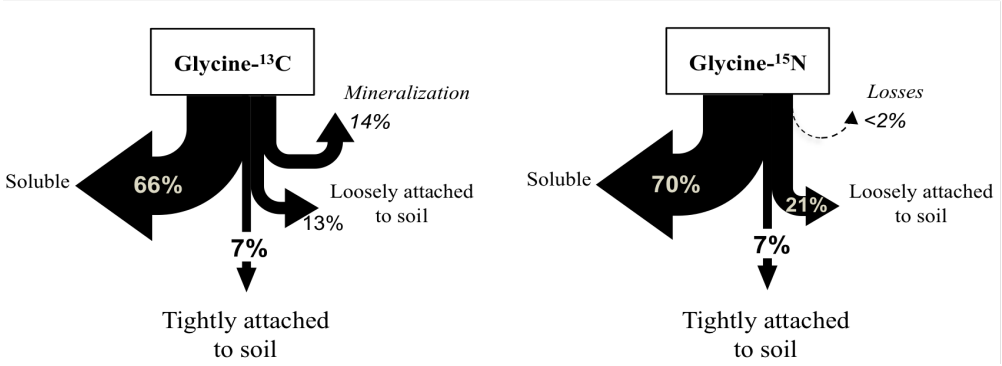

Figure 3: Distribution of glycine-derived ^{13}C and ^{15}N expressed as percent of initially applied. Soluble ^{13}C and ^{15}N tracers were determined from the fraction soluble to 0.025M K_2SO_4. Tightly associated glycine-derived ^{13}C and ^{15}N were determined from the soil recovered after sequential density fractionation, whereas loosely associated glycine-derived ^{13}C and ^{15}N correspond to the difference with the soil extracted using 0.025M K_2SO_4. Mineralization and losses correspond to what was not recovered.

4.2. Quantification of the microbial stabilization of glycine ^{13}C and ^{15}N

Figure 3 reports that 14% of the glycine ^{13}C was mineralized eight hours after addition to soil, indicating the rapid microbial mineralization of the glycine substrate as earlier described by many other studies (Derrien *et al.*, 2007; Henry and Jefferies, 2003; Jones and Murphy, 2007; Webster *et al.*, 1997). This was further confirmed by the large decoupling of the glycine ^{13}C and ^{15}N observed through the set of density fractions (Table 1) and on NanoSIMS images (Figure 1). Our study quantitatively determined the contribution of living microorganisms to stabilized glycine-derived ^{13}C and ^{15}N by comparing the amounts of tracers found in the sterile and non-sterile treatments reported in Table 1.

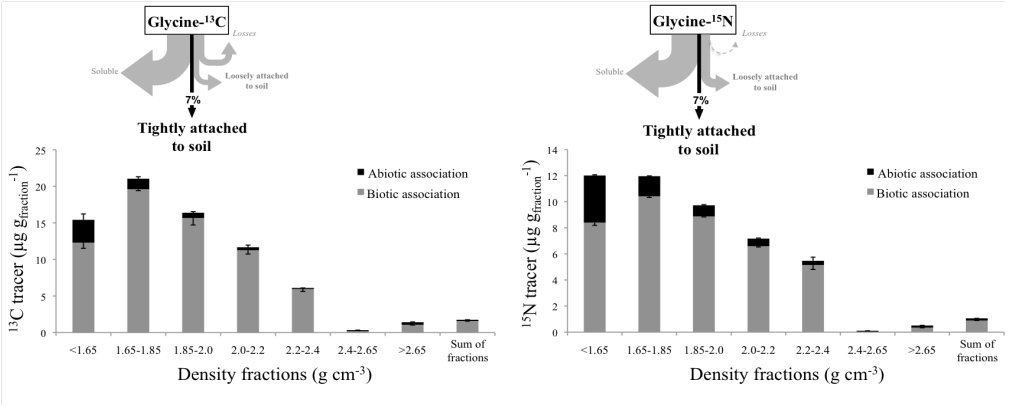

Figure 4: Partition of the glycine ^{13}C (left) and ^{15}N (right) stabilized through the activity of living microorganisms (biotic association - grey) or abiotic processes (black) over the set of density fractions. Abiotic processes were estimated from the quantities of glycine-derived ^{13}C and ^{15}N found in sterile conditions (n=3), while the contribution of living microorganisms was determined by difference to what was found without sterilization. *Sum of fractions* stands for the weighted sum of the density fractions expressed per gram of soil.

Eight hours after the glycine addition, we found that 90% and 85% of the total stabilized ^{13}C and ^{15}N tracers were attached via the activity of living microorganisms (Table 1, Figure 4). Their contribution to the stabilization of the glycine derived C and N varied through the set of density fractions. Aggregates showed the highest contribution of living microorganisms, which regularly increased with increasing aggregate density from 93±2% to 99±3% for the glycine-derived ^{13}C and 87±1% to 95±5% for the glycine-derived ^{15}N. Plant debris and mineral grain fractions showed a slightly lower contribution of living microorganisms, accounting for 68% to 85% of the tight association of glycine-derived ^{13}C and ^{15}N. Moreover, the small proportion of stabilized ^{13}C and ^{15}N tracers attached in sterile conditions in these same fractions was found to be altered glycine residues: $^{13}C_{tracer}/^{15}N_{tracer}$ mass ratios (Table 1) were significantly different from the C/N mass ratio of the glycine initially applied (C/N=1.0 in sterile conditions versus 1.7 for glycine). The alteration of glycine in the γ-irradiated soil might be explained by resilient enzymatic activities and, to a lesser extent, free radicals formed through radiolysis of water in the presence of molecular oxygen (McNamara *et al.*, 2003). This indicates that only a very small amount of unaltered glycine may have been stabilized in the non-sterile soils. This further reveals that soil microorganisms directly and indirectly rule most of the stabilization of the glycine-derived ^{13}C and ^{15}N in the non-sterile soil, which validates the use of glycine to study microbial processes involved in the build up of stable OM.

4.3. Stabilized microbial products

4.3.1. Are they extra- or intra- cellular products?

The stabilized microbial products containing the ^{13}C and ^{15}N tracers were formed through extracellular lysis of glycine and the intracellular biosynthesis of new microbial products, possibly secreted out of the microbial cells (Geisseler *et al.*, 2009, 2010; Knowles *et al.*, 2010). NanoSIMS imaging revealed that the ^{13}C and ^{15}N tracers were found as relatively abundant extracellular products. ^{15}N anomalies always show a strong isotopic enrichment. Given that the probability to find many inorganic ^{15}N exactly at the same locates is low considering the small amount of labeled glycine initially applied (<1% of the total N found in the bulk sample), the ^{15}N anomalies determined by NanoSIMS are more likely to be found as organic N. Together, ^{13}C and ^{15}N tracers occupied thousands times more surfaces (Table 3) than the total soil surface occupied by soil microbes: ^{13}C and ^{15}N anomalies in this study cover $7.4{:}10^3$ of the soil surfaces imaged (Table 3) against $1{:}10^8$ for living microorganisms as proposed by Young and Crawford (2004). The latter number may be questioned even in the extremely favorable conditions of our incubation. Even if few species have been described to respond in such a short period (Bowen and Rovira, 1976; Lee *et al.*, 2011; Murase *et al.*, 2012), the microbial growth usually takes more than a day and could not explain a microbial blow of a 10^4 magnitude (Darrah, 1991; Sato, 1987). Moreover, no microbial cells were identified at the surface of soil particles NanoSIMS imaged. This was not surprising given that soil microbes are expected to cover about $1{:}10^8$ of the total soil surface (Young and Crawford, 2004) and that we only imaged 3796μm^2 of soil particles with a spatial

resolution <0.01µm^2. To statistically ensure the observation of microbial cell, we would have needed to image at least 10^6 µm^2 of soil surfaces. Though unlikely, it cannot be excluded that the sites of joined ^{13}C and ^{15}N association are microbial cells (Figure 2) for two reasons. First, they are found in well-defined clusters consistent in size and C: N ratio with microbial cells (Franklin and Mills, 2003; Nunan *et al.*, 2003; Young, 2006). Second, the ability to identify microbial cells was compromised by the fact that SEM images were acquired after the destructive NanoSIMS imaging. Overall, our observations suggest that the ^{13}C and ^{15}N tracers were rather found as extracellular microbial products than confined in microbial cells.

4.3.2. Stable attachment

Although the mechanisms of attachment for microbial cells are reasonably well known (Chenu and Stotsky, 2002; Young et al., 2006), the mechanisms and controls of the attachment of their extracellular products has received much less consideration. They have been considered as self-assembled within the soil matrix (Kleber *et al.*, 2007; Mikutta *et al.*, 2011; Rillig *et al.*, 2007), but this as never been validated at scales relevant to organo-mineral interactions.

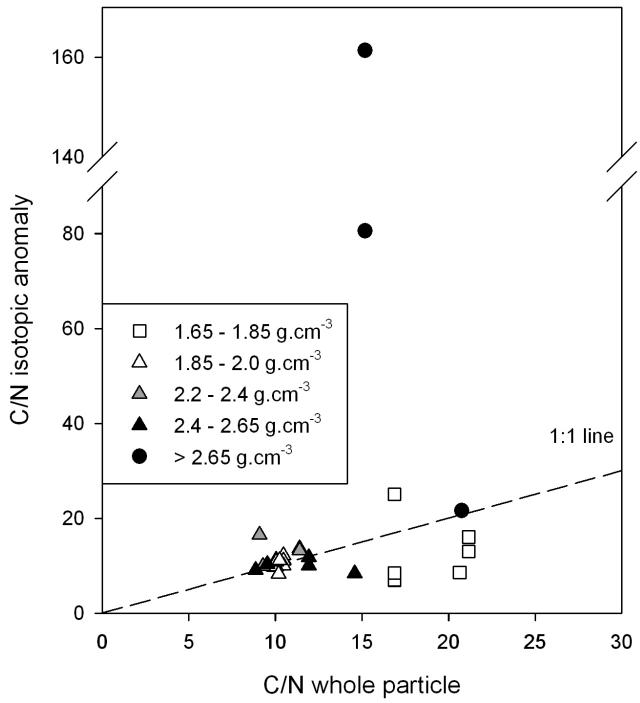

Figure 5: Comparison of the C/N ratios recorded from the isotopic anomalies and from the whole particles in which they were found. The dashed line represents the 1:1 line.

The similar behaviours of the $^{13}C_{tracer}/^{15}N_{tracer}$ ratios recorded throughout the set of density fractions under sterile and non-sterile conditions (R≥0.98; Table 1) might indicate that microbial products interact with distinct organo-mineral associations following similar mechanisms of association in both sterile and non-sterile conditions. It appears that the concentrations in ^{13}C and ^{15}N tracers determined at

the macro-scale (Table 1) were highly correlated with the OM covering rates determined by NanoSIMS at the submicron-scale (R≥0.85; Table 2), suggesting that the extent of glycine ^{13}C and ^{15}N stabilization varied with the surface coverage of mineral-associated OM. NanoSIMS images obtained from the non-sterile treatment further showed that the newly formed microbial products were found on clear agglomeration sites throughout the surfaces of mineral-attached OM from distinct organo-mineral associations, without apparent spatial gradient (Figure 1; Figure 2). Figure 5 shows that glycine ^{13}C and ^{15}N were localized in organic areas with low and homogeneous C/N ratios, between 7.0 and 25, compared with the C/N ratios of the particles in which they were found (Table 2 and 3). The only exceptions were observed in the densest fraction, where the attachment occurred on OM much richer in C than the bulk particle. This fraction differed from the others by the presence of reactive minerals, such as pedogenic oxides, that have been previously described as adsorbing distinct OM types (Hatton *et al.*, 2012b). The highly heterogeneous C/N ratios recorded on the three sites with glycine ^{15}N association may reflect the heterogeneous nature of the mineral-attached OM found in this fraction (Hatton *et al.*, 2012a). We concluded that the chemistry of surface OM constituting the soil assemblages does not exert a primary control for the spatial distribution of glycine-derived ^{13}C and ^{15}N. Our results rather suggest that the reactivity of the underlying minerals control attachment and distribution of the microbial products.

4.3.3. Linking soil OM stabilization and ecology

Soil ecology may explain such distributions of the ^{15}N and ^{13}C tracers through the soil assemblages, as well as the extent to which living microorganisms contribute to their stabilization (Figure 4). Table 1 and Table 3 report macro- and submicron-scale evidences that the stabilized glycine ^{15}N and ^{13}C were quantitatively retained more in light and, to a lesser extent, dense aggregated soil structures, suggesting that the spatial organization of the organo-mineral assemblages favor the build up of stable OM. In an earlier study (Hatton *et al.*, 2012b), we suggested that the microorganisms inhabiting the lightest aggregates were more easily supplied with organic resources, water and gas than in densest ones because of their changing physico-chemical properties: as the aggregate density increases, OM quantitatively decreases and qualitatively shifts from plant to microbial origin and porosity decreases. The distribution and microbial stabilization efficiency of the glycine ^{13}C and ^{15}N reported in the present study (Figure 4) are in agreement with the increasing contribution of microbial biomasses to the total carbon attached to soil organo-mineral associations of increasing density (Hatton *et al.*, 2012a), to suggest that microorganisms preferentially inhabit in dense organo-mineral associations. This supports our previous conceptual model and highlights the strong interconnection among soil OM stabilization and microbial ecology.

The contrasted occurrences of ^{13}C and ^{15}N anomalies identified by NanoSIMS (Table 3) may be attributed to the fact that extracellular microbial products rich in C are more likely found surrounding microorganisms found on soil surfaces than the N-rich ones (Foster, 1988; Young *et al.*, 2008). In the acidic conditions of the

studied soil (pH=3.9), the C-rich products of the microbial activity, such as exopolysaccharides, may develop electrostatic interactions with positively charged organo-mineral assemblages (Mikutta *et al.*, 2011; Omoike and Chorover, 2006), while the positive charge of some N-rich products, such as ammonium and amino-N compounds, would rather favor the attachment to negatively charged organo-mineral assemblages (Kleber *et al.*, 2007).

5. Conclusions

By using labile $^{13}C^{15}N$ glycine, we characterized the attachment of microbial products through a set of ecologically meaningful organo-mineral assemblages and showed that the stabilized microbial products are principally not confined to microbial cells. The glycine derivatives were evenly spread at the surface of the mineral-attached OM as extracellular products and stabilized through physico-chemical interactions, most likely mediated by the reactivity of the underlying minerals rather than by the reactivity of the mineral-attached OM. Their spatial distribution also appear intimately related to soil ecological properties, therein preferential microbial habitats seem to lead to the specific partitioning of microbial C-rich and N-rich products.

Acknowledgment

The Institut National de la Recherche Agronomique (INRA-EFPA) and the Région Lorraine (grants #12000292 and #12000184) have financially supported this work. The National NanoSIMS facility at the Museum National d'Histoire Naturelle was established by funds from the CNRS, Région Île de France, Ministère délégué à l'Enseignement supérieur et à la Recherche, and the Muséum itself. We are in debt to Christian Hossan (PTEF, INRA) for EA-IRMS analyses, Sylvain Pont (LMCM, MNHN) for SEM analyses. We are grateful to Jose Vicente and Daniel Chaumont (CEA Cadarache) for the γ-irradiation of our soil.

References

Andresen, L. C., Jonasson, S., Strom, L., and Michelsen, A., 2008. Uptake of pulse injected nitrogen by soil microbes and mycorrhizal and non-mycorrhizal plants in a species-diverse subarctic heath ecosystem. *Plant and Soil* **313**, 283-295.

Berns, A. E., Philipp, H., Narres, H. D., Burauel, P., Vereecken, H., and Tappe, W., 2008. Effect of gamma-sterilization and autoclaving on soil organic matter structure as studied by solid state NMR, UV and fluorescence spectroscopy. *European Journal of Soil Science* **59**, 540-550.

Bird, J. A., Kleber, M., and Torn, M. S., 2008. C-13 and N-15 stabilization dynamics in soil organic matter fractions during needle and fine root decomposition. *Organic Geochemistry* **39**, 465-477.

Bowen, G. D. and Rovira, A. D., 1976. Microbial colonization of plant roots. *Annual Review of Phytopathology* **14**, 121-144.

Chenu C, Stotzky G (2002). Interactions between micro-organisms ans soil particles: an overview. In: Huang PM, Bollag, J.M., Senesi, N. (ed). *Interactions between soil particles and microorganisms*. John Wiley and Sons: Chichester, UK. pp 3-40.

Craig, H., 1957. Isotopic standards for carbon and oxygen correction factors for mass spectrometric analysis of carbon dioxide. *Geochimica Et Cosmochimica Acta* **12**, 133-149.

Darrah, P. R., 1991. Models of the rhizosphere .2. A quasi 3-Dimensional simulation of the microbial-population dynamics around a growing root releasing soluble exudates. *Plant and Soil* **138**, 147-158.

Derrien, D., Marol, C., and Balesdent, J., 2007. Microbial biosyntheses of individual neutral sugars among sets of substrates and soils. *Geoderma* **139**, 190-198.

Finzi-Hart, J. A., Pett-Ridge, J., Weber, P., Popa, R., Fallon, S. J., Gunderson, T., Hutcheon, I. D., Nealson, K. H., and Capone, D. G., 2009. Fixation and fate of C and N in the cyanobacterium *Trichodesmium* using nano-scale secondary ion mass spectrometry. *Proceedings of the National Academy of Sciences* **106**, 6345-6350.

Foster, R. C., 1988. Microenvironmens of soil-microorganisms. *Biology and Fertility of Soils* **6**, 189-203.

Franklin, R. B. and Mills, A. L., 2003. Multi-scale variation in spatial heterogeneity for microbial community structure in an eastern Virginia agricultural field. *Fems Microbiology Ecology* **44**, 335-346.

Geisseler, D., Horwath, W. R., and Doane, T. A., 2009. Significance of organic nitrogen uptake from plant residues by soil microorganisms as affected by carbon and nitrogen availability. *Soil Biology & Biochemistry* **41**, 1281-1288.

Geisseler, D., Horwath, W. R., Joergensen, R. G., and Ludwig, B., 2010. Pathways of nitrogen utilization by soil microorganisms - A review. *Soil Biology & Biochemistry* **42**, 2058-2067.

Hatton, P.-J., Bode, S., Boeckx, P., Zeller, B., Gelhaye, L., Boiry, S., and Derrien, D., 2012a. Contribution of dead and fresh bacterial and fungal biomasses to soil organo-mineral associations *In Prep. For Soil Biology and Biochemistry*.

Hatton, P.-J., Kleber, M., Zeller, B., Moni, C., Plante, A. F., Townsend, K., Gelhaye, L., Lajtha, K., and Derrien, D., 2012b. Transfer of litter-derived N to soil mineral-organic associations: Evidence from decadal N-15 tracer experiments. *Organic Geochemistry* **42**, 1489-1501.

Hatton, P.-J., Remusat, L., Zeller, B., and Derrien, D., 2012c. A multi-scale approach to determine accurate and isotopic ratios by nano-scale secondary ion mass spectrometry imaging. *Rapid Communications in Mass Spectrometry* **26**, 1363-1371.

Henry, H. A. L. and Jefferies, R. L., 2003. Plant amino acid uptake, soluble N turnover and microbial N capture in soils of a grazed Arctic salt marsh. *Journal of Ecology* **91**, 627-636.

Herrmann, A. M., Clode, P. L., Fletcher, I. R., Nunan, N., Stockdale, E. A., O'Donnell, A. G., and Murphy, D. V., 2007a. A novel method for the study of the biophysical interface in soils using nano-scale secondary ion mass spectrometry. *Rapid Communications in Mass Spectrometry* **21**, 29-34.

Herrmann, A. M., Ritz, K., Nunan, N., Clode, P. L., Pett-Ridge, J., Kilburn, M. R., D.V., M., O'Donnell, A. G., and Stockdale, E. A., 2007b. Nano-scale secondary ion mass spectrometry - A new analytical tool in biogeochemistry and soil ecology: A review article. *Soil Biology & Biochemistry* **39**, 1835-1850.

Jones, D. L. and Hodge, A., 1999. Biodegradation kinetics and sorption reactions of three differently charged amino acids in soil and their effects on plant organic nitrogen availability. *Soil Biology & Biochemistry* **31**, 1331-1342.

Jones, D. L. and Murphy, D. V., 2007. Microbial response time to sugar and amino acid additions to soil. *Soil Biology & Biochemistry* **39**, 2178-2182.

Kinyangi, J., Solomon, D., Liang, B. I., Lerotic, M., Wirick, S., and Lehmann, J., 2006. Nanoscale biogeocomplexity of the organomineral assemblage in soil: Application of STXM microscopy and C 1s-NEXAFS spectroscopy. *Soil Science Society of America Journal* **70**, 1708-1718.

Kleber, M., Sollins, P., and Sutton, R., 2007. A conceptual model of organo-mineral interactions in soils: self-assembly of organic molecular fragments into zonal structures on mineral surfaces. *Biogeochemistry* **85**, 9-24.

Knowles, T. D. J., Chadwick, D. R., Bol, R., and Evershed, R. P., 2010. Tracing the rate and extent of N and C flow from (13)C,(15)N-glycine and glutamate into individual de novo synthesised soil amino acids. *Organic Geochemistry* **41**, 1259-1268.

Koegel-Knabner, I., Guggenberger, G., Kleber, M., Kandeler, E., Kalbitz, K., Scheu, S., Eusterhues, K., and Leinweber, P., 2008. Organo-mineral associations in temperate soils: Integrating biology, mineralogy, and organic matter chemistry. *Journal of Plant Nutrition and Soil Science-Zeitschrift Fur Pflanzenernahrung Und Bodenkunde* **171**, 61-82.

Lee, C. G., Watanabe, T., Sato, Y., Murase, J., Asakawa, S., and Kimura, M., 2011. Bacterial populations assimilating carbon from (13)C-labeled plant residue in soil: Analysis by a DNA-SIP approach. *Soil Biology & Biochemistry* **43**, 814-822.

Lehman, J., Kinyangi, J., and Solomon, D., 2007. Organic matter stabilization in soil microaggregates: implications from spatial heterogeneity of organic carbon contents and carbon forms. *Biogeochemistry* **85**, 45-57.

Lehman, J., Solomon, D., Kinyangi, J., Dathe, L., Wirick, S., and Jacobsen, C., 2008. Spatial complexity of soil organic matter forms at nanometer scales. *Nature geoscience* **1**, 238-242.

Mariotti, A., 1983. Atmospheric nitrogen is a reliable standard for natural 15N abundance measurements. *Nature* **303**, 685-687.

McNamara, N. P., Black, H. I. J., Beresford, N. A., and Parekh, N. R., 2003. Effects of acute gamma irradiation on chemical, physical and biological properties of soils. *Applied Soil Ecology* **24**, 117-132.

Mikutta, R., Zang, U., Chorover, J., Haumaier, L., and Kalbitz, K., 2011. Stabilization of extracellular polymeric substances (Bacillus subtilis) by adsorption to and coprecipitation with Al forms. *Geochimica Et Cosmochimica Acta* **75**, 3135-3154.

Mueller, C., Kölb, A., Hoeschen, C., Hillion, F., Heister, K., Herrmann, A. M., and Koegel-Knabner, I., 2011. Submicron scale imaging of soil organic matter dynamics using NanoSIMS – From single particles to intact aggregates. *Organic Geochemistry*.

Mueller, C. W., Bruggemann, N., Pritsch, K., Stoelken, G., Gayler, S., Winkler, J. B., and Kogel-Knabner, I., 2009. Initial differentiation of vertical soil organic matter distribution and composition under juvenile beech (Fagus sylvatica L.) trees. *Plant and Soil* **323**, 111-123.

Murase, J., Shibata, M., Lee, C. G., Watanabe, T., Asakawa, S., and Kimura, M., 2012. Incorporation of plant residue-derived carbon into the microeukaryotic community in a rice field soil revealed by DNA stable-isotope probing. *FEMS Microbiology Ecology* **79**, 371-379.

Nunan, N., Wu, K. J., Young, I. M., Crawford, J. W., and Ritz, K., 2003. Spatial distribution of bacterial communities and their relationships with the micro-architecture of soil. *FEMS Microbiology Ecology* **44**, 203-215.

Omoike, A. and Chorover, J., 2006. Adsorption to goethite of extracellular polymeric substances from Bacillus subtilis. *Geochimica Et Cosmochimica Acta* **70**, 827-838.

Popa, R., Weber, P. K., Pett-Ridge, J., Finzi, J. A., Fallon, S. J., Hutcheon, I. D., Nealson, K. H., and Capone, D. G., 2007. Carbon and nitrogen fixation and metabolite exchange in and between individual cells of *Anabaena oscillaioides*. *International Society for Microbial Ecology Journal* **1**, 354-360.

Remusat, L., Hatton, P.-J., Nico, P. S., Zeller, B., Kleber, M., and Derrien, D., 2012. NanoSIMS study of organic matter associated with soil aggregates: advantages, limitations and combination with STXM. *Environmental Science & Technology* **46**, 3943-3949.

Rillig, M. C., Caldwell, B. A., Wosten, H. A. B., and Sollins, P., 2007. Role of proteins in soil carbon and nitrogen storage: controls on persistence. *Biogeochemistry* **85**, 25-44.

Sato, K., 1987. Effect of increasing penachlorophenol (PCP) concentrations on bacterial-populations in glycine-percolated soils. *Biology and Fertility of Soils* **5**, 1-5.

Schmidt, M. W. I., Torn, M. S., Abiven, S., Dittmar, T., Guggenberger, G., Janssens, I. A., Kleber, M., Koegel-Knabner, I., Lehmann, J., Manning, D. A. C., Nannipieri, P., Rasse, D. P., Weiner, S., and Trumbore, S. E., 2011. Persistence of soil organic matter as an ecosystem property. *Nature* **478**, 49-56.

Sollins, P., Kramer, M. G., Swanston, C., Lajtha, K., Filley, T., Aufdenkampe, A. K., Wagai, R., and Bowden, R. D., 2009. Sequential density fractionation across soils of contrasting mineralogy: evidence for both microbial- and mineral-controlled soil organic matter stabilization. *Biogeochemistry* **96**, 209-231.

Sollins, P., Swanston, C., Kleber, M., Filley, T., Kramer, M., Crow, S., Caldwell, B. A., Lajtha, K., and Bowden, R., 2006. Organic C and N stabilization in a forest soil: Evidence from sequential density fractionation. *Soil Biology & Biochemistry* **38**, 3313-3324.

van Hees, P. A. W., Jones, D. L., Finlay, R., Godbold, D. L., and Lundstomd, U. S., 2005. The carbon we do not see - the impact of low molecular weight compounds on carbon dynamics and respiration in forest soils: a review. *Soil Biology & Biochemistry* **37**, 1-13.

Vieuble-Gonod, L. V., Jones, D. L., and Chenu, C., 2006. Sorption regulates the fate of the amino acids lysine and leucine in soil aggregates. *European Journal of Soil Science* **57**, 320-329.

Webster, E. A., Chudek, J. A., and Hopkins, D. W., 1997. Fates of C-13 from enriched glucose and glycine in an organic soil determined by solid-state NMR. *Biology and Fertility of Soils* **25**, 389-395.

Young, I. M. and Crawford, J. W., 2004. Interactions and self-organization in the soil-microbe complex. *Science* **304**, 1634-1637.

Young, I. M., Crawford, J. W., Nunan, N., Otten, W., and Spiers, A., 2008. Microbial distribution in soils: physics and scaling. *Advances in Agronomy* **100**, 81-121.

Young, K. D., 2006. The selective value of bacterial shape. *Microbiology and Molecular Biology Reviews* **70**, 660-+.

Zeller, B., Colin-Belgrand, M., Dambrine, E., and Martin, F., 2001. Fate of nitrogen released from N-15-labeled litter in European beech forests. *Tree Physiology* **21**, 153-162.

Zeller, B., Colin-Belgrand, M., Dambrine, E., Martin, F., and Bottner, P., 2000. Decomposition of N-15-labelled beech litter and fate of nitrogen derived from litter in a beech forest. *Oecologia* **123**, 550-559.

Zeller, B. and Dambrine, E., 2011. Coarse particulate organic matter is the primary source of mineral N in the topsoil of three beech forests. *Soil Biology & Biochemistry* **43**, 542-550.

Contribution of dead and fresh bacterial and fungal biomasses to soil organo-mineral associations

Pierre-Joseph Hatton [a]*, Samuel Bodé [b], Nicolas Angeli [c], Pascal Boeckx [b], Bernd Zeller [a], Delphine Derrien [a]

[a] INRA-Nancy, Biogéochimie des Ecosystemes Forestiers, 54280 Champenoux, France

[b] Faculty of Bioscience Engineering, Laboratory of Applied Analytical and Physical Chemistry (ISOFYS), Ghent University, Coupure Links 653, Ghent 9000, Belgium

[c] INRA-Nancy, Ecologie et Ecophysiologie Forestières, 54280 Champenoux, France

* Corresponding author: pierre-joseph.hatton@nancy.inra.fr

VII

In prep. for *Soil Biology and Biochemistry*

Abstract

Soil microorganisms play a key role in soil organic matter dynamics, but little is still known about their distribution through soil organo-mineral associations and how they contribute to the overall soil organic matter. Here, a surface Cambisol was amended with ^{13}C-labeled glycine and beech leaf fragments for 12 weeks. Organo-mineral associations were sequentially isolated by density. Amino sugar ^{13}C analysis was used as a proxy for microbial biomasses to gain insight into bacterial and fungal utilization of the two substrates for the production of biomasses. Total and ^{13}C-labeled glucosamine, galactosamine and muramic acid were quantified throughout density fractions to elucidate the spatial distribution of dead and freshly produced bacterial and fungal biomasses.

Total amino sugars and ^{13}C-labeled amino sugars deriving from glycine were similarly distributed throughout the set of density fractions, and both peaked in microbial aggregates. ^{13}C-labeled amino sugars deriving from leaf fragments were found in all fractions, but mostly in plant debris. Contributions of (i) total amino sugars to the fraction carbon and (ii) ^{13}C-labeled amino sugars deriving from glycine and leaf fragments to the corresponding fraction $^{13}C_{tracer}$ progressively increased along with density.

Dead (total amino sugars) and freshly (^{13}C-labeled amino sugars) produced microbial biomasses increasingly contributed to the cohort of carbon from whom they derive attached with soil organo-mineral associations of increasing density. Bacterial and fungal biomasses are similarly distributed, even though the contribution of the latter is limited. Differences in the distribution of freshly produced amino sugars deriving from the readily accessible glycine and the leaf fragments revealed that bacteria and fungi grow where the resource is, but accumulate in microbial aggregates. This reveals either a higher stabilization efficiency for the microorganisms found in the microbial aggregates than in plant fragments and/ or the transfer of the microbial biomasses from plant debris to microbial aggregates, likely along with the transfers of decaying litter residues.

Keywords

Soil/ amino sugars/ ^{13}C/ density fractions/ LC-IRMS

1. Introduction

Soil microorganisms are increasingly seen as important controlling factors for soil organic matter (SOM) dynamics because their products accumulate in soils (Kindler *et al.*, 2009; Miltner *et al.*, 2009; Nowak *et al.*, 2011) as stable SOM (Hatton *et al.*, 2012b; Sollins *et al.*, 2009). By jointly analyzing fumigation-extracts and biomarkers of the total and living microbial biomasses, Appuhn and Joergensen (2006) showed that half of the SOM of a rhizosphere soil may remain as dead microbial biomass, while 6% might be found in living microorganisms. Although the soil microbial habitats are reasonably well known, the environmental controls for their spatial distribution through the soil system remain not fully understood (Young *et al.*, 2008). Fungal and bacterial contributions to increasingly stable SOM fractions, such as isolated by density (Sollins et al., 2006), are still to explore.

Amino sugars are valuable biomarkers for the total microbial biomass (Amelung *et al.*, 2008; Glaser, 2005a): they are almost totally produced by the microorganisms and they long-survive their producers (Amelung *et al.*, 2001). The most studied amino sugars in soils are glucosamine, galactosamine, and muramic acid. They are quantifiable and inform on bacterial and fungal origins. Fungi cell walls are, by far, the major source of glucosamine in soils, while the bacteria cell walls are the unique purveyor of the muramic acid (Glaser *et al.*, 2004; Liang *et al.*, 2009). Galactosamine has less specific origins (He *et al.*, 2011): it is principally found in bacterial materials, but also in some taxonomic fungal groups. Amino sugars principally account for dead microbial biomass, but a small fraction is included in the living biomass (Glaser *et al.*, 2004) so that tracking the formation of newly synthesized amino sugars has been used for capturing the fates of the resulting microbial residues. Engelking *et al.* (2007) demonstrated that the differences in quality between sucrose and cellulose affect the formation of glucosamine, galactosamine and muramic acid. Many studies further combined stable isotope techniques and amino-sugar ^{13}C or ^{15}N analysis to better quantify the freshly produced amino sugars (Amelung *et al.*, 2008; Glaser, 2005a). Many studies further combined stable isotope techniques and amino-sugar ^{13}C or ^{15}N analyses to better quantify the freshly produced amino sugars (He *et al.*, 2011; Liang *et al.*, 2007). Until recently, however, amino sugar ^{13}C analysis was hampered by undetermined biases on the isotopic signature of the studied amino sugars resulting from a derivatization step for gas chromatography separation. To overcome that issue, Bodé *et al.* (2009) developed a new method for amino-sugar ^{13}C analysis by liquid chromatography that provides more accurate and precise measurement than never before. Such new analytical tool is now available to determine the extent to which the chemical composition of the substrates affects the distribution of fungal and bacterial biomasses through distinct soil compartments.

This study aims at solving the distribution of total and freshly produced bacterial and fungal biomasses within increasingly stable soil organo-mineral associations. Soils amended with ^{13}C-labeled beech leaf fragments (natural substrate) and ^{13}C-labeled glycine were incubated in the laboratory for 12 weeks. Soluble glycine was used as a readily accessible substrate for soil microorganisms. An intermediary sampling was performed for the soil amended with the soluble glycine. Based upon

works of Sollins *et al.* (2009) and Hatton *et al.* (2012a), we hypothesized that the soil microbial biomass increasingly contributes to soil organo-mineral associations of increasing density. We further hypothesized that the incorporation of beech leaf fragments and soluble glycine into the bacterial and fungal biomasses varies with the distribution of soil microorganisms throughout soil organo-mineral associations and their accessibility to the resource. To test these hypotheses, we (i) quantified glucosamine, galactosamine and muramic acid contents through a set of density-isolated soil fractions and (ii) determined the extent to which these amino sugars incorporate the ^{13}C tracers deriving from ^{13}C glycine and ^{13}C leaf fragments. The patterns of ^{13}C incorporation through the soil fractions were traced using elemental analyzer coupled with isotope ratio mass spectrometry (EA-IRMS). The formation of fungal and bacteria biomasses originating from both glycine and leaf fragments was determined overtime by amino sugar ^{13}C analysis using liquid chromatography coupled with isotope ratio mass spectrometry (LC-IRMS).

2. Materials and methods

2.1. Soil

The soil was collected in November 2009 from an even-aged beech forest of 23 year old at Ebrach, Germany (49°52'N, 10°27'E). Both site and soil were described in a previous study (Hatton *et al.*, 2012a). Briefly, the soil is an acidic dystric Cambisol (pH_{H20}=3.9; sand: 80%; loam: 13%; clay: 7%). The first 2.5 cm of the A-horizon were sampled on 2 m^2, mixed and sieved to pass 2mm. Observable roots were removed. The soil stored 2 weeks at +4°C prior pre-incubation.

2.2. Incubated materials

Soils were amended with uniformly ^{13}C-labeled glycine (98% excess; Sigma-Aldrich, France) and ^{13}C-labeled beech leaf fragments (3.27% excess). The labeled leaf litter was obtained from 10 year-old beech trees grown in a chamber at the CEA Cadarache (France) and labeled with $^{13}CO_2$ over the vegetation season by continuous labeling (April-May) and pulse labeling (June-September). Senescent leaves were collected at fall, oven-dried at 25°C and finely ground to powder using a ball mill.

2.3. Conditions of incubation

Soil were pre-incubated for 15 days at 20°C (dark; 1:3 soil to air ratio) prior amendment with labeled glycine and leaf fragments. Both substrates were added in the same amount than the natural annual input in N computed over the first 10cm of the A-horizon: $15\mu g_N.g_{soil}^{-1}$. It corresponds to $80\mu g.g_{soil}^{-1}$ ($26\mu g_C.g_{soil}^{-1}$) for the uniformly ^{13}C-labeled glycine and $2.4mg.g_{soil}^{-1}$ for the ^{13}C-labeled leaf fragments ($1.1mg_C.g_{soil}^{-1}$). The amended soils were thoroughly mixed by hand and sieved twice to ensure a homogeneous mixing. The moisture content was set at half of the water holding capacity (21%). Both treatments were incubated at 20°C (dark; 1:3 soil to air ratio), aerated once a day for 2 weeks and twice a week until collection. The moisture content was readjusted when necessary. The glycine treatment was sampled

after 7 days and 92 days of incubation, against after 92 days for the beech leaf liter treatment. Soils were freezed at -20°C immediately after sampling.

2.4. Isolation of organo-mineral associations

Incubated soils were sequentially separated by density to isolate distinct organo-mineral associations (Hatton *et al.*, 2012a). In short, soils were suspended in a solution of sodium polytungstate with low C and N concentrations (SPT_0, TC-Tungsten Compounds, Germany). The density was set to 1.65 $g.cm^{-3}$ prior separation of light and dense fractions by centrifugation (<2000g). The light fraction is then aspirated, rinsed and freezed at -20°C. The same procedure is repeated with the dense fraction with solutions of increasing density. The same soil was already density fractionated so that the composition of each density fraction is already known (Hatton *et al.*, 2012a). Thus, we separated four density fractions containing plant debris (<1.65 $g.cm^{-3}$), aggregates dominated by plant debris (1.65-1.85 $g.cm^{-3}$), aggregates dominated by phyllosilicates (1.85-2.4 $g.cm^{-3}$) and mineral grains dominated by quartz and feldspar with little organic matter attached (2.4-2.65 $g.cm^{-3}$). Materials denser than 2.65 $g.cm^{-3}$ were not treated because of the presence of pedogenic oxides that could interfere with the LC-IRMS analysis. They accounted for 0.9% and 0.2% of total soil mass and carbon, respectively.

2.5. Elemental and isotopic characterization

2.5.1. Macro-scale composition of the soil fractions

The composition in ^{12}C and ^{13}C of the soil fractions was determined in three replicates using an elemental analyzer (CE instruments, NA 1500 type II) coupled to an isotope ratio mass spectrometer (Finnigan, Delta S) at the Technical Platform of Functional Ecology (OC 081) at INRA Forest Ecology and Ecophysiology Unit, INRA Nancy, France.

2.5.2. Molecular-scale composition of the amino-sugars isolated from the soil fractions

Amino sugars ^{12}C and ^{13}C analyses were obtained in two replicates per soil fraction using a liquid chromatography coupled to isotope ratio mass spectrometer (LC-IRMS) at the Laboratory of Applied Physical Chemistry - ISOFYS, University of Gent, Belgium. We followed the same procedure than Bodé *et al.* (2009): 0.3mg of N were successively hydrolyzed with 6M HCl (20 ml for 1 gram of soil) at 105°C for 8 hours, filtered to pass through 0.45µm (GF/C 25mm, Whatman Cat N°1822-025, Germany). Negatively charged compounds were removed using cationic exchange resin (AG50W-X8, 100-200 Mesh, Hydrogen form, Bio-Rad lab.) prior to LC-IRMS analysis of glucosamine, galactosamine and muramic acid. The chromatographic separation was performed using a LC pump (Surveyor MS-Pump Plus, Thermo Electron, Bremen, Germany) mounted with a PA20 CarboPac analytical anion-echange column (3x150mm, 6.5µm) and a PA20 guard column (Dionex). Two isocratic methods were used: basic amino sugars (glucosamine and galactosamine) were eluted with 2mM NaOH and a column temperature of 15°C;

acid amino sugars (muramic acid) were eluted with 2mM NaOH + 2mM $NaNO_3$ with a column temperature of 30°C. Organic moieties were further converted in CO_2 by the LC Isolink interface (Thermo Electron) using 0.4M $Na_2S_2O_8$ for as oxidizing agent and 1.5M H_3PO_4 to neutralize the pH prior to combustion at 99.9°C. The CO_2 was finally analyzed for ^{12}C and ^{13}C using an isotope ratio mass spectrometer (DELTAPLUS XP, Thermo Electron).

2.6. Calculations

Quantities of ^{13}C tracer ($Q^{13}C_{tracer}$) deriving from the isotopically labeled substrates were calculated as follows:

$$Q^{13}C_{tracer} = \frac{\left(A(\%)_{labeled} - A(\%)_{control}\right)}{100} \times \left[C\right]_{labeled} \quad (1)$$

where $A(\%)_{labeled}$ and $A(\%)_{control}$ are the abundances of ^{13}C isotopes over the total C (%) in labeled and control treatments, respectively. $[C]_{labeled}$ and $[C]_{control}$ are the C concentrations measured in labeled and control treatments, respectively.

Quantities of freshly produced amino sugars were obtained from the $Q^{13}C_{tracer}$ using the amino sugar's stoichiometry:

$$Newly\ formed\ amino\ sugar = Q^{13}C_{tracer} \times {}^{1}\!/\!_{X} \quad (2)$$

where X is the proportion of C found in glucosamine (40.22%), galactosamine (40.22%) and muramic acid (43.03%).

Comparisons were performed using Pearson correlation analysis. The Pearson correlation coefficient (R) was considered as high above 0.8.

3. Results

3.1. Carbon through soil fractions

Table 1 shows that the C contents measured from the control and treatments did not significantly vary. Recovery rates after density fractionation were 99.4±0.4% and 90±4% of total dry weight and total C. Soil masses and total C were similarly distributed through the set of density fractions isolated from control and treatments, indicating that, the density-isolated fractions were globally comparable between treatments and over time. The only exception was in plant debris isolated from the soil amended with beech leaf fragments, what is attributed to the larger inputs in C (Aita *et al.*, 1997).

3.2. Amino sugars through soil fractions

Amino sugars concentrations measured in the bulk soils do not significantly vary between control and the soils incubated with beech leaf fragments for 92 days or with glycine for 7 and 92 days (Table 1). Mean glucosamine, galactosamine and muramic acid concentrations were 664±187µg.g_{soil}^{-1}, 361±76µg.g_{soil}^{-1} and 291±58µg.g_{soil}^{-1}, respectively. Recovery rates after density fractionation did not significantly differ between control and treatments. Glucosamine and galactosamine

were better recovered than muramic acid. In both cases, amino sugars were found throughout the set of density fractions. As observed in the bulk soil, the glucosamine found in each soil fractions was invariably the most abundant amino sugar followed by galactosamine and muramic acid. Based on soil weight, the distributions of these three amino sugars did not significantly differ between the control and the soil amended with beech leaf fragments and glycine. They remain somehow constant through the set of density fractions except in the microbial aggregates fraction in which they peak. The muramic acid shows a slightly less marked tendency. Based on fraction C, the proportions of amino sugars C all regularly increased with fraction density (Figure 1).

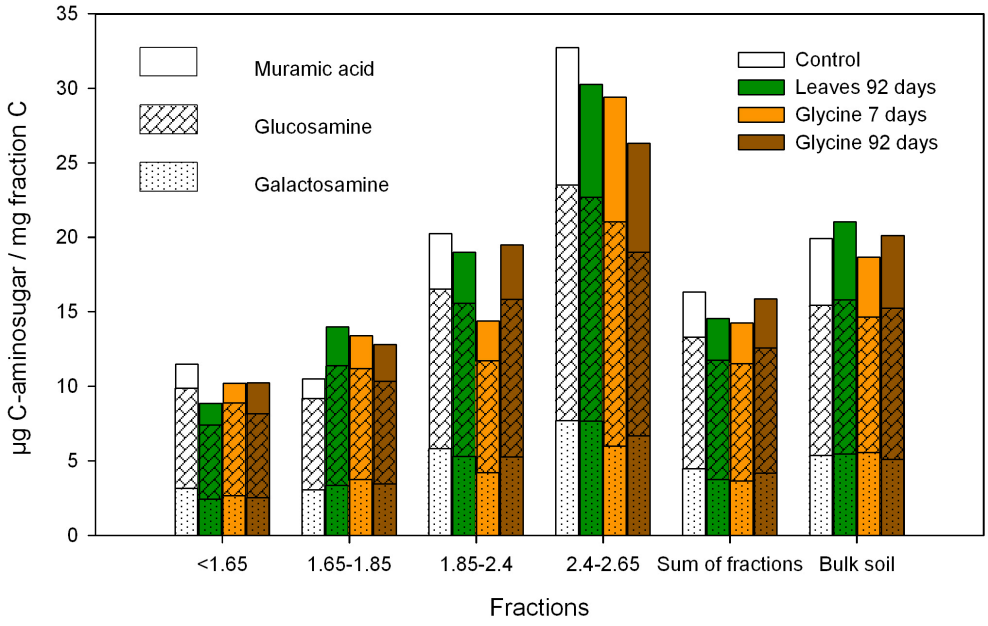

Figure 1: Proportions of amino sugars C relative to fraction C measured in the control (white), beech leaf fragments treatment 92 days after addition (green), glycine treatment 7 days (orange) and 92 days (brown) after addition. Glucosamine, galactosamine and muramic acid C contents were expressed as µg per mg of fraction C. Density fractions are expressed as g cm^{-3}.

Table 1: Carbon, galactosamine, glucosamine and muramic acid contents through soil fractions. The composition of the density fractions is from Hatton *et al.*, (2012a). SD means standard error (n=2).

Treatment	Incubation	Fraction		Dry weight	Carbon		Galactosamine				Glucosamine				Muramic acid			
	days	g/cm^{-3}	Composition	%	mg/ gsoil	SD	µg/gsoil	SD	Distribution (%)	SD	µg/gsoil	SD	Distribution (%)	SD	µg/gsoil	SD	Distribution (%)	SD
Control	0	Bulk soil			27.2	0.5	364	47			680	157			282	32		
		<1.65	Plant debris	2	8.0	0.1	63	7	24	3	134	20	26	4	30	4	18	3
		1.65-1.85	Plant aggregates	1	5.5	0.0	42	7	16	3	84	15	16	3	17	3	10	2
		1.85-2.4	Microbial aggregates	10	7.8	0.4	113	21	42	8	207	20	40	4	67	18	40	11
		2.4-2.65	Mineral grains	86	2.5	0.0	48	2	18	1	98	3	19	1	53	0	32	0
		Sum of fractions		99	23.8	0.4	265	38	79	11	522	59	77	9	167	27	59	9
Beech leaf litter	92	Bulk soil			27.2	0.4	369	60			697	137			330	25		
		<1.65	Plant debris	3	11.1	0.1	68	22	28	9	137	44	26	8	37	2	22	1
		1.65-1.85	Plant aggregates	2	5.3	0.1	44	5	18	2	106	13	20	3	32	8	19	5
		1.85-2.4	Microbial aggregates	9	7.3	0.1	97	20	40	8	187	29	36	6	58	14	34	8
		2.4-2.65	Mineral grains	84	2.4	0.1	46	4	19	2	90	11	17	2	42	8	25	5
		Sum of fractions		99	26.2	0.3	245	51	66	14	520	97	75	14	170	33	51	10
Glycine	7	Bulk soil			26.8	0.1	370	67			605	126			249	11		
		<1.65	Plant debris	2	7.4	0.0	50	10	23	5	115	26	25	6	22	1	15	1
		1.65-1.85	Plant aggregates	2	5.0	0.0	47	7	22	3	93	17	20	4	26	4	17	2
		1.85-2.4	Microbial aggregates	10	8.9	0.0	94	23	43	11	166	41	36	9	55	10	37	7
		2.4-2.65	Mineral grains	85	2.5	0.1	37	3	17	1	92	8	20	2	48	16	32	11
		Sum of fractions		100	23.8	0.2	217	43	59	12	466	92	77	15	151	31	61	13
	92	Bulk soil			26.7	0.1	341	77			673	167			302	27		
		<1.65	Plant debris	2	7.8	0.0	49	13	20	5	109	36	22	7	37	7	21	4
		1.65-1.85	Plant aggregates	2	4.7	0.0	41	10	17	4	81	20	16	4	27	8	15	5
		1.85-2.4	Microbial aggregates	11	8.2	0.0	108	13	44	5	216	26	44	5	70	7	38	4
		2.4-2.65	Mineral grains	84	2.8	0.0	46	4	19	1	85	8	17	2	48	16	26	9
		Sum of fractions		100	23.6	0.1	245	40	72	12	492	90	73	13	182	38	60	13

Table 2: Contents in $^{13}C_{tracer}$ and freshly produced galactosamine, glucosamine and muramic acid through soil fractions. The composition of the density fractions is from Hatton *et al.*, (2012a). SD means standard error (n=2). Total amounts of galactosamine ($GalN_{tot}$), glucosamine ($GluN_{tot}$) and muramic acid ($MurN_{tot}$) are in Table 1.

Treatment	Incubation	Fraction		Dry weight	$^{13}C_{tracer}$		Newly formed Galactosamine						Newly formed Glucosamine						Newly formed Muramic acid					
	days	g/cm^{-3}	Composition	%	µg/ gsoil	SD	µg/ gsoil	SD	Distribution (%)	SD	µg /mg fraction $GalN_{tot}$	SD	µg/ gsoil	SD	Distribution (%)	SD	µg /mg fraction $GluN_{tot}$	SD	µg/ gsoil	SD	Distribution (%)	SD	µg /mg fraction $MurN_{tot}$	SD
Beech leaf litter	92	Bulk soil			35.4	1.2	0.05	0.01			0.12	0.03	0.48	0.02			0.69	0.03	0.39	0.05			1.19	0.17
		<1.65	Plant debris	3	19.3	0.1	0.03	0.00	62	7	0.40	0.04	0.11	0.01	50	3	0.77	0.05	0.07	0.01	38	3	1.78	0.14
		1.65-1.85	Plant aggregates	2	7.4	0.0	0.01	0.00	12	2	0.12	0.02	0.04	0.00	18	1	0.36	0.02	0.04	0.00	24	1	1.30	0.06
		1.85-2.4	Microbial aggregates	9	5.4	0.1	0.01	0.00	16	3	0.07	0.01	0.05	0.00	22	2	0.24	0.02	0.04	0.01	22	3	0.63	0.10
		2.4-2.65	Mineral grains	84	2.1	0.0	0.00	0.00	10	3	0.10	0.03	0.02	0.00	10	1	0.24	0.03	0.03	0.00	16	0	0.65	0.02
		Sum of fractions		99	34.1	0.3	0.04	0.01			0.18	0.03	0.21	0.02			0.40	0.03	0.17	0.01			1.01	0.08
Glycine	7	Bulk soil			7.1	0.0	0.05	0.01			0.14	0.04	0.48	0.03			0.79	0.05	0.04	0.01			0.17	0.03
		<1.65	Plant debris	2	0.8	0.0	0.01	0.00	20	2	0.12	0.01	0.05	0.00	15	1	0.46	0.03	0.00	0.00	11	2	0.18	0.03
		1.65-1.85	Plant aggregates	2	0.9	0.0	0.00	0.00	14	4	0.09	0.03	0.07	0.00	19	1	0.75	0.03	0.00	0.00	14	5	0.19	0.07
		1.85-2.4	Microbial aggregates	10	1.9	0.0	0.02	0.00	51	10	0.17	0.03	0.17	0.01	46	3	1.01	0.07	0.02	0.00	56	4	0.36	0.03
		2.4-2.65	Mineral grains	85	0.6	0.0	0.00	0.00	15	1	0.12	0.01	0.08	0.01	21	3	0.84	0.10	0.01	0.00	19	0	0.14	0.00
		Sum of fractions		100	4.2	0.0	0.03	0.01			0.14	0.03	0.37	0.03			0.79	0.06	0.04	0.00			0.23	0.03
	92	Bulk soil			4.3	0.1	0.05	0.01			0.15	0.04	0.46	0.05			0.68	0.07	0.06	0.01			0.21	0.03
		<1.65	Plant debris	2	0.6	0.0	0.01	0.00	24	11	0.15	0.07	0.06	0.00	14	1	0.52	0.04	0.01	0.00	15	3	0.17	0.04
		1.65-1.85	Plant aggregates	2	0.7	0.0	0.00	0.00	14	5	0.11	0.04	0.06	0.00	16	1	0.78	0.04	0.01	0.00	13	5	0.21	0.09
		1.85-2.4	Microbial aggregates	11	1.5	0.0	0.01	0.00	44	10	0.13	0.03	0.21	0.00	53	1	0.97	0.02	0.03	0.00	58	8	0.37	0.05
		2.4-2.65	Mineral grains	84	0.4	0.0	0.01	0.00	18	1	0.12	0.01	0.07	0.00	17	0	0.79	0.02	0.01	0.00	15	1	0.14	0.01
		Sum of fractions		100	3.3	0.0	0.03	0.01			0.13	0.03	0.40	0.01			0.81	0.03	0.04	0.01			0.25	0.04

3.3. $^{13}C_{tracer}$ through soil fractions

Table 2 shows that 79±3% of the $^{13}C_{tracer}$ initially applied as beech leaf fragments were found in the bulk soil after 92 days of decay, against 28±0% and 17±0% for glycine after 7 and 92 days. This indicates that both substrates, and particularly the glycine, have been mineralized.

Recovery rates after density fractionation were 96±1% for the residual $^{13}C_{tracer}$ deriving from beech leaf fragments. The residual $^{13}C_{tracer}$ was unequally distributed through the set of density fractions: 56% were found in plant debris, 22% in plant aggregates, 16% in microbial aggregates and 6% in mineral grains.

The $^{13}C_{tracer}$ tracer deriving from glycine showed a completely different pattern. Recovery rates after density fractionation increased from 59±1% of the residual $^{13}C_{tracer}$ after 7 days to 76±1% after 92 days, suggesting that the residual $^{13}C_{tracer}$ is increasingly stabilized overtime (Hatton *et al.*, 2012b). Based on fraction weight, the residual $^{13}C_{tracer}$ found at day 7 and day 92 appeared similarly distributed: 19±0% were found in plant debris, 21±0% in plant aggregates, 45±1% in microbial aggregates and 15±2% in mineral grains. This points aggregates, and particularly the microbial aggregates, as preferential sites for the retention of the residual $^{13}C_{tracer}$ deriving from soluble glycine.

3.4. $^{13}C_{tracer}$ within amino sugars

3.4.1. Beech leaf litter amendment

Small amounts of freshly produced amino sugars were found in the soil incubated with beech leaf fragments for 92 days: freshly produced glucosamine, galactosamine and muramic acid accounted for 0.69±0.03 μg mg^{-1}, 0.12±0.03 μg mg^{-1} and 1.19±0.17 μg mg^{-1} of the total glucosamine, galactosamine and muramic acid, respectively (Table 2). This indicates that muramic acid is the most renewed amino sugar followed by glucosamine and galactosamine.

Recovery rates after density fractionation were 44±3%, 94±14% and 44±3% for glucosamine, galactosamine and muramic acid, likely because variable proportions of free forms (Roberts *et al.*, 2007). Based on fraction weight, these three freshly produced amino sugars appeared unequally distributed through the set of density fractions. They all peaked in plant debris that contained 50±3%, 62±7% and 38±3% of the glucosamine, galactosamine and muramic acid recovered after density fractionation. The rest is somewhat equally distributed through plant aggregates, microbial aggregates and mineral grains for glucosamine and galactosamine, while the proportions found within these fractions tend to regularly decrease with fraction density for muramic acid.

^{13}C-labeled amino sugars deriving from beech leaf fragments were quantitatively dominated by glucosamine and muramic acid, but the ^{13}C-labeled produced muramic acid represented a much higher proportion to the total stock of individual amino sugars than the ^{13}C-labeled glucosamine (Table 2). The relatively large formation of muramic acid to compare with glucosamine indicates that bacteria

growth is favored in presence of leaf fragments (Amelung *et al.*, 2001; Bossuyt *et al.*, 2001).

3.4.2.Glycine amendment

Table 2 shows that the quantities of freshly produced glucosamine, galactosamine and muramic acid were statistically equal in the soil incubated with glycine for 7 and 92 days as well as in all density fractions isolated from the two sampling dates. ^{13}C-labeled glucosamine, galactosamine and muramic acid represent 0.74±0.08 μg mg^{-1}, 0.15±0.06 μg mg^{-1} and 0.19±0.05 μg mg^{-1} of the total stock of amino sugars. This indicates that the renewal rates increase is higher for glucosamine than for muramic acid and galactosamine.

Recovery rates after density fractionation did not significantly differ between day 7 and day 92. They were 82±7%, 60±19% and 77±15% for freshly produced glucosamine, galactosamine and muramic acid. Based on soil weight, they all appeared similarly distributed through the set of density fractions: microbial aggregates contained 49±3%, 48±14% and 57±9% of the freshly produced glucosamine, galactosamine and muramic acid, while the rest seemed evenly distributed through other density fractions.

At both sampling dates and in all soil fractions, ^{13}C-labeled amino sugars deriving from glycine were dominated by glucosamine both quantitatively and in term of proportion to the total stock of amino sugars (Table 2). This not only indicates that fungi more efficiently produce biomass from glycine than bacteria over the first 12 weeks after substrate addition, but also that most of the freshly produced amino sugars were produced in less than 7 days after glycine application and remain unaltered for at least 92 days.

4. Discussion

Glucosamine, galactosamine and muramic acid account for 2.0±0.5% and 6.2±1.5% of the total soil C and N (Table 1), which is in line with what have been published before (Glaser, 2005b). However, muramic acid contents are usually much lesser than those reported here. Only Decock *et al.* (2009) reported similar concentrations, which they attributed to the sandy texture of their soil. We also studied a sandy soil and believe that this relatively high proportion of muramic acid may be attributed to the relatively high contribution of bacteria, as revealed by a C/N ratio of 5.5 for the microbial biomass extracted by fumigation, to this biologically active soil (Zeller and Dambrine, 2011).

Table 1 shows amino sugars are unevenly distributed through the set of density fraction: 22% are found in density-isolated plant debris, 54% in aggregates and 24% in mineral grains. Based on fraction C, however, the proportions of amino sugars C to fraction C progressively increase with fraction density (Figure 1). Following Appuhn and Joergensen (2006), who suggested conversion factors to convert glucosasmine in fungal C and muramic acids in bacterial C, we assessed total fungal C and bacterial C contribution to fraction C. Figure 2 shows that the proportion of

microbial C to fraction C regularly increases with increasing density to account for most of the fraction C, what demonstrates earlier thoughts based on $\delta^{13}C$, $\delta^{15}N$ and C/N ratios (Hatton *et al.*, 2012a; Sollins *et al.*, 2009, 2006). Bacterial and fungal C follow the same pattern, but the contribution of the bacterial biomass increases relatively more rapidly with increasing density than for the fungal biomass so that the bacterial biomass exceeds by far the fungal biomass found in the denser fractions. Relatively to the bacterial biomass, fungal biomass appears much more important in low-density fractions where poorly altered plant materials are abundant (Hatton *et al.*, 2012a), as indicated in many different soils by the high contents of poorly oxidized lignin phenols (Sollins *et al.*, 2009). Overall, bacterial and fungal biomasses account for 70% of the total bulk C (95% confidence limits ranging from 52% to 121%), what corroborates earlier estimates (Appuhn and Joergensen, 2006; Simpson *et al.*, 2007).

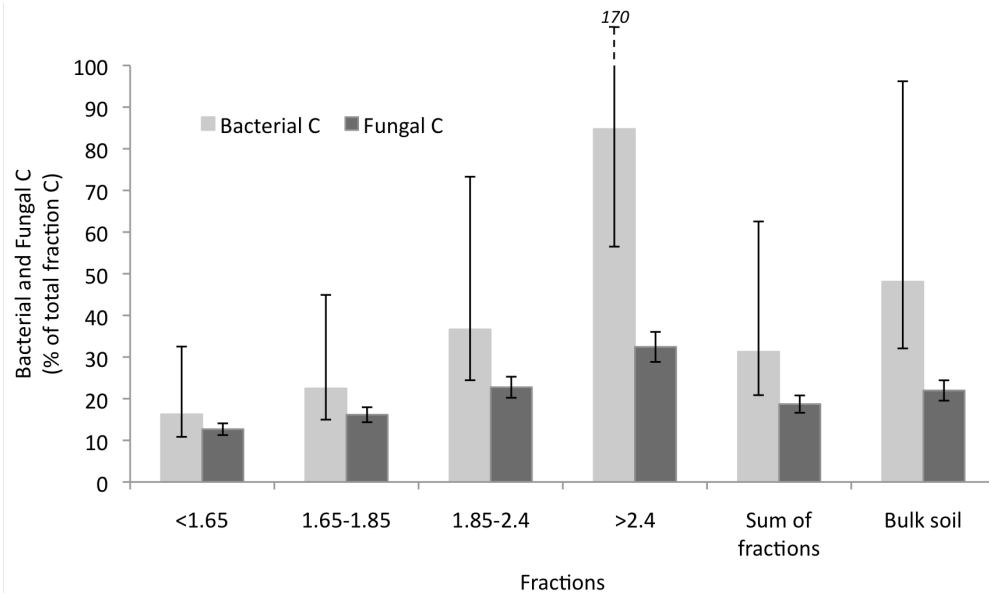

Figure 2: Bacterial and Fungal contributions to fraction C, expressed as percent of the total C of each fraction. Errors bars represent the 95% confidence limits of the factors suggested by Appuhn and Joergensen (2006) for the conversion of glucosamine and muramic acid into fungal (dark grey) and bacterial (light grey) biomasses. Glucosamine and muramic acid contents were averaged from control and treatments.

Contrarily to the total amino sugars that mostly render account for dead microbial biomasses (Amelung *et al.*, 2008), the ^{13}C-labeled amino sugars are indicative of freshly produced biomasses. As recently reported by He *et al.* (2011), our results show that the incorporation of the tracer within amino sugars appears both substrate and compound specific. Our results further reveal that the distributions of ^{13}C-labeled amino sugars deriving from both beech leaf fragment and glycine (reported in Table 2) are highly correlated with the distributions of residual $^{13}C_{tracer}$ found in each treatments ($R \geq 0.97$). Figure 3 shows that the proportions of ^{13}C-labeled amino sugars deriving from both glycine and beech leaf fragment to fraction $^{13}C_{tracer}$ progressively increase with fraction density. Such pattern is highly correlated with

what was observed for total amino sugars C relatively to total fraction C (R≥0.91; Figure 1), corresponding to the integrated state of the different succeeding cohorts overtime. As a consequence, dead and freshly produced bacterial and fungal biomasses are similarly distributed regarding to the C of the cohort from whom they derive.

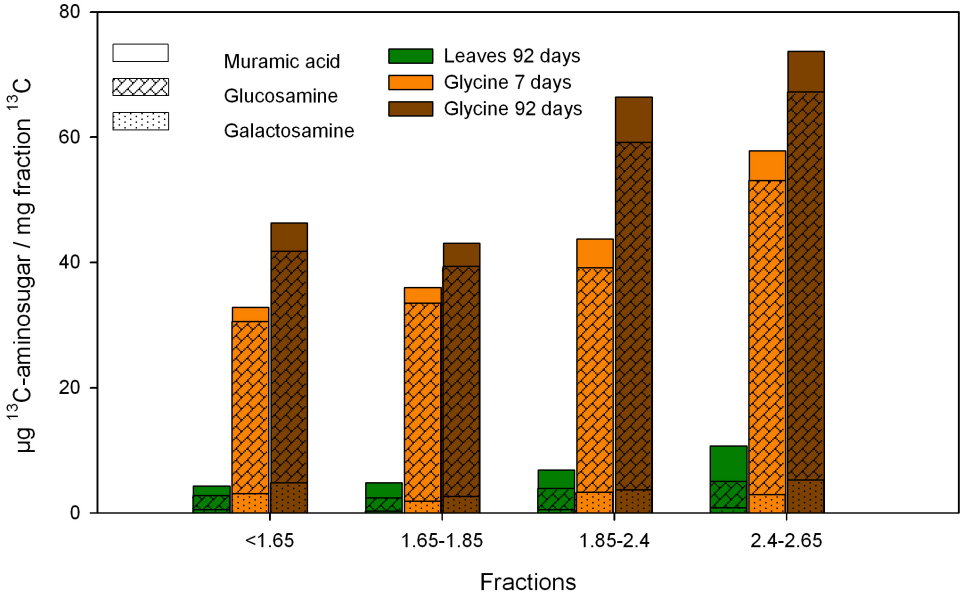

Figure 3: Proportions of $^{13}C_{tracer}$ within the freshly produced glucosamine, galactosamine and muramic acids to residual $^{13}C_{tracer}$ found in the soil fractions isolated from soils amended with beech leaf fragments fragments for 92 days (green), glycine for 7 days (orange) and 92 days (brown). Density fractions are expressed as g cm^{-3}.

Soil ecological interpretations can be derived from the distributions of the freshly produced microbial biomasses. Based on dry weight, amino sugars formed from the soluble glycine quantitatively peak in microbial aggregates where most of the residual ^{13}C-glycine is (Table 2). The ratios ^{13}C-amino sugars/ total amino sugars indicate that the renewal rates for amino sugars are the highest in microbial aggregates. This indicates that active microorganisms preferentially settle in this fraction, what is supported by the distribution of total amino sugars through the set of fractions (R>0.97; Table 1). The comparison with the amino sugars formed from beech leaf fragment reveals that the biological activity evidenced by the renewal rates (Table 2) is principally located where the resource is, as reported by Foster *et al.* (1988) and Young *et al.* (2008). Indeed, the ^{13}C-leaf fragments are mainly isolated in the lightest fraction (Table 2) with other plant debris colonized by microorganisms (Hatton *et al.*, 2012a). Extending our results to naturals ecosystems, where the microbial biomass mostly derives from plant litters, we might assume that the microbial biomass is principally produced on the litter fragments. Integrated state of amino sugars from the succeeding cohort of litter over time, the distribution of the total amino sugars (Table 1) indicates that the microbial biomass does not stay in plant debris. This might be explained by either the progressively movement of soil

assemblages from plant debris to microbial aggregates along with the OM decay, or the higher stabilization efficiency in the microbial aggregates than in plant fragments. Assuming that the microbial biomass found in plant debris turnovers faster than the one found in microbial aggregates, the larger amino sugars contents found in microbial aggregates would result from the accumulation over time.

5. Conclusions

By mapping total and freshly produced glucosamine, galactosamine and muramic acid through density fractions we demonstrated that:

1) Dead and freshly produced microbial biomasses are similarly distributed regarding to the cohort from whom they derive. Dead bacterial and, to a lesser extent fungi, increasingly contribute to SOM attached with soil mineral-organic associations of increasing density. A similar pattern was observed for the small amounts of freshly produced microbial biomasses formed from leaf fragments and glycine relatively to the fraction $^{13}C_{tracer}$.

2) The chemical complexity of substrates influences its microbial utilization and the spatial distribution of the resulting microbial residues. Soluble glycine is rapidly transformed into microbial biomass distributed as the integrated state of the succeeding cohorts, confirming that glycine is readily accessible to all soil microorganisms. At the initial stage of decomposition, the microbial residues deriving from beech leaf litter fragments are mostly located with other plant debris. The difference with the distribution of the total amino sugars might be explained by (i) the progressive movement of soil assemblages from plant debris to microbial aggregates along with the OM decay and/ or (ii) the higher stabilization efficiency in the microbial aggregates than in plant fragments.

Acknowledgments

The Institut National de la Recherche Agronomique (INRA-EFPA), the Région Lorraine (grants #12000292 and #12000184) and the ESF-Molter programme have financially supported this work. We are in debt to Séverine Boiry (GRAP, CEA Cadarache) for producing the ^{13}C-labeled leaves, Louisette Gelhaye (BEF, INRA) for precious lab assistance and Christian Hossan (PTEF, INRA) for EA-IRMS analyses.

References

Aita C, Recous S, Angers DA (1997). Short-term kinetics of residual wheat straw C and N under field conditions: Characterization by (CN)-C-13-N-15 tracing and soil particle size fractionation. *European Journal of Soil Science* **48:** 283-294.

Amelung W, Brodowski S, Sandhage-Hofmann A, Bol R (2008). Combining biomarker with stable isotope analyses for assessing the transformation and turnover of soil organic matter. *Advances in Agronomy, Vol 100* **100:** 155-250.

Amelung W, Miltner A, Zhang X, Zech W (2001). Fate of microbial residues during litter decomposition as affected by minerals. *Soil Science* **166:** 598-606.

Appuhn A, Joergensen RG (2006). Microbial colonisation of roots as a function of plant species. *Soil Biology & Biochemistry* **38:** 1040-1051.

Bodé S, Denef K, Boeckx P (2009). Development and evaluation of a high-performance liquid chromatography/isotope ratio mass spectrometry methodology for delta C-13 analyses of amino sugars in soil. *Rapid Communications in Mass Spectrometry* **23:** 2519-2526.

Bossuyt H, Denef K, Six J, Frey SD, Merckx R, Paustian K (2001). Influence of microbial populations and residue quality on aggregate stability. *Applied Soil Ecology* **16:** 195-208.

Decock C, Denef K, Bode S, Six J, Boeckx P (2009). Critical assessment of the applicability of gas chromatography-combustion-isotope ratio mass spectrometry to determine amino sugar dynamics in soil. *Rapid Communications in Mass Spectrometry* **23:** 1201-1211.

Engelking B, Flessa H, Joergensen RG (2007). Shifts in amino sugar and ergosterol contents after addition of sucrose and cellulose to soil. *Soil Biology & Biochemistry* **39:** 2111-2118.

Foster RC (1988). Microenvironments of soil-microorganisms. *Biology and Fertility of Soils* **6:** 189-203.

Glaser B (2005a). Compound-specific stable-isotope (delta C-13) analysis in soil science. *Journal of Plant Nutrition and Soil Science-Zeitschrift Fur Pflanzenernahrung Und Bodenkunde* **168:** 633-648.

Glaser B, Gross S (2005b). Compound-specific delta C-13 analysis of individual amino sugars - a tool to quantify timing and amount of soil microbial residue stabilization. *Rapid Communications in Mass Spectrometry* **19:** 1409-1416.

Glaser B, Turrion MB, Alef K (2004). Amino sugars and muramic acid - biomarkers for soil microbial community structure analysis. *Soil Biology & Biochemistry* **36:** 399-407.

Hatton P-J, Kleber M, Zeller B, Moni C, Plante AF, Townsend K *et al* (2012a). Transfer of litter-derived N to soil mineral-organic associations: Evidence from decadal N-15 tracer experiments. *Organic Geochemistry* **42:** 1489-1501.

Hatton P-J, Remusat L, Zeller B, Brewer E, Derrien D (2012b) Influence of microbial processes on soil organo-mineral associations. *In prep.* .

He H, Zhang W, Zhang X, Xie H, Zhuang J (2011). Temporal responses of soil microorganisms to substrate addition as indicated by amino sugar differentiation. *Soil Biology & Biochemistry* **43:** 1155-1161.

Kindler R, Miltner A, Thullner M, Richnow H-H, Kaestner M (2009). Fate of bacterial biomass derived fatty acids in soil and their contribution to soil organic matter. *Organic Geochemistry* **40:** 29-37.

Liang C, Read HW, Balser TC (2009). Reliability of Muramic Acid as a Bacterial Biomarker is Influenced by Methodological Artifacts from Streptomycin. *Microbial Ecology* **57:** 494-500.

Liang C, Zhang XD, Balser TC (2007). Net microbial amino sugar accumulation process in soil as influenced by different plant material inputs. *Biology and Fertility of Soils* **44:** 1-7.

Miltner A, Kindler R, Knicker H, Richnow H-H, Kaestner M (2009). Fate of microbial biomass-derived amino acids in soil and their contribution to soil organic matter. *Organic Geochemistry* **40:** 978-985.

Nowak KM, Miltner A, Gehre M, Schaeffer A, Kaestner M (2011). Formation and Fate of Bound Residues from Microbial Biomass during 2,4-D Degradation in Soil. *Environmental Science & Technology* **45:** 999-1006.

Roberts P, Bol R, Jones DL (2007). Free amino sugar reactions in soil in relation to soil carbon and nitrogen cycling. *Soil Biology & Biochemistry* **39**: 3081-3092.

Simpson AJ, Simpson MJ, Smith E, Kelleher BP (2007). Microbially derived inputs to soil organic matter: Are current estimates too low? *Environmental Science & Technology* **41:** 8070-8076.

Sollins P, Kramer MG, Swanston C, Lajtha K, Filley T, Aufdenkampe AK *et al* (2009). Sequential density fractionation across soils of contrasting mineralogy: evidence for both microbial- and mineral-controlled soil organic matter stabilization. *Biogeochemistry* **96:** 209-231.

Sollins P, Swanston C, Kleber M, Filley T, Kramer M, Crow S *et al* (2006). Organic C and N stabilization in a forest soil: Evidence from sequential density fractionation. *Soil Biology & Biochemistry* **38:** 3313-3324.

Young IM, Crawford JW, Nunan N, Otten W, Spiers A (2008). Microbial distribution in soils: physics and scaling. *Advances in Agronomy* **100:** 81-121.

Zeller B, Dambrine E (2011). Coarse particulate organic matter is the primary source of mineral N in the topsoil of three beech forests. *Soil Biology & Biochemistry* **43:** 542-550.

Résumé

Les associations organo-minérales jouent un rôle prépondérant dans la séquestration à long terme des matières organiques des sols forestiers, mais les contributions des différents types d'association organo-minérale à la stabilisation, ainsi que les processus microbiens qui en sont responsables, restent mal connus. Pour y remédier, des techniques de traçage isotopique ont été combinées à la séparation densitométrique séquentielle des associations organo-minérales. Ces dernières ont été investiguées *in* et *ex situ*, à différentes échelles spatiales (macroscopique, submicrométrique et moléculaire) et temporelles (de 8 heures à 12 ans).

Quatre types d'association organo-minérale ont été distingués : les débris végétaux associés à quelques rares minéraux, les agrégats végétaux, les agrégats microbiens et les grains minéraux. Le traçage isotopique du carbone et de l'azote dérivés des litières de feuilles a mis en évidence, à l'échelle de la décennie, des transferts entre les différentes associations organo-minérales. Tous deux entrent dans le sol sous forme de fragments végétaux, puis migrent progressivement vers les agrégats végétaux et microbiens. Les agrégats apparaissent pertinents pour la stabilisation du carbone et de l'azote à l'échelle décennale. Une petite fraction du carbone et de l'azote apparaît rapidement stabilisée dans les grains minéraux denses. Nos observations du devenir du ^{15}N indiquent que l'activité des microorganismes du sol est responsable de ces transferts. Les fragments de feuilles colonisés par les microorganismes sont progressivement incorporés dans les agrégats végétaux. A mesure que la décomposition se poursuit, les agrégats végétaux se disloquent pour former des agrégats plus stables, plus pauvres en matières organiques, plus enrichis en produits microbiens et plus compacts : les agrégats microbiens.

La stabilisation microbienne a été étudiée aux échelles macroscopique, submicrométrique et moléculaire, principalement par NanoSIMS et LC-IRMS. Elle opère (i) directement par immobilisation dans les cellules microbiennes et (ii) indirectement via une abondante production de métabolites extracellulaires. La calibration des C/N obtenus par NanoSIMS a permis de déterminer qu'ils sont stabilisés dans les associations organo-minérales sans contrôle apparent de la chimie des matières organiques. L'incorporation du ^{13}C dans les sucres aminés, biomarqueurs des biomasses bactériennes et fongiques, indique que les microorganismes vivants croissent où la ressource se trouve. Ils s'accumulent dans les agrégats microbiens via les processus de transfert précédemment évoqués.

Ce travail souligne l'importance des agrégats pour la séquestration du carbone et de l'azote dérivés des litières à l'échelle de la décennie. Il met également en évidence le rôle des microorganismes dans les transferts et la stabilisation du carbone et de l'azote dérivés des feuilles au sein d'associations organo-minérales.

Mots clés: Sol forestier, Litière; Stabilisation, Traçage isotopique, Azote, Carbone, Association organo-minérale; Microorganismes; NanoSIMS; STXM-NEXAFS; LC-IRMS; Sucres amines

Abstract

Organo-mineral associations play a key role in the long-term sequestration of organic matter in forest soils. However, knowledge about the contribution of the different types of organo-mineral associations and the microbial processes involved in soil organic matter stabilisation is scant. To solve it, stable isotope techniques have been combined with the sequential density fractionation of organo-mineral associations. Isolated fractions were investigated in field and in lab, at different temporal (from 8 hours to 12 years) and spatial scales (macro-, submicron- and molecular scales).

Four types of organo-mineral associations were distinguished: plant debris with little mineral attached, plant aggregates, microbial aggregates and mineral grains. Isotopically labeled beech leaf litters were tracked at a decadal time-scale to reveal transfers in between organo-mineral associations. Both litter-derived carbon and nitrogen entered the soil as plant fragments to progressively pass through plant and microbial aggregates. Aggregates appeared particularly meaningful for the stabilisation of litter-derived carbon and nitrogen at a decadal time-scale. Little of the litter-derived carbon and nitrogen was found quickly stabilized to mineral grains. Microbial activities appeared as a major controlling factor for the evolvement of organo-mineral associations, responsive for the transfers of litter-derived carbon and nitrogen. Indeed, plant debris colonized by microorganisms are progressively trapped into plant aggregates. As decomposition proceeds, plant aggregates disrupt into denser microbial aggregates. These aggregates are loaded with lesser organic matter, but enriched in stable microbial materials.

Stabilisation by soil microorganisms has been studied at the macro-, submicron- and molecular- scales, using mostly NanoSIMS and LC-IRMS. Microbial stabilization operated (i) directly through immobilization in microbial cells and, (ii) indirectly through large production of extracellular microbial products. By calibrating the NanoSIMS for accurate C/N ratios, extracellular microbial products have been shown to be stabilized onto organo-mineral associations without apparent control of the mineral-attached organic matter chemistry. The incorporation of ^{13}C tracers into amino sugars, biomarkers of bacterial and fungal biomasses, revealed that living microorganisms grow where the resource is, but accumulate in microbial aggregates. Microbial biomasses moved from plant debris to microbial aggregates, likely along with the transfers of decaying litter residues as described above.

This work points aggregates as meaningful organo-mineral associations for the sequestration of litter-derived carbon and nitrogen at the decadal time-scale. It also revealed the role of microorganisms in the transfers and stabilization of litter-derived carbon and nitrogen within organo-mineral associations.

Keywords: Forest soil, Litter ; Isotopique labeling ; Stabilization ; Nitrogen, Carbon, Organo-mineral asociation; Microorganisms ; NanoSIMS ; STXM-NEXAFS ; LC-IRMS ; Amino sugars